University of Southampton

Faculty of Natural and Environmental sciences

National Oceanography Centre

The influence of atmospheric circulation on surface marine temperature

by

Jonathan Harrison

Thesis for the degree of Doctor of Philosophy

January 2019

University of Southampton

Abstract

Faculty of natural and environmental sciences

Department of Ocean and Earth Sciences

Thesis for the degree of Doctor of Philosophy

The influence of atmospheric circulation on surface marine temperature by Jonathan Harrison

Atmospheric circulation is an important influence on local climate, affecting meteorological variables such as temperature, precipitation, cloud cover and humidity. There are strong relationships between surface meteorology and atmospheric circulation in many areas. The extent to which these relationships can explain past climate variability however is unclear, especially over the oceans. A statistical model is developed that can capture the relationships between temperature anomalies and atmospheric circulation. This is then used to estimate the contribution of atmospheric circulation to variations in marine air temperature from as far back as 1770 until 2010. The uncertainty in the relationships is also calculated. Atmospheric circulation patterns are defined from calculations of flow direction, flow strength and average sea level pressure. Estimated and observed marine air temperature anomalies show significant correlations; especially over the northern hemisphere and mid-latitudes of the southern hemisphere. We show that atmospheric circulation has an important influence on past marine air temperature variability. The estimated marine air temperatures are also accompanied with suitable uncertainty estimates. It was concluded that atmospheric circulation is a key factor only in localised short-term climate variability and not the overall global temperature variability. The globally averaged marine air temperature estimates often have an anomaly close to zero. Other factors are more important when considering global marine temperature variability, such as the Atlantic Multidecadal Oscillation and climate change. When focusing on differences between marine air temperature and sea surface temperature (SST) the climate change signal becomes less important and atmospheric circulation is the main contributor to differences seen.

Table of Contents

List of Tables

List of Figures

Abbreviations

20CR – 20th Century Reanalysis

AMO – Atlantic Multidecadal Oscillation

ASL – Above Sea Level

CBTA – Circulation based temperature anomaly

CET – Central England Temperature

COWL - Cold Ocean Warm Land index

ENSO - El Niño Southern Oscillation

GISS – Goddard Institute for Space Studies

GMST – Global Mean Surface Temperature

ICOADS - International Comprehensive Ocean-Atmosphere Data Set

ISPD – International Surface Pressure Databank

J12 – Jones, Harpham and Briffa (2012)

LST – Land Surface Temperature

MAT – Marine Air Temperature

NAG – Numerical Algorithms group

NAO – North Atlantic Oscillation

NOAA – National Oceanic and Atmospheric Administration

PDO – Pacific Decadal Oscillation

SLP – Sea Level Pressure

SOI – Southern Oscillation Index

SST – Sea Surface Temperature

Research Thesis: Declaration of Authorship

Print name:	Jonathan Harrison

Title of thesis:	The influence of atmospheric circulation on surface marine temperature

I declare that this thesis and the work presented in it are my own and has been generated by me as the result of my own original research.

I confirm that:

1. This work was done wholly or mainly while in candidature for a research degree at this University;
2. Where any part of this thesis has previously been submitted for a degree or any other qualification at this University or any other institution, this has been clearly stated;
3. Where I have consulted the published work of others, this is always clearly attributed;
4. Where I have quoted from the work of others, the source is always given. With the exception of such quotations, this thesis is entirely my own work;
5. I have acknowledged all main sources of help;
6. Where the thesis is based on work done by myself jointly with others, I have made clear exactly what was done by others and what I have contributed myself;
7. None of this work has been published before submission

Signature:		Date:	

Acknowledgements

Firstly, I would like to thank my main supervisor Elizabeth Kent for her support, help and enthusiasm. I am especially grateful for her maintaining her belief in me through the whole of this project when there have been difficult times. This in combination with her consistently quick feedback kept my motivation levels up. I would also like to thank David Berry for his feedback through the project.

As I have become older and progressed through academia I have become more thankful of the support I have received from my family, they have played a key role in helping me get this far and on my more difficult days I remind myself how lucky I am to be in my current position in my life.

Thanks to all my friends that I met at NOC as they helped me enjoy my time here also. I would like to thank Steve, Age, Gavin, Harry, Caspar, Xiaodong, Amaya, Lissette and Neela (plus many others) for your company and I enjoyed our many conversations here. I miss them already. I would also like to thank my furry friend Rubens for his company during the later write up stages.

Finally, I would like to thank Rob Allan and Victoria Slonosky for their supply of station Sea Level Pressure data for this thesis.

Chapter 1 Introduction

Historical records of past temperature are important for understanding the earth's climate, helping confirm an unequivocal surface warming trend associated with increasing greenhouse gas emissions (Hartmann *et al.*, 2013). Global mean surface temperature (GMST) is expected to increase by more than 2^{o}C from pre-industrial levels (1850) by the year 2050 in most emissions scenarios (Karmalkar and Bradley, 2017), passing a threshold for dangerous climate change. Such a warming trend is predicted to cause summers free of arctic sea ice later this century (Stroeve *et al.*, 2012), an increasing intensity of tropical cyclones (Holland and Bruyère, 2014), greater precipitation extremes (O'Gorman, 2015) and rising sea levels (Carson *et al.*, 2016). Our estimates of future climate variability and extremes come from climate models and the ability of these models to reproduce historical GMST gives an indication of their skill (Hartmann *et al.*, 2013). Developing accurate estimates of GMST is therefore an important area of research.

The GMST record consists of three components; land, sea and ice. A time series of the land and ocean components with their uncertainties can be seen in Figure 1.1 (Jones, 2016). The land component shows 4 different temperature series which are all in generally close agreement from the 1890s onwards though uncertainties until the 1910s are large (~1^{o}C). This close agreement is apparent because most of the land air temperature (LAT) biases tend to be random in nature over annual timescales (e.g., Böhm *et al.*, 2010, Brandsma and van der Meulen, 2007, Hansen *et al.*, 2010, Moberg *et al.*, 2003). LAT data also has the advantage of all of the observations being recorded at stations, meaning they are generally at fixed locations for long periods of time (Jones, 2016) and metadata also aids the homogenisation process (removal of relative biases (Kent, Woodruff and Berry, 2007, Jones, 2016)).

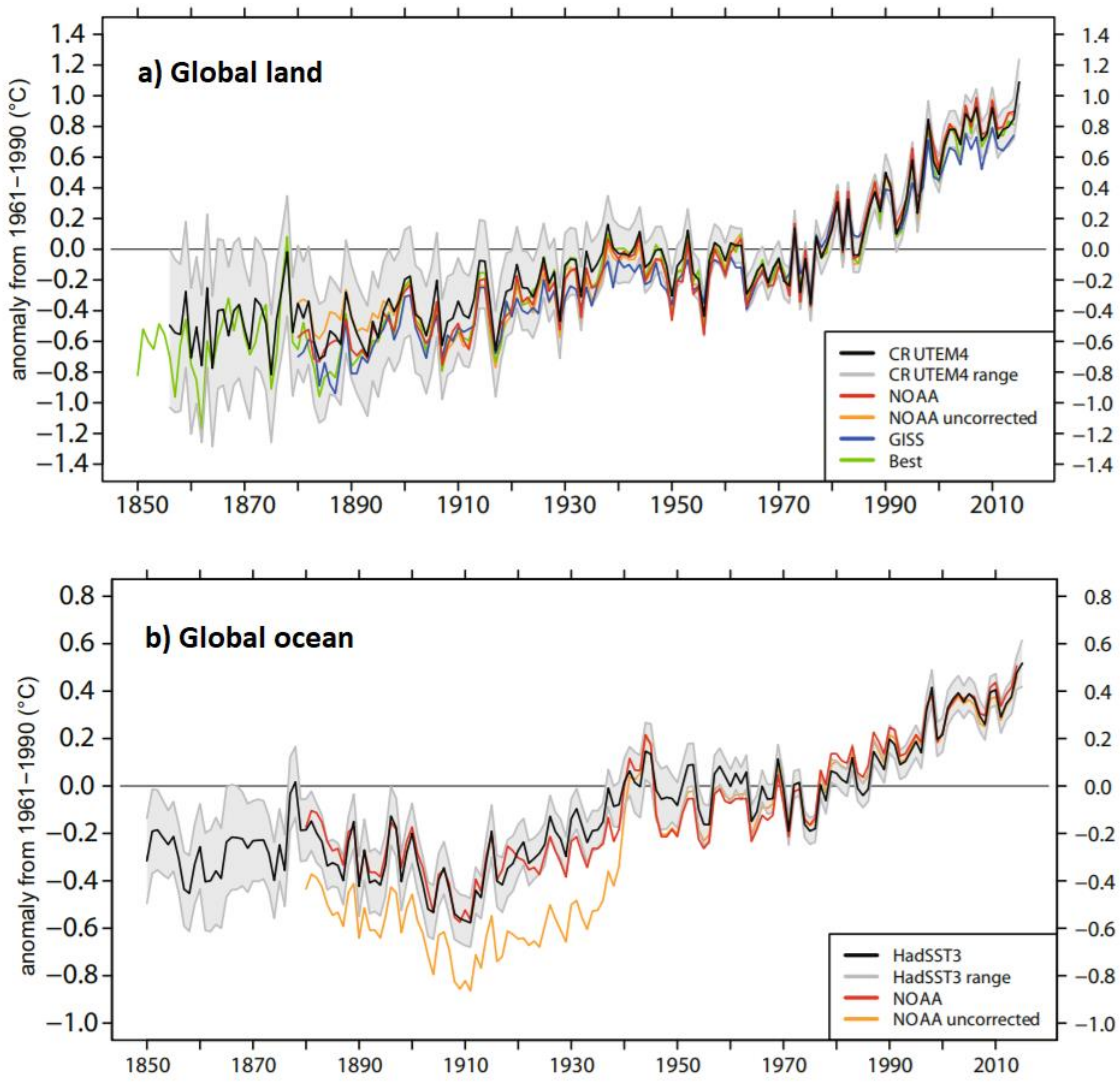

Figure 1.1: Time series of land and marine temperature data (°C). Panel a) Globally averaged land surface from 4 different datasets, CRUTEM4 (black, Morice *et al.*, 2012) with uncertainty bounds within the 5% - 95% range of 100 ensemble members (grey), NOAA corrected (red) and uncorrected (orange, Karl *et al.*, 2015), GISS (Blue, Hansen *et al.*, 2010) and Berkeley Earth (Green, Muller *et al.*, (2013)). b) Global averaged sea surface temperature from two datasets; HadSST3 (black line) with uncertainty calculated from 100 ensemble members (grey areas, Kennedy *et al.*, 2011) and adjusted/unadjusted SST data from NOAA (red and orange respectively, Karl *et al.*, 2015).

The unadjusted sea surface temperature record (SST) however is characterised by systematic errors associated with changes in observational methods over time (Kennedy, 2014, Kent *et al.*, 2017). The SST observations have sufficient coverage to create global SST datasets as far back as 1850 (e.g. Kennedy *et al.*, 2011) but observations were initially taken to improve understanding of ocean currents and to help improve ship navigation

(Maury, 1858, Rennell, 1832), rather than for the purpose of climate change studies. The nature of the observations has varied greatly over time as ships and technology have evolved, with Figure 1.2 demonstrating these changes (taken from Kent *et al.*, 2017).

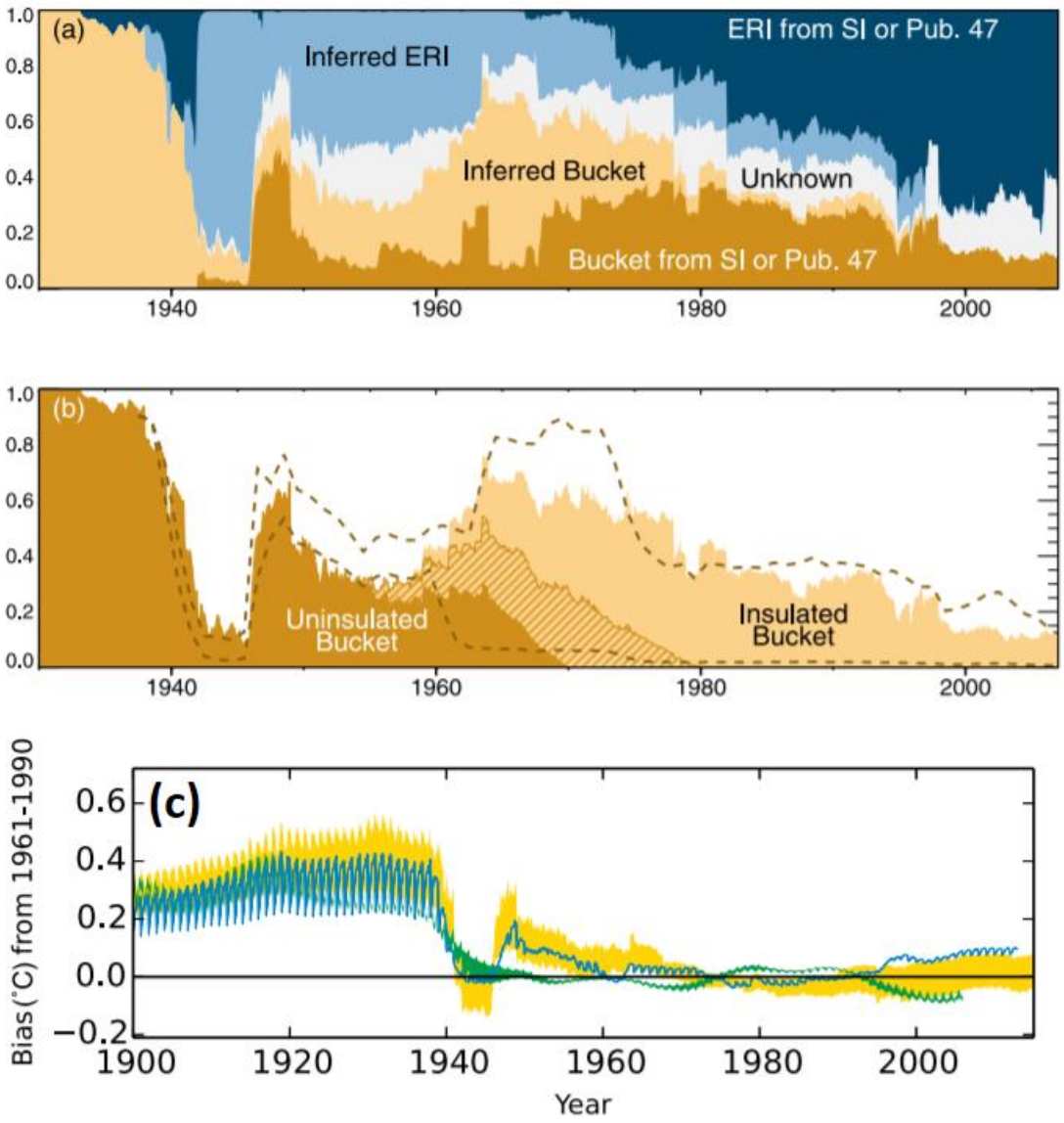

Figure 1.1: Time series of SST observation methods and biases. Panel (a) Measurement method of SST (each contribution expressed as a fraction of 1) from ships covering the period from 1930-2007 produced from results by Kennedy *et al.*, 2011. Darker shading indicates where the measurement method is taken from ICOADS whilst lighter shading indicates where metadata is taken from other sources. (b) As with (a) but showing the different types of bucket observations taken. Hatched areas represent uncertainty in the type of bucket assignment. Dashed lines represent estimates of measurement methods by Hirahara, Ishii and Fukuda, (2014) (c) Estimated bias adjustments to raw SST data based on the observation methods. Adjustments are shown for HadSST3 (yellow, Kennedy *et al.*, 2011), ERSSTv4 (green, Huang *et al.*, 2015) and COBE-SST2 (blue, Hirahara, Ishii and Fukuda, 2014).

Before World War II (WWII), buckets were the main source of SST measurement (Kennedy, 2014), these were initially wooden and well insulated. From the 1930s onwards, canvas buckets were more popular as increasing ship size and speed meant wooden buckets were at higher risk of breaking when hauled from the side of a ship. Canvas buckets however do not insulate as well as the wooden buckets (Folland and Parker, 1995). This is important because the water in buckets often lose heat to the atmosphere whilst being hauled onto the surface of the ship. This results in a cool bias in the unadjusted SST data, evident in Figures 1.1b and 1.2c. WWII meanwhile was dominated by Engine Room Intake measurements of SST (Figure 1.2a) which are generally biased warm whilst data from 1946-1980 contains a range of different methods. Since then the proportion of floating and drifting buoy measurements has increased until the present day to become the dominant source of SST observations (Kent *et al.*, 2017).

The changes in observation methods in Figures 1.2a and b led to the adjustments shown in Figure 1.2c but these adjustments are uncertain. The proportions of observations using these different methods remains an estimate during earlier years due to a lack of metadata (Carella, Kent and Berry, 2017; Kent *et al.*, 2017) so further study of biases in the SST record is needed. Further uncertainty in the SST bias adjustments comes from uncertainty in the weather conditions at the time of the SST measurement (Folland and Parker, 1995), the depth of the water sample (Donlon *et al.*, 2007) and uncertainty in ship positions (Carella, Kent and Berry, 2017). Uncertainties even in the 21st century have been the subject of much debate (e.g. Karl *et al.*, 2015; Cowtan, Rohde and Hausfather, 2018). The uncertainties still surrounding SST adjustments has therefore led to calls for further investigation of the SST record (Kennedy, 2014; Kent *et al.*, 2017).

Two main methods are presently used to estimate biases in the SST data. The first was by Folland and Parker, (1995) who developed numerical models for temperature change in bucket-derived temperatures to help identify bias adjustments needed with raw SST data. The second was by Smith and Reynolds, (2002) who compared the SST and marine air temperature (MAT) records to also understand when the SST record may require adjustments. Some problems are apparent with both of these studies however; the Smith and Reynolds, (2002) method requires MAT observations to be accurate to find the correct level of SST bias adjustment. Unfortunately, there are known biases in the MAT

record (Bottomley *et al.*, 1990; Kent *et al.*, 2013) and the two SST bias adjustment methods are not fully independent (Kent *et al.*, 2017). The study by Smith and Reynolds, (2002) also assumes that the differences between MAT and SST remain constant over time but certain factors besides biases can also affect the differences. Huang *et al.*, (2015) tested the assumption of constant MAT / SST differences over time and found evidence of the differences changing because land is warming faster than the oceans, which may influence MAT in regions where advection of air from land is common. Additionally, synoptic variations may also affect MAT/SST differences. Cold air outbreaks from the North American continent for example often move eastwards into the North Atlantic and this often encourages cyclogenesis as seen in the winter of 2013/14 (Huntingford *et al.*, 2014). This is because in such instances the MAT is much colder than the ocean below it as it is more directly influenced by variations in atmospheric circulation (Kent *et al.*, 2013) Finally, anomalous sea ice melting in the summer can cause SSTs to vary much more in regions that are usually covered. This was particularly evident in the summer of 2007 in the Arctic over Siberia as SSTs were often 3-5^{o}C above normal (Stroeve *et al.*, 2008). The high SSTs were the result of increased solar absorption over areas which are typically covered with sea ice (Steele, Ermold and Zhang, 2008). In periods when sea ice coverage is evident, SSTs are given a value of -1.8^{o}C as this tends to be the temperature in which sea water turns to ice (e.g. used to fill in ice fields by Kennedy *et al.*, (2011)).

Globally the small-scale (~ 1000km) differences between MAT and SST often cancel out, especially over annual timescales as shown by the HadNMAT2 time series comparison with SSTs (Figure 14, Kent *et al.*, (2013)). However, over some periods HadNMAT2 and SST comparisons did expose more potential unadjusted biases and these are discussed further in Section 1.3. Overall the Smith and Reynolds, (2002) method works well when looking at global data but due to differences that may arise in regions such as near the continental US, it does not work as well on smaller scales. The issues with these correction methods highlight the importance of studying MAT as well as SST, given how accurate time series of MAT are needed for providing the correct level of bias adjustment to SST. MAT is also an important climate variable in its own right so independent estimates are useful anyway (Bojinski *et al.*, 2014).

One way in which the MAT record can be improved is to understand what causes it to vary, the available literature suggests atmospheric circulation can be a key factor (e.g. Visbeck *et al.*, 2001; Kent *et al.*, 2013). Many studies have demonstrated connections between atmospheric circulation and temperature over land (e.g. Chen, 2000; Moberg *et al.*, 2003) but studies over the ocean are lacking. These studies have shown that atmospheric circulation can explain historic variations in air temperature well (*r* values occasionally over 0.80). Such studies show it can be possible to reduce the level of interannual variability in a temperature dataset and allow other influences to show more strongly.

The aim of this thesis is to develop quantitative relationships between atmospheric circulation and MAT anomalies to understand the contribution of variability in atmospheric circulation to the observed MAT variability. Isolating this contribution will enable other contributions to variability in observed MAT to be identified. These contributions might arise from biases in the data or the effects of secular climate change.

This chapter proceeds to first introduce the MAT temperature record in Section 1.1, going through the issues already known in its record and then showing comparisons made with SST in the literature and discussing where further adjustments may be required. Section 1.2 goes through the importance of Thompson *et al.*, (2008) study to this thesis which assumed a bias in SST after reducing noise in the data. Section 1.3 then introduces the main variable used to define atmospheric circulation in this study, sea level pressure (SLP). Then the literature describing connections between temperature and atmospheric circulation is discussed (Section 1.4). The final introductory section outlines the structure of the thesis (Section 1.5).

1.1 An introduction to the marine air temperature record

1.1.1 Available data and known issues

Marine air temperature data extend back to the 17th Century and are available from the International Comprehensive Ocean-Atmosphere Data Set (ICOADS, (Freeman *et al.*, 2017). The latest version is release 3.0 (Freeman *et al.*, 2017) but releases 2-2.5 are used in the data products taken for this thesis (Woodruff *et al.*, 2011). Release 3.0 does contain

an increase in coverage of MAT data from 1853-1868, World War I and data after 2000 (Figure 1.3), but release 2.5 is used in many gridded SLP datasets discussed in this thesis (Compo *et al.*, 2011; Poli *et al.*, 2016).

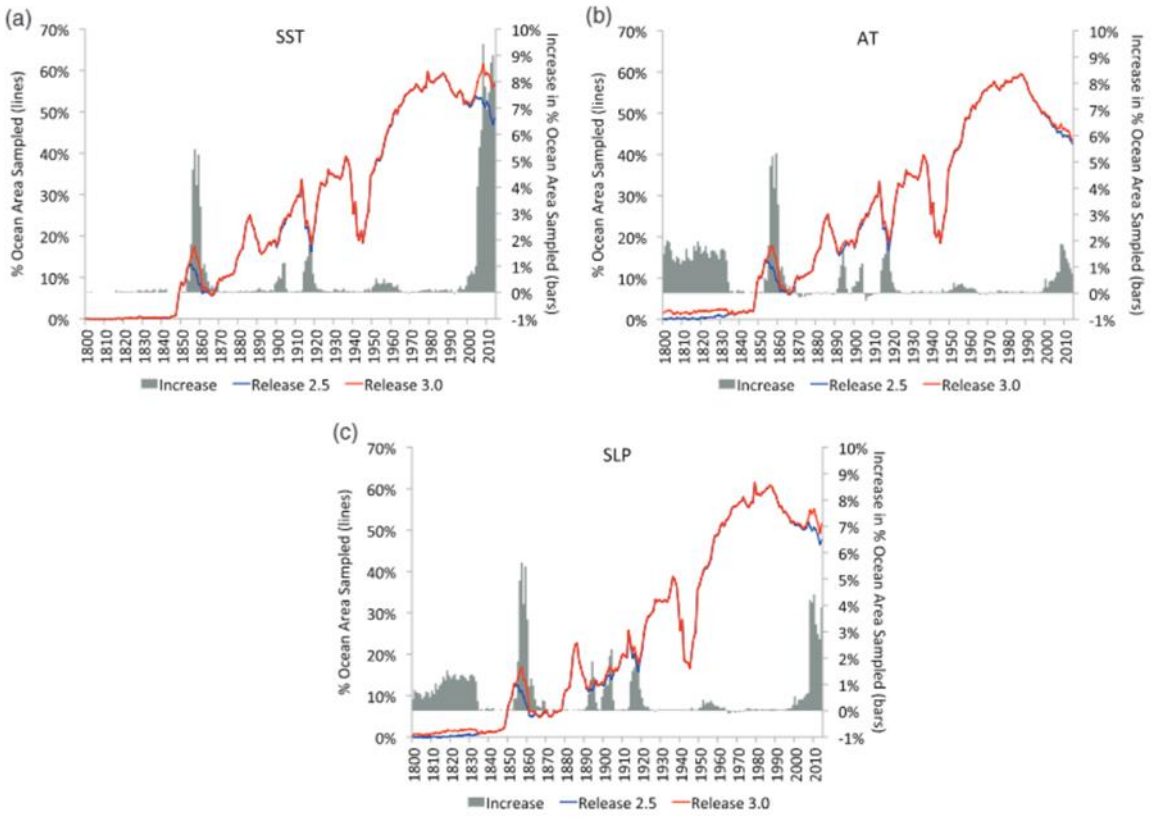

Figure 1.2. Annual percentage of global ocean and coastal area sampled for different meteorological variables. Panel (a) shows SST for ICOADS release 3.0 from 1800 onwards (red line) and ICOADS release 2.5 (blue line) as shown by Freeman *et al.*, (2017). The right axis and bars represent the percentage change of observations from ICOADS release 2.5 to 3.0 (b) same as (a) but for MAT (c) SLP.

The ICOADS data have been used to create gridded global datasets of MAT (e.g. Bottomley *et al.*, 1990; Kent *et al.*, 2013) but like SST, the MAT data in ICOADS requires adjustments to improve its accuracy. The early data up until ~1880 mostly consists of observations in the North Atlantic and there is evidence to suggest this data may be warm biased. Bottomley *et al.*, (1990) for example identified that MAT over the Atlantic Ocean up until 1885 was anomalously warm when compared to SST data at the same time. The reasons for this are not clear although Bottomley *et al.*, (1990) found that the differences between MAT and SST were largest when the winds were at their strongest. Bottomley *et*

al., (1990) indicated this may have been due to air temperature observations being taken inside the ship when the weather conditions were poor. Evidence of this was also found by Chenoweth, (2000) when examining earlier North Atlantic marine climate data from 1796-1843. To overcome this issue, Bottomley et al., (1990) adjusted MAT anomalies for each month so the long-term average equalled the monthly SST anomalies averaged over the period from 1856-1885. Due to the MAT issues of the mid-19th century, Kent *et al.*, (2013) developed their HadNMAT2 dataset to cover the 1880-2010 period only, stating more analysis is needed on MAT data prior to 1880.

There are also some MAT adjustments that are made on a global scale, daytime MAT observations for example are often warm biased because of solar heating of the ship superstructure. For HadNMAT2, Kent *et al.*, (2013) use MAT observations taken between an hour after sunset and an hour before sunrise. These hours were picked because it has been shown to be a period where the influence of solar heating is at a minimum (Parker, Folland and Jackson, 1995) Over time ships have also become larger which means the thermometer is often a greater height above sea level (ASL), leading to an increasing cool bias in unadjusted MAT over time. To overcome this issue, MAT is adjusted to a reference height of 10 metres ASL (Berry and Kent, 2011). A time series of estimated ship height is shown in Figure 1.4a (from Kent *et al.*, 2013) and this assumes that observation height increased slowly up to 1890. After the emergence of steam ships in the late 19th century however, ship size is estimated to have increased substantially (Bottomley *et al.*, 1990; Rayner *et al.*, 2003; Kent *et al.*, 2013).

In WWII there may have been a drop in the average observational height of MAT as ships that were lost in war were replaced with smaller ships (Kent *et al.*, 2013). From 1946 to 1969 ship height is assumed to increase linearly again before the availability of metadata became much more widespread during the 1970s (Kent, Woodruff and Berry, 2007). This means uncertainties in ship height are generally lower after the 1970s; before this time information on ship height is based on general descriptions of ships from the literature.

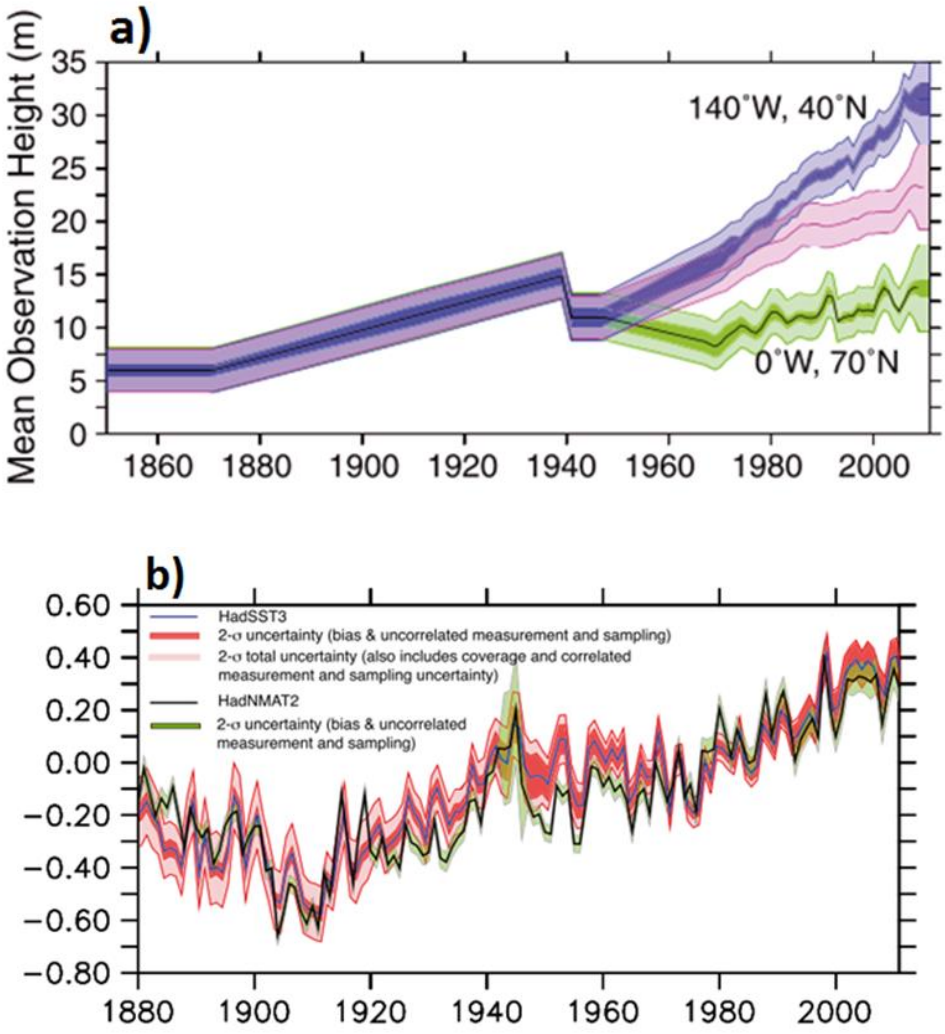

Figure 1.3. Time series of observational height and anomalies for HadNMAT2. Panel a) Annual mean of the observational height (solid lines) of the MAT data from 1850-2010 and uncertainties to 2 standard deviations represented by shaded areas. The global mean uncertainty is shown in pink, a region in the north Pacific with above average ship height in purple and a region in the North Atlantic with below average ship height in green. b) Global annual average timeseries of HadNMAT2 and HadSST3 mean anomalies (with respect to 1961-1990 average in ^{o}C) compared with each other. Uncertainties are represented by shaded areas (Kent *et al.*, 2013).

1.1.2 Comparing the MAT and SST records from 1880-2010

Despite the detailed study of the MAT record, further bias adjustments to the data may be required. Figure 1.4b shows a comparison between HadSST3 and HadNMAT2 from 1880-2010. Whilst both agree on a warming trend from the early 20th century to the present day, there are still discrepancies which appear separate to those highlighted in Section 1.1. Some small additional differences between HadNMAT2 and HadSST3 data are

expected, given the restriction of HadNMAT2 observations to night hours and the remaining uncertainties in ship height used for temperature adjustments. There are also some differences evident after the mid-1990s which Kent *et al.*, (2013) stated could be due to geographical differences in coverage as the HadSST3 and satellite measurements (Merchant *et al.*, 2014) are in strong agreement.

Other periods of larger differences between the marine temperature datasets however are more difficult to explain. From ~1930 to 1970 for example HadNMAT2 anomalies are consistently below the uncertainty bounds of HadSST3, especially for the period after WWII. A separate SST analysis by Cowtan, Rohde and Hausfather, (2018) also highlighted this discrepancy by examining a separate SST time series, created by comparing island and coastal station temperature data with different SST datasets. The comparison of this data with HadSST3 also indicated HadSST3 may have been too warm after WWII until the 1970s. Kent *et al.*, (2013) conclude that differences may be due to unresolved biases in either HadSST3 or HadNMAT2 and will require further investigation.

From the 1970s onwards metadata availability is far greater (Kent, Woodruff and Berry, 2007) and the level of agreement between SST and MAT is good. Differences before this period however highlight the need for further intercomparisons of MAT and SST to improve the marine climate record. The next section discusses a study by Thompson *et al.*, (2008) which demonstrates the potential of noise reduction of time series data to help identify these potential biases.

1.2 The potential for further validation of the MAT record

In order to provide further insight into the variability of SST since the 19th Century, Thompson *et al.*, (2008) took two climate indices which represent significant interannual variability in global temperature; the El Niño Southern Oscillation (ENSO) and the Cold Ocean Warm Land (COWL) index. ENSO is the single biggest source of interannual variability in GMST and typically fluctuates between an El Niño and La Niña state every 3-7 years. The period where an El Niño or La Niña event is at its strongest is typically around Christmas and both types of event have an impact on global climate. During an El Niño event ocean heat intake is reduced and as a result, global temperatures can rise

substantially relative to the expected average for the following year (seen with global temperatures during 1998 and 2016 following major El Niño's). The opposite pattern is seen during a La Niña (Yulaeva and Wallace, 1994). The COWL index meanwhile is strongly linked to temperature variability of the Northern hemisphere during winter (Wallace, Zhang and Renwick, 1995). The COWL index is most closely related to differences in temperature over the land and ocean during the winter. In the North Atlantic for example, if cold air outbreaks from Canada are frequently pouring over the North Atlantic, SSTs typically drop to around 1-2^{o}C below normal (Visbeck *et al.*, 2001). However, such a pattern is likely to encourage cyclogenesis, deeper low-pressure systems and as a result stronger westerly winds across parts of the northern hemisphere. These westerly winds usually carry mild Atlantic air over the whole of Europe and sometimes into Eurasia, producing temperature anomalies 5-10^{o}C above normal in some areas. This in turn also increases the GMST.

By identifying and removing the estimated influence of COWL and ENSO from GMST, a smoother variation in GMST should be seen over time. Numerous discontinuities in GMST are still evident despite this, most of which are associated with volcanic eruptions such as Pinatubo in 1991 (Soden *et al.*, 2002). However, a discontinuity is seen after 1945 that cannot be explained by any volcanic eruptions (Figure 1.5). When comparing the trends from LST to those from SST, Thompson *et al.*, (2008) found the discontinuity was only present in the SST record. This provided the rationale for another bias adjustment after WWII, which was attributed to the increase in use of rubber buckets by ships after WWII (Kennedy *et al.*, 2011). The SST data after WWII until the mid-1960s were therefore adjusted upwards in HadSST3.

Despite the results by Thompson *et al.*, (2008) some problems still remain. As Figures 1.1b and 1.4b show, there is still a difference between the SST and MAT datasets after WWII with HadSST3 (which bases its adjustments on models of heat loss from buckets) being most strongly influenced by the results from Thompson *et al.*, (2008). The scale of the upwards adjustments in HadSST3 is not backed up by other subsequent marine temperature datasets and an additional recent analysis by Cowtan, Rohde and Hausfather, (2018) also indicates HadSST3 data after WWII may be too warm. The SST

anomalies based on coastal temperature data supports the results from NOAA's ERSST product (Huang *et al.*, 2017) rather than the HadSST3 time series.

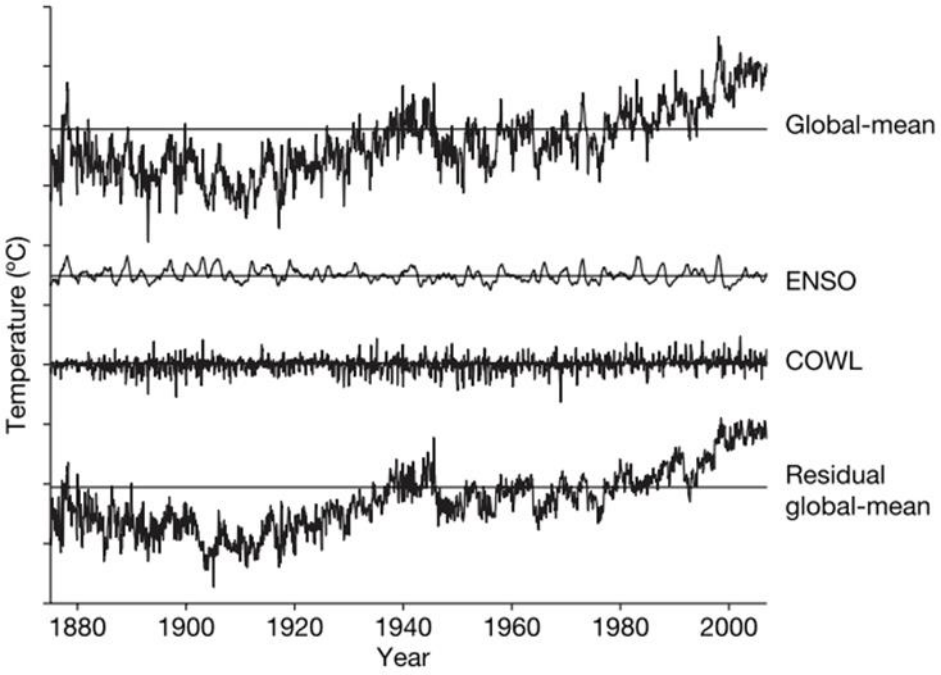

Figure 1.4: Contribution of COWL and ENSO to global temperature. From top to bottom: Time series of monthly global mean temperature from HadCRUT3 combining SST and LST data; the estimated contribution of ENSO to global temperature variability; the contribution of COWL to monthly global temperature variability; the residual global monthly mean temperature series once the estimated influences of ENSO and COWL have been removed. Horizontal lines represent the 1961-1990 monthly mean global temperature. The vertical axis represents global temperature anomalies with tick marks indicating steps of 0.5°C (Thompson *et al.*, 2008).

The method used by Thompson *et al.*, (2008) to identify a potential SST bias was based on atmospheric circulation. COWL is closely tied to the Arctic Oscillation which is an expression of the frequency of mid latitude cold air outbreaks from the arctic using variations in SLP over the Arctic (Wallace, Zhang and Renwick, 1995). ENSO meanwhile can be estimated by using the differences in SLP between Tahiti and Darwin (Ropelewski and Halpert, 1987). Their method though is based on global indices of atmospheric circulation, so what can be found when the role of atmospheric circulation on marine climate is explored in much more detail? Is there a further reduction of interannual variability in the data? Interesting results were found by the Thompson *et al.*, (2008)

study, despite the focus on SST rather than MAT and it's this study that provides the motivation for this thesis. The next section describes the independent variable used in this thesis, SLP.

1.3 Introduction to SLP observations and available datasets

Sea level pressure has been recorded since the early 17th century with Blaise Pascal being the first to recognise that pressure decreases with altitude. Later in the 1660s, Robert Hooke used the barometer to forecast the weather as he noticed unsettled conditions frequently occurred with low pressure and settled conditions with high pressure. The earliest observers sparked much research into the barometer and its potential to help understand the weather (Golinksi, 2007). With this research the level of knowledge about potential errors and bias adjustments grew. Even in the mid-17th century, the observations by philosophers were regarded to be highly accurate and were used to create daily series of SLP over London and Paris from 1670-2007 (Cornes *et al.*, 2012). Schmith *et al.*, (1997) concluded in their review of European SLP data that the level of error is lower than for other climate variables.

There are still biases in SLP data that must be accounted for however and these are particularly problematic in areas where SLP does not vary much (such as the tropics). Most of the earliest SLP observations were taken using a mercury barometer (Schmith *et al.*, 1997) with expansion of the mercury being sensitive to temperature changes so a reference value of 0^{o}C is used for correcting SLP observations (WMO, 1983).

Temperature based adjustments of SLP from mercury barometers are therefore much greater in warmer areas of the world. It is important to know whether adjustments for temperature have been made but despite this some biases relating to temperature have only recently been found. Early observations from the US and Germany Maury collections (ship data from 1853 to the mid-1860s) were found to have biases, believed to be due to mercury barometer observations being uncorrected for temperature in some areas (Wallbrink, Koek and Brandsma, 2009). Aneroid barometers were developed later in the 19th century which do not need to be corrected for temperature, but the timing of the transition from mercury to aneroid barometer usage in ships is uncertain in some regions.

In contrast some land stations document the changes in barometer equipment used over time in detail (e.g. the meteorological logbooks at Greenwich, http://www.geomag.bgs.ac.uk/data_service/data/yearbooks/grw.html). SLP observations should also be adjusted to account for the changes in gravity between the equator and the poles (Smith and Reynolds, 2004), with the value at 45˚ latitude being used as a reference (Basnett and Parker, 1997), requiring adjustment of - 2.6/+2.6mb at the equator/poles respectively. It is unclear however whether such adjustments have been made in some marine SLP data sources (Allan and Ansell, 2006). Other unknown errors in SLP may be present even with the most used time series of SLP data. Jones, Jonsson and Wheeler, (1997) for example analysed the SLP time series at Gibraltar and Iceland and concluded that data before the 1860s in Gibraltar was less reliable. A later analysis by Vinther *et al.*, (2003) compared nearby SLP in Cadiz and San Fernando to that in Gibraltar and concluded errors in SLP of around 4mb in the Gibraltar time series before the 1870s due to issues with the barometer.

Such biases will introduce uncertainties in the SLP data but there are also fewer observations in earlier years, especially over the oceans. Like MAT, SLP is prone to high frequency daily fluctuations meaning the missing daily data can have a notable impact on the monthly mean. It is also unclear as to the level of care taken with the marine observations, or the height in which they were taken, though pressure on voluntary observing ships is likely to be adjusted to sea level (Freeman *et al.*, 2017). For these reasons gridded datasets of SLP are likely to be less accurate during earlier years.

Compo, Whitaker and Sardeshmukh, (2006) evaluated the accuracy of SLP fields from a weather model when modern SLP data was subsampled to the level of coverage seen in the 1890s. Uncertainties were high in the southern hemisphere but results were more promising in the Northern hemisphere. This led to the 20th Century Reanalysis (20CR, Compo *et al.*, 2011) which consists of a globally complete gridded SLP dataset based on output from a weather model, with SST and sea ice concentration used as boundary conditions and assimilation of SLP observation (described further in Chapter 2). The analysis originally covered the 1871-2008 period but has now been extended to cover the period from 1851-2014 (Compo, 2014). However, reanalysis products can have numerous issues when going back further in time (Thorne and Vose, 2010), a concern when

numerous studies are looking at long range climate variability from this dataset without fully considering the uncertainties involved (e.g. Johnstone and Mantua, 2014; Peña-Angulo *et al.*, 2016).

Recent studies of the 20CR SLP output highlight the need for caution when using the product. Jones, Harpham and Lister (2016) for example found an abrupt change in the atmospheric circulation variability in the Falkland Islands region from the opening of the Panama canal (1914) to the 1970s, attributed to changes in numbers of nearby daily SLP observations assimilated into the 20CR. SLP biases in the 20CR have also been reported in the Arctic (Przybylak *et al.*, 2013) and also across Eastern Europe as recently as the 1960s (Stryhal and Huth, 2017). Even in areas such as the Southern USA where levels of daily SLP coverage are high, discontinuities (step changes in a time series of a variable) in 20CR air temperature have been found in the 1930s (Ferguson and Villarini, 2012).

Ferguson and Villarini, (2014) subsequently expanded the Southern US analysis across the world with a map of SLP discontinuities shown in Figure 1.6. The reanalysis showed little in the way of discontinuities in the North Atlantic during the DJF (December, January, February) period which is encouraging given marine data can be lacking in this basin during earlier years. In the North Pacific discontinuities are apparent up until the 1910s, whereas in the Southern Ocean, discontinuities can occur up until the 1970s. Discontinuities in the winter are less common then in summer however and the discontinuity reported earlier by Ferguson and Villarini, (2012) over the southern/central US was also limited to the summer months only.

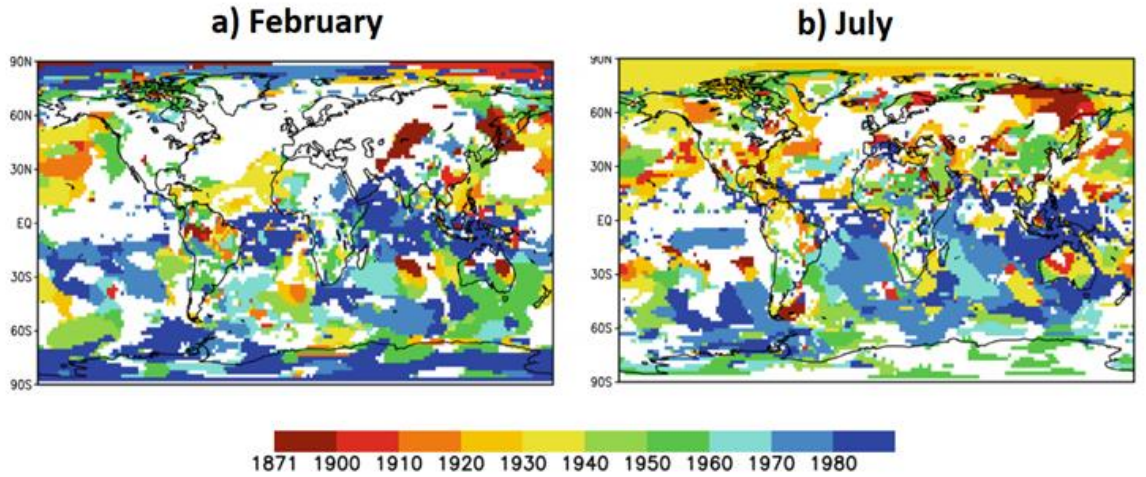

Figure 1.5: Maps of the most recent decade of detected discontinuities in SLP data in the 20CR. Discontinuities are represented by sudden changes in mean SLP and increases in the ensemble spread of the 20CR (Ferguson and Villarini, 2014). Plots are shown for February (a) and July (b).

The issues in the 20CR highlight the importance of comparisons between different SLP products (Trenberth and Paolino, 1980; Jones *et al.*, 1999; Allan and Ansell, 2006; Poli *et al.*, 2016). The ERA-20C is developed using a different reanalysis model and also assimilates surface winds from the oceans (Poli *et al.*, 2016). HadSLP2 meanwhile takes monthly mean SLP values to build its gridded SLP product. Numerous stations used in HadSLP2 are not assimilated into the 20CR as this requires timescales of a daily resolution to be used (Allan, pers. comm.). Some monthly SLP stations used in HadSLP2 therefore may not be used in the 20CR.

The literature indicates fewer sources of error in SLP observations compared to other meteorological variables though some errors may occur in earlier years (Schmith *et al.*, 1997) and the sizes of such errors are important, especially in tropical areas where SLP variations are smaller. Numerous SLP products are available however to compare with the 20CR and it is important these are used to validate any results based on 20CR data.

1.4 Connections between temperature and atmospheric circulation

Atmospheric circulation is a key influence on local climate and has been associated with variations in past air temperature over numerous locations. In addition to air temperature, links have been found with rainfall and cloud cover (Osborn and Jones, 2000; Moberg *et al.*, 2003; Wilby and Quinn, 2013). Variations in atmospheric circulation itself has been linked to climate change, ocean circulation and volcanic eruptions (Robock, 2000; Gillett *et al.*, 2003; Alexander, Halimeda Kilbourne and Nye, 2014). Therefore, atmospheric circulation is a useful indicator of past variability.

Despite its importance, little research has explored the extent to which atmospheric circulation can explain past variations in MAT. Many studies have at least shown there are connections between atmospheric circulation and MAT or SST over different ocean basins (Visbeck *et al.*, 2001; Johnstone and Mantua, 2014; Cortesi *et al.*, 2018) although many have looked at relationships with respect to SLP gradients between two stations.

Two examples would be the SLP gradient between Iceland and Gibraltar (a definition of the North Atlantic Oscillation (NAO, Jones, Jonsson and Wheeler, 1997)) and that between Tahiti and Darwin (the Southern Oscillation Index (SOI)). These approaches can have their limitations, the NAO for example only has a strong influence on climate across the North Atlantic during November to March (Hurrell, 1995). Relationships between temperature and atmospheric circulation can change throughout the year (e.g. the NAO, Folland *et al.*, (2009)) so more detailed approaches to defining atmospheric circulation parameters than the NAO may be required in certain areas.

One potential alternative is to focus on small-scale atmospheric circulation variability, which can be achieved by defining atmospheric circulation parameters such as flow direction, strength or shear from the SLP data (e.g. Jones, Harpham and Briffa, (2012), abbreviated from here as J12). Several studies focusing on smaller scale atmospheric circulation patterns have demonstrated that there are relationships between temperature and atmospheric circulation throughout the year (e.g. Chen, 2000; Osborn and Jones, 2000; Moberg *et al.*, 2003; Jones *et al.*, 2014; Peña-Angulo *et al.*, 2016). These relationships have been used to predict temperatures from the observed atmospheric circulation patterns (Circulation Based Temperature Anomalies – CBTA) as far back as the

18th Century in Europe (Moberg *et al.*, 2003; Beck, Jacobeit and Jones, 2006). Two different methods were used in these studies to relate atmospheric circulation variability and temperature. Jones *et al.*, (2014) opted for a binning-based approach to identify connections between Central England Temperature (CET) and atmospheric circulation, whilst others have identified connections using regression methods (Chen, 2000; Osborn and Jones, 2000; Moberg *et al.*, 2003).

Both methods can create long time series of CBTAs to give an estimate of the contribution of atmospheric circulation to the observed temperature variability. If this estimated signal is identified other influences on temperature variability can be highlighted, such as climate change or potential observational biases (Osborn and Jones, 2000; Moberg *et al.*, 2003). Moberg et al., (2003) for example identified a strong relationship between Southern Sweden June-August air temperature and atmospheric circulation. Removing the estimated influence of atmospheric circulation on air temperature revealed a positive bias before the 1870s, which was attributed to exposure of thermometers to solar radiation.

Studies exploring the connections between temperature and small-scale atmospheric circulation however have mostly focused on Europe and other land regions, although Cortesi et al., (2018) did look at the oceans. In the study by Cortesi et al., (2018), the link between weather types (classification of weather patterns, e.g. Lamb, 1972) and 20CR MAT were explored. Some patterns similar to those over land were seen, with northerlies in the northern hemisphere for example coinciding with colder than average temperatures throughout the year. The extent to which atmospheric circulation influenced past temperature variability however was not explored and the weather types used involved the categorisation of data which has its disadvantages as there could be important variations of atmospheric circulation within a category itself. Additionally, this analysis only looked at fields from ERA interim from 1979-2010 (Dee *et al.*, 2011). The analysis was also restricted to daily data, whereas most observational marine temperature datasets are at a monthly time resolution (e.g. Kent et al., 2013, Kennedy et al., 2011).

There are also indications that climate change may be influencing the way in which temperature responds to certain atmospheric circulation patterns (Osborn and Jones, 2000; Van Oldenborgh and Van Ulden, 2003) or alternatively that SLP patterns may be changing as a result of climate change (Gillett et al., 2003). Figure 1.7 shows the global trend in SLP, with the trend over Europe during the DJF period since the 1950s being particularly notable. DJF temperatures across Europe have risen rapidly since the 1980s and this is likely to be due to increased south-westerly winds across much of Europe, advecting warm air from the North Atlantic over Europe.

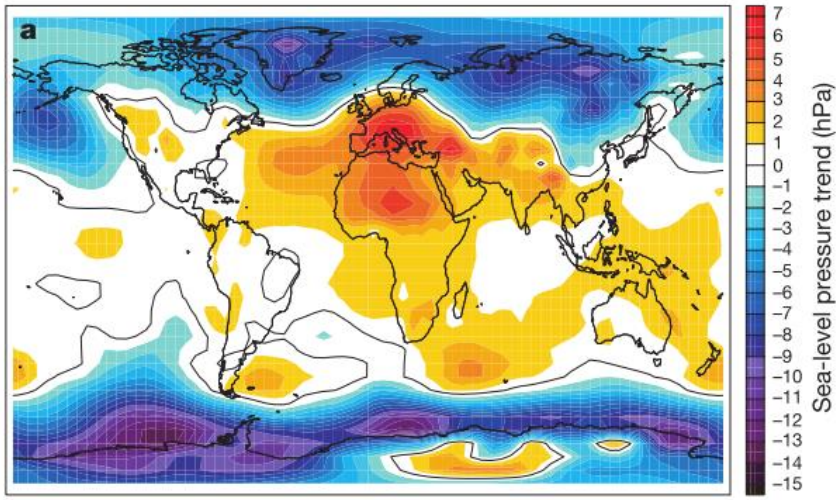

Figure 1.6: December to February (DJF) SLP trends in SLP (mb) in the NCEP reanalysis (Kalnay et al., 1996), over the period 1948-1998 (Gillett et al., 2003).

Can the changes in SLP shown in Figure 1.7 explain the temperature changes seen outside of Europe and during other seasons? The study by Gillett et al., (2003) suggests that, in some areas at least, increases in temperature are also occurring alongside changes in atmospheric circulation patterns.

The literature suggests atmospheric circulation could provide an insight into the MAT record, especially if relationships between MAT and atmospheric circulation are strong. SLP observational errors are independent of those in MAT and SST, though there is evidence to suggest that in some weather models SLP can be influenced by SST, especially in the tropics (Kushnir *et al.*, 2002). If this is the case then some errors associated with SST may affect the SLP in reanalysis products.

Most studies investigating the impact of atmospheric circulation on climate variables have been confined to Europe where the greatest amount of meteorological data is available (J12). However, with the development of the 20th Century Reanalysis (20CR: Compo et al., 2011) and other gridded SLP products, (HadSLP2: Allen and Ansell, 2006), global SLP fields have become available for analysis over long time scales and can be used to improve our understanding of small-scale atmospheric circulation variability. Studies using the 20CR have begun to look outside Europe and have focused on the Falkland Islands (Jones, Harpham and Lister, 2016), Russia (Spellman, 2017) and Mexico (Pérez *et al.*, 2014). However, few studies have taken advantage of all the SLP data becoming available over the oceans to understand past marine climate at this time of writing, this thesis will address that gap.

1.5 Summary and thesis structure

A literature review was carried out to produce a rationale for the research in this thesis. The main findings are as follows:

- There are large systematic biases in raw SST data which require correction. MAT plays an important role in calculating the extent of these corrections which help produce datasets of GMST.

- MAT has its own biases though which need to be understood to assist bias corrections in the SST record.

- Atmospheric circulation was highlighted as a useful source of intercomparison with land air temperature, but not so much is known over the oceans.

- The 20CR is being used to study historic variations in atmospheric circulation but some studies have expressed concerns over the quality of SLP in earlier years. Issues with gridded SLP datasets in earlier years mean comparisons with station data would be useful.

- The extent to which climate change affects relationships between temperature and atmospheric circulation requires further understanding, especially over the oceans.

The aims of this thesis are to:

1) Develop a method which can define atmospheric circulation parameters with gridded or station SLP data over any of the world's oceans (Chapters 2 and 5).
2) Develop suitable uncertainty estimates for the CBTAs (Chapter 3).
3) Use these circulation parameters to estimate the circulation-dependent contribution to MAT variability over all of the world's oceans using the 20CR. (Chapters 2-4).
4) Analyse whether the CBTAs could potentially identify biases in MAT over the course of its record or other influences (Chapters 4 and 5).
5) Compare the 20CR CBTAs to those based upon other SLP and temperature datasets to further assess the quality of the 20CR reanalysis product (Chapter 5).

The structure of the work is as follows. Chapter 2 looks at different ways of linking atmospheric circulation to variations in MAT and determines which approach may be best, with an initial focus at a point in the North Sea. Chapter 3 then discusses in more detail the choices made with the method chosen in Chapter 2 and how the uncertainties are calculated. Chapter 4 then applies the method globally using 20CR fields and discusses connections between temperature and atmospheric circulation over different ocean basins. It also provides insight into the contribution of atmospheric circulation to past MAT variability. Chapter 5 then analyses the MAT data further looking at differences with SST, coastal air temperature, Central England temperature (Parker et al., 1992) and HadNMAT2. The quality of the SLP data is assessed by comparing CBTAs derived from 20CR SLP data with that from ERA-20C and station SLP data. This chapter aims to clarify the results in Chapter 4 and show that the method of defining atmospheric circulation parameters is not dependent on gridded SLP data. Chapter 6 discusses the results, outlines the potential for further improvements and draws conclusions.

Chapter 2 Producing circulation-based temperature anomalies

In this chapter, the two methods used to predict MAT are introduced. These predictions are then used to produce an example time series of MAT based on atmospheric circulation patterns at a point in the North Sea. This time series is then compared to the anomalies from 20CR MAT over the same location. The advantages and disadvantages of each method at the North Sea point are discussed.

2.1 Introduction

In the previous section, a potential additional insight into the marine climate record was hypothesised by using atmospheric circulation patterns to predict past variations in MAT. However, when performing such analyses over the oceans, some additional challenges compared to the land series used in previous studies are present. First is the issue of potential biases and changing coverage of MAT (discussed in Section 1.2). Previous studies that have generated time series of CBTAs selected well-sampled cases. Osborn and Jones, (2000) for example used the daily CET time series from 1880-2000, one of the most accurate and longest temperature series in the world (Parker, Legg and Folland, 1992). MAT on the other hand declines in coverage before the 1970s in the southern oceans and biases are believed to exist in earlier years (Kent et al., 2013). For this reason, the thesis mainly focuses on developing a model from relationships between temperature and atmospheric circulation from 1971-2010. This is because it represents a period where confidence in MAT estimates are high. For reanalysis products a longer period can be used but there are still issues with SST in earlier years, and this is used as a boundary condition in the 20CR (Compo et al., 2011).

One of the aims of this thesis is to assess the quality of the 20CR SLP by comparing results with station SLP data but there are numerous data sources only available at a monthly time resolution. Previous studies looking into connections between temperature and atmospheric circulation have focused on daily data. Jones et al., (2014) for example created CBTAs over the Central England region using daily CET data from 1871-2012, a

total of over 10,000 individual data points. This thesis is developing relationships between temperature and atmospheric circulation for each month of the year meaning any relationships developed between atmospheric circulation and MAT are based on a small number of months. Steps can be taken to deal with the small sample sizes however with more details given in Section 2.3.1.

If atmospheric circulation parameters are to be calculated without reliance on gridded SLP data, the methods from existing literature need to be simplified. The most common method used to define atmospheric circulation parameters is that used by J12. This method uses a defined grid of 16 points of SLP to define atmospheric circulation parameters which is not readily applicable to station SLP data, especially in earlier years. The method requires gridded SLP data rather than irregularly distributed points of SLP from individual stations. In this chapter, simpler ways of defining atmospheric circulation parameters are therefore discussed to try and develop a method which can work well with both station and gridded SLP data.

Finally, the atmospheric circulation parameters developed by J12 were originally developed to identify North Sea Storms or predict rainfall (El Dessouky and Jenkinson, 1975; Jenkinson and Collison, 1977). Therefore, it is uncertain whether the flow parameters used by J12 are also the best for predicting monthly temperature. With these issues identified, the following questions are posed:

1) Are there strong connections between atmospheric circulation and North Sea MAT?
2) Are the flow parameters defined by J12 the best for developing CBTAs and predicting monthly MAT at this location?
3) How much can current methods used to define atmospheric circulation parameters be simplified?

Section 2.2 introduces two different SLP grid configurations used to calculate atmospheric circulation parameters and compares the results to those developed by J12. Section 2.3 then introduces the method used to develop the CBTAs, based on flow parameters developed in Section 2.2. Section 2.3 also introduces the stepwise regression method also used to predict past MAT and will be used as a comparator to the prediction method from

flow parameters. Section 2.4 presents time series of CBTAs at the North Sea point which are compared with 20CR MAT anomalies from 1881-2010 and with the results of different methods used to develop the CBTAs. Some conclusions of the chapter are then provided in Section 2.5.

2.2 Defining atmospheric circulation parameters

2.2.1 Data sources used in this chapter

The data used in this chapter is from the 20CR which is a model-based atmospheric reanalysis with limited observational input from SLP, SST and sea ice (Compo et al., 2011). The 20CR version 2c used here is available at 4 times daily, 2^{o} grid resolution from 1851-2014 (Compo, 2014). Observations of SLP over land are from the International Surface Pressure Databank version 3 (Cram *et al.*, 2015) whilst marine SLP observations are from the ICOADS (Release 2, Woodruff et al., 2011). SST fields are from the Simple Ocean Data Assimilation (Giese and Ray, 2011) along with sea ice concentration estimates from the COBE-SST2 dataset (Hirahara et al., 2014).

SLP observations are integrated into the forecasting model through data assimilation. During the data assimilation process, uncertainties in the observations and model fields of SLP are accounted for and the resulting SLP field is the most consistent combination of model and data given the estimated uncertainties. SST and sea ice meanwhile are imposed boundary conditions and are not changed by the model (Compo et al., 2011).

Once assimilation is complete, the model provides an estimate of the atmospheric state, used as the initial condition for the next 6 hourly time steps. Assimilation of SLP brings this new model estimate closer to the observations, attempting to correct for model error and bias and then the process is repeated for the next time step. Uncertainty estimates are available for all the meteorological variables in the 20CR which are based on the standard deviation of 52 ensemble members (Compo et al., 2011) each with different initial conditions. 20CR MAT is derived from the reanalysis model and is estimated at the height of 2 metres, using model values, including SST, to estimate the effects of atmospheric stability on near surface temperature gradients. A climatological average is calculated for each of these days using data from a 40-year period (1971-2010), to create

an annual cycle. The difference of each value from the climatological average annual cycle determines the temperature anomaly at each time step. Both SLP and MAT anomalies are converted into 30 day running means to improve the calculation of the CBTA fields (discussed further in Section 2.3.1).

2.2.2 Calculating flow parameters with different grid configurations

The flow parameters defined by the J12 method are flow direction, shear and strength. These variables are calculated using SLP gradients because air generally flows parallel to isobars. Air should move straight from high pressure to low pressure but the Coriolis effect deflects air to the right in the Northern Hemisphere and to the left in the southern hemisphere (Wallace and Hobbs, 2006). Flow parameters calculated from SLP gradients therefore are a good proxy for the source of an airmass. The grid pattern of the J12 method is shown in Figure 2.1 with SLP extracted at each of the 16 points. The calculations involving this method are shown in Section A of the Appendix.

The J12 method is a popular approach for defining atmospheric circulation because it can be applied anywhere except near the poles and around the equator. It has been used in the research field of synoptic climatology (Jones, Hulme and Briffa, 1993) predicting rainfall and flood events (Wilby and Quinn, 2013) and the downscaling of weather models (Conway, Wilby and Jones, 1996). However, it has rarely been used for predicting past temperature anomalies, only to highlight there are relationships between atmospheric circulation and temperature.

Other methods of defining atmospheric circulation patterns have been used (e.g. James, 2007; Philipp *et al.*, 2010) but some of these refer to specific synoptic features at certain locations (such as the Scandinavian high) and cannot be applied so readily elsewhere (James, 2007), or they rely on even more points than the J12 method. In this section it is argued that the J12 method can be reduced to fewer than 16 points.

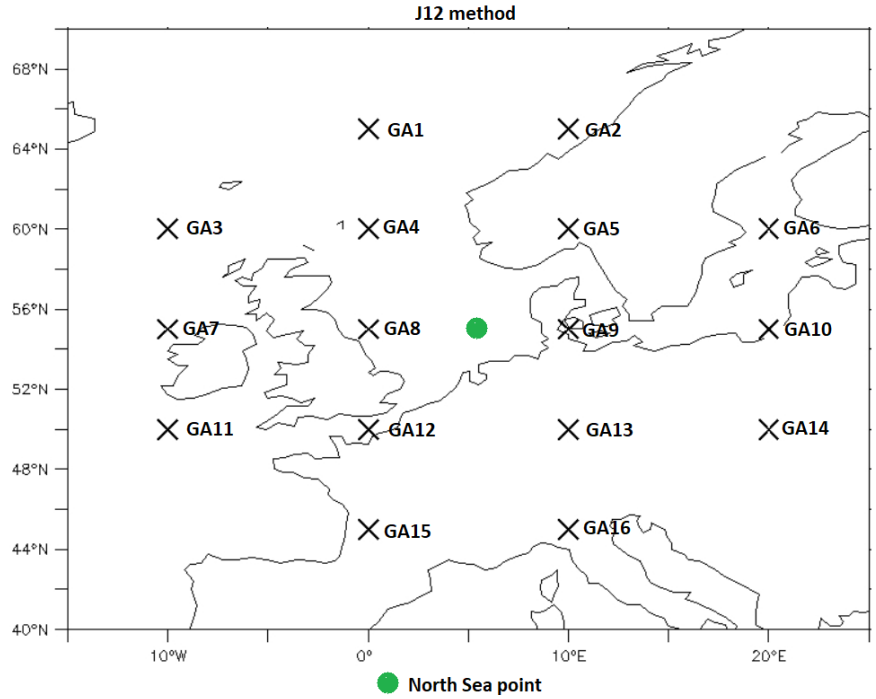

Figure 2.1: Locations of points where SLP is extracted from the 20CR reanalysis for the method developed by J12.

The first step was to verify the calculations of flow parameters made in this thesis. A FORTRAN routine was set up to calculate flow parameters using the J12 method and compare the results to those from the J12 study over the Northern area of the UK (available at: https://crudata.uea.ac.uk/cru/data/lwt/static_files/20CR_1871-2010_00hrs_UK.dat). This location meant some points of SLP between the 20CR grid locations required bilinear interpolation. All flow parameters at this location were reproduced consistent with rounding of the output reported by J12.

Some changes to the J12 approach were then made. Firstly, the number of points used to define atmospheric circulation patterns is reduced, an example of two of the six generalised grid configurations used in this thesis is shown in Figure 2.2. The calculation of the westerly and southerly flow components is similar to J12 and outlined in Appendix A.

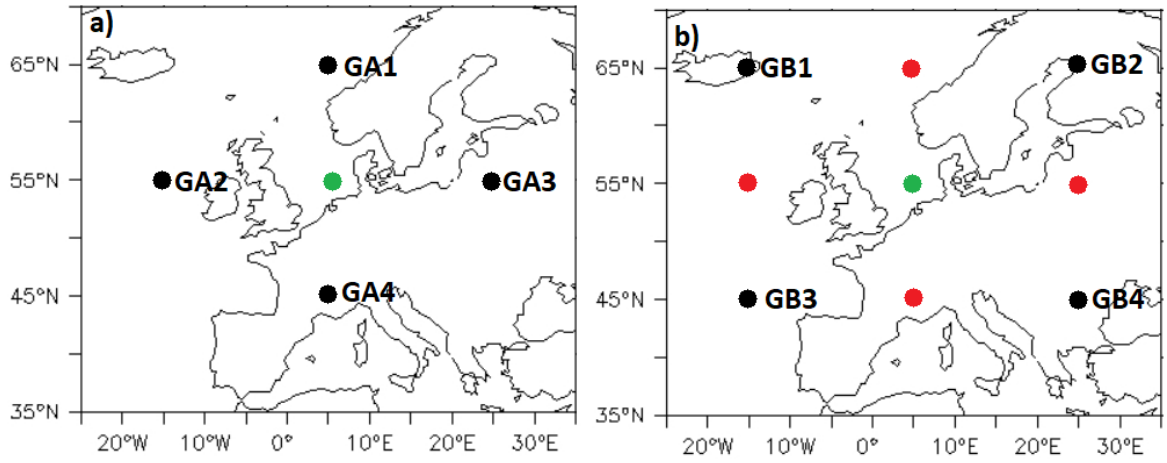

Figure 2.2: The grid configurations used to define atmospheric circulation parameters in this chapter. SLP is not extracted from the North Sea point shown in green. Red points represent interpolated SLP values.

J12 use a weighting to account for differences in distances between lines of longitude with changing latitude. Lines of longitude are closer together in terms of absolute distances towards the poles and furthest at the equator. The weighting calculation used by J12 only works for two points that are at the same latitude (e.g. the southerly flow calculation for the J12 method shown in Appendix A). The haversine formula (Inman, 1835) is therefore used to calculate the distance between two points in kilometres. This method can be applied to calculate weightings for a SLP gradient even if the two points are at different longitudes and latitudes.

Additionally, the shear calculations from J12 are not used to develop the CBTAs in this thesis with the average SLP value across the 4 points being used instead. Other studies defining atmospheric circulation types have done this, such as the Lynetski weather type catalogue for Eastern Europe (Philipp et al., 2010). A comparison with the calculated flow shear and SLP values shows the two are strongly correlated. Figure 2.3 shows a point at the North Sea only but Figure A3 in the appendix shows that this pattern is evident throughout the Extra tropics. The scatterplot in Figure 2.3a shows the strongest correlation out of the two panels because this is taking the SLP from the North Sea point itself (green dot in Figure 2.2). Figure 2.3b uses the average SLP from the 4 grid points in Figure 2.2a. Although the correlation coefficient is lower (to be expected when

considering large scale averages), it was still higher than the other attempts used to try and estimate the flow shear itself.

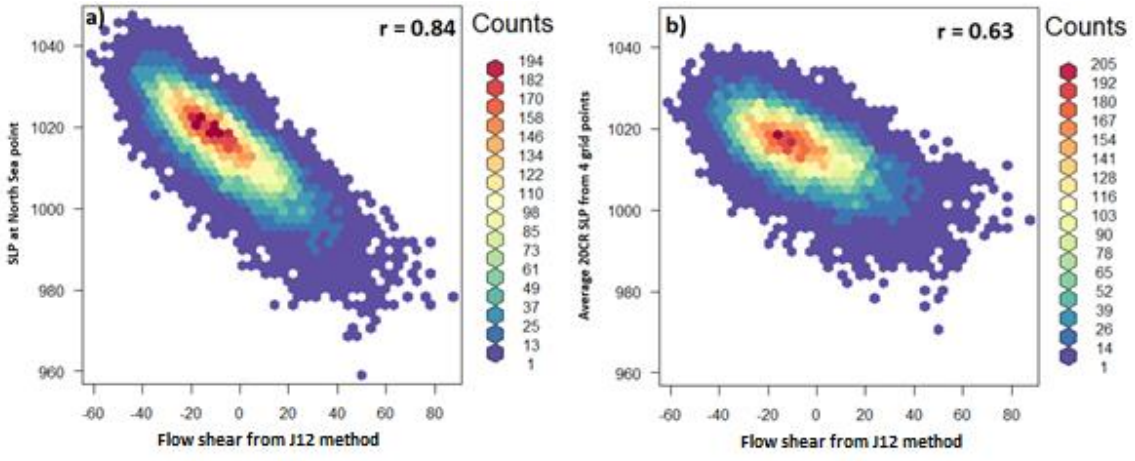

Figure 2.3: Scatterplots of the SLP (in millibars) and total flow shear (also in millibars) from the J12 method (x axis) and; a) SLP extracted at the North Sea point (y axis); b) SLP extracted at the 16 points used in the J12 grid configuration. Scatterplots consist of daily data from 1971-2010.

To generate the atmospheric circulation parameters from the grid configuration in Figure 2.2a, the average SLP value and the North/South and East/West SLP gradients are also taken. The haversine formula (Inman, 1835) is used to calculate the distances between the points used in the SLP gradients. The calculations are as follows:

$$a = sin^2(\varphi B - \varphi A/2) + cos\,\varphi A * cos\,\varphi B * sin^2(\lambda B - \lambda A/2)$$

$$b = 2 * asin(\sqrt{a})$$

$$\Delta n = b * R \quad (2.1)$$

Where φB and φA represent the two different latitudes and λA and λB the two different longitudes. Δn is the total distance between two geographical points in kilometres. All angles are expressed as radians whilst R is the earth's radius of 6371km. Using these distances, the geostrophic wind can be calculated. Geostrophic motion assumes air moves parallel to isobars and no other forces such as friction and vertical motion are at play. The magnitude of the geostrophic wind can be calculated as follows:

$$Vg = \frac{\Delta P}{\Delta n} \quad (2.2)$$

Where:

Vg = Pressure gradient [in millibars per kilometre]

Δ*P* = Sea level pressure difference [in millibars]

Δ*n* = Distance between two points [in kilometres]

A final calculation converts to a flow strength in ms^{-1}:

$$Flow\ strength\ (ms^{-1}) = \frac{\mathrm{Vg}}{\rho * 2\Omega * sin\varphi} \quad (2.3)$$

Where:

Ω = Earth rotation speed [7.272 x 10^{-5} radians per second]

ρ = Density of the air [kg/m^3]

Vg = Pressure gradient [in millibars per kilometre]

For Figure 2.2b the same calculations are applied but SLP is interpolated at the 4 red points before calculating westerly and southerly flow components. The flow direction and strength values can be estimated anywhere using these calculations away from the equator or the North and South Poles. The approach is generalised and can be used for grid configurations with 4 points as long as they contain a reasonable range of both latitudes and longitudes as demonstrated in Chapter 5.

In order to test whether a reduced number of points compared to the J12 approach can be taken, this chapter compared the flow parameter values from J12 with those used in this thesis. The results are shown in Figure 2.4. Panel (a) shows a scatterplot of the two westerly flow components which are very strongly correlated (r = 0.99) from the grid configuration in Figure 2.2a. The southerly flow components are also strongly correlated (r = 0.97, panel b), meaning that flow direction (except when a flow is very weak) and strength are also very highly correlated (calculations shown in Appendix Section A). For the grid configuration in Figure 2.2b, westerly flow estimates are strongly correlated (r > 0.9, Figure 2.4c), whereas correlations for southerly flow are slightly weaker. There is

some deviation in the scatterplots from the 1-1 line but these are likely to be minor differences related to grid spacing and the level of interpolation required for the three methods.

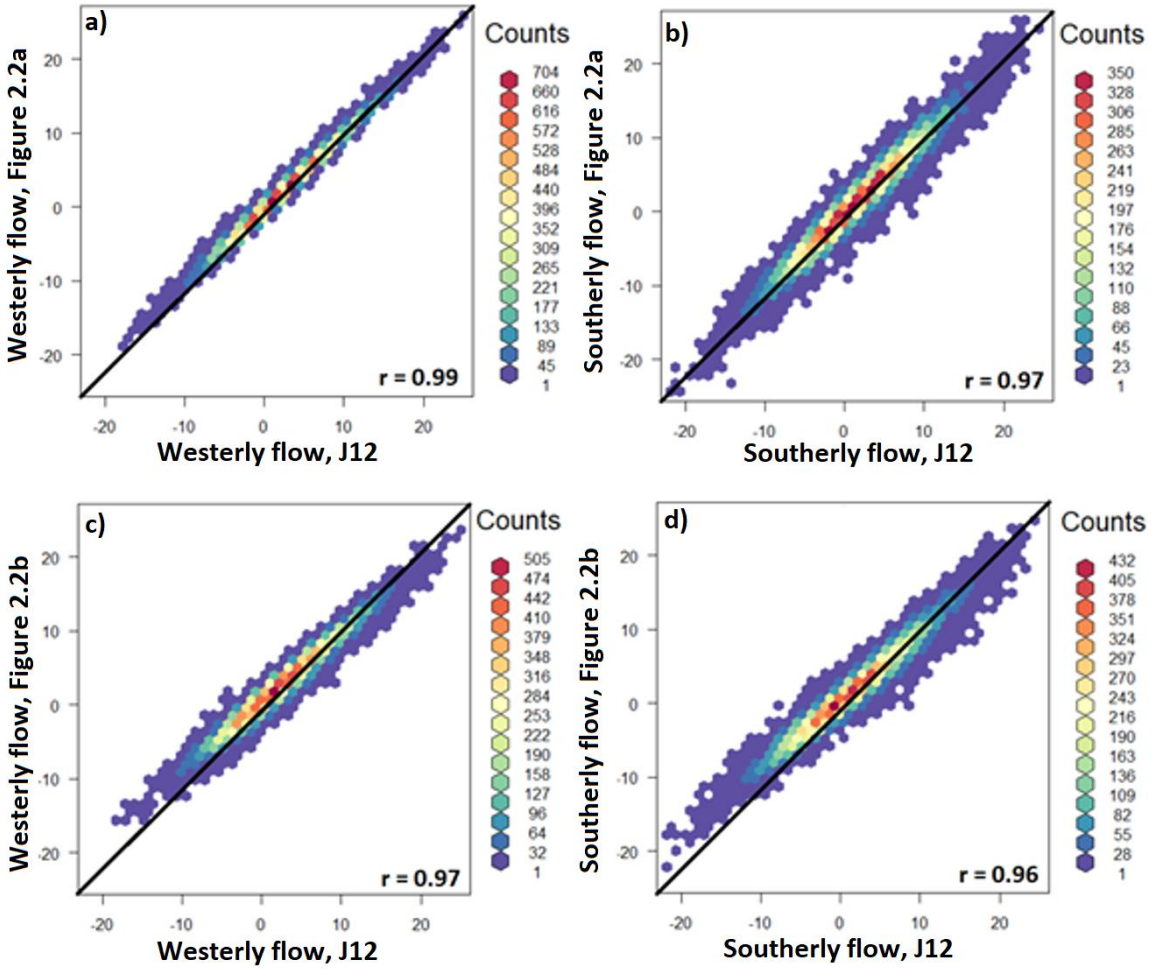

Figure 2.4: Comparisons of flow parameters between the J12 method and the grid configurations in Figure 2.2. Panels a-b) show comparisons for westerly and southerly flow strength using the panel a) configuration whilst panels c-d) show the same parameters for the panel b) configuration. Flow parameters calculated for the North Sea point, using daily data from the 20CRv2c from 1971-2014 and units are expressed as ms^{-1}.

As an alternative to flow shear, average SLP values over the 4 points is used as these show a strong correlation with the total shear values (Figure 2.3) and is much easier to calculate, and therefore more flexible to apply to different grid configurations. The synoptic charts in Figure 2.5 show different instances where SLP and flow shear calculations are similar to each other. Figure 2.5a for example shows a flow from the east

with a cyclonic component. The flow to the east of the North Sea point is from the east whilst the flow to its west is from the North-east, indicating an anticlockwise circulation (Northern hemisphere). SLP is lower than average overall when taking the value from 16 points so this gives an indication of the cyclonic circulation. Figure 2.5b shows a chart which has a moderate flow strength from the NNW but SLP is above average suggesting an anticyclonic northerly, which the synoptic chart shows.

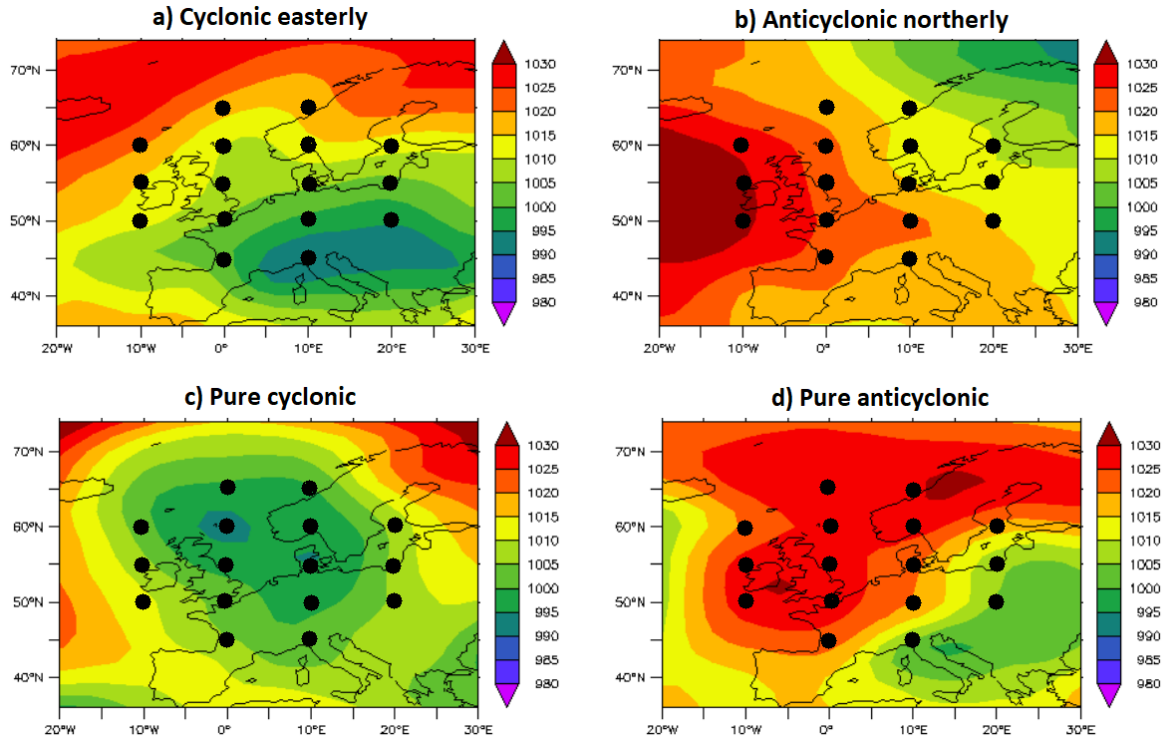

Figure 2.5: Four different circulation types across the North Sea region on different days with the SLP values (in millibars) indicated by the colours. Red values indicate higher SLP whilst blue values represent low SLP.

Figures 2.5c and d) show synoptic patterns where a cyclone and anticyclone respectively are directly over the UK, SLP gradients between the 16 points are smaller than panels a) and b) in both cases but SLP is either well below or above average. One issue with using average SLP values is that they may not be able to distinguish shallow low or high pressure systems (cyclones or anticyclones which don't have particularly high or low SLP values), but this will be more of an issue when looking at daily timescales (where shallow high and low pressure systems can occur giving very different meteorological conditions at the surface in spite of very slack SLP gradients.). The findings suggest that using only SLP data as an alternative to shear calculations is feasible. This approach is particularly beneficial in Chapter 5 and is taken forward in this thesis.

2.3 Creating marine air temperature predictions

2.3.1 Using the flow parameters

In this section, the bicubic spline method used to link MAT anomalies to atmospheric circulation is introduced, using flow parameters as they are a good proxy for air mass source. Flow strength for example (Figure 2.6a) gives an indication of the persistence of atmospheric circulation patterns through a given month. A month with a strong South-westerly flow strength is likely to be dominated throughout the month by air coming from that direction whilst a weak South-westerly flow is likely to be characterised by a variation of circulation patterns within the month, with only a slight South-westerly bias.

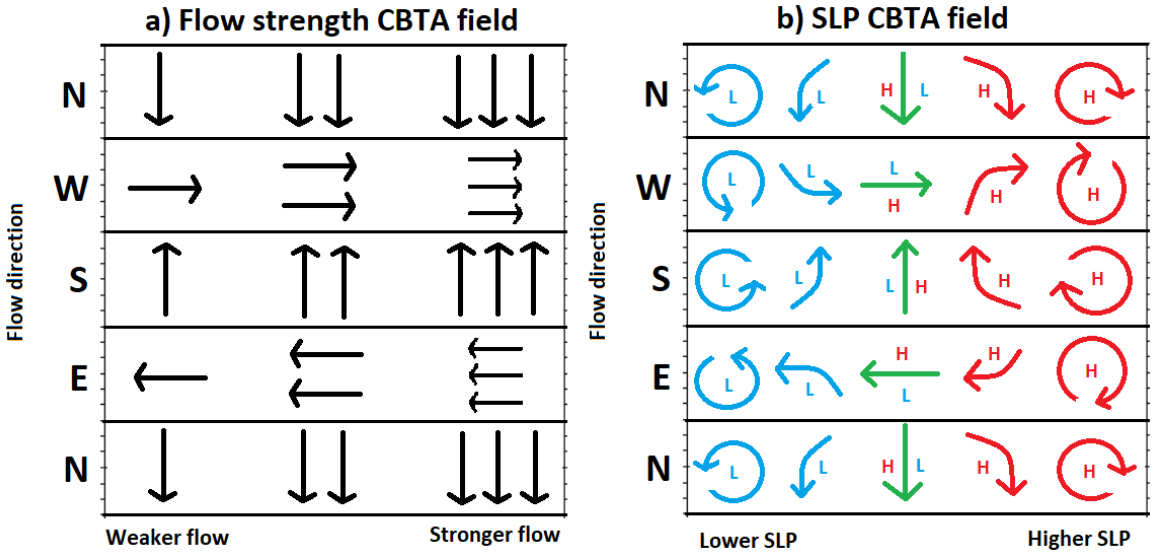

Figure 2.6: The source of the air mass as a result of flow direction and strength (a) or SLP (b). Panel b shows the circulation patterns expected in the northern hemisphere, with lower SLP likely to contain an anticlockwise flow component and vice versa.

The average SLP value for a synoptic pattern is another important parameter to consider. At the North Sea point for example, a southerly flow with low SLP is likely to have a cyclonic flow (anti-clockwise component) drawing in air from the subtropical North Atlantic (Figure 2.6b). A southerly flow with high SLP meanwhile is likely to have an anticyclonic flow (clockwise component), drawing in air from the continent. Air flows in the opposite direction around pressure cells in the Southern Hemisphere. The differences in SLP/curvature are important because they also have a bearing on the weather

conditions at the surface. Wilby and Quinn, (2013) for example found that cyclonic (low pressure dominated patterns) lead to increased rainfall which is also likely to lead to more cloud cover (e.g. Moberg et al., 2003). Placing the variables of SLP and flow strength on a 2d field can capture the variations of MAT alongside the flow direction and indicate where an air mass may be coming from.

An alternative method developed by Parker, (2009) looked at predicting variations in air temperature by calculating air mass source directly. This method predicted past CET variability with more skill than the studies by Osborn and Jones, (2000) and Jones et al., (2014). This is because they used MSLP patterns from reanalysis products from the preceding 1-6 days to track air mass source, whereas Jones et al., (2014) for example just used daily flow indices. Such results demonstrate that persistence of atmospheric circulation patterns is key (as air masses are advected from further away in such instances), but this is captured by the flow strength values in this thesis when looking at monthly means. In addition to this, monthly means obscure daily variations in atmospheric circulation meaning it is not possible to track the source of an airmass directly from monthly mean SLP. For these reasons, the 2d grids shown in Figure 2.6 are used for this thesis although the Parker, (2009) method may be better suited to daily timescales.

To capture the relationships between MAT and atmospheric circulation, 20CR MAT anomalies are placed onto a 2d grid with flow strength or SLP on the x-axis and flow direction on the y axis. Data from 1971-2010 is used to build the relationships for the model as this is a period when uncertainty in 20CR MAT and HadNMAT2 is low due to better knowledge of metadata and more widespread coverage of marine meteorological data (Kent *et al*., 2013, Freeman *et al*., 2017). Using monthly data would mean only 40 values would be available to place on the 2d field whereas the 30-day running means results in over 1000 values to place for the month of February during the 1971-2010 period, though these many of these points are not independent. February 2010 for example would contain 28 different values covering the periods from January 16th 2010 February 13th 2010 (earliest point) to February 16th 2010 – March 17th 2010 (latest point) at one day intervals.

Figure 2.7a shows an example of the 30-day running means placed onto a 2d grid according to flow direction and SLP. Placement onto the 2d field is done for all of the February 30-day running means from 1971-2010 but to predict temperature outside the 1971-2010 period the CBTA field needs to be complete. Completion by infilling of the CBTA field is possible with the use of a bicubic spline, with the anomalies shown in the SLP CBTA field of Figure 2.7b. This was calculated by using the Numerical Algorithms Group (NAG) subroutines E02DDF and E02DFF (NAG, 2015), with these subroutines explained further in Chapter 3.

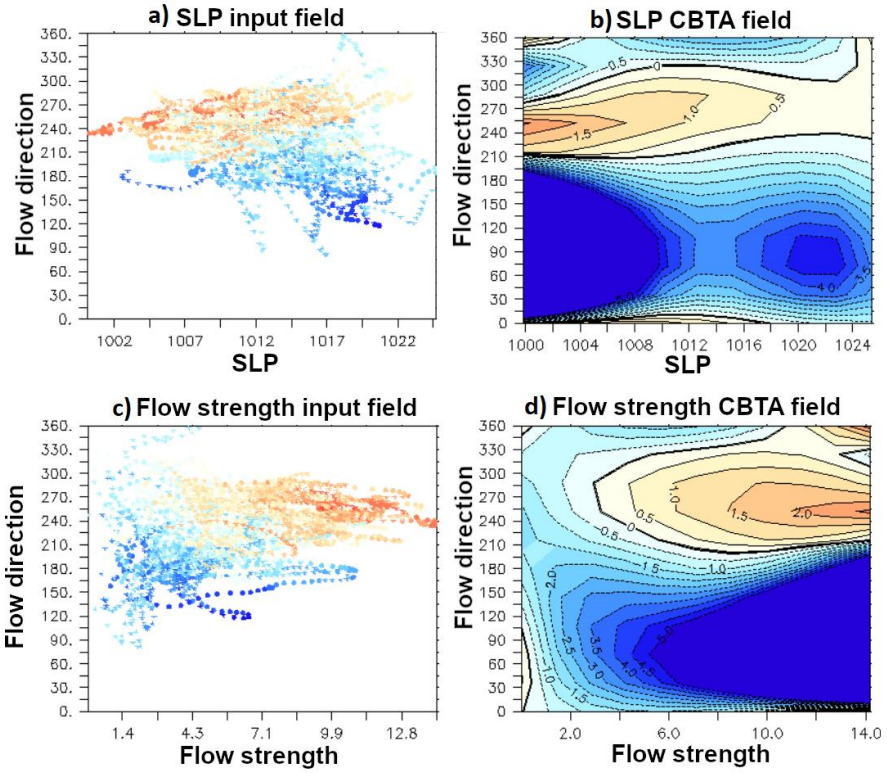

Figure 2.7: CBTA fields for flow direction and SLP. Panel a) shows the input data based on SLP and flow direction, with MAT anomalies (°C) colour coded relative to their deviation from the 1971-2010 climatological average ; b) CBTA field consisting of SLP on the x axis (mb) and flow direction on the y axis.; c) As with panel a) but with flow strength on the x axis instead; d) as with b) but a CBTA field consisting of flow direction and flow strength (ms^{-1}) . Flow parameters are based on calculations from the diamond grid pattern in Figure 2.2a.

A bicubic spline consists of several piecewise cubic polynomials, each with different coefficients. The polynomials are joined together at particular points (knots) with

constraints on the consistency of the line through the knot point. How closely the CBTA field fits the data placed into it depends on the number of knots picked with more knots meaning a closer fit to the input data. The suitable number of knots for any given month varies but it's an important issue to consider as too few knots may result in an underfit and miss important variability within the input data. Too many knots meanwhile may result in an overfit, producing unrealistic looking CBTA fields. For Figure 2.7, 8 knots are picked for the CBTA fields as these fit best to a period of trained (1971-2010) and untrained data (1931-1970, explained further in Chapter 3).

Several other choices can be made for the CBTA field, data from January and March is also included to improve coverage for the CBTA fields and such data is assigned a reduced weighting (1.0 is the standard weighting). A weighting is also applied at the 0^o and 360^o lines respectively (extremes of the y axis) to make these ends of the CBTA field loop. The stronger the weighting of the values at 0^o and 360^o, the closer the anomalies are to each other but this has implications for the rest of the CBTA field. The issue of weightings and knots is also discussed further in Chapter 3.

The relationship between temperature and atmospheric circulation is clearly illustrated in Figure 2.7b with warmer Februaries associated with a westerly flow from the North Atlantic and colder Februaries with easterlies from the continent as seen in the UK region (Jones et al., 2014). The infilled SLP CBTA field appears realistic although easterlies with a low SLP probably have an anomaly too low and vice versa for northerlies with low SLP. In these regions input data are still lacking. Figures 2.7 c) and d) show plots relevant to the flow strength CBTA field. Like the SLP CBTA field, easterlies coincide with cold Februaries and westerlies mild ones, however westerlies for example show a substantial variation in anomalies depending on the strength of the flow (more positive the stronger the flow is). There is a lack of coverage in some areas, especially with strong easterlies and northerlies for example, explaining the more extreme anomalies in the CBTA fields. In Chapter 3 uncertainty estimates are developed for the CBTA fields which are large in these poorly sampled conditions.

2.3.2 Stepwise regression with SLP values

In this section a second method of predicting MAT is introduced and is used as a comparator to the bicubic spline method. One of the disadvantages of the bicubic spline method is that it requires many observations to avoid too much extrapolation with the CBTA fields and the risk of overfitting exists. Therefore, another method was developed to assess whether these factors were an issue for time series analysis (judged by comparing correlation coefficients in Chapter 4). A forward selection stepwise regression is used (Myers, 1990) as it is simple and can be applied using only monthly means. The stepwise regression method does not require the calculation of atmospheric circulation parameters, instead it is just based on regressions on the available SLP data only.

The first step in developing the stepwise regression model is to take the 4 points of SLP (Figure 2.2) used in grid configuration of Figure 2.2a (as used to produce the time series in Section 2.4). Correlations between North Sea SLP and MAT are calculated. The next step involves selecting the point on the grid from Figure 2.2a where SLP has the strongest correlation with North Sea MAT. From Figure 2.8a, it can be seen that this is west of Norway at 65^{o} N ($r = 0.77$). A scatterplot of this relationship (Figure 2.8b) shows a non-linear relationship. The data shows that warmer temperatures during the month of February are associated with lower pressure over Northern Europe and such a pattern is more likely to coincide with westerlies. Above average temperatures are smaller in magnitude than the below average temperatures but are more common and the scatterplot in Figure 2.8b has a non-linear shape.

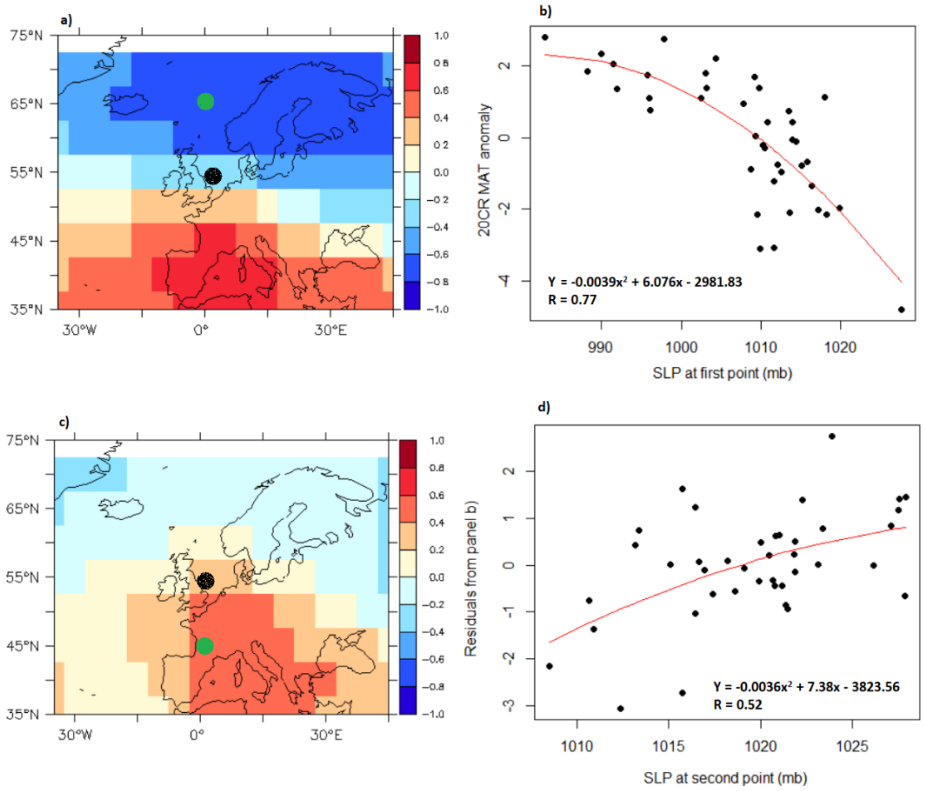

Figure 2.8: Plot of the 2 steps taken for the regression method at the North Sea point (in black) for the month of February. Panel a) correlation between 20CR MAT and SLP over surrounding 20CR grid boxes; b) A quadratic regression of SLP at the point with the highest correlation coefficient shown by the green marker in Figure 2.8a). Panels c) and d) show the same plots but the regression is applied to the residuals from the model of Figure 2.8b.

The residuals from Figure 2.8b are then calculated (predicted MAT – 20CR MAT) and these represent the variability not captured by SLP variations to the west of Norway (Figure 2.8c). There is still a strong positive correlation between residual MAT with SLP over Southern Europe so a point of SLP over this region is taken for the 2nd regression step (Figure 2.8d). These steps are repeated until none of the remaining SLP points have a significant correlation with MAT. The threshold for adding another step to the regression is that the p-value must be below 0.05 for a correlation to be significantly different from zero (with the analysis containing 38 degrees of freedom). For the prediction of North Sea February MAT, SLP from only 2 points is picked. To produce the final predicted temperature using the regression method, the values from each regression step are summed. These values are derived from the SLP and regression equations shown in Figures 2.8c and d.

The model is developed in individual steps to avoid multicollinearity as the SLP field is spatially correlated. High SLP over Gibraltar for example is often associated with low SLP over Iceland (Jones et al., 1997; Hurrell 1995). Validation of the regression model is possible through examination of the residuals. If these are normally distributed then the regression model is working well, whilst a non-normal distribution indicates that other methods could possibly provide a better fit to the data. Some histogram plots are presented in Figure 2.9 and these show that the residuals that have a normal distribution with the exception of Autumn (due to September and October outliers, perhaps due to the use of too few points during these months) as p-values from the Shapiro-Wilk tests are greater than 0.05 (tested using Minitab version 18). A normal distribution of the residuals indicates the choices made for the regression method are suitable. Overall the regression method provides evidence of a relationship between MAT in the North Sea and atmospheric circulation, with westerly flow patterns being picked up on by the correlations (low SLP near Scandinavia, high SLP over Southern Europe). However, it still gives a less clear picture of how exactly atmospheric circulation influences MAT. For this reason and because the regression does not work as well with values not used in the regression (i.e. outside the 1971-2010 period, shown in Chapter 4); a regression method is used as a comparator only to the CBTA estimates based on flow parameters.

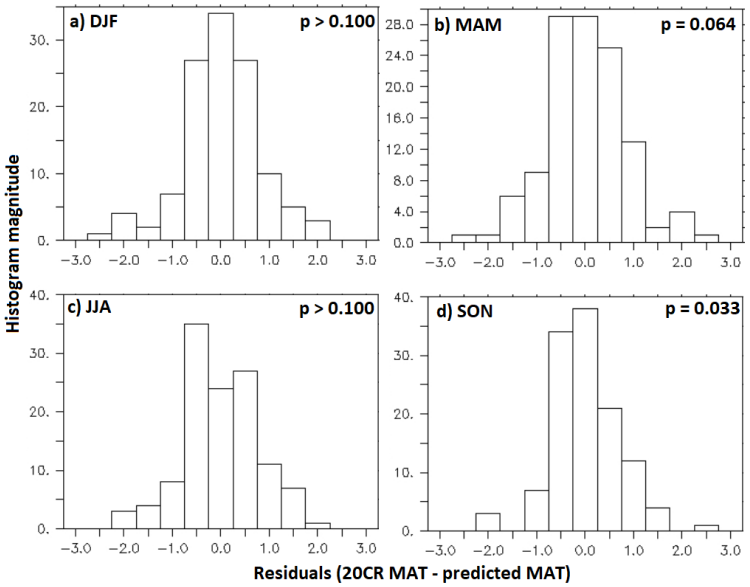

Figure 2.9: Regression residuals for MAT anomalies at the North Sea Point for the 4 seasons of the year. Panel a) shows a histogram plot of the residuals from the regression model presented in Figure 2.8 for the boreal winter b) shows regression residuals for the boreal Spring; panel c) Summer; d) Autumn. P values from Shapiro-Wilk normality test shown in each chart.

2.4 Time series analysis of North Sea MAT anomaly predictions

In this section the results for different time series of data are compared to demonstrate the importance of atmospheric circulation's influence on MAT variability at the North Sea point. Results from the 2 methods used to develop CBTAs are analysed by comparing their correlation coefficients with 20CR MAT anomalies. Time series are created covering the period 1881-2010 as this covers the range of years available for HadNMAT2 analysed later (Kent et al., 2013).

Figure 2.10 shows time series of CBTAs and 20CR MAT anomalies for the months of February, May, August and November respectively, based on the flow strength CBTA fields described in Section 2.3. There are strong connections between temperature and the CBTAs from this method, especially during February for both the 1971-2010 period and from 1880-2010 ($r = 0.81$). This indicates that (for February at least), the relationships between temperature and atmospheric circulation are genuine, given they are apparent with data not used to construct the model relationships. A few outliers are apparent however, which may be a consequence of using a short time period to develop the model.

Whatever the amount of data included to develop the model, there will be situations that are not represented by other periods. The extent of the cold for the Februaries of 1929 and 1956 for example is not well reproduced. These months were characterised by persistently strong Scandinavian highs advecting cold air from Siberia across the region, weather patterns which were not seen to such an extent during 1971 to 2010.

For other months relationships between temperature and atmospheric circulation are apparent but weaker, as also seen with nearby studies over land (e.g. Osborn and Jones, 2000). The correlation coefficient is generally lower when applying to time periods not included in the model (r value is about 0.10 lower for unused model data) but the causes of this are uncertain (Table 2.1). In addition to the short period used to develop the model, other factors may have an influence on MAT. Overall though the largest decreases in the correlation coefficients generally occur when the relationships between temperature and atmospheric circulation are weakest (such as May). For January, February and March relationships are consistent throughout.

Method	JAN	FEB	MAR	APR	MAY	JUN	JUL	AUG	SEP	OCT	NOV	DEC
Strength CBTAs	-0.08	-0.08	0.03	-0.11	-0.22	-0.01	-0.22	0.01	-0.31	-0.16	0.08	-0.05
SLP CBTAs	0.00	-0.10	-0.05	-0.18	-0.08	0.00	-0.16	-0.06	-0.44	-0.23	-0.23	-0.24
Regression	-0.12	-0.04	0.00	-0.14	-0.17	-0.26	-0.38	-0.14	-0.29	-0.29	-0.19	-0.10

Table 2.1 Differences between the correlation coefficients for 1971-2010 period and data from 1881-1970 for the two different methods. Negative values indicate where the model performs worse with the 1881-1970 data.

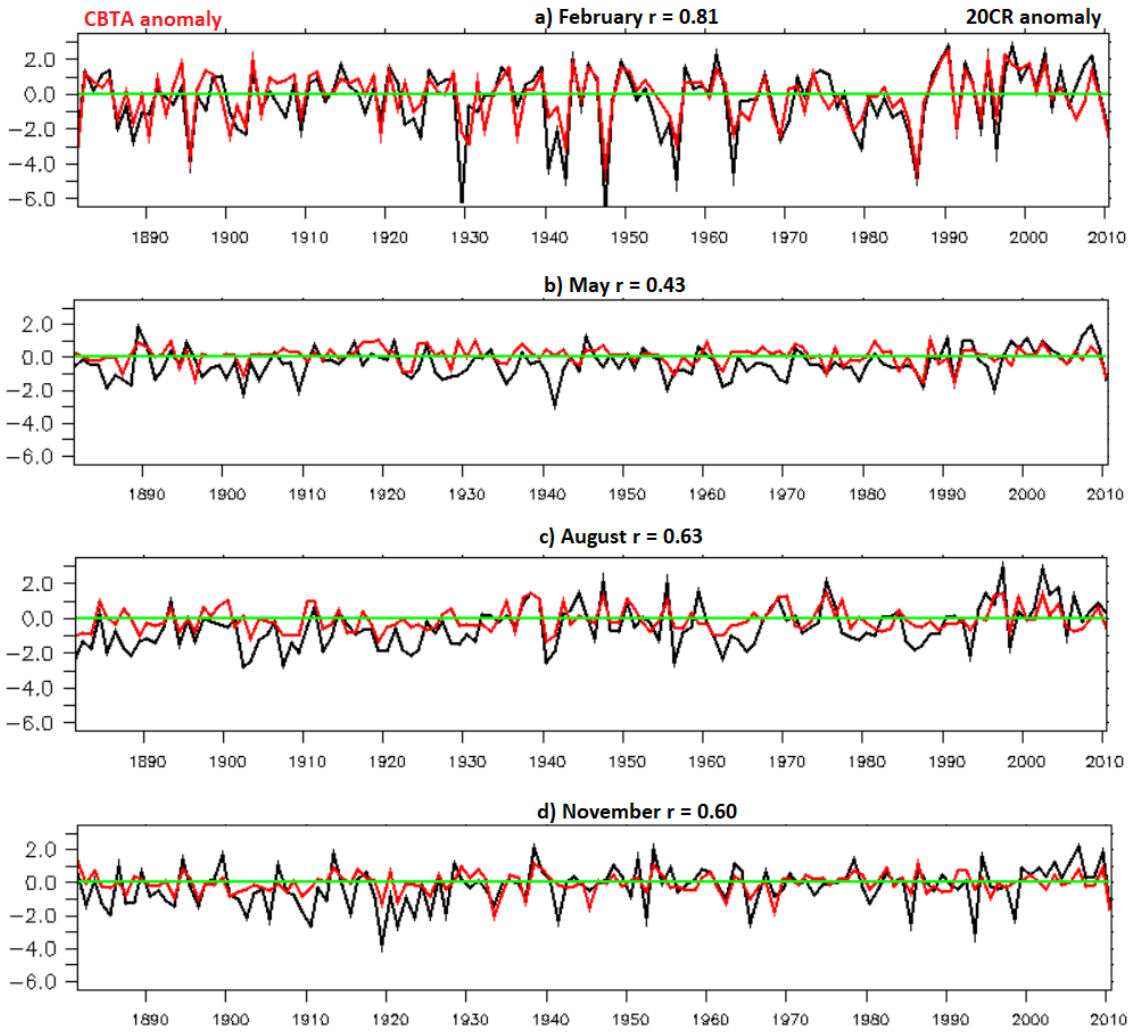

Figure 2.9: Time series of predicted MAT and 20CR anomalies for a) February; b) May; c) August; d) November.

Finally, Table 2.2 shows a comparison of the correlation coefficients for the two different methods of developing the CBTAs for each month of the year. This indicates that the stepwise regression method presented in Section 2.3 generally performs worse than the method based on the flow parameters with the only exceptions being April, October and December. At this location flow strength is the most influential variable on MAT, but this is not the case in other locations.

	JAN	FEB	MAR	APR	MAY	JUN	JUL	AUG	SEP	OCT	NOV	DEC
Strength CBTAs	**0.85**	**0.81**	**0.69**	0.28	**0.43**	**0.63**	**0.67**	**0.63**	**0.56**	0.62	**0.60**	0.76
SLP CBTAs	0.75	0.74	0.57	0.25	0.36	0.55	0.59	0.62	0.38	0.46	0.43	0.60
Regression	0.82	0.81	0.68	**0.35**	0.32	0.45	0.58	0.54	0.50	**0.65**	0.52	**0.80**

Table 2.2 Correlations between CBTAs and 20CR MAT anomalies during the period of 1881-2010 for the two different methods. The highest correlation for each month is highlighted in bold.

Although some strong relationships have been found at this location between MAT anomalies and atmospheric circulation, things can be improved further. There needs to be uncertainty estimates so they can be used to combine the flow strength and SLP based CBTAs by generating weighted means. The uncertainty estimates also aid interpretation of time series data. The next chapter therefore goes through the uncertainties of the model and how they are used to produce a final time series of CBTAs for this location.

2.5 Conclusions

In this chapter relationships between MAT anomalies and atmospheric circulation were explored over the North Sea. The chapter sought to answer three questions:

1) Are there strong connections between atmospheric circulation and North Sea MAT?

Strong relationships have been shown between atmospheric circulation and MAT anomalies. The two models performed particularly well when looking at predictions covering the period used in the model (1971-2010) but when moving outside this period there is a decrease in predictability, as expected. Despite this, relationships between temperature anomalies and atmospheric circulation are still apparent. Variations in the relationship between temperature and atmospheric circulation could be due to the use of a limited time period for developing the CBTA model (1971-2010), other aspects of atmospheric circulation, methodological choices and non-circulation effects. With this information the next question could be answered:

2) Are the flow parameters defined by J12 the best for developing CBTAs and predicting monthly MAT at this location?

There were two ways in which these relationships between MAT and atmospheric circulation were developed, using either a bicubic spline or forward selection stepwise regression. For the bicubic spline method, temperature anomalies were placed onto a 2d field depending on the corresponding flow parameter observations of flow strength, SLP and direction (defined by J12). The regression method just focused on individual points of SLP and the time series analysis found the bicubic spline method was slightly better.

3) How much can current methods used to define atmospheric circulation parameters be simplified?

Flow parameters using the J12 method required 16 points of SLP but the method in this chapter reduced the number of points to calculate the flow parameters of westerly flow, southerly flow and SLP down to 4. The average SLP value was used to replace the flow shear calculations as the two variables are similar but the average SLP value is easier to calculate. The simplification makes it possible to analyse station SLP data in Chapter 5.

Results in this section were promising and the spline method can be improved further to aid time series interpretation and it can be combined with SLP CBTAs by developing uncertainty estimates. Chapter 3 describes the method of calculating the uncertainties relevant to the method presented in this chapter.

Chapter 3 Uncertainties of the circulation-based temperature anomalies

3.1 Introduction

In Chapter 2 it was demonstrated that there were strong connections between MAT anomalies and atmospheric circulation over the North Sea during some seasons. These connections were identified by examining how MAT varied as a result of flow direction, strength and SLP. Despite these connections, numerous questions emerged. Firstly, why does the relationship between temperature and atmospheric circulation weaken further back in time? And what are the causes of the differences between predicted and observed temperatures? Uncertainty estimates are required to answer these questions and an uncertainty framework is developed, with the North Sea point being used as an example in this chapter.

Uncertainty estimates are provided in many MAT/SST datasets (e.g. Kennedy et al., 2011; Kent et al., 2013; Huang et al., 2017) and these assist interpretation of the past MAT/SST variability from the 19th Century to the present day. However, within the research field of analysing relationships between temperature and atmospheric circulation, uncertainty estimates have been less common. Developing uncertainty estimates is important because the aim of this thesis is to assess the extent to which atmospheric circulation has influenced marine climate and also identify any unusual occurrences. For interpretations of the MAT data to be made, it is necessary to assess what can cause the anomalies in the CBTA field vary to identify potential irregularities. Moberg et al., (2003) for example were able to interpret their time series because they developed uncertainty estimates and this led to identifying a potential bias. A bias was assumed because the observed temperature fell outside the calculated uncertainty bounds for a prolonged period of time. The uncertainty estimate was developed using data from 1870-2000 and because the observed temperature prior to this period consistently fell well outside the uncertainty bounds, another external factor was assumed to be influencing the observed temperature. However, their model used a multiple linear regression and is different to the method used here.

For this chapter a new approach to calculating uncertainties will be taken, focusing on the CBTA field developed in Chapter 2. The aims of this chapter are to:

1) Develop individual uncertainty components which are not related to each other. These uncertainty components should capture the variability in MAT not captured by the CBTA field.
2) Combine the individual uncertainty components to create a total uncertainty estimate and demonstrate this can be used for time series analysis.

An uncertainty estimate can be defined as the potential dispersion of values which can be attributed to a measured value (Bulgin, Embury and Merchant, 2016) and in this thesis that uncertainty will be presented as one standard deviation. Two key uncertainties were already highlighted in the previous chapter which are outlined in this one. Those are the potential for other factors besides flow direction, strength and SLP to influence MAT (referred to in this chapter as category uncertainty). The other is the level of smoothing done by the spline approximation itself due to the variation of anomalies in areas of the input field (misfit uncertainty). A standard error calculation for the category uncertainty would lead to this capturing some element of misfit uncertainty. This is because standard error considers the sample size being considered and as section 3.3.2 shows, the misfit uncertainty is heavily influenced by sample sizes and small sample sizes usually result in a greater degree of smoothing.

The chapter is structured as follows; Section 3.2 examines the NAG routine used to produce the CBTA field and how changes to its input data can affect the final spline approximation and these are used to calculate parametric uncertainties. Section 3.3 will then focus on other uncertainty components that can affect the final CBTA field. Section 3.4 then demonstrates how these uncertainties can be combined to produce a final uncertainty estimate. Section 3.5 then provides some conclusions of the chapter.

3.2 Methodological choices and their uncertainties

To produce a complete CBTA field with a bicubic spline (as shown in Chapter 2), a number of subjective choices must be made with regards to the NAG subroutines E02DDF (calculates positions of knots and coefficients for spline approximation) and E02DFF

(produces the CBTAs from coefficients and knot positions). In the subroutine E02DDF for example decisions can be made with regards to the weighting of individual categories and the closeness of fit. Additionally, the values at 0^o and 360^o should be continuous but making this occur has an impact on the rest of the CBTA field, so a weighting is considered for this adjustment too. The decisions taken to produce a CBTA field are shown in a flow chart (Figure 3.1) with the justification for each choice made described in this section. The most important choice is the number of knots that are used to create the CBTA field.

Knots represent the start/end points for cubic polynomials so an increasing number of knots means a closer fit to the input data. To determine the closeness of fit a smoothing factor must be stated before entering the subroutine E02DDF as this determines knot placement for the flow strength/SLP and direction variables.

In Figure 3.2a, the input data for the February CBTA field is shown at the North Sea point (as in Chapter 2) with the first spline approximation shown in Figure 3.2b (using 4 knots). The positions of the knots are also shown for the CBTA field in Figure 3.2b and the locations of them are automatically picked by the subroutine E02DDF to provide the closest fit of the anomalies to those seen in the input data. A second spline approximation is then taken to ensure that the 0^o and 360^o values are linked (Figure 3.2c, using 8 knots). The implications of this are discussed with the parametric uncertainties later in this section.

Finally, it is important to pick a suitable number of knots because too few knots can result in an underfit and a CBTA field too smooth, whilst too many knots may provide an overfit. Too many knots can also lead to numerical instability which results in extreme values in the final CBTA field. Overall Figure 3.2b and 3.2c however illustrate a close fit to the input data and are both numerically stable and a quality checking procedure is put into place for numerical stability. This quality checking procedure checks the sum of the square residuals to examine whether there are too many knots.

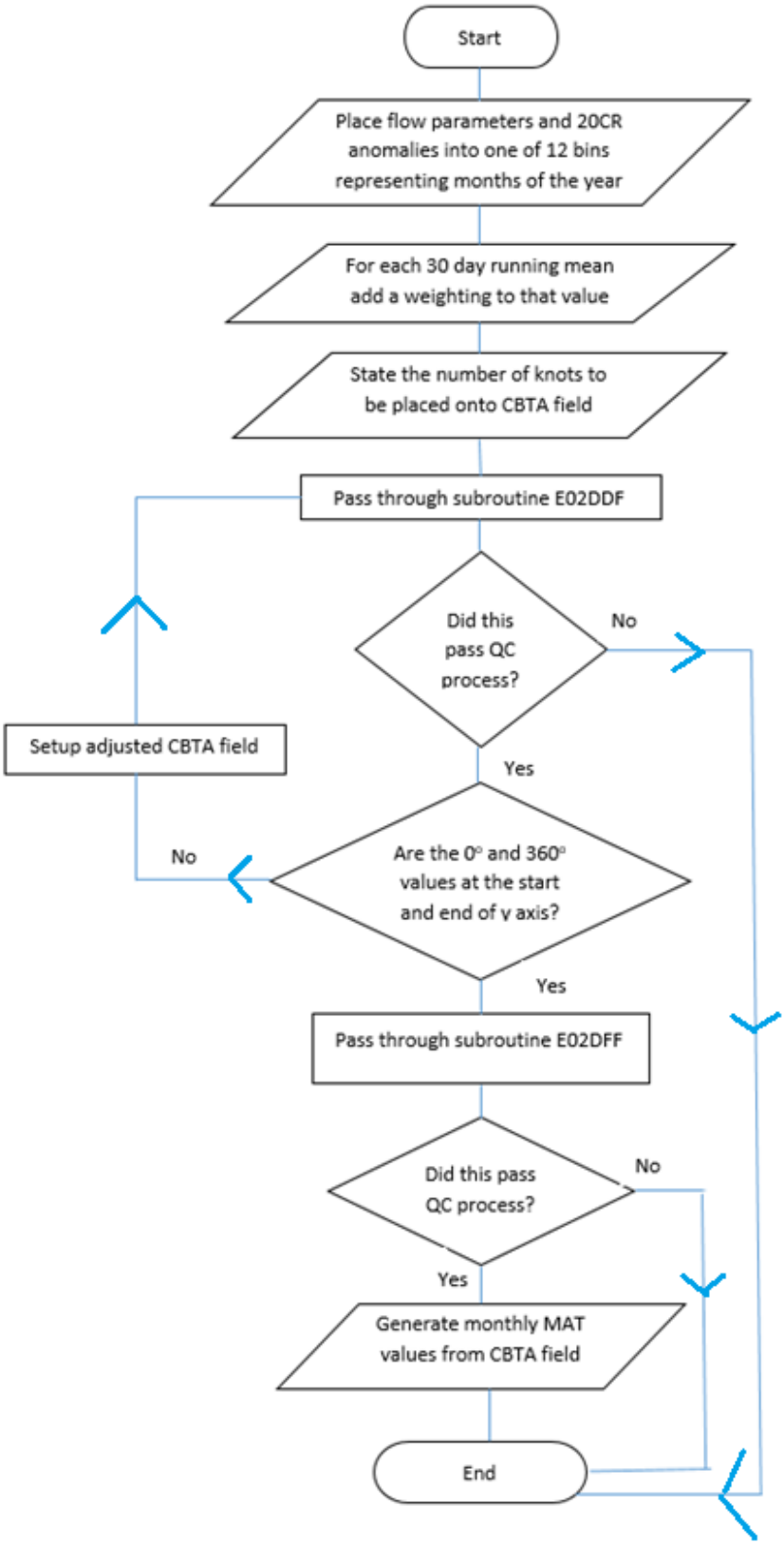

Figure 3.1: Flow chart showing the process for creating a CBTA field, ovals represent terminals, rectangles represent processes, parallelograms show data input steps and diamonds show decisions made by the data user/program.

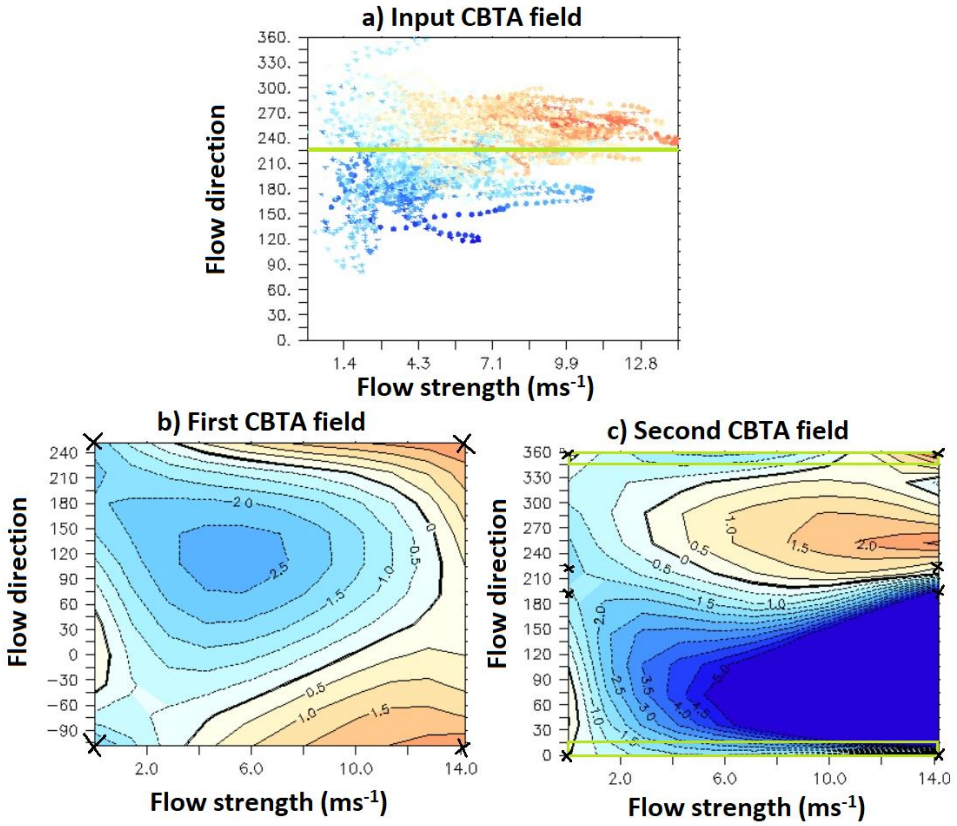

Figure 3.2: a) input field of 20CR MAT anomalies (°C) for the North Sea point during the months of January to March. Placement of MAT anomalies on the 2d grid is based on the flow direction and strength; b) Spline approximation of the input field with the start and end points represented by the green line in panel a). The crosses represent the positions of knots; c) as with panel b) but the start and end points are 0° and 360°. Extra data for the input field of this approximation is added from the values within the green box of panel b).

To assess the uncertainty arising from knot selection, 7 ensemble members were created with 4 to 10 knots each and 1 standard deviation was calculated from the 7 corresponding CBTA fields. The standard deviations can be seen in Figure 3.3a which shows that the variability of the CBTA field as a result of the different number of knots. The uncertainty due to the number of knots chosen is generally small (mostly < 0.2°C where there is input data). There is a risk of unrealistic temperature anomalies where the bicubic spline approximation is unconstrained and this explains the large uncertainties with a strong easterly flow for example as no observations are present here.

The second issue is the impact of weightings of the values at the 0-360° lines. The input data are set up to make the temperature estimates over these regions as realistic as

possible. This is done by first setting up an input field where the edges of the y axis are taken up by as many observations as possible, so the extremes of the y axis will have similar anomalies (green line, Figure 3.2a). A first bicubic spline is then made from the input field with the start and end points denoted by the green line from Figure 3.2a (with the initial spline approximation shown in Figure 3.2b). The values at the 0° line from this initial spline approximation are then taken and added to another input field but the y axis is adjusted to 0 -360° (Figure 3.2c) rather than the -108° to 252° axis initially taken based on the position of the green line.

An alternative approach to linking the 0° and 360° values is to develop one CBTA field covering the range of -360° to 720° and then just take the values between 0° and 360°, however this presents two problems. The first is that the subroutine E02DDF places knots with no input from the user, so there is no way of knowing which of the three fields between -360° and 720° contains the best fit. Secondly, the program would require at least three times the number of knots shown in Figure 3.2c which would greatly increase processing time.

Whichever method is used, the weighting of the 0° and 360° values has an impact on the rest of the CBTA field so 30 ensemble members were generated with different weightings to assess this impact. The standard deviation of these 30 ensemble members is shown in Figure 3.3b and shows a similar pattern to the uncertainty from the number of knots.

When producing the February CBTA field, the weighting of data for surrounding months can also be changed before entering the E02DDF subroutine. The decision to include surrounding months was taken to help improve coverage for the spline approximation. The uncertainty due to adding these months was explored by randomly changing their weighting to values between zero and one for each ensemble member. Figure 3.3c shows one standard deviation of 30 ensemble members with the random weightings for the surrounding months. This standard deviation captures the uncertainty due to the changing relationship between temperature and atmospheric circulation from month to month which becomes more of an issue if a higher weighting is used.

Uncertainties are small at the North Sea point during February however indicating that the temperature response to atmospheric circulation from January to March is very

similar in both months. For example, cold periods during both January and March are almost always associated with easterlies whereas mild periods are associated with westerlies.

To provide a complete picture of the uncertainty due to the choices made with the NAG routine, an uncertainty field in Figure 3.3d is shown which is calculated from 30 ensemble members, each with different numbers of knots and various weightings. These are all changed simultaneously to investigate the combined effect of the choices made with the NAG routine and is referred to from here as the parametric uncertainty.

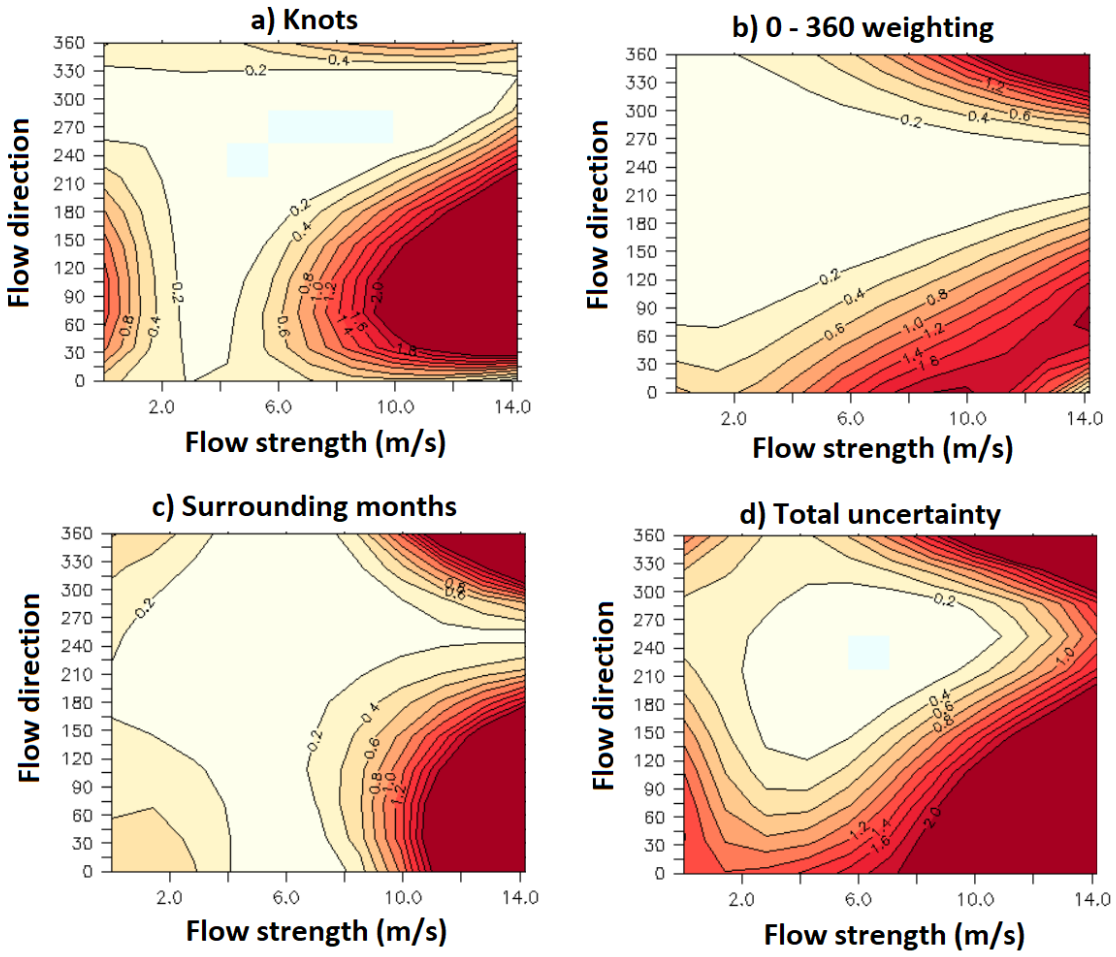

Figure 3.3: Panel a) Standard deviation of the temperature anomalies (°C) in the CBTA field in Figure 3.2b using different numbers of knots in 7 ensemble members; b) Standard deviation of 30 CBTA fields each with a different weighting for the 0° and 360° values; c) Standard deviation of 30 CBTA fields each with a different weighting for the surrounding months of January and March; d) Standard deviation of 30 ensemble members using a combination of different knots and weightings.

For the final CBTA field (as shown in Figure 3.2c), the weightings for values on the 0° to 360° points on the y axis are set to 0.53. The weightings of surrounding months are set at 0.5 whilst the number of knots for this CBTA field is 8. These values were chosen because this combination for the February CBTA field results in the strongest correlation coefficient between the CBTA estimates and 20CR MAT for the period 1931-2010 at the North Sea point (therefore including data used and not used by the model). For other areas of the globe the number of knots and weightings may vary from those at the North Sea point as the values picked are those from the best performing ensemble member. It is assumed that the ensemble member which produces the strongest correlation represents a combination that avoids underfitting and overfitting to the greatest extent. Overall however the parametric uncertainty at this location is small and suggests that despite the array of options available with regards to knots and weightings, they only have a small contribution to the total uncertainty. Other uncertainty components are more important in the model but critically, the parametric uncertainties emphasise where the anomalies of CBTA field are unrealistic.

3.3 Additional uncertainties

3.3.1 Category uncertainty

The category uncertainty is defined as variation due to influences on temperature other than flow direction and strength. This could be due to other atmospheric circulation parameters not considered by the CBTA field in Figure 3.2c (e.g. mean SLP). However other external factors such as climate change and variability outside a defined region can also be an issue (Osborn and Jones, 2000; Van Oldenborgh and Van Ulden, 2003). To calculate the category uncertainty component, it was decided to place the 30-day running means into category bins, rather than directly on the 2d bivariate grid. There are 121 categories overall represented by 11 categories each on the x and y axes. Each category is represented by the average of all the anomalies in that category.

The number of observations in each category is shown in Figure 3.4a and this shows that westerlies are by far the most common circulation type at the North Sea point during February with over 75% of the 30-day running means containing a westerly component.

The consequence of this is that most other categories will have fewer than 10 values in them. When few values are in the same category, the uncertainty of that category is likely to be underestimated. This is because some of the 30-day running means in the same category may be strongly correlated to each other resulting in a small standard deviation. A 30-day running mean from February 1st 2010 – March 3rd 2010 for example is likely to have a very similar flow direction, strength and SLP value to a 30-day running mean from February 5th to March 7th 2010, meaning two strongly overlapping values are placed into the same bin. In the most populated category of the CBTA field (216° flow direction / 5.7ms^{-1}) flow strength there is data from only 36 separate months despite 284 values being in that bin when including January and March data as well. Non-independent data points are therefore an issue, however the 30-day running means do improve the coverage of the CBTA field and this is why they are included.

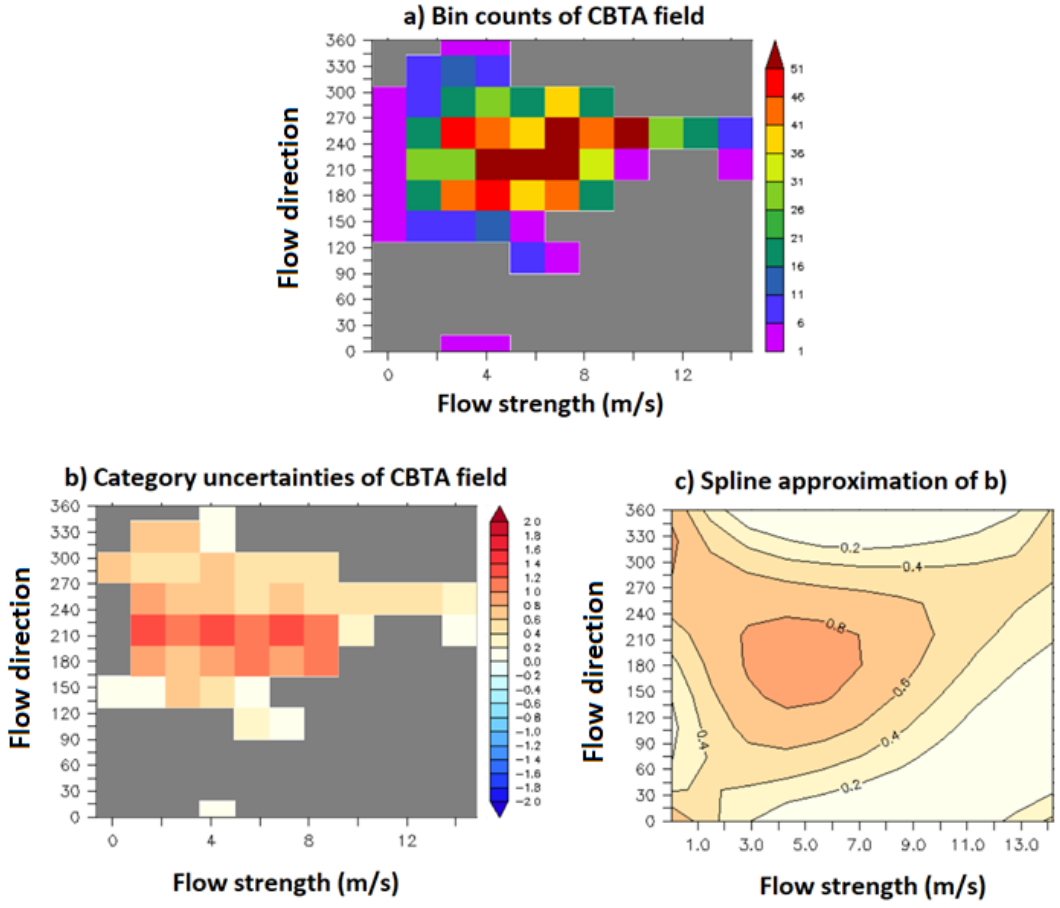

Figure 3.4: a) bin counts of the binned 30-day running means; b) Standard deviation of MAT (°C) in the input field categories shown in panel a); c) Weighted spline approximation of Figure 3.4b. Categories with less than 10 observations are given a weighting of 0.25. Unconstrained areas of the spline approximation may have values less than zero. In these instances, the uncertainty category uncertainty is set to zero as it cannot be negative.

The standard deviations of MAT anomalies within each category show a pattern related to the number of 30-day running means placed into them (Figure 3.4b). Where category counts are highest (198-234^{o} bins) the uncertainties are often close to 1^{o}C whereas categories with fewer values in them see uncertainties close to 0.4^{o}C. Categories with 1 value in them or less have no uncertainty value as it is not possible to calculate the standard deviation in these cases. It is assumed that categories with more values in them are likely to have uncertainty estimates of a higher quality (a standard deviation which is representative of the real uncertainty), which raises the question of whether a uniform standard deviation should be used based on the value from the bin with the most values in it. This approach was not taken because there is some evidence that category uncertainty may vary depending on the weather pattern. During the boreal winter for example, daily CET values may be over 10^{o}C below average for a south-easterly if the air source is from Siberia. Conversely if the south-easterly is picking up warmer air from Africa, temperatures may be above normal. Such variations would not occur with a westerly flow from the warmer North Atlantic for example (Parker, 2009). Therefore, categories with few observations in them are given a lower weighting (0.25), so the categories with more observations in them are of greater importance when constructing the final category uncertainty field (Figure 3.4c).

The final category uncertainty field in Figure 3.4c shows the distribution that might be expected given the input field it is based upon (Figure 3.4b), with uncertainties greatest for westerly and southerly flow types, especially when the flow strength is weaker. Where there are no observations in the input field, the corresponding category uncertainty field in Figure 3.4c shows category uncertainties close to 0^{o}C. These uncertainty estimates are likely to be too low, but are compensated by the parametric uncertainties which are very high in these regions, shown in Figure 3.5 which compares the category and parametric uncertainty fields. More category and parametric uncertainty contrasts are shown in Figure B1 in Appendix B.

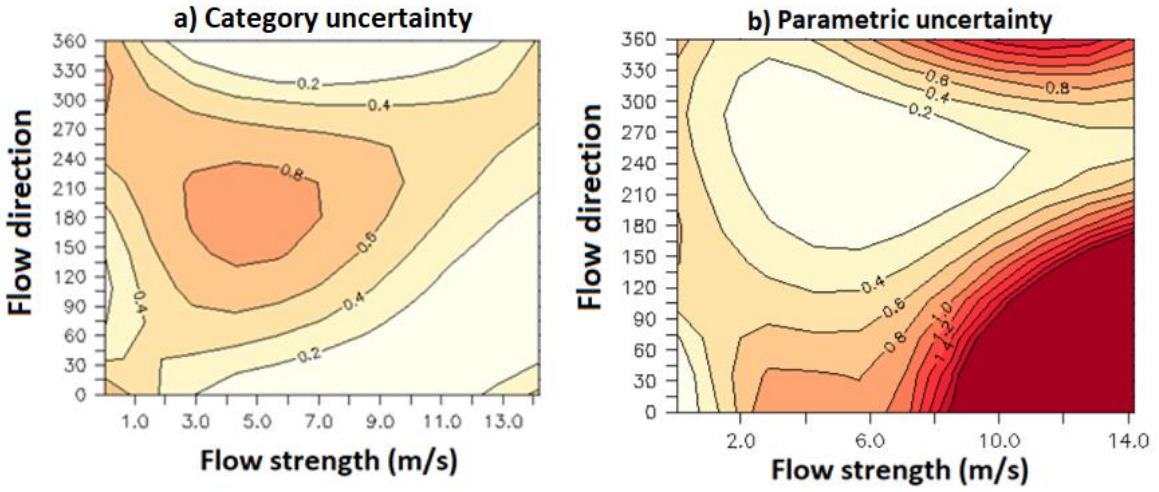

Figure 3.5: Category and Parametric uncertainties of MAT anomalies (°C) from Figure 3.4c and Figure 3.3d respectively shown alongside each other.

3.3.2 Misfit uncertainty

The third uncertainty component is due to the smoothing of the input field in order to produce the spline approximation. The degree of smoothing required to produce a complete field of CBTAs can be quite large. Where category bins contain few observations (e.g. <10), the input field for the misfit uncertainty is likely to contain a greater variation of temperature anomalies from one category to the next because the mean MAT of such bins is likely to deviate from the true population mean (due to the potential for a low number of independent samples). Figure 3.6a shows an example of high misfit uncertainty, with southerly flows which generally contain anomalies slightly below normal whilst south-easterlies contain temperatures 4-5°C below the 1971-2010 climatological average. The final CBTA field therefore contains a large difference from the input anomaly field in these regions because they are smoothed more heavily.

One way to represent the degree of smoothing is to take a category anomaly in the input field and also take all the other category anomalies immediately surrounding it (e.g. black box in Figure 3.6a) and then calculate a standard deviation of all the values. This can be a maximum of 9 category anomalies when all the surrounding categories have anomalies in them. Instances where there are less than 2 categories of observations are assigned no value since it is not possible to calculate a standard deviation.

The standard deviation of all these categories is then taken (Figure 3.6b) and a spline approximation is applied to this field of standard deviations, with the uncertainty field shown in Figure 3.6c. This uncertainty component is referred to as the misfit uncertainty. This captures the degree of smoothing taken with the bicubic spline, with uncertainties over 1^{o}C showing for moderate strength south-easterly flows and near zero where there are no observations (no inferences can be made about the level of smoothing in these regions).

A potential disadvantage of the misfit uncertainty is that it may not differentiate between noise due to varying sampling and differences due to sharp gradients. As the February CBTA fields have shown for example, there is a sharp temperature gradient between south-easterlies and south-westerlies which is expected given they are often associated with continental and maritime airmasses respectively (e.g. Jones et al 2014). However, the misfit uncertainty is an important uncertainty component which must be considered.

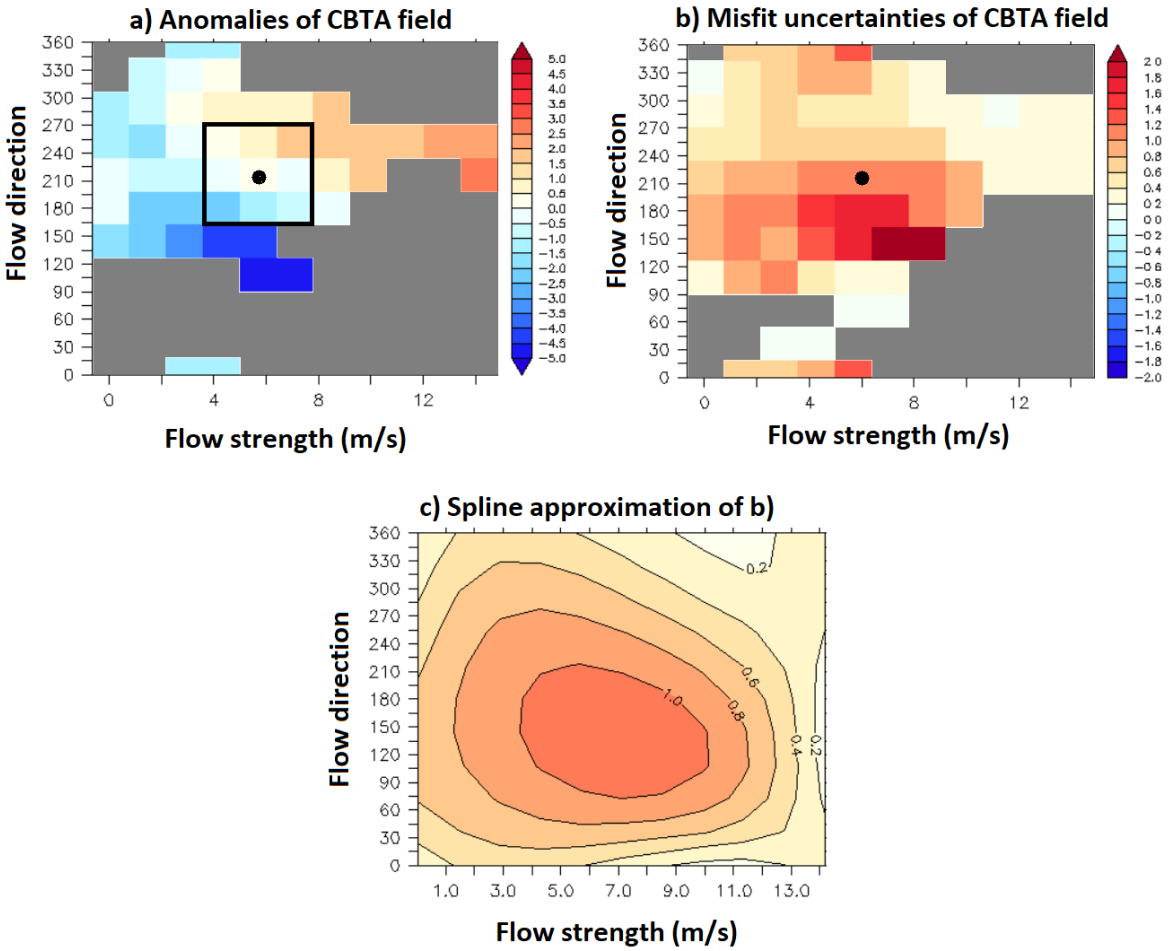

Figure 3.6: Panels showing the development of the misfit uncertainties. Panel a) Input field of CBTAs (°C) when placed into the 121 possible bins. To calculate the uncertainty at the point highlighted, all 9 categories within the black square are taken and the standard deviation is calculated, giving the uncertainty estimate shown in panel b); panel b) shows the input field of all the misfit uncertainties; c) spline approximation of panel b).

3.3.3 Circulation and SLP uncertainties

Another uncertainty component of the spline method arises from the values of flow direction, strength and SLP themselves in relation to the prevailing atmospheric circulation pattern. One way in which this can be calculated is by comparing the CBTA anomalies for each month produced by different grid configurations. There are six different grid configurations (referred to as conventional grid configurations) used for the 20CR analyses from Chapters 2-4. These grid configurations are used to calculate the uncertainty component and are shown in Figure 3.7. Although the method has been generalised in Chapter 2, smaller grid configurations often coincide with higher flow strengths. This is because larger scale grid configurations are more likely to contain

anticyclones or cyclones within them, which themselves contain smaller SLP gradients (because the lowest / highest SLP values are in the middle of the 4 points and the SLP gradient calculations may not calculate this well). In Figure 3.8, the smallest grid configuration contains a maximum flow strength value of ~15m/s yet the larger scale configuration contains a maximum flow strength value of only ~9m/s meaning it's essential to create individual CBTA fields for each grid configuration, rather than just use one CBTA field to predict anomalies from different grid configurations.

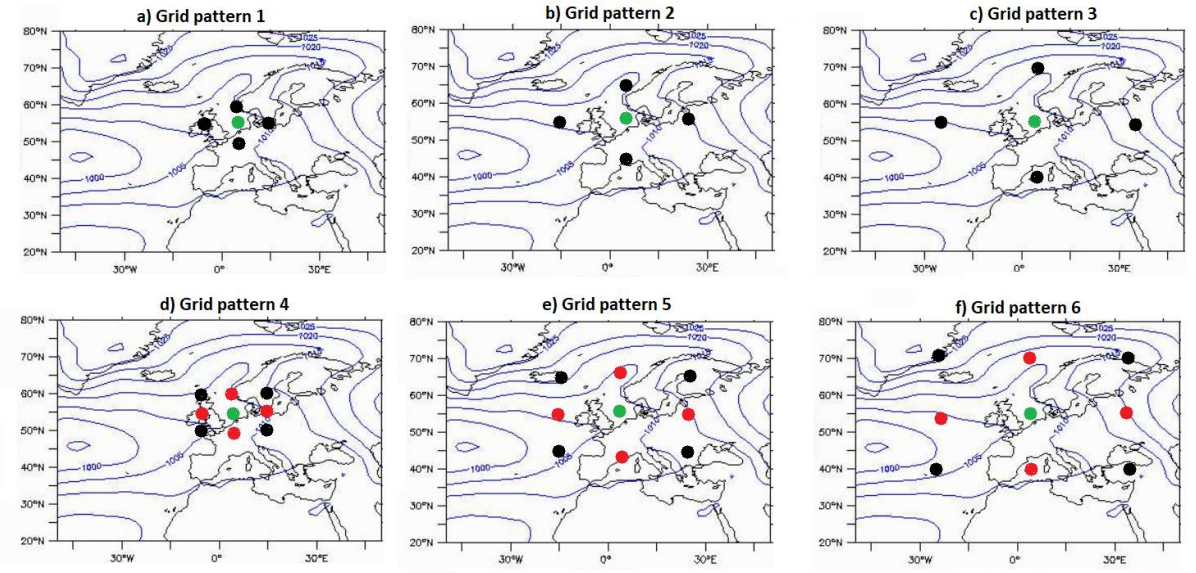

Figure 3.7: The six grid configurations used to calculate the flow parameters for the category uncertainty. Black points indicate the locations of SLP extracted from the 20CR. Red points indicate where SLP is interpolated. The green point represents the North Sea point used for analysis in this chapter.

The six CBTA fields for the six grid configurations are shown in Figure 3.8 for the month of February. The predicted anomalies for the month of February 2010 are shown for each grid configuration below the corresponding CBTA fields in Figure 3.8. The flow direction and strength values for February 2010 are represented by the location of the black dots in each CBTA field. The standard deviation of these six predictions is the circulation uncertainty. It is often highest when the atmospheric circulation patterns are poorly defined as these months are sensitive to changes in flow direction when changing the grid configurations for the flow parameter calculations. The circulation uncertainties overlap with the misfit uncertainty to an extent because it is often taking the standard deviation

of a set of anomalies from similar areas of the CBTA field and these may well be neighbouring categories.

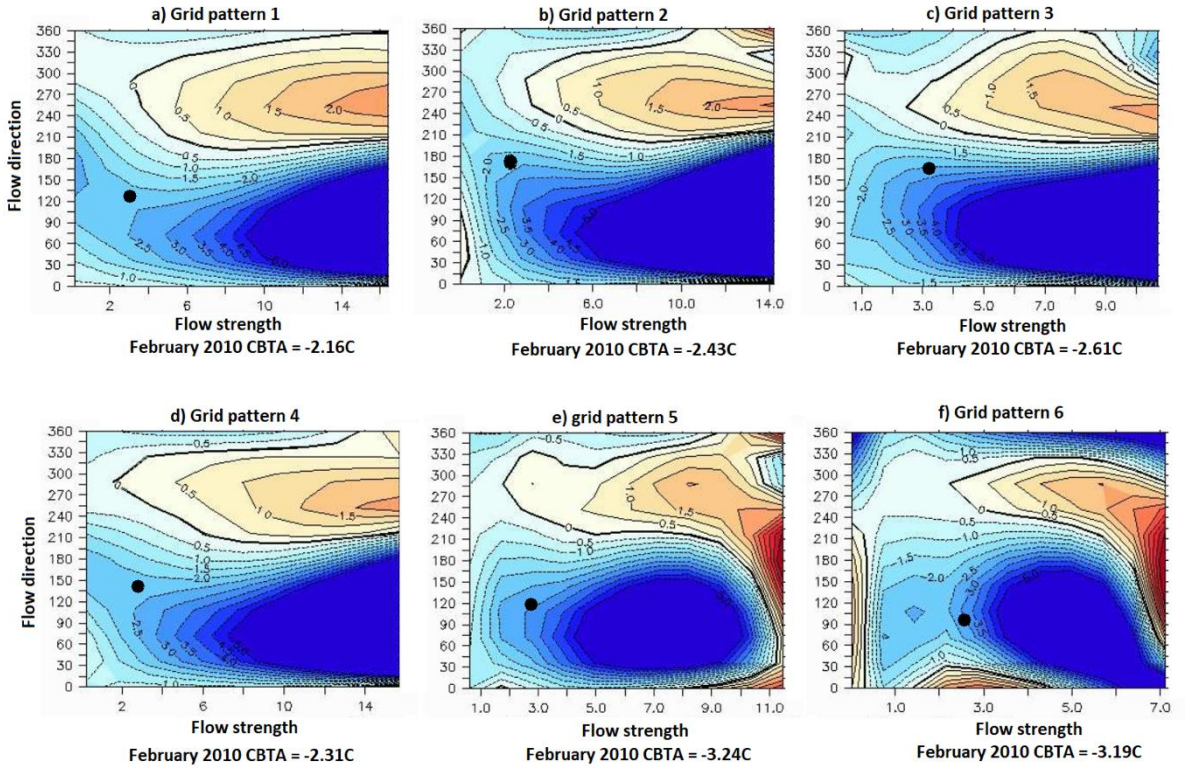

Figure 3.8: February CBTA fields for the grid configurations shown in Figure 3.7. The black dot represents the atmospheric circulation pattern for February 2010 for the different grid configurations. The CBTA anomaly for February 2010 is listed under each CBTA field, taking the standard deviation of these estimates gives the category uncertainty.

Finally, The SLP uncertainty is calculated by producing a predicted anomaly from 26 different SLP ensemble members of the 20CR reanalysis. Flow direction, average SLP and strength are defined for each ensemble member and then assigned a predicted anomaly from the CBTA field in Figure 3.8b. The SLP uncertainty is expressed as the standard deviation of these 26 ensemble members.

3.4 Combining uncertainties to produce a final time series

The aim of this section is to demonstrate that the combined uncertainty components developed from this chapter are accurate and that the spline provides a good fit to the data. The fit to the spline to the input data was examined first. To do this, the CBTA field

was cut through in several places, showing the CBTA anomalies, the actual anomalies and the uncertainties which could be combined and shown for this cut through (category, misfit and parametric uncertainty). The cross sections can be seen for two parts in Figure 3.9 for a westerly flow and a weak flow strength.

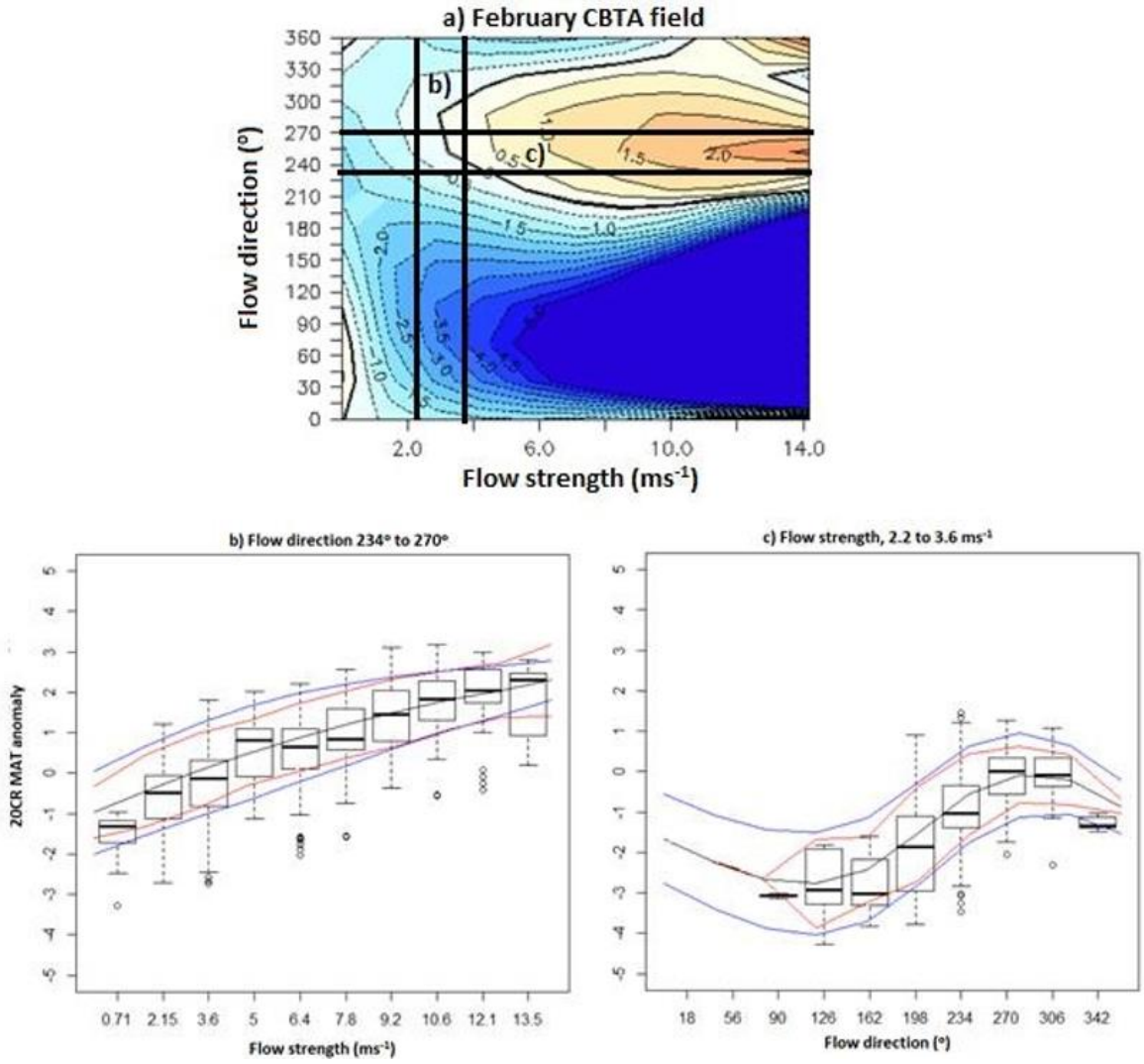

Figure 3.9: A cut through of 2 sections of the February flow strength CBTA field. Panel a) shows the same CBTA field as that in Figures 2.7 and 3.2. Panel b) shows a boxplot of input anomalies placed in bins with the upper and lower quartile ranges shown. The lines in the middle of the boxes represents the median of the bins. Red lines represent the standard deviation of the bins and blue lines show the combined category, misfit and parametric uncertainties. The green line shows the anomalies from the CBTA field. Panels c) shows a section of a weak flow strength.

The cut through in panel b) shows that the CBTA anomalies generally increase with a stronger westerly flow. Both the means of the CBTA fields and the medians of the bins show only small differences from each other (< 0.3°C) that are only larger when there are smaller sample sizes in the bins. The total uncertainties are generally larger than the standard deviation of the MAT anomalies in the bins but only by a small margin (0.2°C). The same pattern can be seen in panel c) with the combined uncertainty here again a slight overestimate. The southerly flow direction (168° to 192°) appear to be slightly warmer in the CBTA field compared to the observations but there is little difference elsewhere.

The two cut sections here appear to be encouraging when compared to the observations, but there are other uncertainty components that need adding and combining to produce a final total uncertainty estimate. There are five uncertainty components overall which are as follows:

- Parametric uncertainty (μ_{par}) – Dispersion of predicted temperature anomalies due to changes in setting up the CBTA field
- Category uncertainty (μ_{cat}) – Variation within a category (a section of the CBTA field) due to factors other than flow direction and curvature.
- Misfit uncertainty (μ_{mis}) – Range of anomalies over several neighbouring categories in a CBTA field.
- Circulation uncertainty (μ_{circ}) – Variation in CBTA estimates due to uncertainty in the category allocation of flow direction and strength / SLP.
- 20CR SLP uncertainty (μ_{20CR}) – Uncertainty due to variations of SLP within 20CR ensemble members.

The five uncertainty components should be added in quadrature (Taylor, 1997) if the uncertainties are not linked with one another. However, the correlation matrix for the flow strength CBTA field shows that some of the uncertainty components are correlated (Figure 3.10). The most noteworthy is the correlation between parametric and category uncertainties, though this may well be coincidental as other points aside from the North Sea show little correlation (and parametric uncertainties are generally very small). The misfit / parametric and parametric / circulation uncertainties also don't show any persistent correlations when looking at other points besides the North Sea. Given that

these are different components of uncertainty with no clear reason for a relationship, these correlations are not considered when adding the uncertainties in quadrature.

However, a correlation between misfit and circulation uncertainty appears at many points and here there is a link because the circulation uncertainty is likely to take anomalies from nearby points in the CBTA field. Given the misfit uncertainty takes the standard deviation of neighbouring points some correlation can be expected.

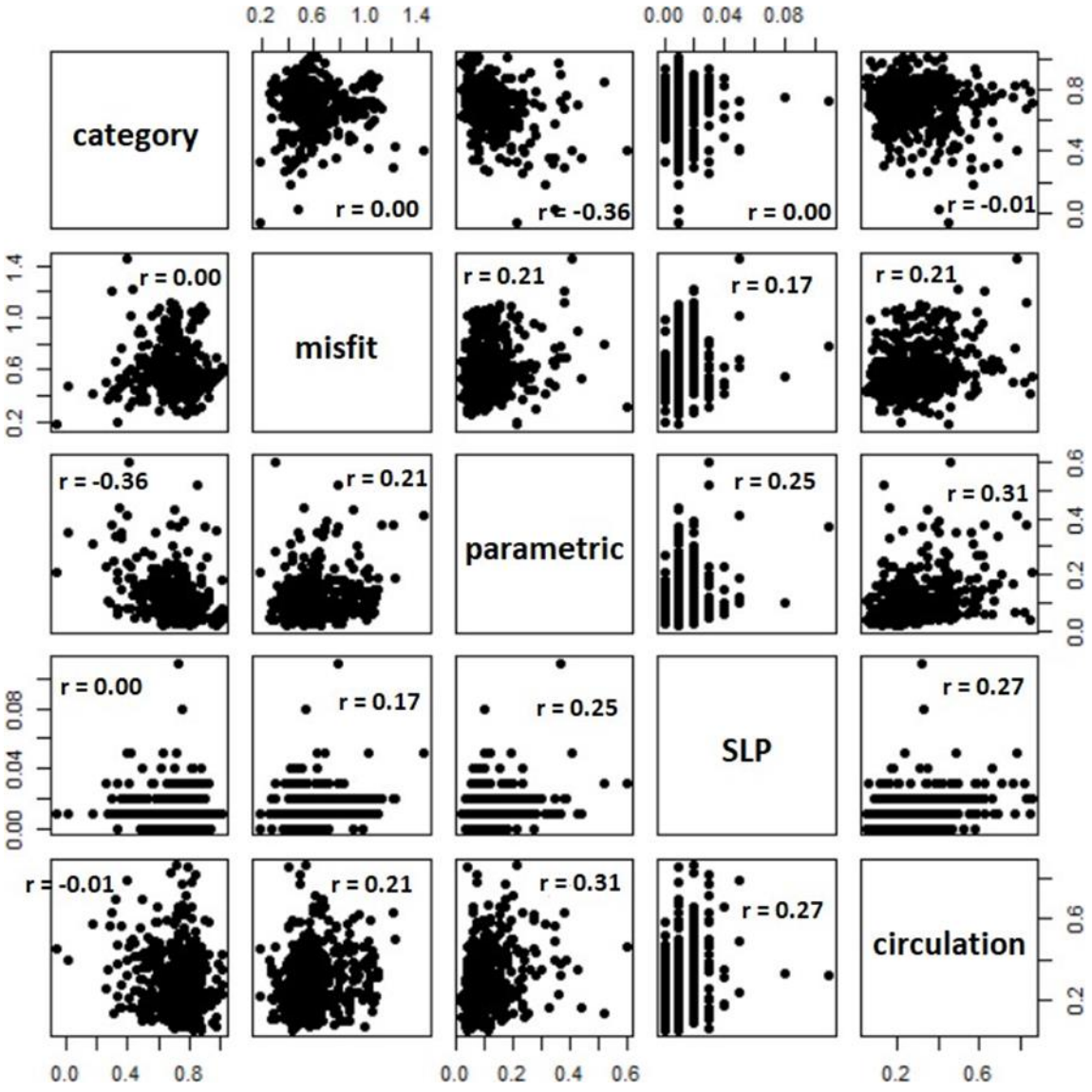

Figure 3.10: Correlation matrix between the 5 uncertainty components during the 1971-2010 period. Data taken from the North Sea point for the flow strength model.

Instead of just adding up all the components in quadrature, calculation 3.1 is done as follows:

$$\text{Total uncertainty} = \sqrt{\mu_{par}{}^2 + \mu_{cat}{}^2 + \mu_{mis}{}^2 + \mu_{20CR}{}^2 + \mu_{Circ}{}^2 - (\mu_{mis} * \mu_{Circ} * \rho)} \quad (3.1)$$

Where ρ represents the correlation between the misfit and category uncertainties for the month of the year in question and is part of the covariance calculation. The covariance is subtracted at the end of (3.1) to reduce the total uncertainty. If two uncertainty components are strongly linked and the correlation isn't taken into account, then uncertainties will be overestimated due to double accounting.

To check whether the uncertainty calculations work successfully, a comparison was made between the uncertainties and the residuals (20CR MAT – predicted MAT) in a few areas at and around the North Sea point. Then the total uncertainty estimates from the flow strength CBTA time series were binned into categories at 0.1°C uncertainty intervals with the interquartile range of each bin shown in the Figure 3.11a boxplot (for data covering the 1971-2010 period).

A good set of uncertainty estimates should see the total uncertainty increase as the residuals become larger, whilst the standard deviation of the residuals should also be similar to the uncertainty estimates as well (Bulgin, Embury and Merchant, 2016). In Figure 3.11a this relationship is evident with a cone shape shown in the box and whisker plot. The boxes represent the interquartile range of a bin although the standard deviation also generally increases, indicated by the red lines. The magnitude of the total uncertainty is slightly higher than the standard deviation of the residuals which is due to the steps taken to calculate the category uncertainty. In Section 3.3.1 it was stated that categories with more values in them have a higher weighting and these categories are likely to have higher uncertainties.

Figure 3.11a shows a clear steady increase in the standard deviation of the residuals as the total uncertainties increase (with the exception of some of the data sparse bins) with increasing uncertainty, meaning the total uncertainties for the flow strength CBTA field are of good quality. Similar promising results are also found for the SLP CBTA field in Figure 3.11b to demonstrate the uncertainty model works for both types of CBTA field.

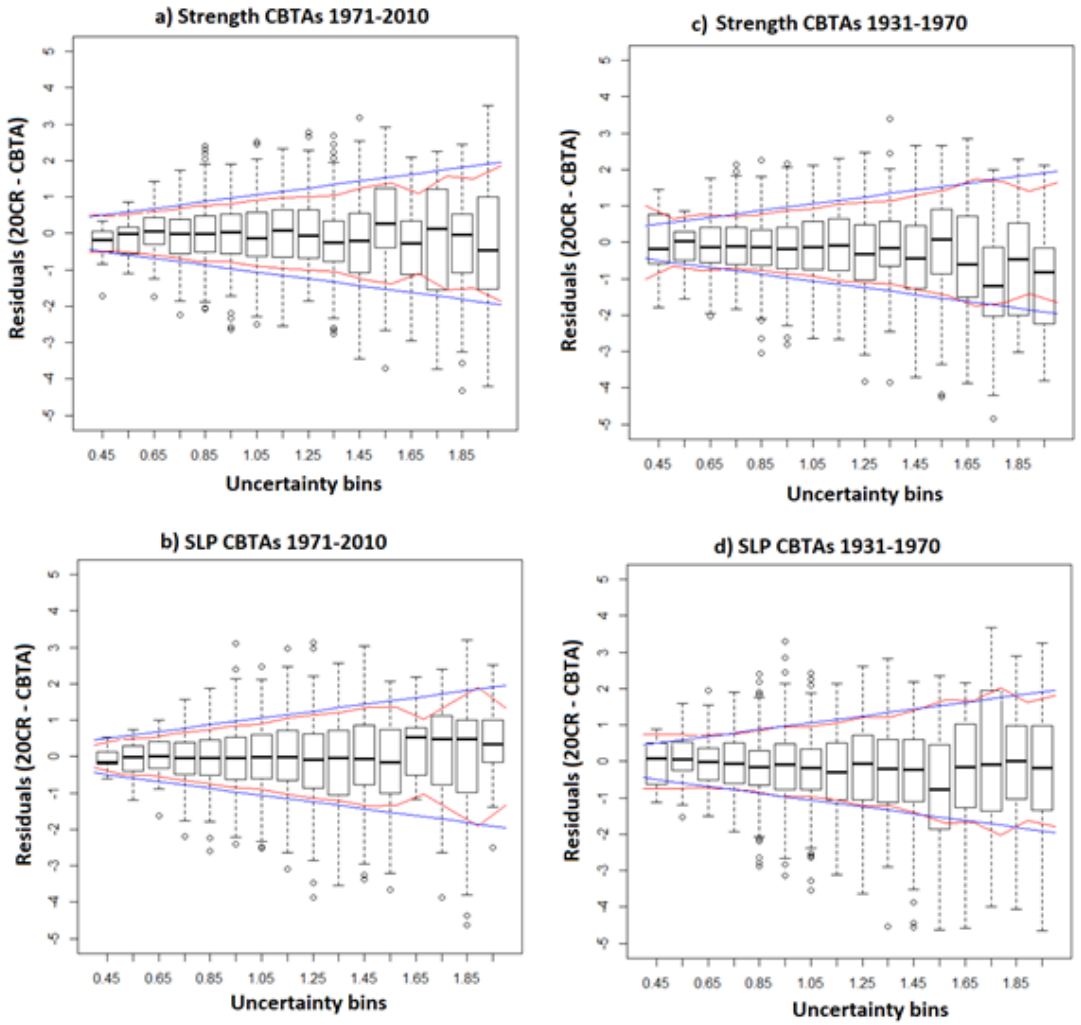

Figure 3.11: Panel a) boxplot containing data for all months during the 1971-2010 period with the total uncertainty on the x axis placed into 0.1°C bins and the distribution of residuals (also in °C) on the y axis. The bins represent the upper and lower quartile range of the uncertainty bins whereas the lower and upper extremes of the bins. The line in the middle of the boxes represents the median whilst the circles represent outliers. The red lines represent the standard deviations of the residuals in each bin and the blue lines represent the average total uncertainty of each bin; b) as with panel a) but for the SLP CBTA model. Panels c) and d) as a) and b) but for data from 1931-1970.

In panels c) and d) boxplots are shown for the 1931-1970 period which consists only of data from 1931-1970. Overall higher uncertainties are associated with higher variability in the residuals but there are likely to be some different circulation patterns which are not observed in the 1971-2010 period. The influence of climate change may mean uncertainties are underestimated, if a longer period of data is used to develop the model relationships then uncertainties would be larger as the variations in the anomalies would

include the warming trend. Figure 3.11c shows a climate change signal as the medians of the bins are often below zero (therefore indicating the model overestimates observed 20CR temperature in earlier years as expected).

The standard deviation of the residuals in Figures 3.11c and d) still increases with total uncertainty so even outside the 1971-2010 period this method still works well. This uncertainty information can also be used to combine the temperature estimates from the flow strength and SLP CBTA fields. The first step is to give priority to the temperature estimate with the lowest uncertainty from the flow strength and SLP CBTA fields. This is done by initially dividing the CBTA value by the total uncertainty squared (calculation 3.2). The total uncertainty is squared to increase the importance of the lower uncertainty estimates when combining the data. The individual weighting is expressed as a fraction by dividing by the total of the weighted values.

$$a_i = \left(\frac{1}{\sigma_i^2}\right) \Big/ \sum_i \left(\frac{1}{\sigma_i^2}\right) \quad (3.2)$$

Where:

a_i = Weighting for CBTA anomaly

σ_i = Uncertainty estimate of CBTA anomaly

The two CBTA time series for flow strength and SLP respectively will be strongly correlated, because both of the fields contain flow direction on the Y axis. As with calculation 3.1 the uncertainties from the flow strength and SLP based CBTA anomalies are added in quadrature. However, the covariance is added onto the quadrature calculation in 3.3:

$$\sigma_f^2 = \sum_i a_i^2 \sigma_i^2 + \sum_i \sum_{j(j \neq i)} a_i a_j \sigma_i \sigma_j \rho_{ij} \quad (3.3)$$

Where:

σ_f^2 = Uncertainty of weighted mean

a_i = Weighting for CBTA anomaly

σ_i = Uncertainty estimate of CBTA anomaly

ρ_{ij} = Correlation between two CBTA time series

Due to quadrature summation, the uncertainty for the weighted mean time series can be lower than the uncertainties from the individual flow strength and SLP time series. The weighted mean should improve the time series of CBTAs so the decrease in uncertainty is expected, as the SLP and strength CBTA time series are not perfectly correlated (overall r = 0.78). Due to the use of a weighted mean however, the amplitude of this time series compared to the 20CR anomalies is reduced despite the decrease in uncertainty. In Figure 3.12 it can be seen that the slope of the regression equations is over 1 giving indication of the reduced amplitude of the combined model. The slopes are also bigger than those seen for the individual models as shown in Table 3.1. To adjust the amplitude, The CBTAs are multiplied by the monthly slope values with examples shown in Figure 3.12.

Model	FEB	MAY	AUG	NOV
Strength	1.06	0.87	1.11	1.04
SLP	1.11	1	1.05	1.28
Combined	1.12	1.12	1.21	1.43

Table 3.1: Slope of the regression applied to the CBTAs and 20CR MAT for 4 different months. The results for the combined CBTAs, flow strength CBTAs and SLP CBTAs are shown. A plot of the regressions for the combined model is shown below in Figure 3.12

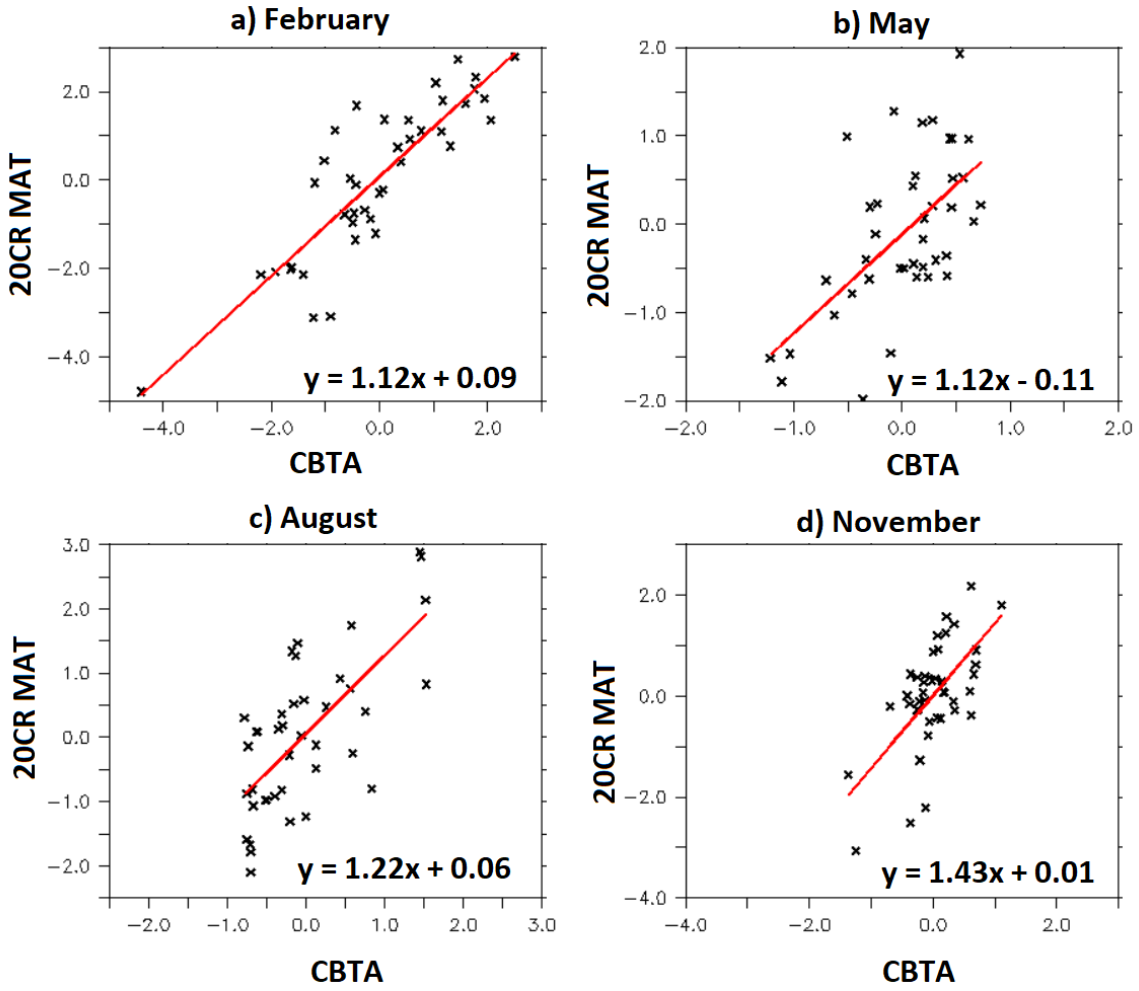

Figure 3.12: Linear regressions of MAT anomalies from the combined model (CBTA) and 20CR MAT anomalies for 4 different months of the year during the 1971-2010 period. The regression lines and equations are also shown for the 4 months. When the slope coefficient is greater than 1 the amplitude of the combined CBTAs are smaller than the 20CR MAT anomalies.

To show that the uncertainties are still being accurately calculated when the temperature estimates are combined, Figure 3.13 shows a boxplot for the 1971-2010 and 1931-1970 data of the combined CBTA model. Again, there is still a general increase in the uncertainty estimates when the standard deviation of the residuals is higher. The ratio of the uncertainties to the standard deviation of the residuals is 0.93 during the 1971-2010 period and the standard deviations of the residuals for each uncertainty bin (red lines) are close to the expected values (blue lines). The only exception to this is for the smaller uncertainties with the data from 1931-1970 period (Figure 3.13b) indicating that the smallest uncertainties from the 1971-2010 period are underestimated to an extent.

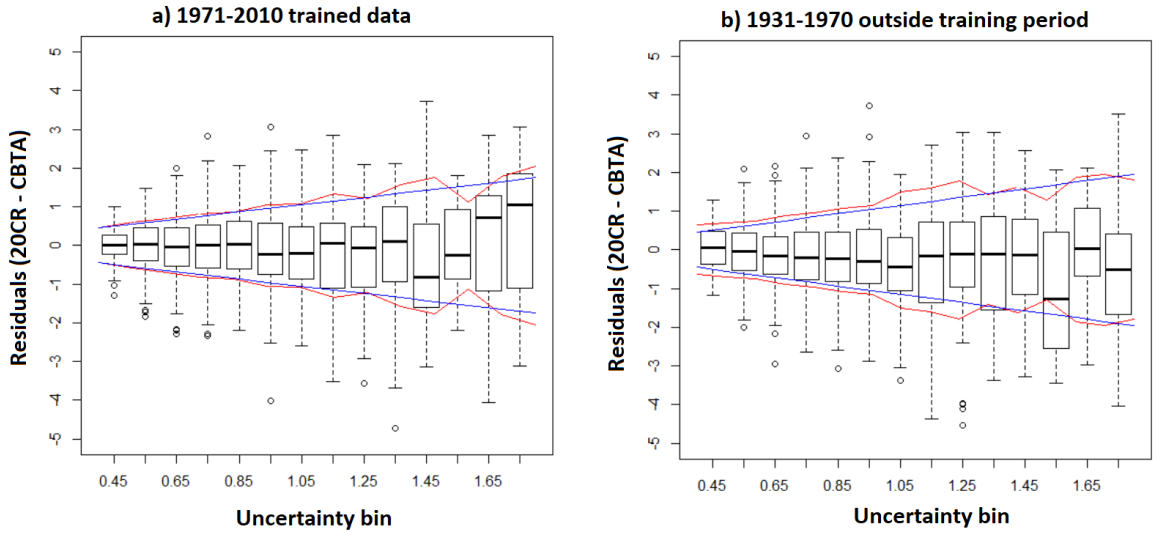

Figure 3.13: As Figure 3.11 but boxplots for the combined CBTA time series during a) the 1971-2010 period and b) with the 1931-1970 period. The blue lines represent the expected standard deviations of the residuals given the uncertainty estimate.

Figure 3.14 shows the time series of the weighted means plotted against the 20CR anomalies for the period of 1881-2010 at the North Sea point. The error bars appear smallest when a strong correlation with observed temperature is seen (e.g. February in Figure 3.14a) giving another indication that uncertainties associated with this method are being captured successfully. Outside the 1971-2010 period some outliers (particularly large differences not explained by uncertainties) are evident such as those seen in February 1929 and 1956 but both of these had unusual circulation patterns. For months outside the DJF period, the weaker relationship between temperature and atmospheric circulation is evident especially for May which contains a large uncertainty range in comparison to the variability of the predicted temperatures.

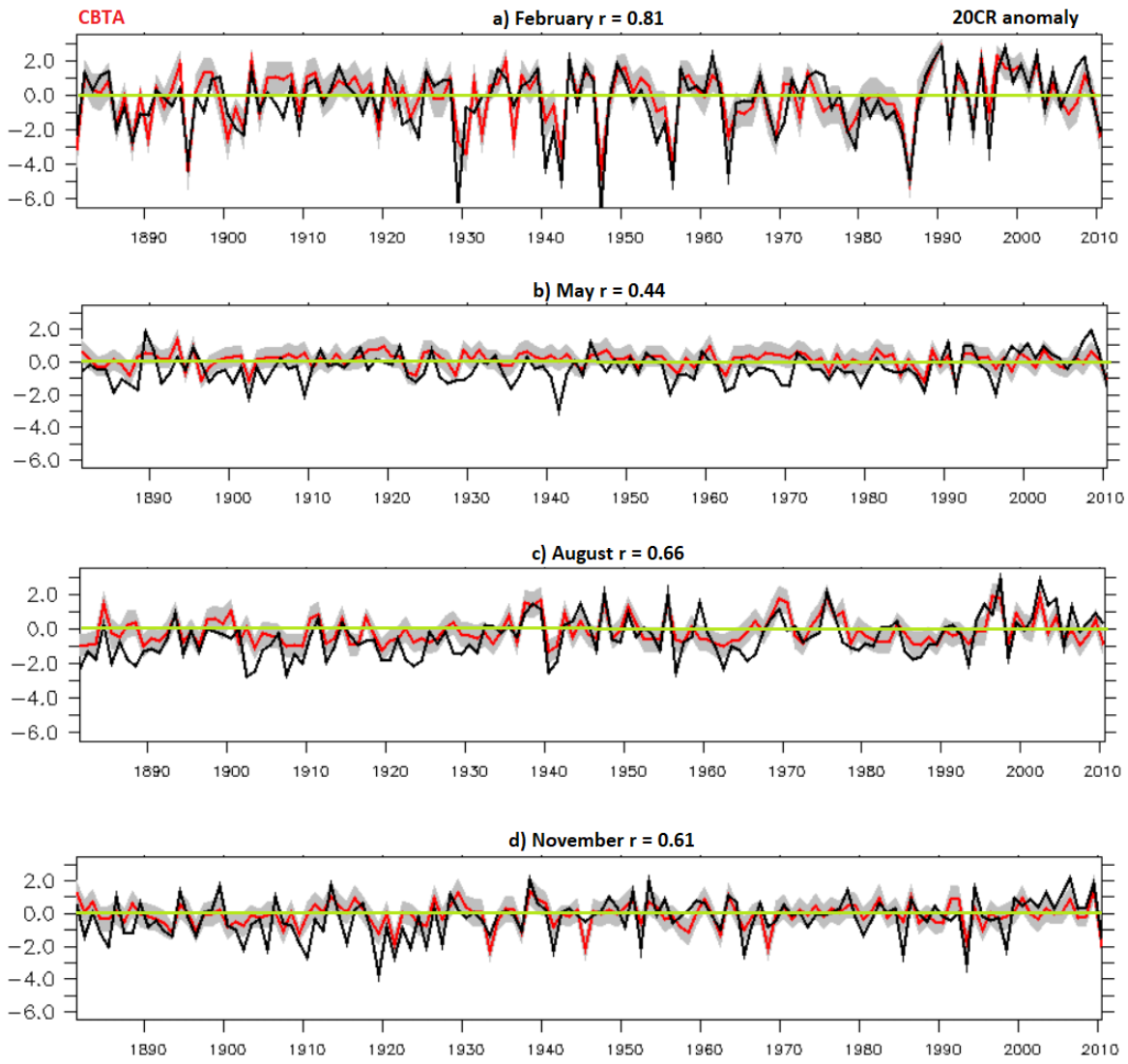

Figure 3.14: Time series of MAT anomalies at the North Sea point for a) February; b) May; c) August; d) November. Predicted anomalies shown in red and 20CR 2 metre air temperature anomalies in black. Uncertainty bounds of predicted anomalies shown in grey (to 1SD).

Over the whole time series some interesting features occur. For example, during the 1900's Februaries contain CBTAs notably lower than the 20CR MAT anomalies and the CBTAs are not accompanied by large uncertainties in the predicted temperatures. Persistent negative residuals are also seen during August in the 1920's which fall outside the uncertainty bounds. The time series analysis in this section however represents a single point in the North Sea and it is unclear at this point whether the time series here is representative of the variability seen over a larger region.

Finally, in Figure 3.15, bar charts of the different uncertainty components over 4 periods of the year are shown for different 40-year periods. For all periods of the year the dominant uncertainty components are the category and misfit uncertainty components (explaining 70-80% of the total uncertainty) meaning meteorological factors other than flow direction, SLP or flow strength are contributing most to residual variability. The contribution of parametric uncertainty in contrast is small (typically 10% of the total uncertainty) so issues relating to the method are minimal during the 1971-2010 period.

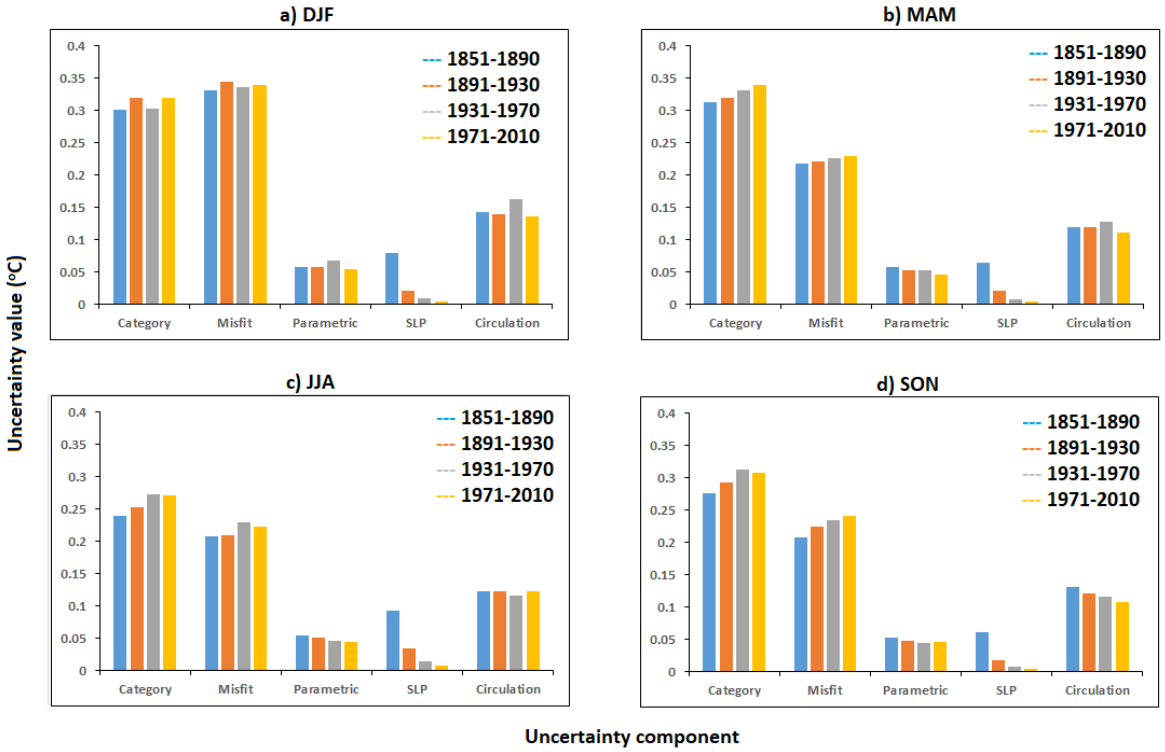

Figure 3.15: a) Bar charts of the five uncertainty components for different 40 year periods in the 20CR. Data shown for 4 different periods with panel a) showing the DJF period; b) MAM period (March to May); c) JJA Period (July to August) and d) SON period (September to November).

The contribution of each uncertainty component to the total remains similar outside of the 1971-2010 period also. Interestingly the parametric uncertainty component still only contributes to around 5% of the total uncertainty for periods before 1971-2010. It was noted in Section 3.2 that parametric uncertainties are particularly high where there is no data in the CBTA field. Therefore, the low parametric uncertainties seen with data before 1971-2010 period suggest that the atmospheric circulation patterns during earlier 40-year

periods have also been seen during the 1971-2010 period. The 20CR SLP uncertainty is even smaller suggesting that there is high confidence in the SLP data since 1851 in the North Sea region. Comparisons with station data in this area are shown in Section 5.2 to see whether the 20CR SLP uncertainties may be an underestimate.

The total uncertainty has been calculated for the time series in Chapter 2 and the uncertainty estimates appear sensible (the distribution of the residuals is well represented by the uncertainty estimates), especially during 1971-2010 period (but also during other periods to an extent as well). This uncertainty method can be readily applied to almost any other marine location (shown in Chapter 4) and is also useful for combining the SLP and Strength CBTA time series to produce a final CBTA series. The improvements in the correlation coefficient aren't particularly large here because the role of average SLP over the whole region in itself isn't influential unlike flow direction and strength, but this is not the case in other areas of the world.

3.5 Conclusions

In this chapter uncertainty estimates were calculated for predicted MAT anomalies based on atmospheric circulation for a point in the North Sea. The important contributions to uncertainty were identified, estimated, and combined to form a total uncertainty estimate for each CBTA time series. The process of creating a CBTA field was first described and used to define the parametric uncertainty. This only made up a small proportion of the total uncertainty estimate. The largest component of uncertainty in the model was found to be the category uncertainty (standard deviation of anomalies in an area of a CBTA field). This indicates that other factors besides flow direction, strength and SLP are contributing to the most residual variability during the 1971-2010 period. The SLP and parametric uncertainties were found to be small throughout.

Overall the dispersion of the residuals increases with the total uncertainties during the 1971-2010 period, indicating the key components of uncertainty were being captured. However outside of the 1971-2010 period this increase was rather less clear. A reason for this could be a signal from climate change as taking a 40-year period won't capture this fully. The uncertainties allowed for the possibility of producing a weighted mean time

series that combined the influences of flow direction, strength and SLP into one CBTA time series which yielded some small improvements at the North Sea point; however, Chapter 4 will show that the weighted mean approach is particularly beneficial in other regions. The next step is to examine how well this process works worldwide and begin to examine the contribution of atmospheric circulation to past MAT air temperature variability across the world oceans, using 20CR data.

Chapter 4 Global relationships between MAT and SLP based on the 20th Century Reanalysis

4.1 Introduction

In Chapters 2 and 3, the methods used to produce CBTAs were introduced and an example was shown of how to create a time series of flow direction and strength/SLP based CBTAs at a point in the North Sea. The uncertainties of the CBTA time series were calculated and used to combine the CBTA estimates from the flow/direction strength and flow direction/SLP time series. Encouraging results were found with strong correlations ($r > 0.7$) between the CBTAs and 20CR MAT anomalies from 1881-2010. It was also concluded that these were accompanied by suitable uncertainty estimates to help interpret the time series of data. This next chapter takes the methods of developing CBTAs introduced in Chapters 2 and 3 and applies them globally. The global application of these methods will help answer the key questions for this section:

1) Can the model developed in Chapters 2 and 3 be applied successfully? Success here is regarded as model output that demonstrates there are strong ($r > 0.7$) connections between MAT and atmospheric circulation with realistic uncertainty estimates.
2) Can other influences on 20CR MAT be exposed when removing the estimated effects of atmospheric circulation on temperature?
3) Do the relationships between temperature and atmospheric circulation change over time?

Whilst many studies have explored connections between temperature and atmospheric circulation, few have developed a time series analysis out of these relationships. Time series analyses of air temperature variability using CBTAs have been limited to land regions over Europe (Chen, 2000; Osborn and Jones, 2000; Moberg *et al.*, 2003; Peña-Angulo *et al.*, 2016). By developing CBTAs over the world's oceans and subtracting them from the 20CR MAT anomalies; it is hypothesised that this could reduce the level of variability to reveal other potential influences on MAT besides atmospheric circulation.

The various plots in this chapter will provide an insight into the three questions highlighted above but the following three sections will focus on one in particular. The chapter will first show some global maps to assess the model and its uncertainties to answer question 1 (Section 4.2). Section 4.3 then looks at time series of CBTAs across the world's oceans and to try and see whether different influences of global MAT can be identified (question 2). Section 4.4 then looks at time series of CBTAs over a small region (specific grid points) and attempt to answer whether the relationships between temperature and atmospheric circulation are changing over different locations (question 3). Some conclusions are then provided in Section 4.5.

4.2 Global model assessment

This section goes through some of the decisions made for developing the model, presents some correlation statistics and then discuss the uncertainties.

4.2.1 Developing the model

The first step for the global analysis was to compare the flow parameters from the 20CR product to those calculated in Chapter 2. This step was performed to check whether the calculations in Chapter 2 are suitable for defining atmospheric circulation patterns, with focus on the westerly and southerly flow strength values. The wind data taken from the 20CR is wind at 10 metres above sea level and the flow parameters are calculated from the 4-point grid configuration in Figure 3.7b. Strong correlations between 20CR winds and those derived from atmospheric circulation parameters were found especially away from the local influences of land.

Global maps of the correlation coefficients for westerly flow and southerly flow are plotted in Figure 4.1. For the westerly flow parameter (panel a), correlation coefficients above 0.80 are seen over most grid boxes away from the equator and areas close to land. Local effects such as topography may play a role in the lower correlation coefficients over coastal areas, whilst near the equator, calculating the flow components accurately is not possible. Future map plots in this chapter therefore do not consider the model output between 10N and 10S around the equator.

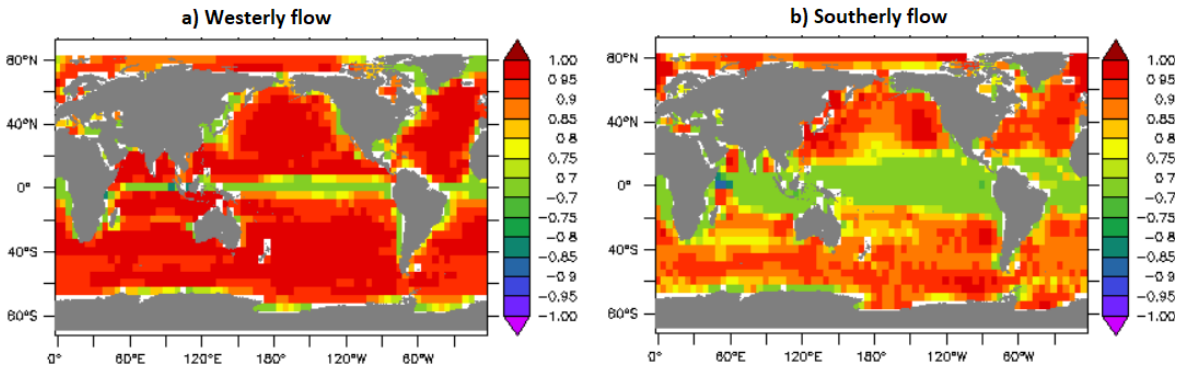

Figure 4.1: Correlation between westerly and southerly flow strength parameters defined in Chapter 2 and the 20CR westerly and southerly winds at a 10-metre height. Correlations generated from data covering 1971-2010.

For the southerly flow parameter (4.1b), correlations between the 20CR southerly wind component and those calculated from the pressure fields are a bit lower than for westerly flow. This is because the southerly flow components over high latitudes are often much weaker than the westerlies that typically dominate over these regions (especially during winter months), so southerly flow components are more sensitive to grid configuration changes. Therefore, some differences between the correlations of the two different time series can be expected. Plots for other time periods look very similar to those shown in Figure 4.1.

The method used to produce a time series of CBTAs in Chapter 3 (combining strength and SLP CBTAs using grid pattern 2) was implemented globally over 5° lat/lon ocean grid points. The CBTAs for 3 different months can be seen in Figure 4.2. Panel a) displays the CBTAs for December 2010 with the anomalies showing many similar patterns to the 20CR anomalies in panel b). Over the North Atlantic for example, a clear tripole pattern can be seen in both panels (a - CBTAs, b – 20CR MAT), with positive anomalies over the Greenland and tropical North Atlantic regions. A region of negative temperature anomalies extending from roughly the SE USA to the UK can also be seen in both temperature anomaly plots. In the North Pacific there is a pattern of negative anomalies to the south of Alaska and positive anomalies to the South of Siberia. Similar patterns between both panels are seen in other regions also. From panel a) the anomalies off the west coast of South America indicate the presence of a La Niña in the equatorial Pacific, a

large region of above average MAT in the South Atlantic and around Australia. In some regions the uncertainties themselves are uncertain as there is little variation in the overall atmospheric circulation pattern. In low latitudes of the eastern Pacific for example the only variations in atmospheric circulation are minor changes in the intensity of easterly winds from month to month. Judging by the uncertainty panels in Figure 4.2 however this does not appear to be a problem.

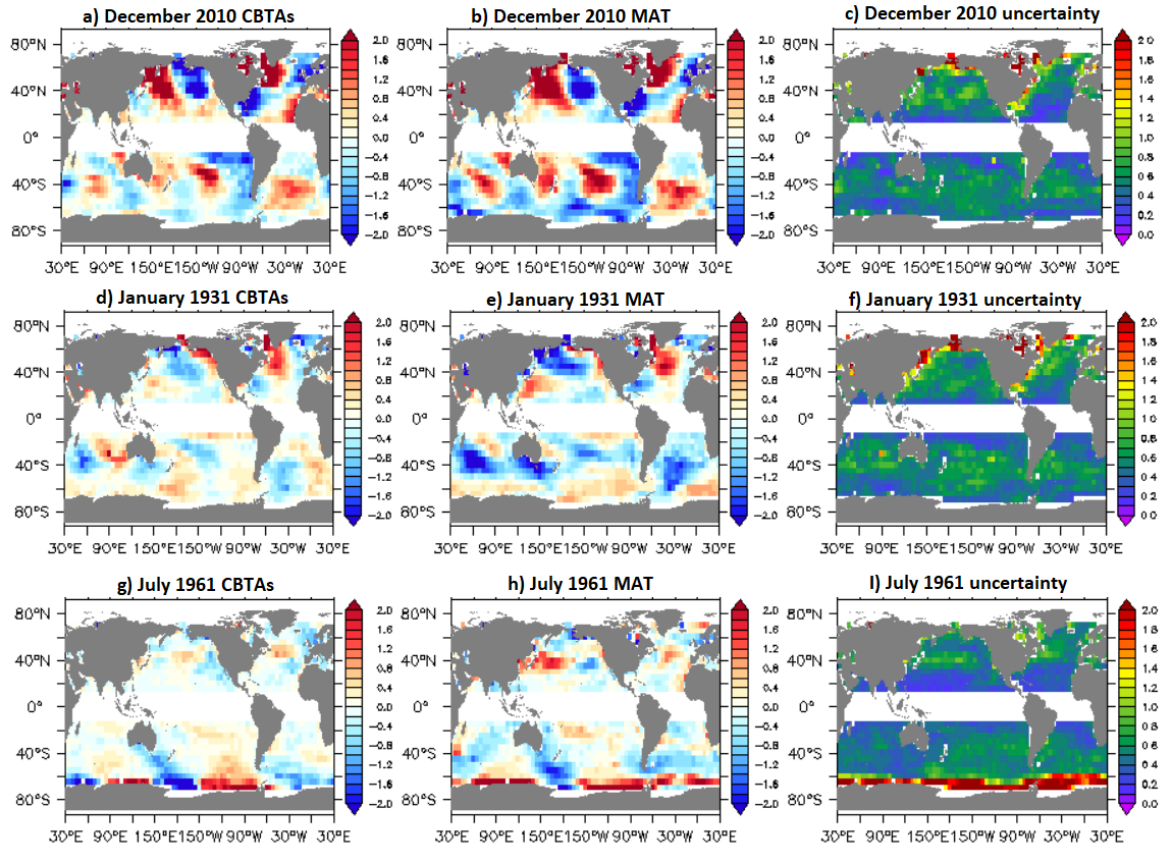

Figure 4.2: Temperature anomalies (°C) for three example months in the CBTA time series and the 20CR. Panels a), b) and c) show anomalies for December 2010 for the CBTA model, the 20CR model and total uncertainties (1SD) from the CBTA model respectively. Panels d), e) and f) present the same information but for January 1931. Panels g), h) and i) are for July 1961. All anomalies are from the 1971-2010 climatological average.

The CBTA model can still work well with months outside the 1971-2010 period as panel d) shows for January 1931. The patterns of CBTAs over the North Atlantic are again very similar to those seen with the 20CR anomalies. In the North Pacific both the CBTAs and 20CR anomalies agree that temperatures were generally below average whilst an El Niño

event is indicated from the anomalies over the Pacific in both plots. There are some notable differences in the anomaly patterns seen over the Southern Hemisphere however with the extent and magnitude of below average temperatures in the CBTA time series not as strong as those seen in the 20CR (panel e). Differences between the CBTAs and the 20CR anomalies are more profound in the third month selected for this figure (July 1961), particularly for the South Indian and North Pacific Ocean basins. The more extreme anomalies in the far Southern Ocean however are seen in both panels, these are also accompanied by increased uncertainty estimates (panel i).

The CBTAs in Figure 4.2 were developed by combining the CBTA fields from flow strength and SLP, with a breakdown of the correlations for these individual CBTA fields is shown in Figure 4.3. Both the correlation fields for flow strength and SLP are similar for the DJF period (a and b) but the flow strength variable is not linked to the average SLP value. The performance of both models varies with the average SLP value appearing to be more influential over lower latitude regions (c). Due to these differences the decision was made to combine the two estimates using the total uncertainty estimates as explained in Chapter 3. The result of combining these two CBTA estimates is an improved model.

Improvements over most areas are slight but the blue areas in (d) show where the combined model works better than the flow strength model. Improvements are notable over many areas of the Southern hemisphere and NE North Atlantic. The improvements of the combined model also give another indication that the total uncertainty estimates are realistic (otherwise the model may get worse if not). This is because the combined model gives priority to the CBTA model with the lowest uncertainty estimate as it is assumed to be more accurate. The histogram of panel d (e) shows that combined model most often has a correlation coefficient 0.025-0.1 higher than the flow strength model. In a small number of cases the flow strength model is still better and this may be because in these such instances flow strength is much better at predicting temperature then the average SLP (hence weighted means become less beneficial). However, the combined model generally improves the correlations seen from the individual CBTA estimates.

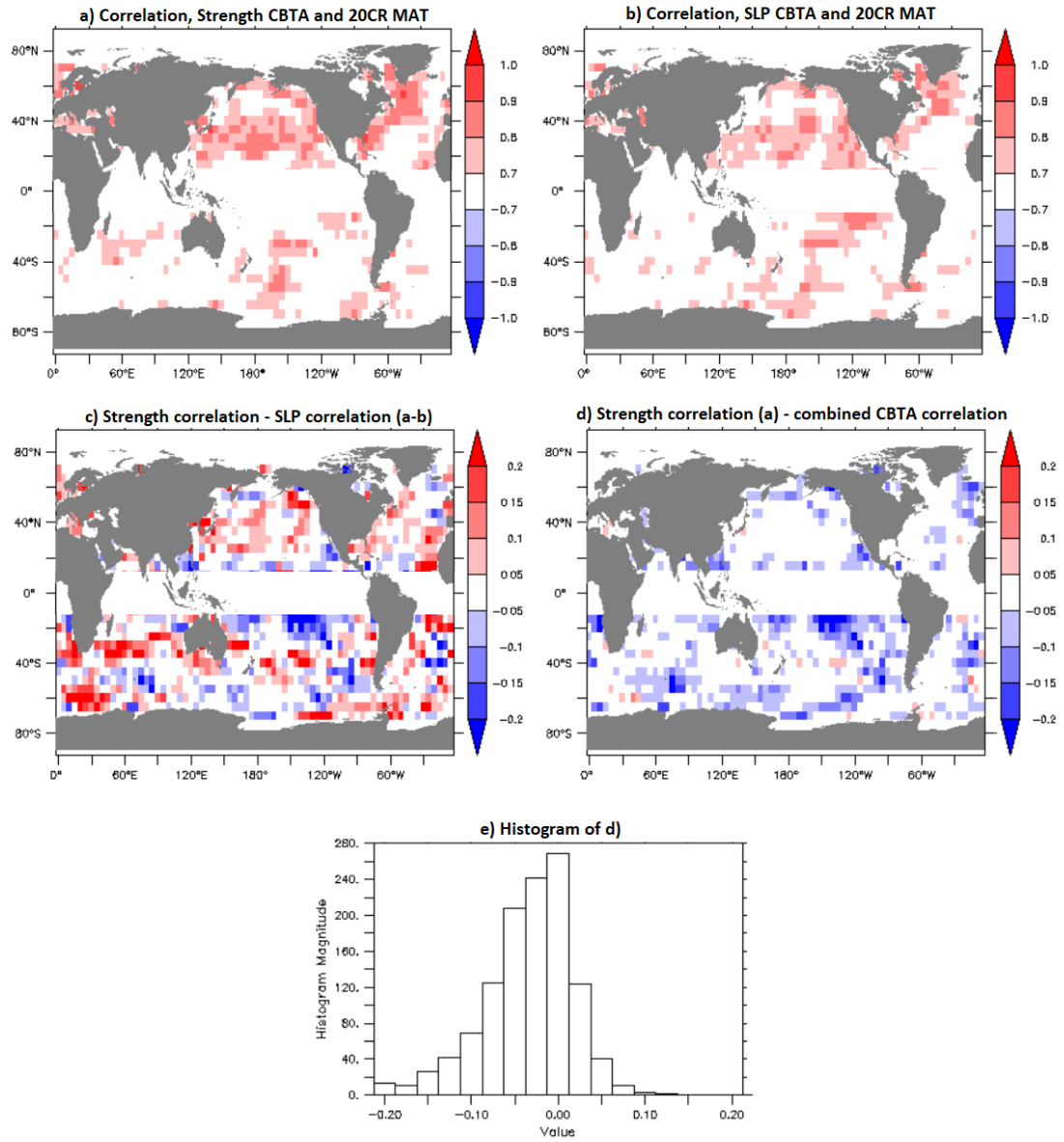

Figure 4.3: a) DJF correlation map for the flow strength CBTA fields; b) as with panel a but for the SLP fields; c) difference in the correlation coefficients for the SLP and flow strength fields, blue areas show where the SLP model performs better and vice versa; d) the differences between the flow strength correlation coefficients and those from the combined model. Blue boxes indicate where the combined model performs better; e) Histogram of the differences from panel d). Units are dimensionless.

The correlations in Figure 4.3 show the values of the individual CBTA fields for the DJF period. Figure 4.4 shows correlations for the combined model and this works all year round in a number of places. These plots show the correlations between the CBTAs and 20CR anomalies for each season for both the 1971-2010 period and the 1931-1970 period

(where data is not used to build the model in this section). For the 1971-2010 period, correlations of above 0.7 are seen over many areas of the world's oceans. In panel a) for example the model performs very well over large parts of the North Atlantic, North Pacific and equatorial Pacific. Model performance is particularly strong over the NW North Atlantic with correlation coefficients ~0.9 indicating atmospheric circulation is a dominant influence on MAT in this region during the 1971-2010 period.

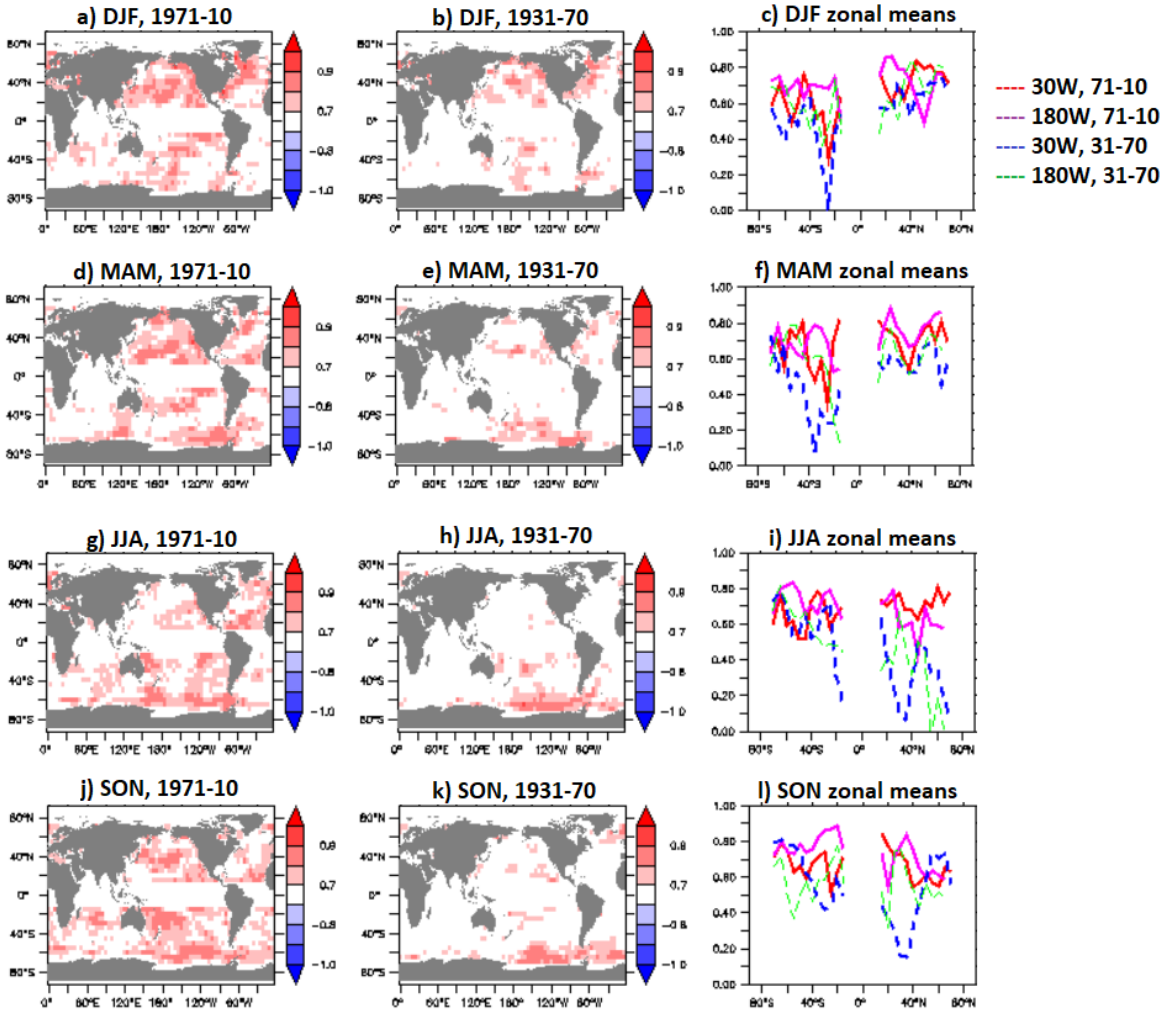

Figure 4.4: Correlation coefficients between the CBTAs and 20CR MAT anomalies for different time periods and seasons. Panel a) shows the correlation coefficient during the DJF period from 1971-2010. Panel b) shows the DJF correlation coefficient from 1931-1970 and panel c) shows the variation of the correlation coefficients over two lines of longitude (30W and 180W); d-f) As with panels a-c) but for the MAM; Panels g-i) JJA; j-m) SON.

Previous literature has indicated that the role of atmospheric circulation is strongest during the DJF period across the Northern hemisphere (Osborn and Jones, 2000; Vautard and Yiou, 2009). However model performance is also very strong over much of the North Pacific and North Atlantic during the MAM period (panel d), with similar levels of success seen during the SON period also (panel j). Outside of Europe, there appears to be some areas of the northern hemisphere where atmospheric circulation is influential outside the DJF period. The only areas where the model doesn't perform as well during the DJF period are over the central North Atlantic, Southern Atlantic and North Indian Ocean areas ($r < 0.5$).

The middle panels of Figure 4.4 however show that the correlation coefficients are generally weaker for the period 1931-1970 than those seen during the 1971-2010 period. A drop in the correlation coefficients should be expected given the middle panels represent months outside the 1971-2010 period used to build the model but the drops are large over many areas (r values over 0.2 lower in places). This is shown by the zonal mean plots in the right-hand columns in Figure 4.4. Only parts of the North Atlantic and Pacific during the DJF period and the South Pacific (in general) during the JJA period are notable exceptions as the correlation coefficients for both periods are similar. Drops in the correlation coefficient from the 1971-2010 to 1931-1970 period are particularly large over both hemispheres during the JJA period (i), with the far Southern Ocean being an exception (though data coverage is sparse here).

The results in this section however are encouraging and it appears that the spline method is the best to take forward for this thesis after a comparison between the methods used to develop CBTAs. In Chapter 2 the method of calculating CBTAs built from the Jones *et al.,* (2014) approach and a forward selection stepwise regression approach were introduced. A comparison between the correlation coefficients from the two methods was made, with the differences shown in Figure 4.5 for data during the 1931-1970 period. The figure shows that the spline model performs noticeably better for all seasons. Correlation coefficients during the 1931-1970 period are often 0.1 higher or more for the spline method then the regression method. For the 1971-2010 period model performance is similar (shown in Appendix C) but the better performance of the spline model during

earlier years is key and demonstrates the method is more suitable for time series analysis of CBTAs.

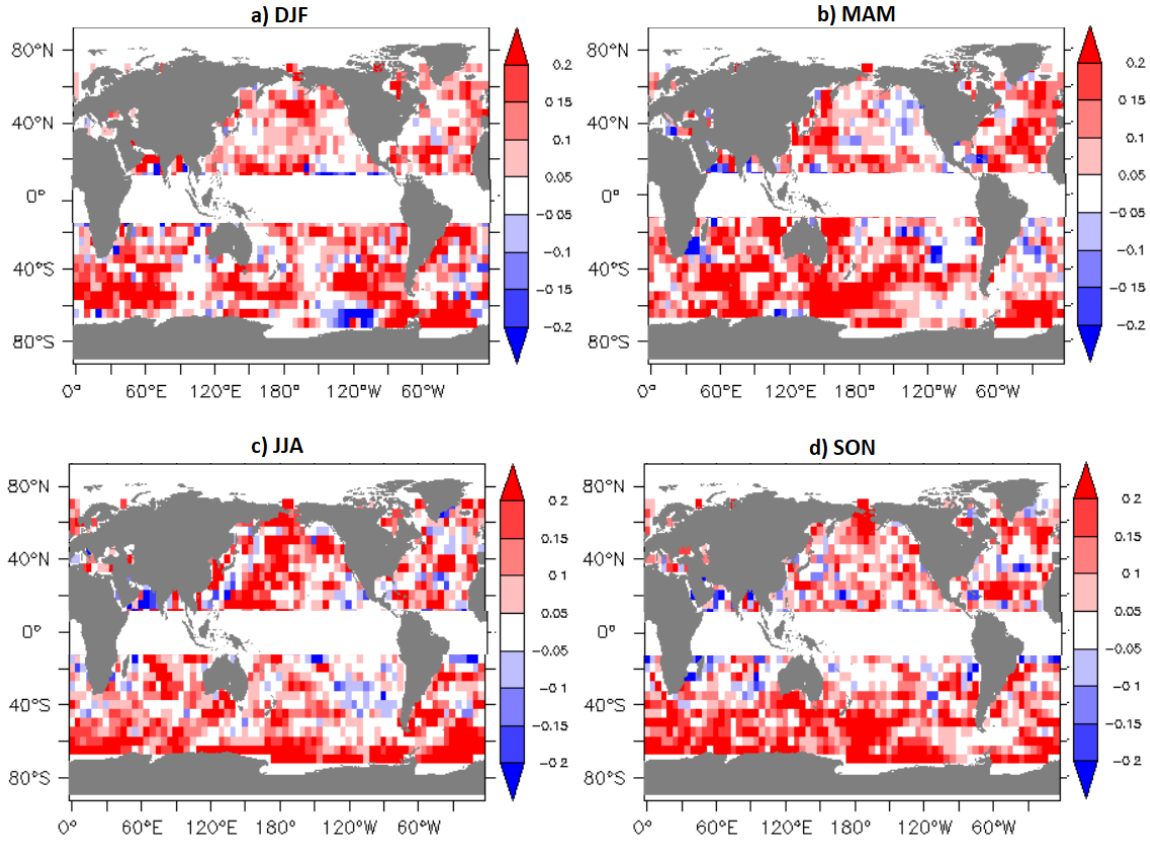

Figure 4.5: Comparison between the correlation coefficients from the CBTA method and regression method for each season. Red grid cells indicate where the CBTA method performs better whereas blue cells indicate where the regression method is best. White cells show where there is little difference in performance between the two methods. Results are shown for the 1931-1970 period.

For the CBTA method there is also the issue of which grid configuration to choose to calculate the flow parameters. For this thesis chapter the results are presented using flow parameters calculated from the grid configuration in Figure 3.7b (grid pattern 2). However, there are 5 other additional 'conventional' grid configurations shown in Figure 3.7. There were two reasons for examining the effect of different grid patterns on the CBTAs. First is that many of the studies examining the role of atmospheric circulation on temperature still used the Jenkinson and Collison, (1977) grid pattern to define flow parameters and haven't explored whether other grid patterns are better suited for

predicting temperature. Secondly it is well established that in some areas closer to the equator, temperature responds to variations in atmospheric circulation on much larger scales. Over ENSO regions for example, one of the best predictors of SSTs is the SLP difference between Tahiti and Darwin (Xu, Takeuchi and Ishidaira, 2004).

CBTAs were produced from flow parameters, calculated from each of these grid configurations. The correlations of the time series of these CBTAs were then compared. The results are shown in Figure 4.6 for selected comparisons and these show that the levels of performance of the model are similar for all grid configurations. Panels a) to d) show little geographical pattern in the correlation coefficient differences. There is a small improvement in model performance when using larger grid configurations (correlation coefficient increases of < 5%, c and d) but nothing significant (students t-test, $p > 0.05$). There is only the hint at some genuine improvements over parts of the Southern Hemisphere and the Gulf of Mexico (d).

Overall these results are consistent with those found in the Falklands by Jones, Harpham and Lister, (2016) and are encouraging because they suggest the model output is not sensitive to the grid configuration, providing the latitude/longitude spacing is not too large. At daily time scales the grid pattern chosen may become more important as small areas of low pressure may fall within the grid points themselves. Although spatial variations in the role of atmospheric circulation are evident, there is no clear differences evident in the correlations shown in Figure 4.6. Therefore, this thesis continues to present results from grid pattern 2. The only issue with the results presented in this section is the decrease in the correlation coefficients when looking at the data from 1931-1970. The uncertainties can provide an insight into this and some will be provided in the next section, to demonstrate that this is not associated with any issues surrounding the method taken.

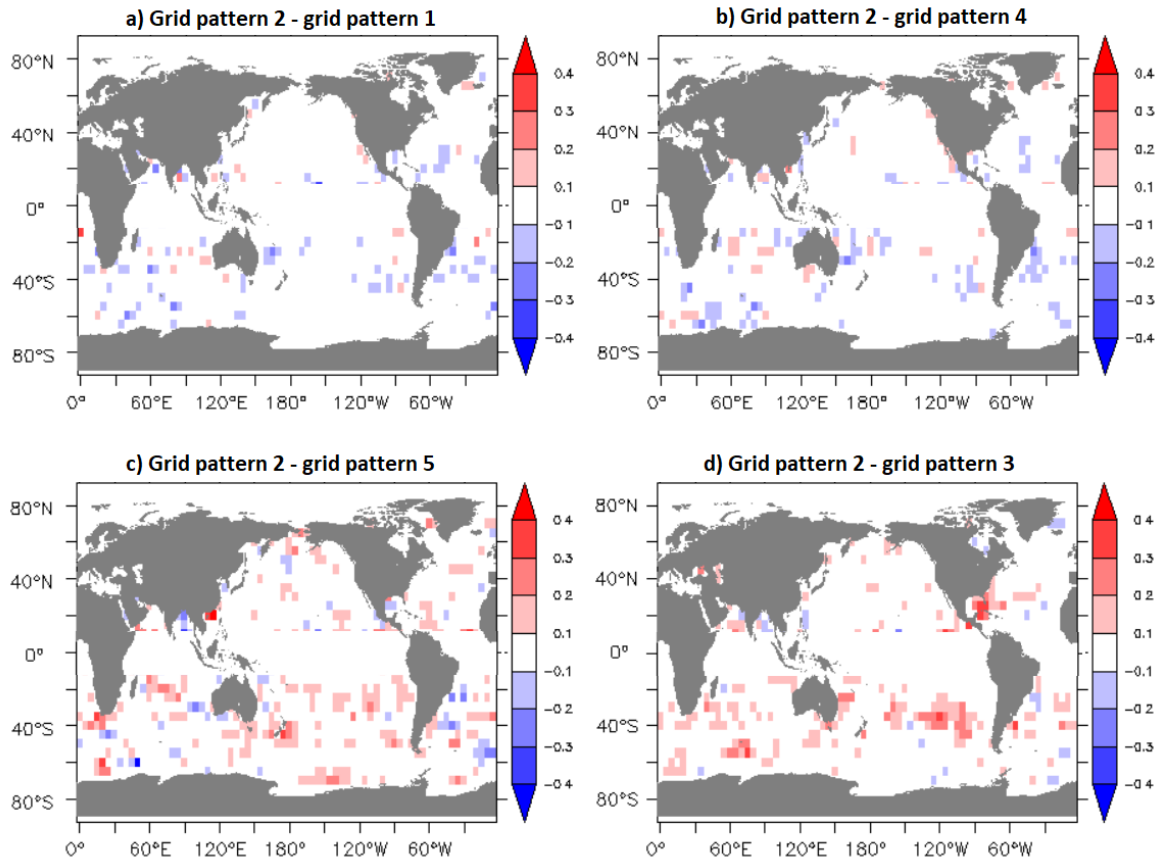

Figure 4.6: Differences in correlation coefficient between CBTA time series calculated from different grid configurations (see Figure 3.7). Red cells indicate where CBTA time series from grid configuration 2 (Figure 3.7b) has a lower correlation coefficient, whilst blue colours show where the alternative grid configuration performs worse. Plots are for the DJF and 1971-2010 period.

4.2.2 Global uncertainties of the CBTA model

Uncertainty estimates were calculated for every CBTA value. Five uncertainty components were presented in Chapter 3 and combined to produce the estimates shown in this section. At the North Sea point it was concluded based on Figure 3.12 that a useful uncertainty model had been developed at that location as the uncertainties were consistent with the standard deviation of the residuals.

The uncertainties were first assessed by looking at the ratio of the total uncertainty to the standard deviations of the residuals. These ratios are shown in Figure 4.7 for both DJF (a) and JJA (b), with the blue areas showing were the uncertainties of the model are underestimates and the red areas where they are overestimates. White regions show

areas where the magnitude of the uncertainty estimates is similar to the expected value. For the DJF period it can be seen that most of the uncertainty ratios (~80%) are between 0.85 and 1.15 due to the amount of white shading and from the histograms. There appears to be some structure to the uncertainty ratios with the DJF period containing more ratios close to 1 away from the far Southern Oceans. Meanwhile, during the JJA period there appears to be more underestimates in the Northern Hemisphere (most prevalent in the Pacific) and overestimates in areas surrounding Australia. The causes of this pattern are unclear but the uncertainties generally tend to be more accurate when the relationships between the CBTAs are 20CR anomalies are stronger.

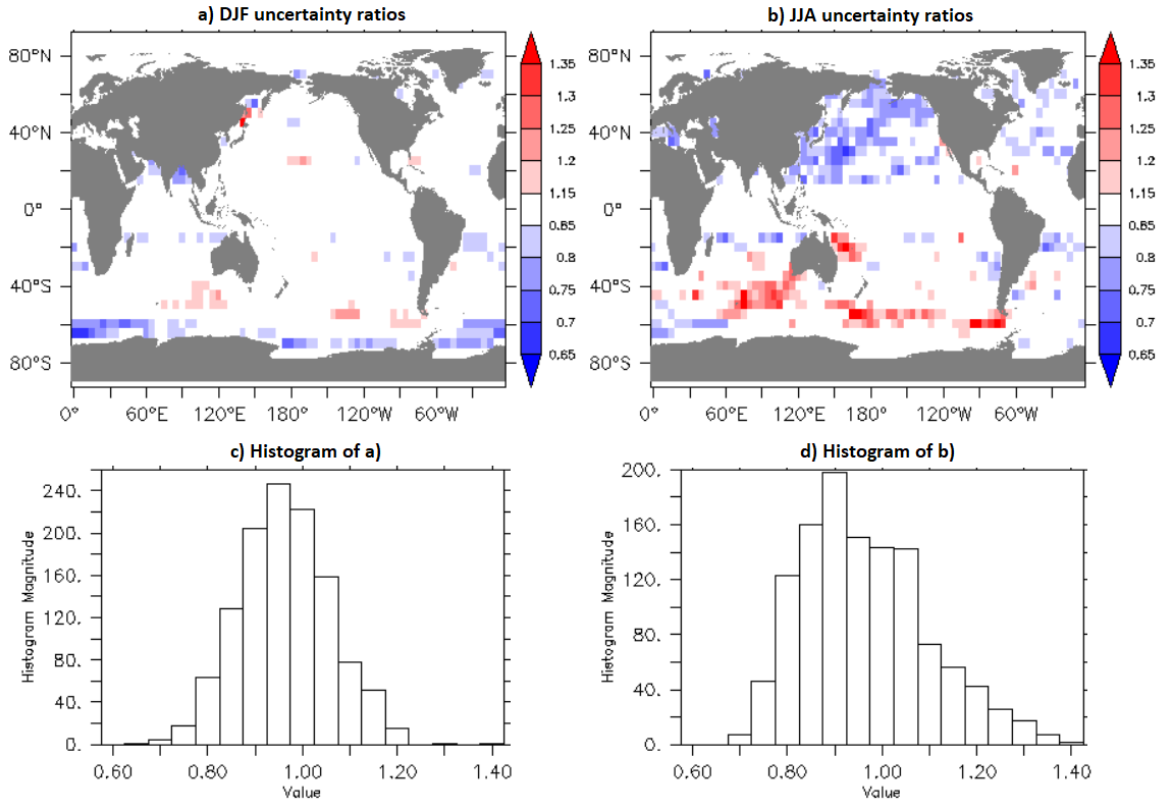

Figure 4.7: A plot of the ratio of the standard deviation of the residuals (20CR MAT – CBTA) to the total uncertainty estimates. Red (blue) areas indicate where uncertainties in the CBTA model are overestimated (underestimated). Panels a) and b) show maps of ratios for DJF and MAM during the 1971-2010 period whilst panels c) and d) show histograms.

Despite some seasonal variations with the uncertainty ratios however, the uncertainty estimates look realistic (the distribution of the residuals is well represented by the uncertainty estimates as with Bulgin, Embury and Merchant, (2016)). This is shown in Figure 4.8 by some further uncertainty boxplots from four different locations. As expected, these show an increasing standard deviation of the residuals with increasing total uncertainty. For all 4 locations (chosen at random) in Figure 4.8 the uncertainty estimates look realistic as they show the same pattern of increasing residuals with uncertainties for data during the 1971-2010 period only. For data outside the 1971-2010 period at these locations, the same issues as the boxplots shown in Chapter 3 arise (e.g. climate change) but they have the same pattern of an increasing total uncertainty as the residuals of the model increase. The uncertainty estimates are of useful accuracy at other locations besides the North Sea region.

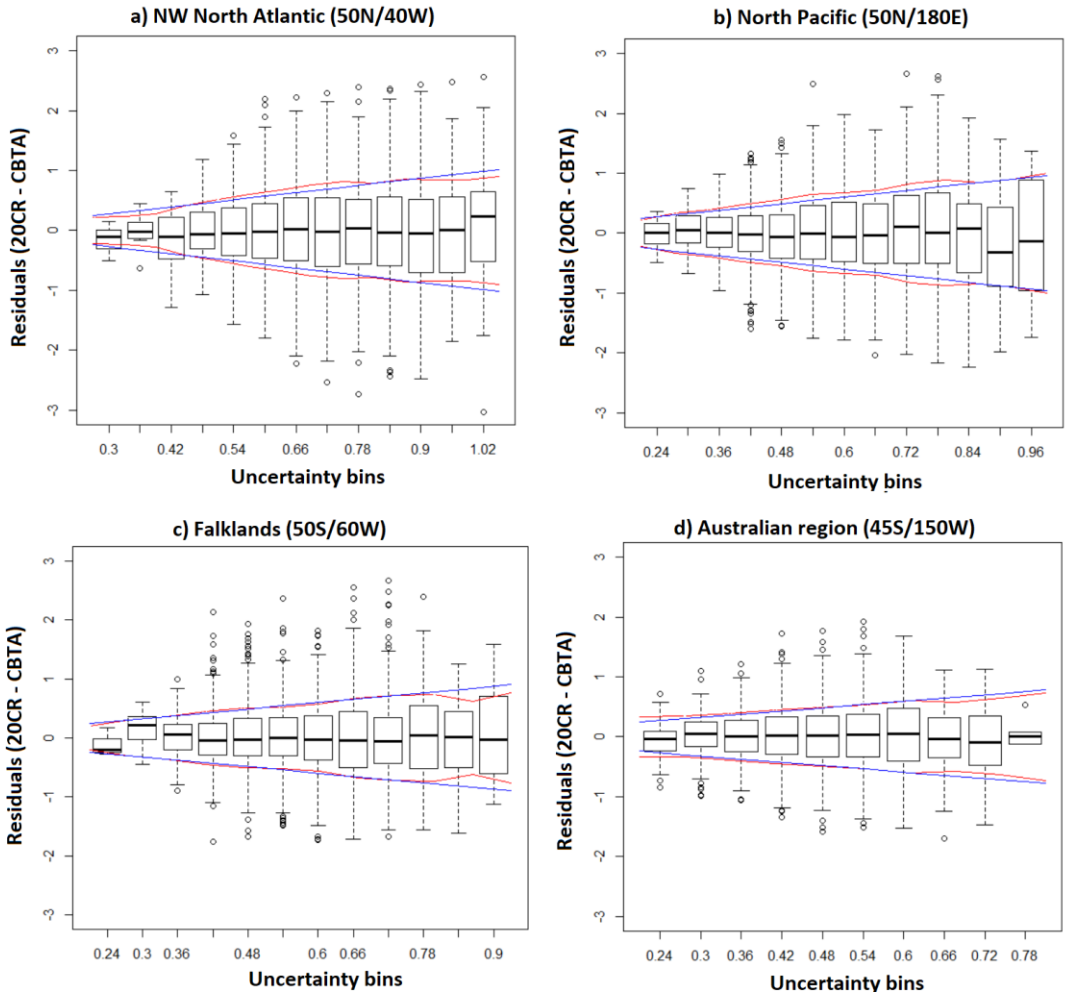

Figure 4.8: As with Figure 3.12a but for 4 different locations: the NW North Atlantic, Central North Pacific, Falklands and between Australia and New Zealand.

Another aspect of the uncertainty estimates that can be explored in more detail is the regional contribution of individual uncertainty components to the total (Figure 4.9). The most dominant uncertainty component is the category uncertainty which typically contributes 35-55% of the total uncertainty at each grid point, with the actual category uncertainty values shown in panel a). This indicates that during the 1971-2010 period, factors other than atmospheric circulation contribute the most uncertainty to the CBTA estimate. The misfit uncertainty is also important, typically contributing to 25%-40% of the total uncertainty. Where the misfit uncertainties are highest the CBTA fields are either not well defined or sensitive to small changes in atmospheric circulation as the variability between adjacent categories is large. The highest uncertainties are in mid to high latitudes with the lowest in tropical regions. The parametric uncertainty component is small over all ocean grid points (between 0.05 and 0.15°C, panel c) indicating that methodological choices don't have much impact on model performance. The circulation uncertainties are also fairly small typically consisting of 10-20% of the total uncertainty (d).

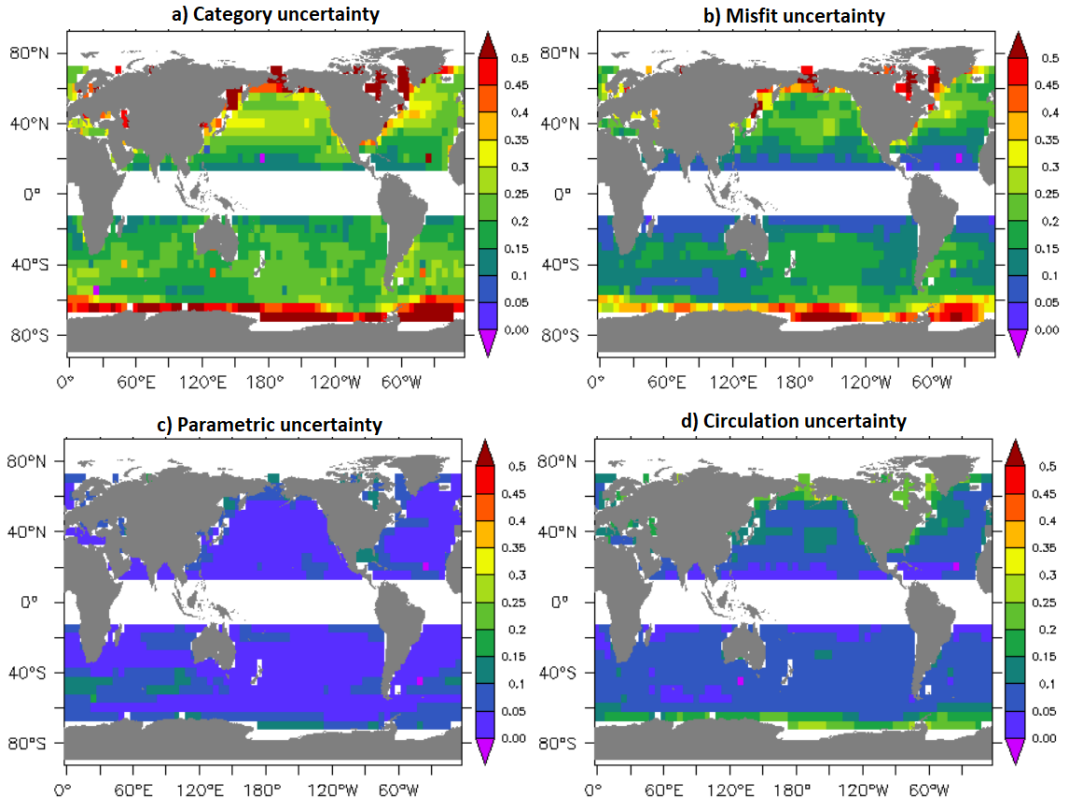

Figure 4.9: The uncertainty estimate (°C) of each uncertainty component for all months from the 1971-2010 period.

The parametric uncertainties are particularly important in the context of this chapter because they are very high in areas of the CBTA field that are unconstrained by the 20CR anomalies (as shown in Figure 3.3). If atmospheric circulation patterns show a dramatic change in earlier years from the 1971-2010 period then the parametric uncertainties should be large in the earlier period (there is likely to be poor sampling in the CBTA field if this is the case). The zonal means of Figure 4.10 however show that the parametric uncertainty increases by a factor of two for the 1931-1970 period, judging by the results for 30W and 180W but the uncertainties are still very small. The only exception to this is high southern latitudes but there are coverage issues in this region (Freeman *et al.,* 2017). There also appears to be no seasonal variations in the changes of the parametric uncertainty either. From this it is concluded that the atmospheric circulation patterns during the 1931-1970 period were also seen during the 1971-2010 period. Variations in atmospheric circulation patterns appear to not be responsible for the drop in the correlation coefficient in earlier years seen in Figure 4.4. Either the relationships between temperature and atmospheric circulation are changing or other influences besides atmospheric circulation are playing a role. In the next section it is examined whether any of these influences appear when looking at MAT variations globally or within ocean basins.

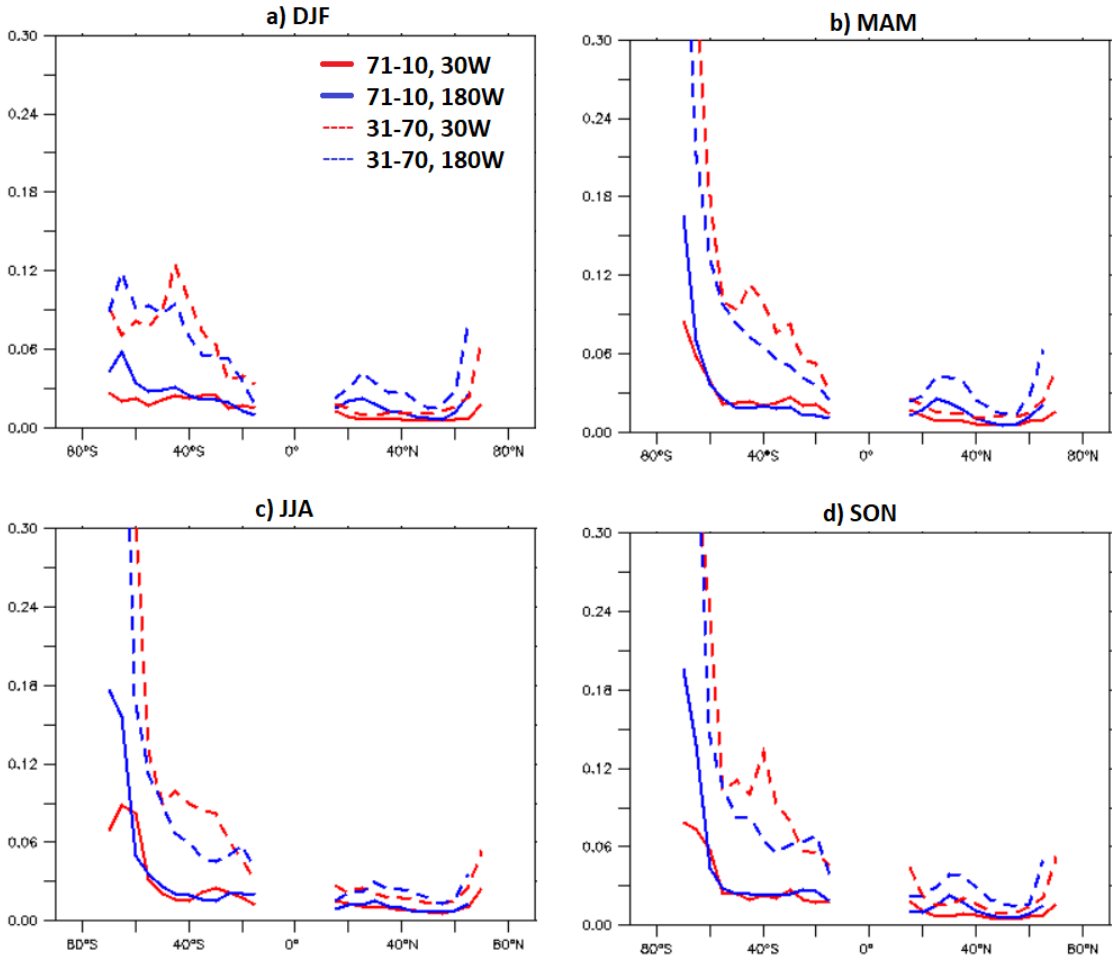

Figure 4.10: Parametric uncertainties over 2 different longitudes (30W and 180W) for the 1971-2010 developed model. Uncertainties are shown over two time periods (1931-1970 and 1971-2010). Panels a-d) show plots for the DJF, MAM, JJA and SON periods respectively. Latitudes are shown on the x axis and parametric uncertainties (°C) on the y axis.

4.3 Large scale time series analysis of CBTAs

In this section variations in the CBTAs are examined from 1880-2010 to see what variations in 20CR MAT the model predicts over time. The first sub-section looks at changes in global CBTAs and 20CR MAT whilst the second focuses more specifically on MAT in the North Atlantic basin. The aim of this chapter is to highlight other influences on global temperature besides atmospheric circulation. Then it will be discussed whether this can explain any decline in the correlation coefficient when looking at periods not used to build the model, as shown for 1931-1970 in Figure 4.4. The regions examined in this chapter are shown in Figure 4.11.

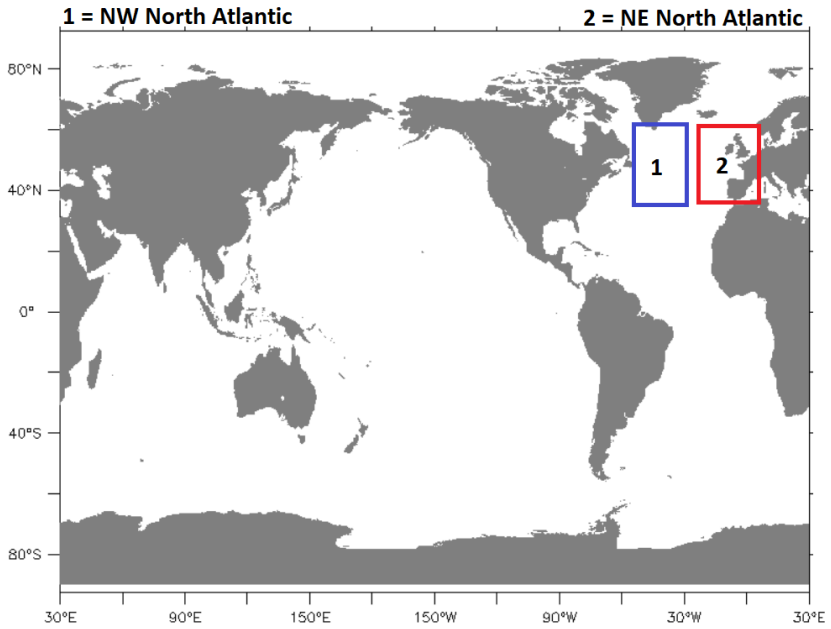

Figure 4.11: The two regions of CBTAs examined in this chapter, in addition to global MAT.

4.3.1 Global time series of CBTA model

The annual time series of global CBTAs (with exception to the tropics and the poles) is shown in Figure 4.12 and this shows that the CBTAs have varied little over time whilst 20CR MAT has warmed substantially since the 20th Century, in agreement with other MAT and SST datasets (e.g. Huang *et al.,* 2017, Kennedy *et al.,* 2011, Kent *et al.,* 2013). Despite the strong correlations between the CBTAs and 20CR MAT over grid cells, little can be seen from the global annual CBTA time series and as a result a large residual warming trend still remains. The monthly CBTAs since 1880 show a little more variability (b) but the CBTAs do little to reduce the global residuals which highlights the influence of climate change. From these plots it is concluded that regardless of how the atmospheric circulation varies, global temperatures will still continue to warm (as expected).

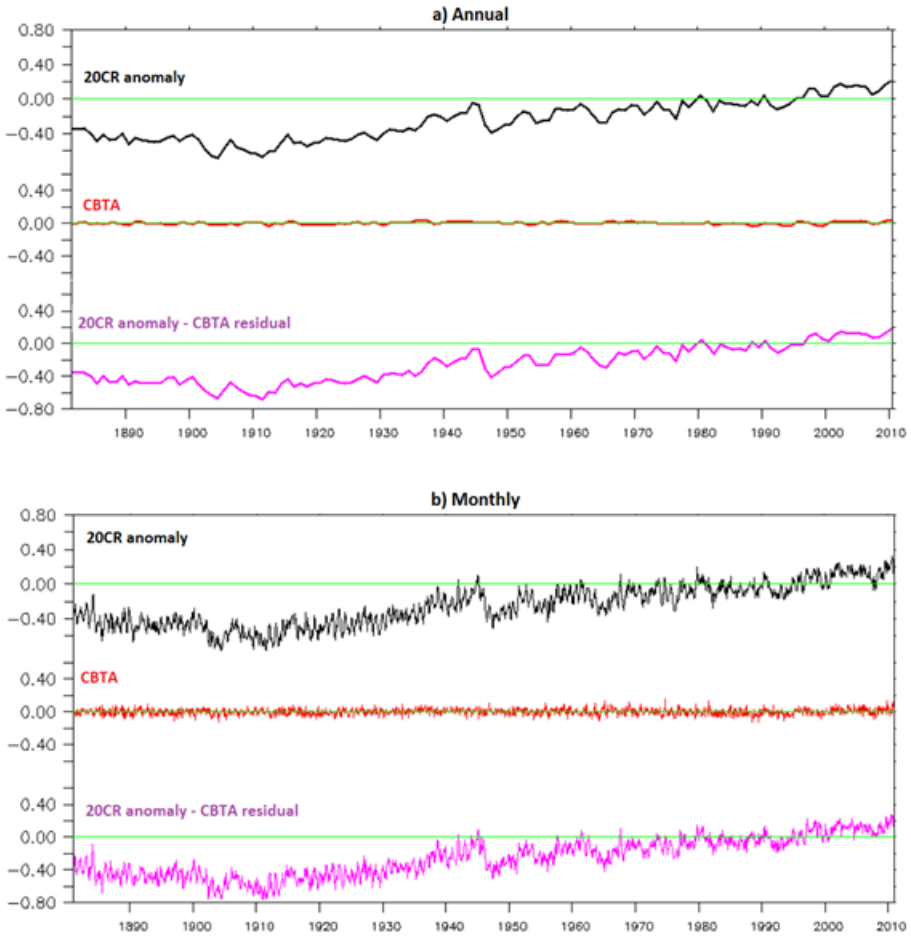

Figure 4.12: a) Plot of annual temperature anomalies (°C) from 1880 to 2010, b) As with a) but with monthly data. The upper time series in each panel shows the 20CR anomalies, the middle panel shows CBTAs developed using data from 1971-2010. The lower time series show the remaining temperature variability when the CBTA has been subtracted from the 20CR anomaly.

There are several reasons as to why the CBTAs have a smaller amount of variability compared to the study by Thompson *et al.,* (2008). The first reason is that this thesis does not consider temperature anomaly variations over land which are often far greater than the oceans (Thompson *et al.,* 2008). Secondly the CBTA time series in Figure 4.12 does not consider the MAT variability in the ENSO region which is one of the most variable regions of MAT and SST in the world (Clarke, 2014). Finally, this thesis looks at local MAT variability in response to local atmospheric circulation patterns. It is well known that ENSO affects temperatures across different areas of the world (e.g. Webster and Yang, 1992; Fraedrich, 1994). The final point is a key difference to the Thompson *et al.,* (2008)

study, as they looked at how global influences on global temperature contributed to past global temperature variability. As this thesis examines the contribution of atmospheric circulation on local temperature variability, more useful results are found when looking at specific different regions instead.

Decadal plots of the CBTAs reveal more about temperature variability over different regions in the 20CR (Figure 4.13). In earlier years, 20CR MAT as might be expected, is below average over most ocean basins. With exception of the Southern Oceans (data coverage here is especially sparse), much of the southern hemisphere contains 20CR anomalies over 0.5C below the 1971-2010 climatological average as do large areas of the Pacific and Indian Oceans.

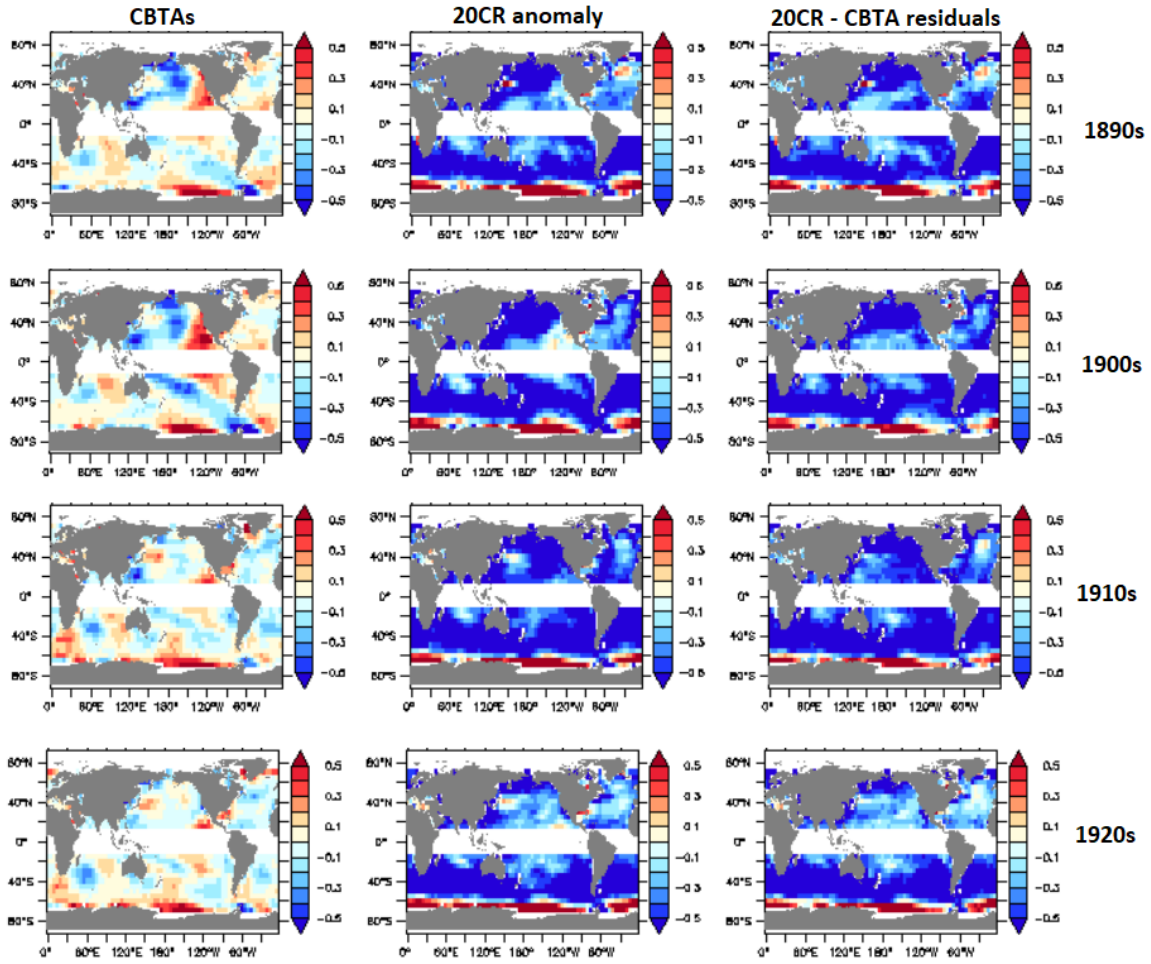

Figure 4.13: Decadal anomalies of the CBTAs (left columns), 20CR anomalies (°C, middle columns) and the 20CR MAT – CBTA residuals (right columns). Each row shows a different decade which from top to bottom show the 1890s, 1900s, 1910s and 1920s. Anomalies from the 1971-2010 climatological average.

The CBTAs however are markedly different and show some notable variations from the mean temperature, especially over the Pacific. The Central Northern and Eastern Pacific (to the south of Japan) contain CBTAs -0.2 to -0.4^{o}C below average up until the 1900s. The 1910s and 1920s show a similar CBTA pattern but to less of an extent. Meanwhile the Western Pacific has CBTAs well above average extending towards the ENSO region. ENSO during the 1890s and 1900s was more often in a La Niña phase than El Niño (Wolter and Timlin, 2011) so to see this pattern is surprising. The amplitude of the anomalies in these regions are more likely to point towards certain SLP patterns persisting frequently. This in itself may be a result of a lack of assimilated SLP observations in earlier years and SLP analysis over the Pacific region has suggested issues with 20CR SLP during previous decades (Abatzoglou, Rupp and Mote, 2014). Over the North Atlantic things look more realistic as CBTAs should average close to zero when taking averages over numerous years given how variable atmospheric circulation is and shows no overall long-term trend. The 1890s and 1900s appear warmer whilst the 1910s and 1920s look rather cool.

Towards the middle of the 20th century, the number of SLP observations assimilated into the 20CR increases. The CBTAs in areas such as the Pacific appear to be less amplified as a result (Figure 4.14). The 1930s and 1940s are slightly milder than average over the US Pacific which coincides with a period of a positive Pacific Decadal Oscillation (PDO, an SST pattern in the Pacific (McCabe, Palecki and Betancourt, 2004)). Signals for below average temperatures in the CBTAs appear in the South Pacific and Atlantic but again these don't appear to the same extent as they do with the 20CR anomalies. One area where the CBTA model and the 20CR disagree in particular is in the North Atlantic Ocean. A recurring pattern here in the CBTAs is for above average temperatures between Greenland and Canada, the tropical Atlantic near Africa and below average temperatures in between. This is at odds with the 20CR anomalies which indicate that the Central North Atlantic contained MAT anomalies much above average from the 1930s to the 1950s. The residuals (20CR MAT – CBTA anomaly) in the right-hand panel for the North Atlantic are therefore particularly large. It's only from the 1960s onwards that the North Atlantic CBTAs and 20CR MAT patterns have some strong similarities.

The most anomalous results overall in earlier decades are found in the Southern Oceans, especially in the areas near the boundaries of Antarctic sea ice as anomalies are

persistently above the 1971-2010 climatological average. This also coincides with a region where the category and misfit uncertainties are also very high during the 1971-2010 period (Figure 4.9) but lower during the 1931-1970 period (discussed further with Figure 4.28). Atmospheric circulation patterns favour higher temperatures in earlier years over Southern Oceans and SLP is less variable, so the decadal CBTAs are well above average. With the lack of assimilated SLP data in this region, some changes in atmospheric circulation patterns should be expected in earlier years (especially given the results found further north in the Falklands by Jones, Harpham and Lister (2016)).

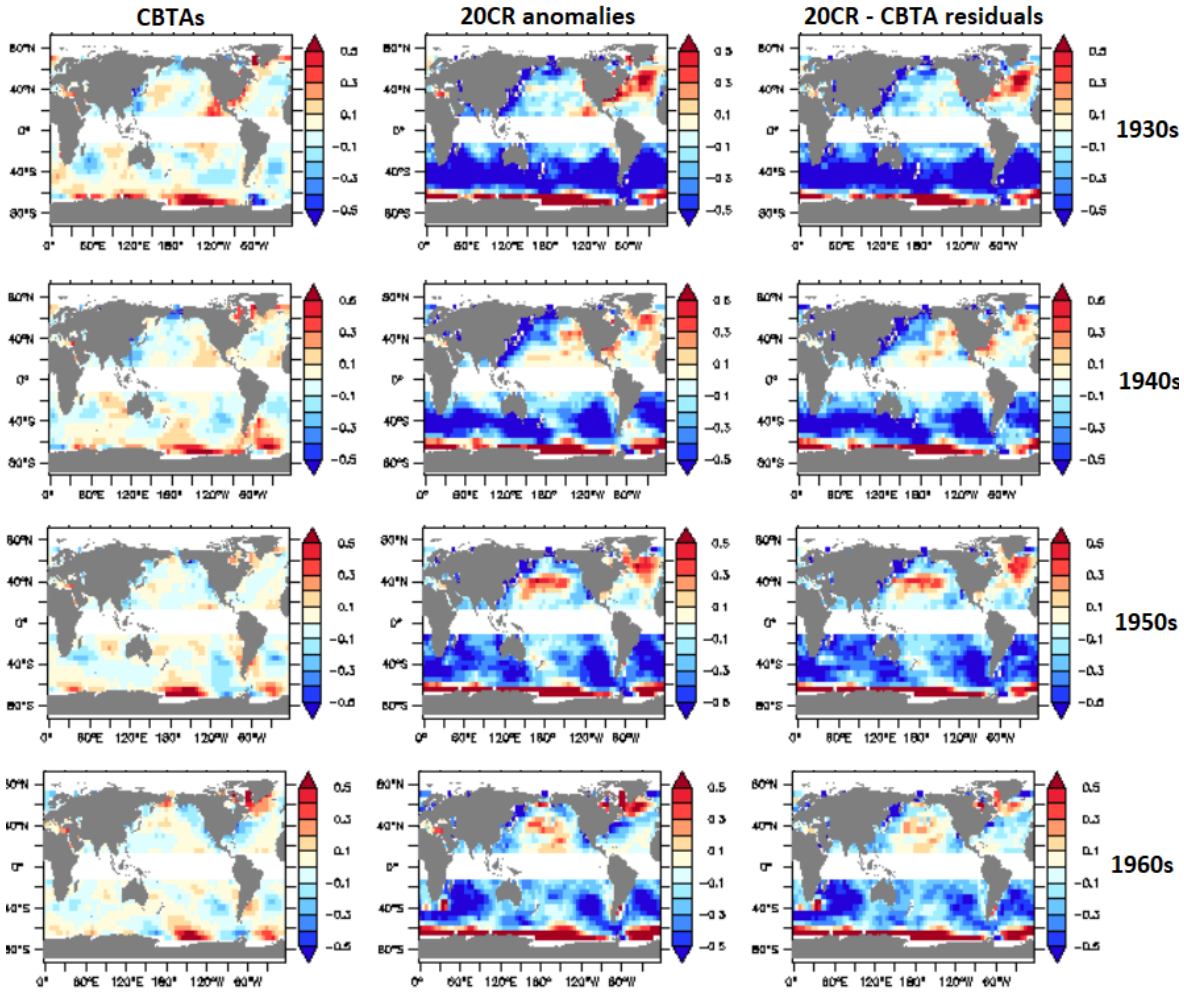

Figure 4.14: As with Figure 4.13 but showing anomalies from the 1930s to the 1960s.

From the 1970s to the 2000s the anomaly patterns of the CBTAs bear a much closer resemblance to those from the 20CR (Figure 4.15) which should be expected given these decades include data used to develop the model. The 1970s for example were a cold decade in the Pacific with strong La Niña events frequent in the first half of the decade

with a negative PDO (Newman, Compo and Alexander, 2003). Above average temperatures preside over the lower latitudes of the Pacific during the 1980s and 1990s when El Niño events were much more common. Results for the North Atlantic are encouraging also with below average CBTAs in the North Atlantic during the 1970s and 1980s. Above average MAT is more common during parts of the Atlantic during the 1990s and 2000s, in line with variations of the Atlantic Multidecadal Oscillation (AMO, Kerr (2000)). The fact that CBTAs can show decadal variations is notable as it may be indicative of ocean influences (given there is a persistent signal over a long timescale). The other notable feature is that the variability of the CBTAs is smaller than the 20CR MAT anomalies. The result of this is that the residuals in all the right-hand panels are large but these show decadal means and hide some of the greater variations in the CBTAs seen with seasonal data (as expected).

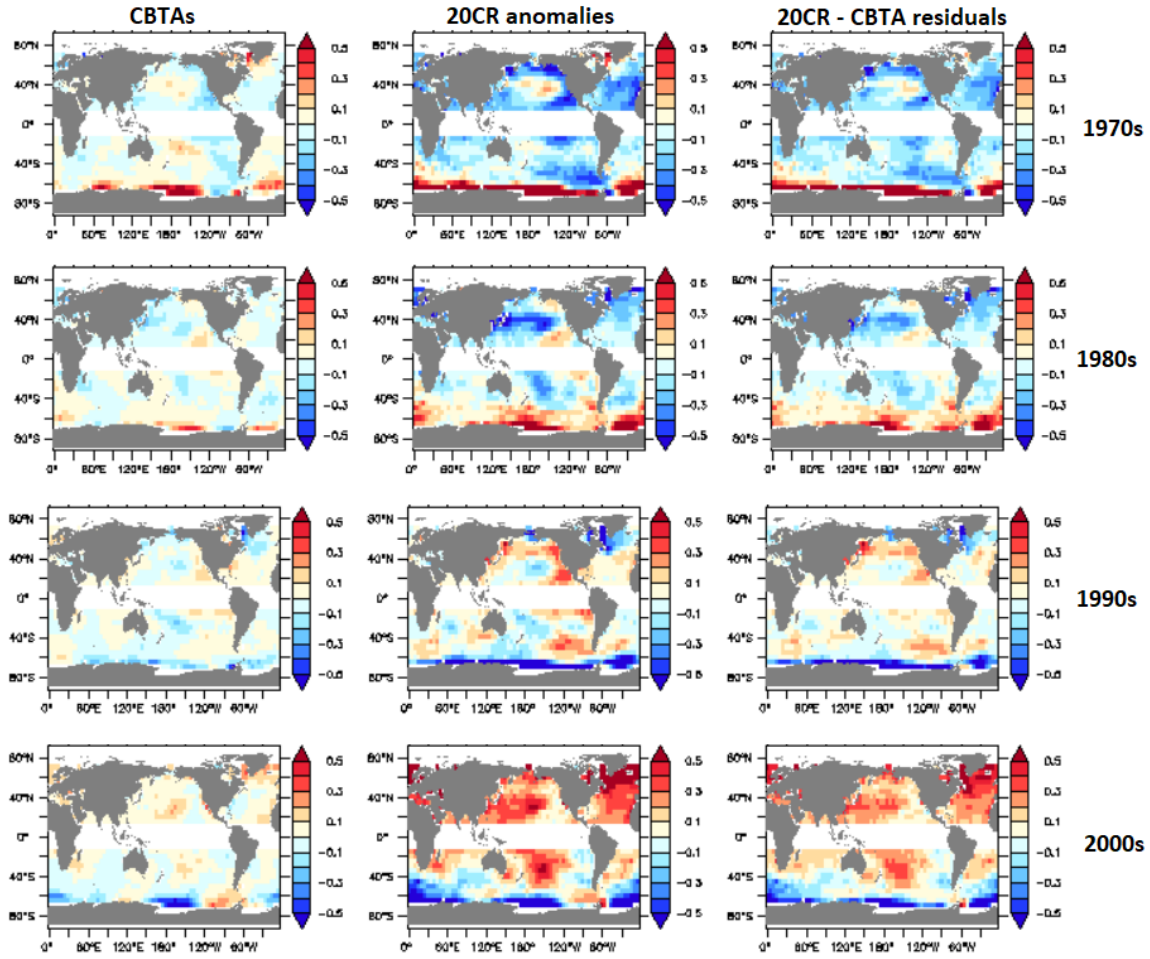

Figure 4.15: As with Figure 4.13 but showing anomalies from the 1970s to the 2000s.

4.3.2 North Atlantic regional time series

For seasonal CBTAs the impact of atmospheric circulation becomes much more apparent. Figure 4.16 shows the variances of 20CR MAT from 1971-2010 for the 4 seasons of the year. As expected, variances in 20CR MAT are largest over mid-latitudes, especially during the DJF period in the Northern hemisphere. The variances of the CBTAs however are also high and as a result, the residual variances (20CR MAT – CBTA) in the middle column of Figure 4.16 are much smaller. The drop in the variance as a result of taking the estimated influence of atmospheric circulation away is clear in the right-hand column of Figure 4.16, with blue areas showing the reduced variance. Variance is particularly reduced over the North Atlantic and North Pacific during the DJF and MAM periods. These findings should not be surprising for the 1971-2010 period given the correlations shown in Figure 4.4 but they emphasise the advantage of looking at small scale atmospheric circulation patterns over specific grid points, rather than just global averages.

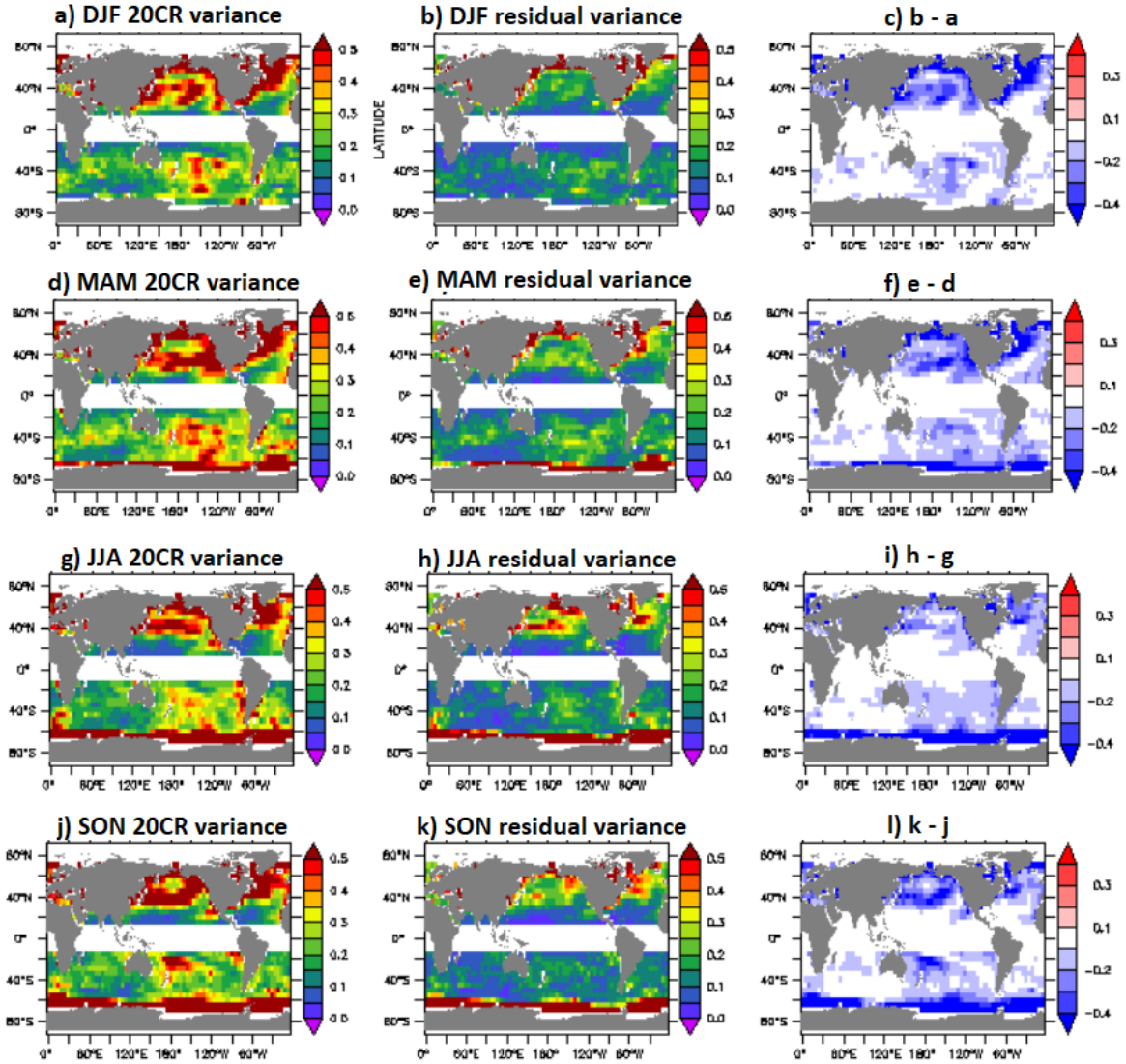

Figure 4.16: Global maps of variances (˚C^2) and their differences for the 1971- 2010 period. Panel a) shows DJF variances in the 20CR; b) Variance remaining in the 20CR when the CBTA variance has been subtracted from panel a); c) the differences between the residual and 20CR MAT variance. Blue areas indicate where 20CR MAT variance has been reduced due to taking the estimated influence of atmospheric circulation away from 20CR MAT; Panels (d-f) as with panels a-c) but for the MAM period; Panels (g-i) JJA; Panels (j-k) SON.

Some particularly interesting results are found in the North Atlantic, especially when looking at two contrasting regions such as the NW and NE North Atlantic (regions shown in Figure 4.11). The DJF time series of both regions are rather poorly correlated ($r < 0.5$) shown in the upper time series of Figure 4.17. During the 1960s for example, 20CR MAT was below average in the NE and much above average in the NW. The middle panel

shows the time series of CBTAs since 1880 for both regions and from these, the NW Atlantic DJF MAT appears to be particularly sensitive to variations in atmospheric circulation. Time series of 20CR MAT and the CBTAs here are strongly correlated (r ~0.80).

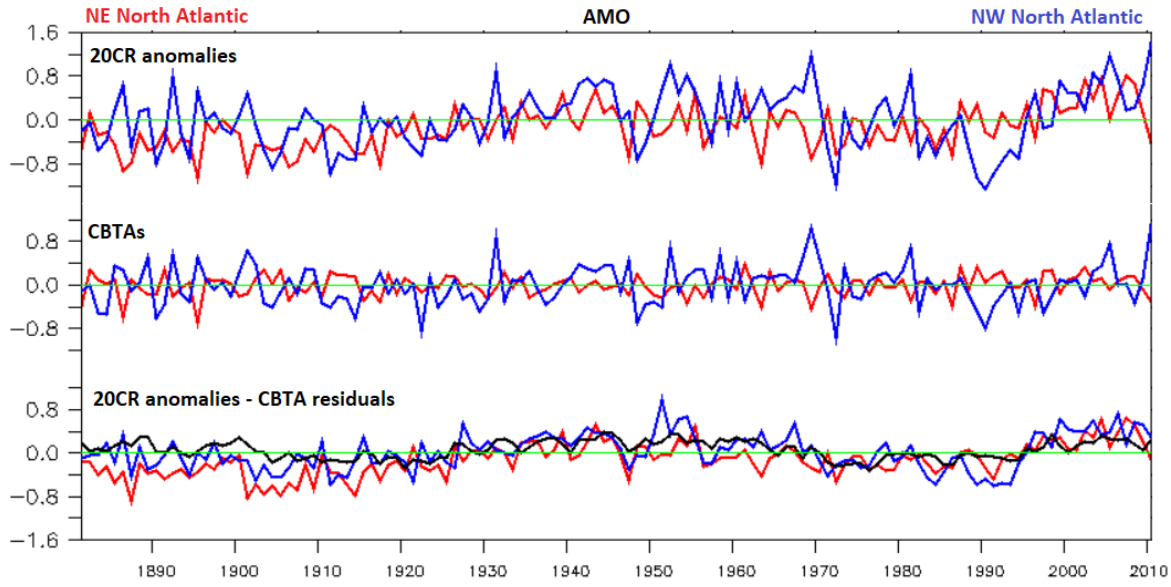

Figure 4.17: Time series of anomalies over the NE Atlantic (red) and the NW Atlantic (blue) from 1880 to 2010. Time series in the top part of the plot show the 20CR anomalies, the middle shows the CBTAs and the bottom part shows the residuals. The AMO time series from Enfield, Mestas-Nuñez and Trimble (2001) is overlaid for comparison (black).

After subtracting the estimated contribution of atmospheric circulation to 20CR MAT, a multidecadal signal becomes clearer in the residuals. This is also apparent in the NE Atlantic with the residual time series of both in the bottom panel. Both of these time series indicate a period of generally positive residuals from 1930 to 1960 and 1995 to present and persistently cool residuals seen from 1900 to 1925 and 1965 to 1995. These periods coincide with positive and negative AMO phases (Msadek *et al.*, 2014) and provide further evidence that ocean signals can be found from the residuals of the CBTAs.

There are periods with conflicting signals in the bottom time series of Figure 4.17. Some years in the 1950s for example have a strongly positive AMO and 20CR anomalies that are at times not represented by the CBTAs. The winter of 1950/51 is a particularly notable

example with a map of the CBTAs shown in Figure 4.18 for January 1951. The atmospheric circulation patterns suggest a large region of below average temperatures in the NW North Atlantic (a) but this is at odds with the 20CR anomaly pattern (b). This region according the 20CR had notably above average temperatures and the contrast is highlighted further when looking at the residuals. The residuals are above +2^{o}C over a large number of grid cells (c) and there is some evidence to suggest that it may be the 20CR anomalies that are too high. The atmospheric circulation pattern backs up the argument that the WNW Atlantic should have been cold (d). This is because mean SLP values for January 1951 indicate a deeper than average Icelandic low. The NW North Atlantic therefore saw air more frequently advected from the Greenland region which is usually associated with cold continental/arctic airmasses. Either the 20CR MAT is warm biased or the ocean circulation signal was strong enough to overwhelm the cold signal from atmospheric circulation.

Whilst the global average CBTAs are small, as expected, results from Sections 4.3.1 and 4.3.2 suggest that the CBTAs can be used to help explain past MAT variability, especially in the North Atlantic. The AMO was suggested to be a strong background influence on temperature over the North Atlantic whilst globally climate change is the dominant factor influencing MAT. Despite these factors appearing to be influential during the 1971 to 2010 period, strong correlations were found between temperature and atmospheric circulation during this time over many locations. What is clear is that the first two questions from the introduction of this chapter have been addressed. The CBTA model developed in Chapters 2 and 3 has been successful globally (question 1) and other influences on MAT such as the AMO and climate change are exposed (question 2).

This results in this section do not answer the third question from the introduction of what causes the decrease in the correlation coefficients between temperature and

atmospheric circulation. If it's not climate change or the AMO causing this, could the relationships between temperature and atmospheric circulation be different in earlier years? To investigate this the CBTAs are analysed further over some other grid points in the world's oceans to see if anything further can be found.

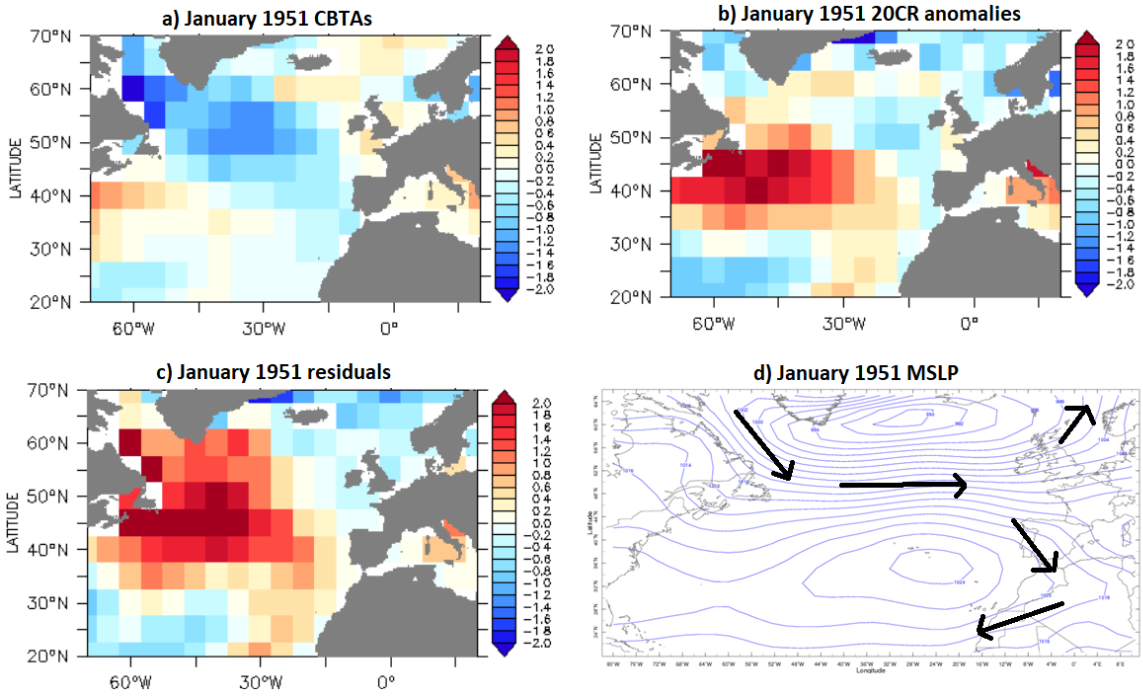

Figure 4.18: Anomalies and synoptic charts over the North Atlantic for the month of January 1951. Panel a) shows the CBTAs developed from the 1971-2010 relationships; b) The 20CR anomalies; c) The 20CR MAT – CBTA residuals and d) The mean SLP pattern for that month, arrows show the general circulation pattern.

4.4 Small scale analysis of CBTA time series

In this section, time series of CBTAs are shown over several different points of the world's oceans, with locations shown by the map in Figure 4.19. The aim is to investigate how the relationships between temperature and atmospheric circulation are changing over time and to explore MAT variability over different areas in detail. In order to assess whether relationships between temperature and atmospheric circulation are changing, a CBTA model is developed for two periods. One is developed for the 1971-2010 period as with previous results in this chapter. The second CBTA time series is developed from data covering the period from 1931-1970. The same climatological average is used for the MAT anomalies for both datasets (1971-2010) and given the global warming trend shown in Figure 4.12, the 1931-1970 CBTAs and the fields should be colder than average. This study will focus on three points in particular: the Falklands (where results that would be expected appear), the US Pacific (with an example given for a month which has varying model performance) and the NW Atlantic (where some more unusual results are found).

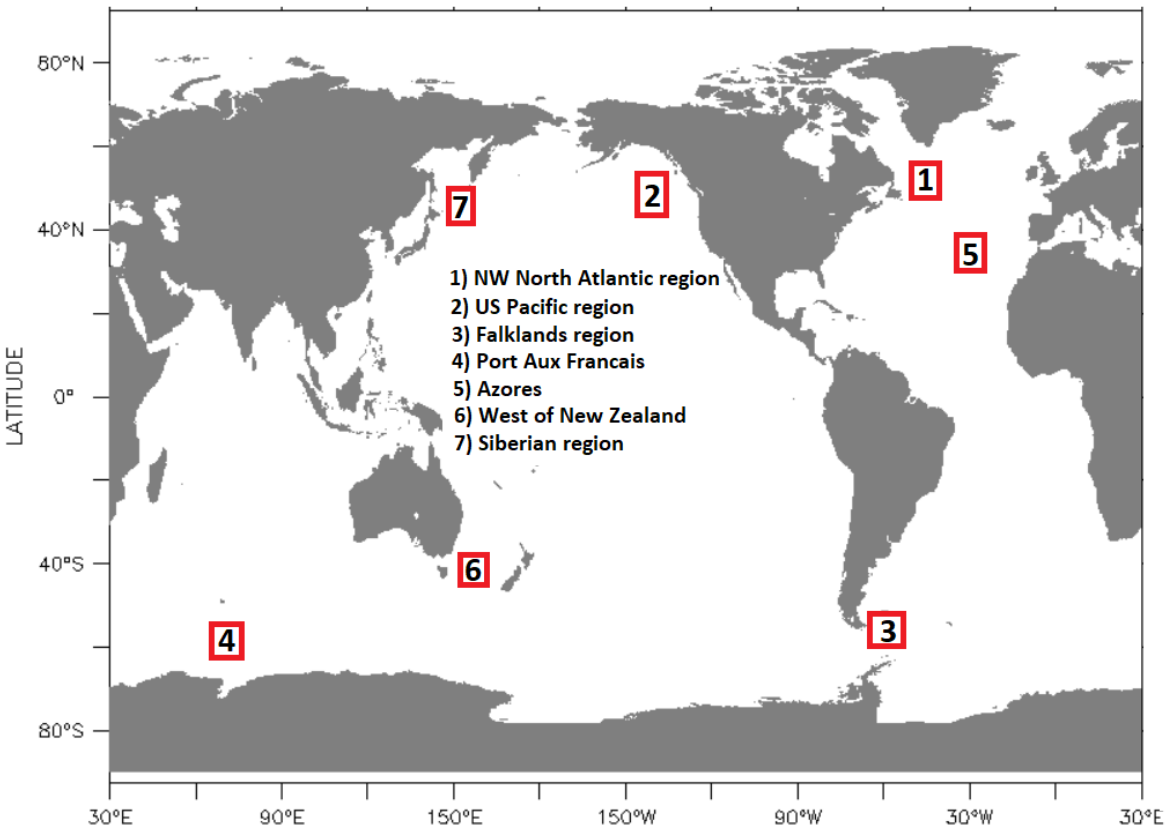

Figure 4.19: Locations where CBTAs are analysed in this chapter.

4.4.1 The Falklands

The Falklands time series is introduced first as this shows the variations in a time series that would be expected of a CBTA model. The expected trends are that the CBTAs should be warmer when building a model on more recent time periods, the relationships between temperature and atmospheric circulation remain consistent and there should be a general steady increase in the residual temperature over time (due to the climate change signal). Time series of CBTAs in the Falklands region are shown in Figure 4.20 for the DJF period as this is when relationships are at their strongest here (r = 0.67 from 1880-2010). The 20CR MAT anomalies for this time series generally show below average temperatures from 1880-1980 (with the exception of the two world wars), and above average temperatures since. The MAT anomalies during the world wars look suspiciously high (as it is known marine observational quality also declined during these periods) but they are supported to an extent by the atmospheric circulation patterns. Evidence of this comes from the CBTAs shown in the middle time series of the panel because they are also

above the 1971-2010 climatological average during the World War periods. The CBTA time series for the two different periods are very strongly correlated (r > 0.9) indicating that the relationships between temperature and atmospheric circulation haven't changed that much. The residuals in the bottom time series show a smoothed version of the 20CR MAT anomalies and contain a weak warming trend (0.08°C per decade using data from 1961-2010 and 0.09°C from 1881 - 1950) that bears some resemblance to the climate change signal discussed in Figure 4.12. The time series for other seasons are similar in nature and the correlations are also reasonably strong as shown by Table 4.1. In some cases, the relationships between temperature and atmospheric circulation are stronger during the 1931-1970 period than the 1971-2010 period.

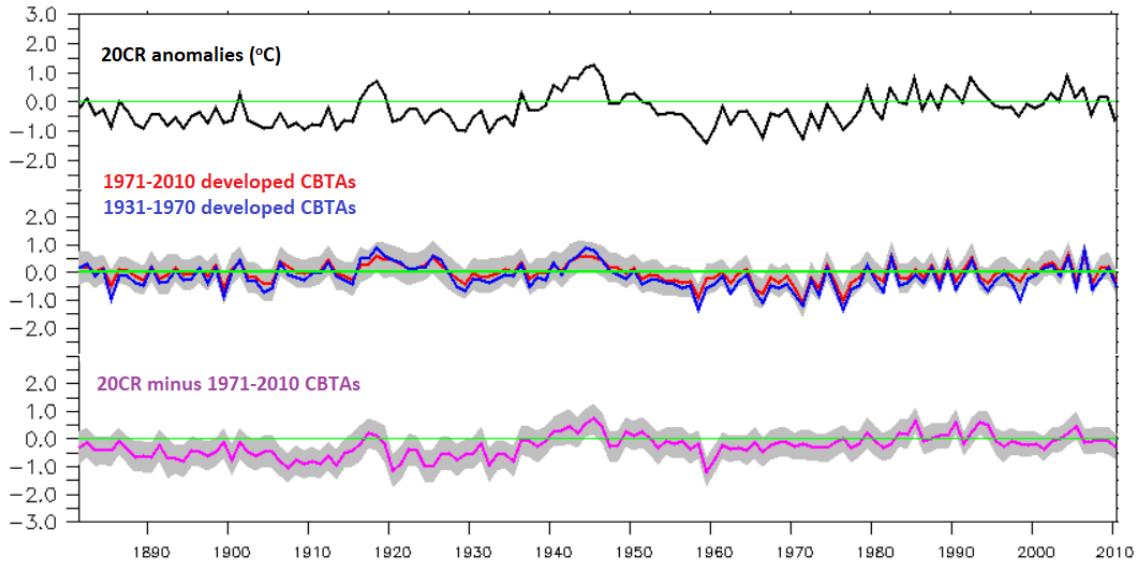

Figure 4.20: Time series of DJF anomalies at a point near the Falklands (55S/60W, shown in Figure 4.19). The top time series shows the 20CR anomalies, the middle shows the CBTAs predicted from the 1971-2010 data developed model (blue) and the 1931-1970 developed model (red). The bottom time series shows the residuals.

Period for building model	Correlations during period	DJF	MAM	JJA	SON
1971-2010	1971-2010	0.83	0.73	0.74	0.76
1971-2010	1931-1970	0.84	0.60	0.81	0.78
1931-1970	1971-2010	0.79	0.63	0.66	0.73
1931-1970	1931-1970	0.87	0.77	0.84	0.79

Table 4.1: Falkland's region seasonal correlation coefficients. The correlations are shown for the models built over different periods with the 20CR MAT from the two different time periods.

An example of how the atmospheric circulation patterns generally affect MAT in this region is shown by the field of anomalies in Figure 4.21. Panel a) shows that the April MAT anomalies for SW winds generally coincided with anomalies 1-3°C below normal from 1931-1970, a much bigger difference than that seen from 1971-2010 (b). Milder Aprils in this region are more often associated with stronger NW winds and this is probably the result of NW winds in this region advecting air from the sub-tropics. The CBTA fields reveal that the increase in temperatures over this region outside of the DJF period are due to less cold south-westerly winds. The April flow direction histogram actually shows that NW winds were actually more common during the 1931-1970 period (d) but the colder SW winds meant that the 1931-1970 period was colder than from 1971-2010 (for the month of April in this case but also for most other months of the year).

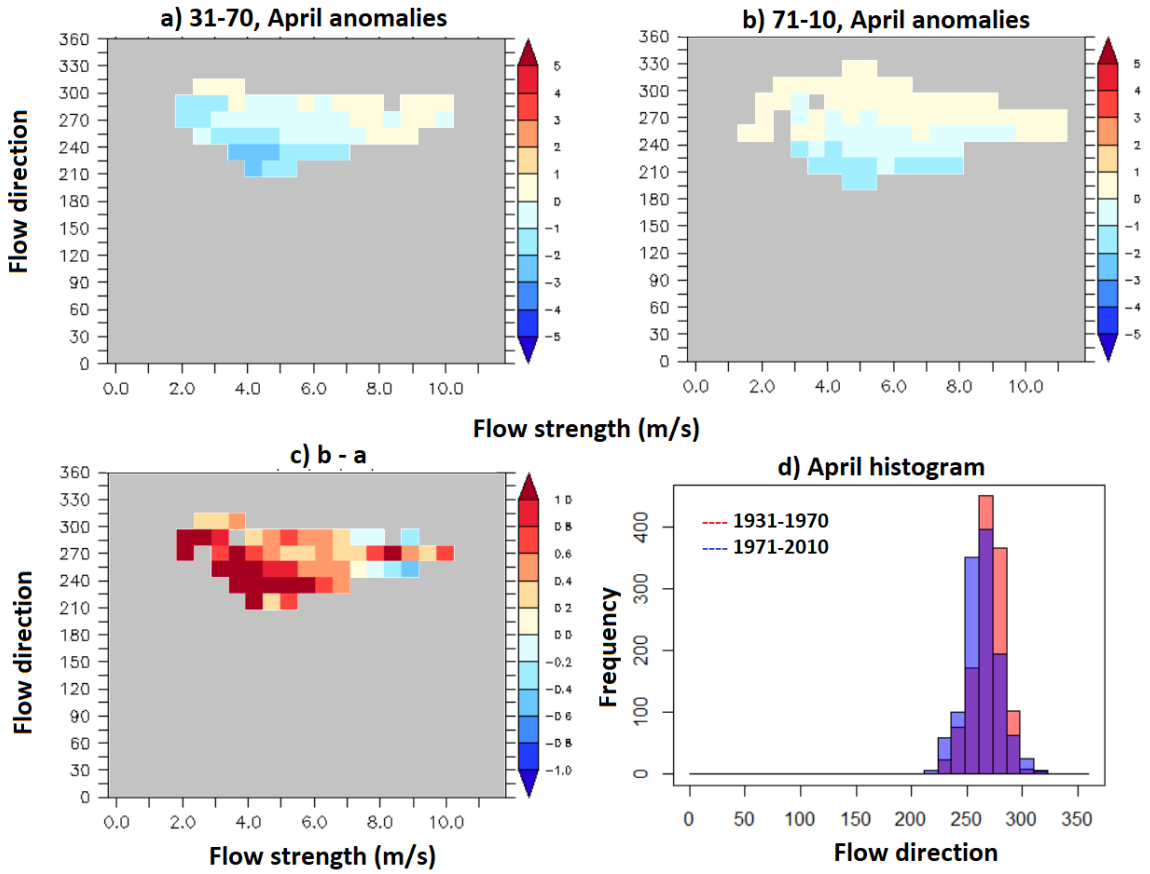

Figure 4.21: April CBTA fields and histograms for the Falklands region. Panel a) shows the 20CR anomalies (°C) on the CBTA field, with data taken from 1931-1970; b) As with a) but data taken from the 1971-2010 period. All anomalies are expressed as differences from the 1971-2010 climatological average; c) 1971-10 minus 1931-70 CBTA field differences where both fields have 20CR anomalies available; d) April histogram of the 30-day running means of flow direction (degrees) from 1931-1970 (red) and 1971-2010 (blue).

To summarise, over the Falklands region strong relationships between temperature and atmospheric circulation persist from 1931-2010 for all seasons. The residuals with the exception of the World Wars show a slow warming trend and the relationships between temperature and atmospheric circulation are consistent over time (NW winds are warmer; SW winds are colder). The analysis was able to reveal that the warming trend appears partly due to the SW winds becoming warmer over time. Some caution should be applied to the results of this region however as the early 20th century SSTs have been noted as being unusually cold (Hegerl *et al.*, 2018) and concerns over SLP in this region have been expressed during the mid-20th Century (Jones, Harpham and Lister, 2016). The residuals from Figure 4.20 also appear too low as the upper limits of uncertainty are still below the 1971- 2010 climatological average. These issues are discussed further in Chapter 5, the next section meanwhile moves on to look at results over a location in the US Pacific.

4.4.2 The US Pacific

The (US Pacific is another region where the connections between temperature and atmospheric circulation are strong, with the strongest relationships again seen during the DJF period from 1880-2010 (r = 0.65). A time series of the DJF 20CR and CBTA anomalies is seen in Figure 4.22. Looking at the 1971-2010 developed model, the time series shows a period of below average temperatures during the 1970s and then mainly fluctuates between average and above average afterwards until the late 2000s. These periods of below and above average temperatures correspond to different phases of the Pacific Decadal Oscillation (Mantua *et al.*, 1997) and suggest that atmospheric circulation is an important driver behind its variability during the 1971-2010 period in agreement with other studies (e.g. Johnstone and Mantua, 2014). However, there is an overlying warming trend in 20CR MAT (0.13^{o}C per decade from 1881-1950 and 0.09^{o}C since then) not captured by the time series of CBTAs which should be expected given the increase in global temperatures since the 20th Century (Hartmann *et al.,* 2013). Before the 1971-2010 period some interesting results appear. Firstly, the notably cold 20CR MAT from 1880- 1910 has no backing from the CBTA anomalies with the CBTA time indicating that this period should have seen average/above average temperatures. The 20CR anomalies

also fall outside the 1SD uncertainty bounds of the time series from 1971-2010 developed CBTAs. The residuals at the bottom of Figure 4.22 emphasise this as the upper uncertainty bounds are well below zero especially 1904 for example).

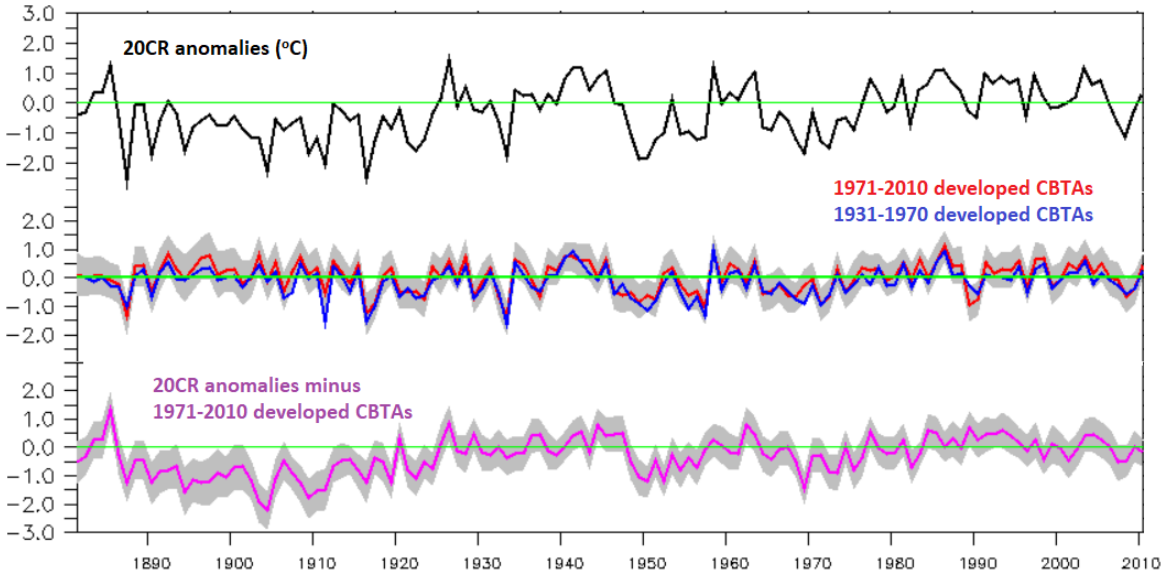

Figure 4.22: As with Figure 4.20 but for the US Pacific region (135W / 50N shown in Figure 4.19).

Period for building model	Correlations during period	DJF	MAM	JJA	SON
1971-2010	1971-2010	0.80	0.76	0.51	0.64
1971-2010	1931-1970	0.83	0.55	0.22	0.64
1931-1970	1971-2010	0.78	0.66	0.00	0.55
1931-1970	1931-1970	0.88	0.65	0.66	0.74

Table 4.2: As with Table 4.1 but for the US Pacific region.

Meanwhile the period from 1925-1945 shows little in the way of difference between the CBTAs and 20CR MAT (emphasised by the residual time series) although the PDO was markedly positive during this period (McCabe, Palecki and Betancourt, 2004) so a shift in the PDO not captured by the CBTA model may explain why there is a shift upwards in the residuals from the mid-1900s to the early 1930s. The 1931-1970 period was slightly colder than the 1971-2010 period despite the strongly positive PDO, shown by the blue line which represents a time series of CBTAs developed by using 1931-1970 data. The variability of the two different time series is strongly correlated ($r > 0.9$ as seen with the Falklands time series) indicating the relationships between temperature and atmospheric circulation in the 20CR are consistent but there is a slight offset in the temperature

anomalies between the two different time series. For other seasons the relationships between temperature and atmospheric circulation are weaker, especially in the JJA period (and also September most of all) where relationships are almost non-existent when looking at time periods not developed by a model (Table 4.2). Whilst the overlying atmospheric circulation pattern is a dominant driver of interannual MAT variability during the DJF period, other factors appear to be influencing MAT at other points of the year.

The JJA statistics from Table 4.2 are interesting because the correlations between the 1971-2010 built model and the anomalies for the same period show some predictability (r=0.51) as do the comparisons for the 1931-1970 built model with its corresponding time period (r = 0.66). Yet outside of their respective time periods, the two models perform very poorly (r = 0.22 and 0.00 for the two models). This indicates that the CBTA fields must be very different for these months and September (the pattern is not seen in October and November – hence it disappears from Table 4.2). Therefore, CBTA fields for a month that correspond closest to this pattern (September) are shown in Figure 4.23.

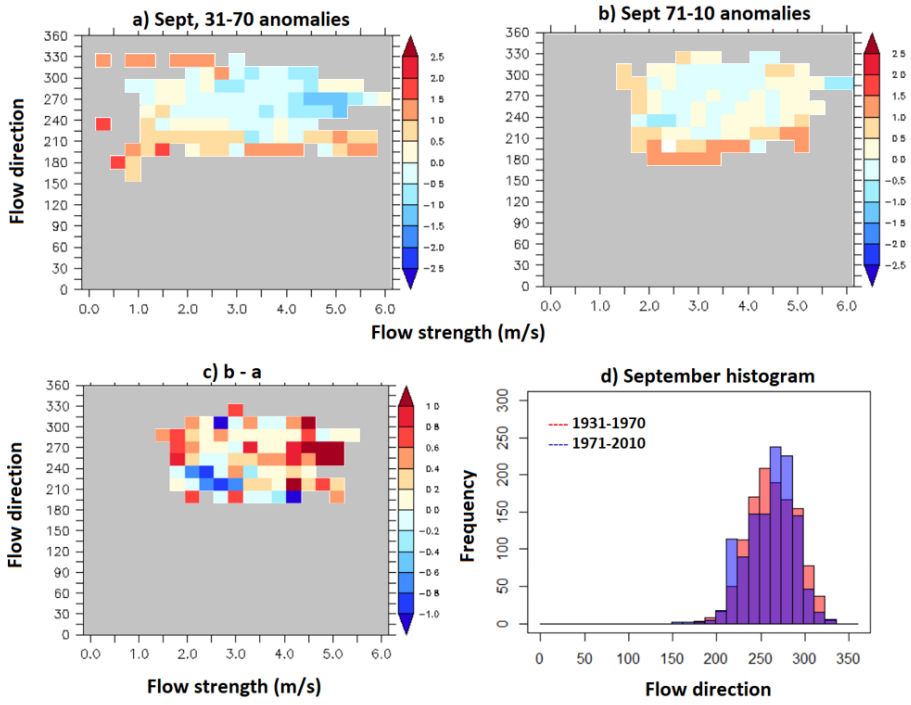

Figure 4.23: As with Figure 4.21 but for the US Pacific region and for the month of September.

The CBTA fields are quite different for the two periods as panels a) and b) show. The CBTA field for the 1931-1970 period (a) shows that strong westerlies coincide with below average temperatures whilst from 1971-2010 they coincide with slightly above average temperatures. The differences between the CBTA fields in panel (c) show a further complicated picture as there are areas in the field where categories are warmer or colder during the 1931-1970 period compared to 1971-2010. Overall, the decline in the correlation coefficient or changes in temperature cannot be attributed to shifts in atmospheric circulation as the overlapping histograms in (d) show no major change. From this information it is concluded that the JJA relationships between temperature and atmospheric circulation during the 1971-2010 and 1931-1970 periods are different. This is therefore likely to explain the dip in the correlation coefficients seen over the North Pacific in Figure 4.4 (g-i).

4.4.3 The NW North Atlantic

The NW North Atlantic is the focus for this section and is an interesting area because in contrast to much of the world, temperatures have not significantly increased since the 19th century (Dima and Lohmann, 2010; Drijfhout, van Oldenborgh and Cimatoribus, 2012). The absence of a long-term warming trend is in part due to some particularly warm years in the mid-20th Century and cold years in the early 1990s and 2010s. Some papers have speculated that the recent cooling trend in this region could be associated with a slowing down of the Atlantic meridional overturning circulation (Robson *et al.*, 2014; Rahmstorf *et al.*, 2015) but what role does atmospheric circulation play in this region in influencing MAT?

To understand how atmospheric circulation influences MAT in this region some flow strength CBTA fields are shown for the month of November which are typical for the extended winter months at this location (Figure 4.24, extended winter means from November-March in this section). Both (a) and (b) show that the coldest Novembers in this region are associated with strong westerlies and the mildest being southerlies. Months with a predominant S/SW flow can see anomalies in the NW North Atlantic up to 2-3^{o}C above the 1971-2010 climatological average. Such differences in the temperature anomalies are likely to be related to the contrast in temperature between the oceans and

continents. Cold air outbreaks over North America are often advected westwards into this region. Meanwhile S/SW flows are likely to advect warmer air from the Gulf of Mexico and Subtropical North Atlantic. The higher the flow strength for the WNW flow for during November (and for the extended winter period), the more frequently continental cold air outbreaks pour into this region, hence strong WNW flows coincide with the coldest anomalies (panels a and b). NE Canada was one of the fastest warming areas on the planet during the 20th century, especially during the extended winter months (Zhang *et al.*, 2000) so one would expect the westerlies in this region to have become warmer over time as the continental cold air outbreaks over Canada have become less intense. Surprisingly however the flow strength CBTA field for (c) in Figure 4.24 show that westerlies have actually turned colder over the space of two periods.

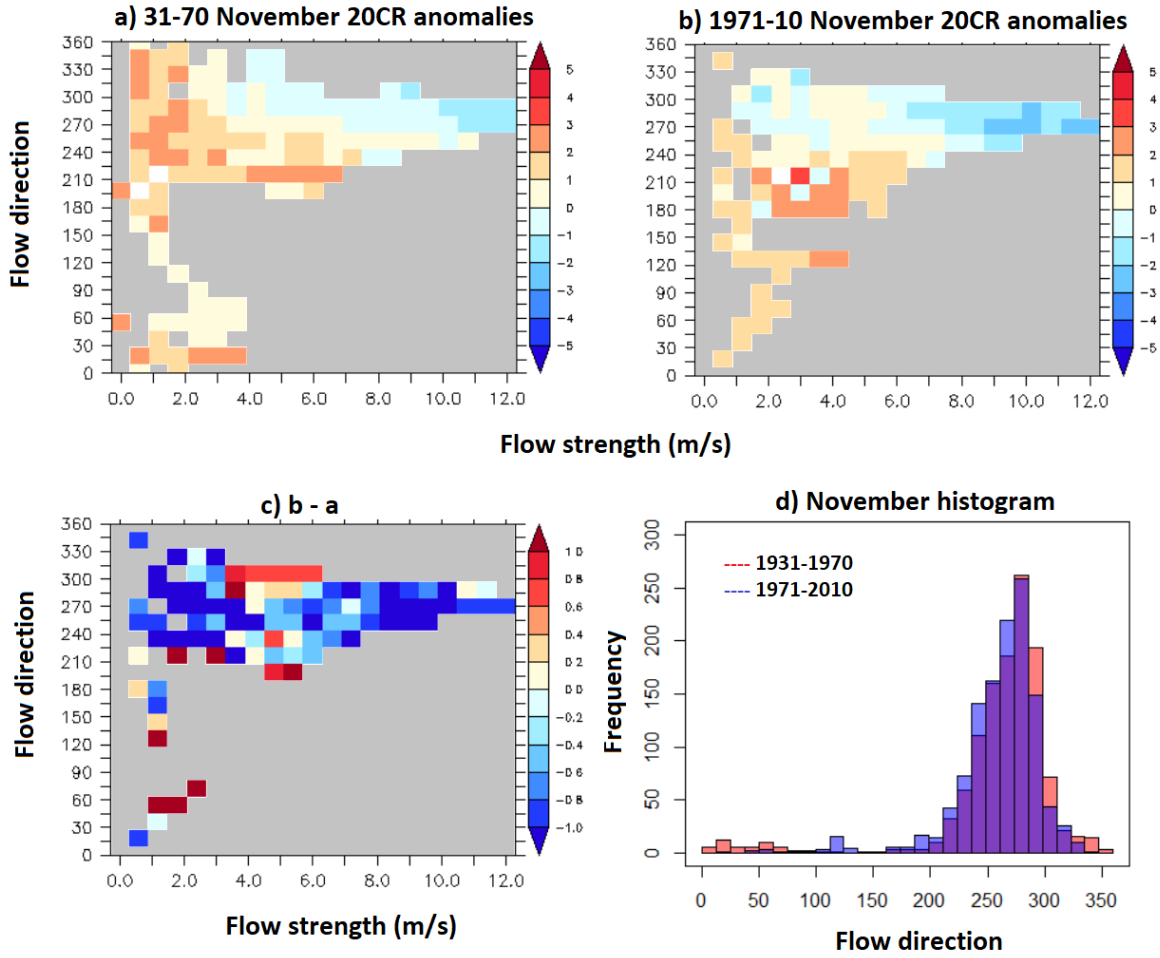

Figure 4.24: As with Figure 4.21 but for the NW North Atlantic region and for the month of November.

Westerlies were generally 0.5-1.5^{o}C cooler during November from 1971-2010 compared to the 1931-1970 period (calculated from the differences in the two CBTA fields, panel c). The CBTA fields would therefore suggest that the 1971-2010 period had an additional source of colder air from either the west or NW. Temperatures during the extended winter period over Greenland weren't particularly cold from 1971-2010 either though, with exception of some DJF periods in the 1980s and 1990s (Vinther *et al.*, 2006). With no obvious source of colder air, it appears that the 20CR MAT from 1931-1970 could be too warm over this location, especially given the contrast with the North Pacific and Falklands CBTA fields which commonly show negative residuals at various points in earlier years. Alternatively, the impact of ocean circulation may have been strong enough to overwhelm any cooling signal from atmospheric circulation patterns (a slight shift to more NW winds during the 1931-70 period is shown in panel d also). Such conclusions are similar to those made from the analysis in Figure 4.18 that the 20CR MAT anomalies are not consistent with the atmospheric circulation patterns in this region.

When plotting the two different time series of NW North Atlantic CBTAs developed using data from either 1971-2010 or 1931-1970, the differences between the CBTA fields and the implications of them become clearer to see (Figure 4.25). The 1971-2010 developed CBTAs appear to be ~1.0^{o}C cooler than the 1931-70 trained CBTAs. Strangely, the differences between the two sets of trained data are minimal during the MAM period with the 1931-70 developed data being only slightly warmer at times (not shown). There appears to be a seasonal cycle to the offsets between the two different time series. The 1931- 70 CBTA time series has higher temperatures than expected given the atmospheric circulation pattern in the colder, stormier boreal winter months. Conversely, there is no clear differences during the boreal summer months. The two CBTA time series are very strongly correlated however for all seasons ($r > 0.85$) and the relationships between temperature and atmospheric circulation are consistent (Table 4.3) but there is an offset in the estimated temperature for different periods of time. The uncertainty bounds of this time series however are larger compared to the Falklands and Pacific time series, which is due to the anomalous cold of the early 1990s not being picked up well by the CBTA model.

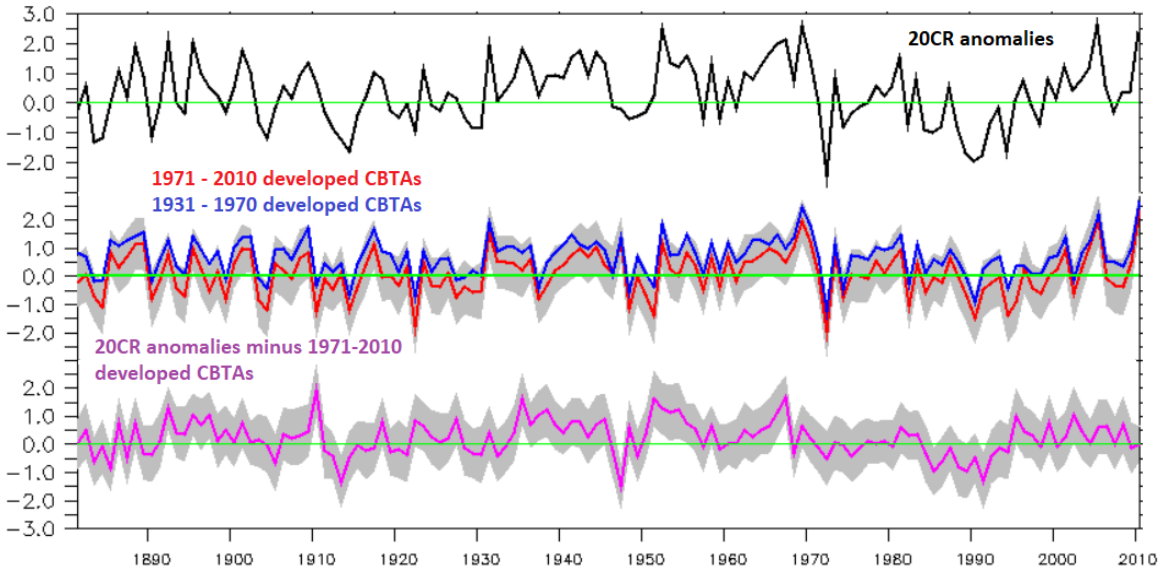

Figure 4.25: As with Figure 4.20 but for the NW North Atlantic region.

Period for building model	Correlations during period	DJF	MAM	JJA	SON
1971-2010	1971-2010	0.88	0.86	0.71	0.69
1971-2010	1931-1970	0.69	0.71	0.53	0.56
1931-1970	1971-2010	0.87	0.79	0.42	0.61
1931-1970	1931-1970	0.73	0.75	0.63	0.75

Table 4.3: As with Table 4.1 but for the NW North Atlantic region.

4.4.4 Further statistics other regions of the world

In this subsection it is demonstrated that useful insights are possible over other regions of the world's oceans as shown by the additional time series in Figure 4.26. These contain some further interesting features, the time series for panel a) for example indicates that during the 1971-2010 period the climate turned notably colder in this region during the SON period, with changes in atmospheric circulation appearing to an important contributing factor. The 1971-2010 developed model shows a strong correlation between 20CR MAT and the CBTAs (red line). The 1931-1970 period however doesn't and was much warmer. The 1931-70 model based CBTAs are (blue line) notably warmer than the 1971-2010 based CBTAs as a result (over 1°C). The two different time series of CBTAs are also poorly correlated over this location so the CBTA time series are suggesting that the relationships between temperature and atmospheric circulation have changed. It must be

noted that SLP and SST observations in this region are sparse in earlier years (Cram *et al.,* 2015; Kennedy, 2014) so building accurate long time series in this region is challenging.

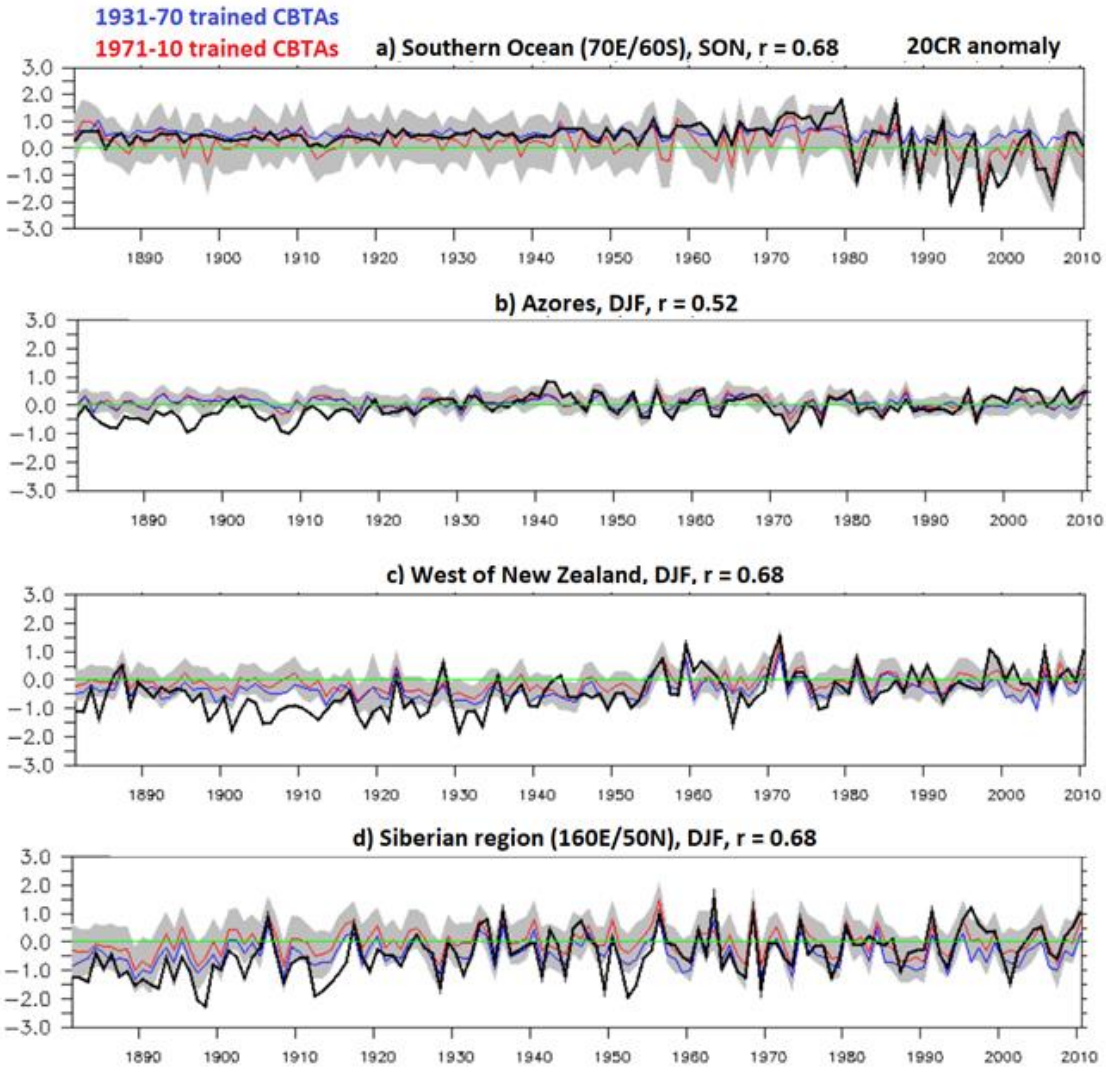

Figure 4.26: Time series of predicted anomalies for a) the Southern Ocean (SON period); b) Azores (DJF period); c) West of New Zealand (DJF period); d) the Siberian region. Predicted anomalies (°C) shown in red and 20CR 2 metre air temperature in black. Uncertainty bounds of predicted anomalies shown in grey (to 1SD). The blue line represents CBTAs developed using 1931-1970 20CR MAT and SLP, red line represents 1971-2010 developed CBTAs.

Three time series at other locations are shown in Figure 4.26 (panels b-d) and these show some similar patterns to those seen in the North Pacific and Falklands with 20CR anomalies much colder than CBTAs from ~1880-1930. For the Azores however,

correlation coefficients are lower than many other areas in the North Atlantic and this is largely because atmospheric circulation cannot explain the warmth seen in the 2000s and 1940s. Model performance in the Australian and Siberian regions is better ($r > 0.6$) but once again the earlier years (~1881-1930) show that the cold 20CR anomalies aren't captured well by the CBTAs like in the Falkland's and US Pacific, further highlighting potential climate change influences.

Overall the results in this section show very strong connections between CBTA and MAT on a local scale. In response to the third question in the introduction, relationships between temperature and atmospheric circulation generally haven't changed much over the course of 80 years. Some exceptions are areas such as the Southern Ocean and during the JJA period in the North Pacific (Figure 4.27). The seasonal plots of the correlation coefficients of the two CBTA models shown in Figure 4.27 further demonstrate that the relationships between temperature and atmospheric circulation haven't changed much as most areas show a correlation coefficient over 0.9.

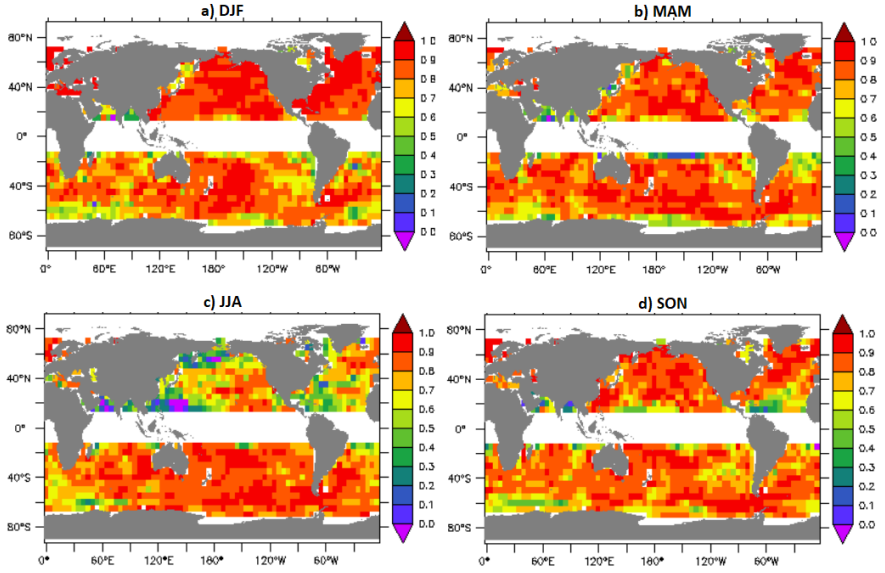

Figure 4.27: Correlations coefficients between the 1971-2010 developed CBTAs and 1931-1970 developed CBTAs for different seasons. Panel a) shows data for the DJF period; b) MAM period; c) JJA period; d) SON period. Correlations are from data during the 1971-2010 period.

The decline in the correlation coefficient seen in Figure 4.4 therefore cannot be explained by changing relationships between temperature and atmospheric circulation. The

decrease in the correlation coefficients however mean the 1931-70 period should be accompanied by increases in uncertainty estimates (assuming 20CR MAT variances are not smaller). Figure 4.28 does show an increase in uncertainty estimates for both the category and misfit uncertainties from the 1931-70 built model (compared to the 1971-2010 model). This suggests that whatever is causing the decrease in the correlation coefficient can be captured by the uncertainties. This is most evident in the North Pacific during the 1931-1970 period for the category uncertainty which appears realistic given that Figure 4.4 showed the largest decreases in the correlation coefficient from 1971-2010 to 1931-1970 here. The southern oceans however see a large drop in the uncertainties of panels a) and b) despite the 1931-1970 period having a weaker relationship between temperature and atmospheric circulation compared to 1971-2010. A comparison of the variances of these two periods shows that temperatures in the 20CR over the far Southern Oceans are a lot less variable in earlier years and because of this lower variability, the uncertainties are also lower (Figure C2 in Appendix C). This is likely to be associated with sparse data coverage over these regions in early decades.

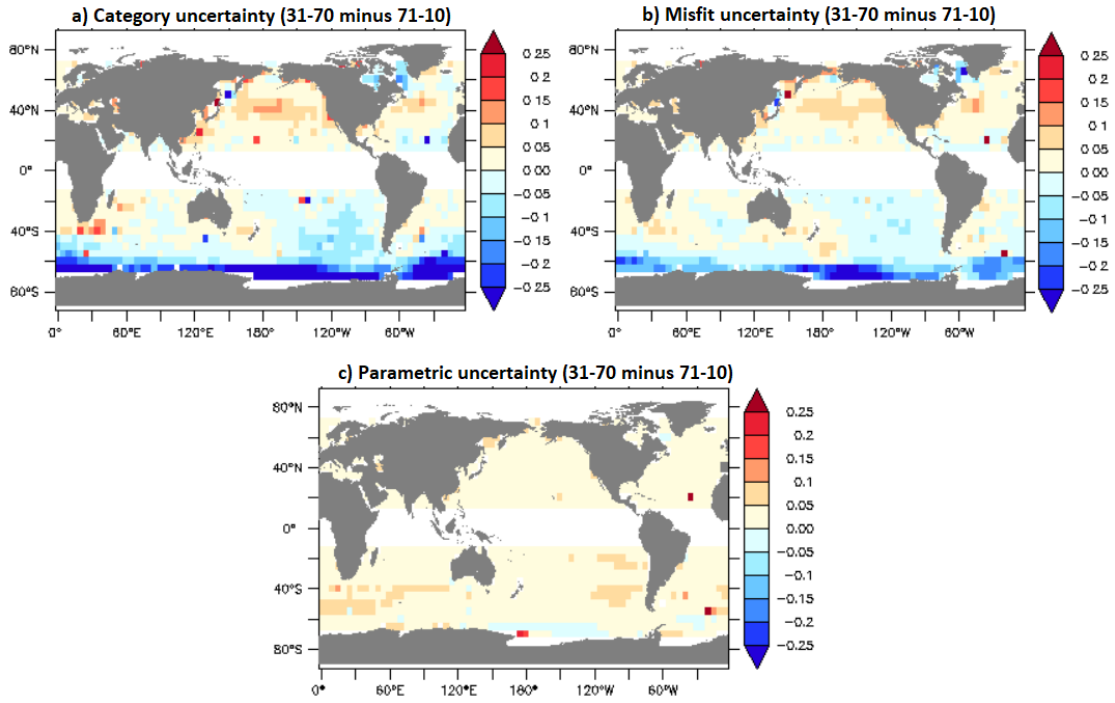

Figure 4.28: Difference between the average uncertainty estimates (°C) for the models developed using data from the 1931-1970 and 1971-2010 periods). Plots refer to all data from the 1971-2010 period. Oranges indicate where the 1931-1970 uncertainty estimates are bigger than the 1971-2010 uncertainty estimates. Panel a) looks at the category uncertainties; b) the misfit uncertainties and c) the parametric uncertainties.

4.5 Conclusions

This chapter expanded on the methods shown in Chapters 2 and 3 and applied them globally to analyse MAT from the 20CR. The results in Section 4.2 found that there were strong connections between temperature and atmospheric circulation in a variety of locations over much of the world's oceans from 1971 to 2010. These strong relationships appear with any of the 'conventional' grid configurations and show that changing them has little impact provided the choices of grid spacing for latitude and longitude are not too large. Comparisons between the spline and stepwise regression method shows that the spline method works much better over many areas with months not used to develop the model and this was used to justify choosing the spline method. Meanwhile an analysis of the uncertainties suggest that they provide accurate uncertainty estimates in many locations. In answer to the first question of whether the spline model can be applied successfully globally, the results in this chapter suggest they can. Looking at months outside the 1971-2010 period however showed that the relationships between temperature and atmospheric circulation appeared to weaken. Section 4.2 analysed either global CBTAs or regional CBTAs to see whether any other influences on temperature besides atmospheric circulation were responsible. Other influences on temperature such as climate change and the AMO were exposed answering the second question in the introduction. Strong correlations between CBTAs and 20CR MAT were found on smaller scales despite these influences acting on the period when the modern model for this chapter was built up (1971-2010), so they were not responsible for the declines in the correlation coefficients.

This led to the question as to whether the relationships between MAT and atmospheric circulation themselves were different during different 40-year periods (an issue raised in the 3rd aim of the introduction to this chapter). To investigate this, Section 4.3 analysed time series and CBTA fields over small regions. There was evidence to suggest relationships between atmospheric circulation and MAT varied over the North Pacific during the JJA period but this was an area and period when relationships were already rather weak anyway. The time series of CBTAs for the 1971-10 built model and 1931-70 model were very strongly correlated over most locations, indicating relationships are consistent between temperature and atmospheric temperature in the 20CR over time.

The thesis so far however has been restricted to the 20CR only and concerns about the quality of SLP and temperature data have been expressed in various studies (e.g. Ferguson and Villarini (2014), Jones, Harpham and Lister (2016)). How much can the results shown in this chapter for the 20CR be trusted? Chapter 5 provides further evaluation of the results in this chapter by comparing SLP and MAT from the 20CR with different datasets.

Chapter 5 Further applications of the CBTA model

5.1 Introduction

In Chapter 4, it was demonstrated that a model could be developed to estimate historical variations in 20CR MAT globally using flow parameters. Strong relationships were found in many regions between the CBTAs and the 20CR anomalies when examining 1971-2010 developed data but relationships weakened when looking at data outside the 1971-2010 period. The results from Chapter 4 indicate that this weakening relationship may be due to the CBTAs inability to capture the climate change signal but some other unusual patterns were found.

Could uncertainties in SLP be playing a role and how widely applicable are the findings from the 20CR in Chapter 4? The analysis so far has only been applied to the 20CR and literature has suggested the quality of this product is lower in earlier years as fewer SLP observations are available and potential issues with SST arise (Ferguson and Villarini, 2014; Jones, Harpham and Lister, 2015; Thorne and Vose, 2010).

The aim of this chapter is to analyse some of the results seen in Chapter 4 further by looking at different temperature and SLP data sources, but to also demonstrate that the model developed can be applied to station data. Such applications will demonstrate that the method developed for calculating flow parameters in this thesis can be generalised and have a variety of uses. The chapter will aim to answer the following questions:

- Can the method of defining atmospheric circulation be applied to different grid configurations of SLP observations?
- Can there be confidence about the time series of 20CR CBTAs based on comparisons with CBTAs generated from other SLP datasets?
- Can any further insights into MAT be found where there are strong relationships between temperature and atmospheric circulation as well as good SLP data?

The chapter will first describe the different SLP datasets in Section 5.2. The data sources for the station SLP are discussed and it is demonstrated that calculating atmospheric

circulation parameters accurately is possible using different grid configurations. For Section 5.3 CBTAs are generated from the flow parameters derived from different SLP datasets. Section 5.4 shows some brief additional analysis by looking at HadNMAT2 and some land air temperature datasets over the North Sea region and Newfoundland. The final section provides some conclusions for this chapter.

5.2 Developing a generalised method for calculating flow parameters

This section first describes the SLP sources used in this chapter and then compares the flow parameters from different grid configurations to show the method developed in Chapter 2 works with station data.

Most of the station SLP data outside of Europe comes from the Global Historical Climatology Network version 2 (GHCN2, Peterson and Vose, 1997). For this dataset station-level pressure data is corrected to sea level and suspected duplicate values (repeated SLP values over 3 consecutive years) are removed. Station-level pressure during earlier years over some locations may not be corrected to SLP in GHCN2 but corrections were made for the construction of the HADSLP2 dataset (Allen and Ansell, 2006). As a result of these corrections there are many station SLP series that extend back well into the 19th century and are available from the Met Office website (https://www.metoffice.gov.uk/hadobs/hadslp2/data/download.html). SLP data for many of these series are updated to the present month with data available from the world monthly surface station climatology dataset (https://rda.ucar.edu/datasets/ds570.0/). In some regions, such as western Greenland and NE Canada, SLP data needs to be taken from multiple locations in order to provide a complete series of SLP data as there can be some gaps. For Western Greenland for example, SLP observations are mainly taken from Nuuk, with data from Jakobshavn used to fill in most of the gaps. The latitude and longitude of each station is noted so the change in location can be accounted for when producing the flow parameter calculations.

SLP observations over Europe often go back further then 1850 as monthly SLP data in this region has been used for long range climate analysis (e.g. Jones *et al.,* 1997). Many of these stations were digitised as part of the ADVICE project (Jones *et al.*, 1999) and some

of the stations can be used to define atmospheric circulation parameters as far back as 1770 in the North Sea region. A full list of the stations used in this chapter can be seen in Table D1 in the appendix Section D. The long SLP series in Hobart and the Falklands have been created in recent studies and are available on the CRU webpage (http://www.cru.uea.ac.uk/data/). Station data for Japan and New Zealand are available from the Japanese and New Zealand websites (https://www.data.jma.go.jp/obd/stats/data/en/smp/index.html, https://cliflo.niwa.co.nz/, abbreviated to JMA and NIWA respectively)

Figure 5.1 shows a map of all the locations where atmospheric circulation parameters are defined in this section. In many instances during earlier decades, SLP from these stations are not assimilated into the 20CR because daily SLP data is required for the assimilation process. The benefit of using monthly SLP data is clear as it is possible to analyse atmospheric circulation patterns outside of Europe going back to the mid-late 19th Century in many places (start years shown in captions of Figure 5.1). Atmospheric circulation parameters can also be defined back to 1770 over the North Sea which can be used to give an insight into climate variability over this region during the Katla and Tambora volcanic eruptions which caused a string of severely cold winters and a year without a summer (1816) respectively (Schmidt *et al.*, 2010; Veale and Endfield, 2016). Even in the Tasman Sea it is possible to define atmospheric circulation parameters going back to 1864 using the grid pattern in panel g). The station SLP data may have its own biases however (e.g. over South America, Jones, Harpham and Lister, 2016) so for further validation, ERA-20C SLP data is taken from all the points where the station data is located also. The ERA-20C like the 20CR is also a reanalysis product but data is generated using a different model and it also assimilates surface marine wind observations (Poli *et al.,* 2016).

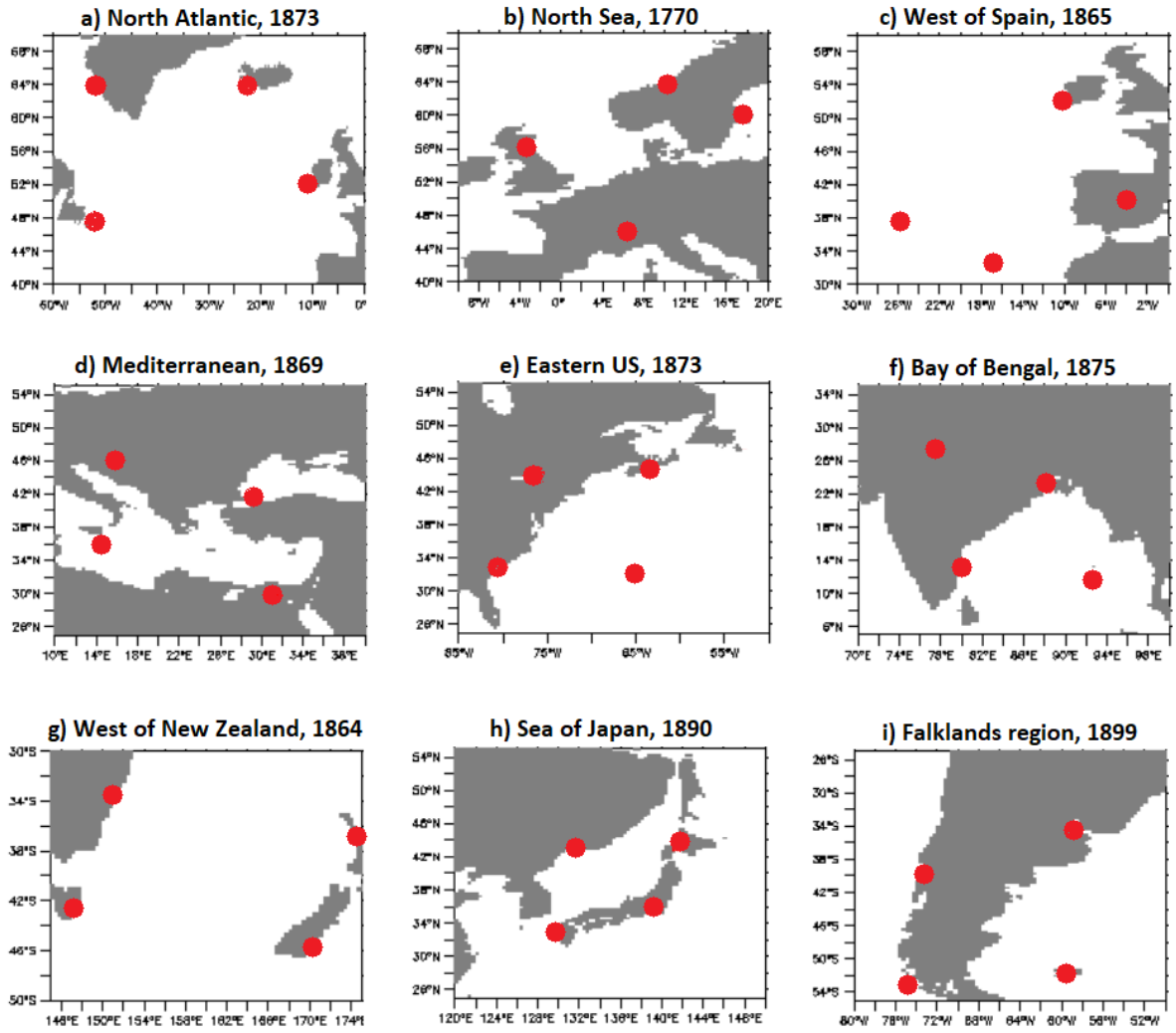

Figure 5.1: Stations of SLP data from Table D1 and the regions for which they are used to help calculate atmospheric circulation parameters. The first year on which all 4 points in each panel have SLP data is listed on each caption.

The advantages of looking at monthly SLP data are emphasised further when looking at the coverage of the International Surface Pressure Databank (ISPD, Cram *et al.,* 2015) during earlier years. The 20CR assimilates daily ICOADS SLP and Land SLP from the ISPD version 3 for its product (Compo, 2014). The levels of coverage are particularly low before the 1900s as seen by the plots for 1870 and 1885 in Figure 5.2. The majority of SLP observations assimilated into the 20CR are from the Northern Hemisphere and are especially concentrated over the USA, Europe and Eurasia. The number of observations is particularly low in the southern hemisphere during 1885 for example with daily station data only assimilated into the 20CR from the Falklands, 3 stations from East Africa, 6 from

Australia and 2 from Indonesia. There are also no assimilated land observations from the Bay of Bengal, Japan, New Zealand or the NW North Atlantic though some ship observations are available. Some SLP observations may be available from ICOADS but the lack of assimilated SLP observations raises the question of what impact the change in coverage has.

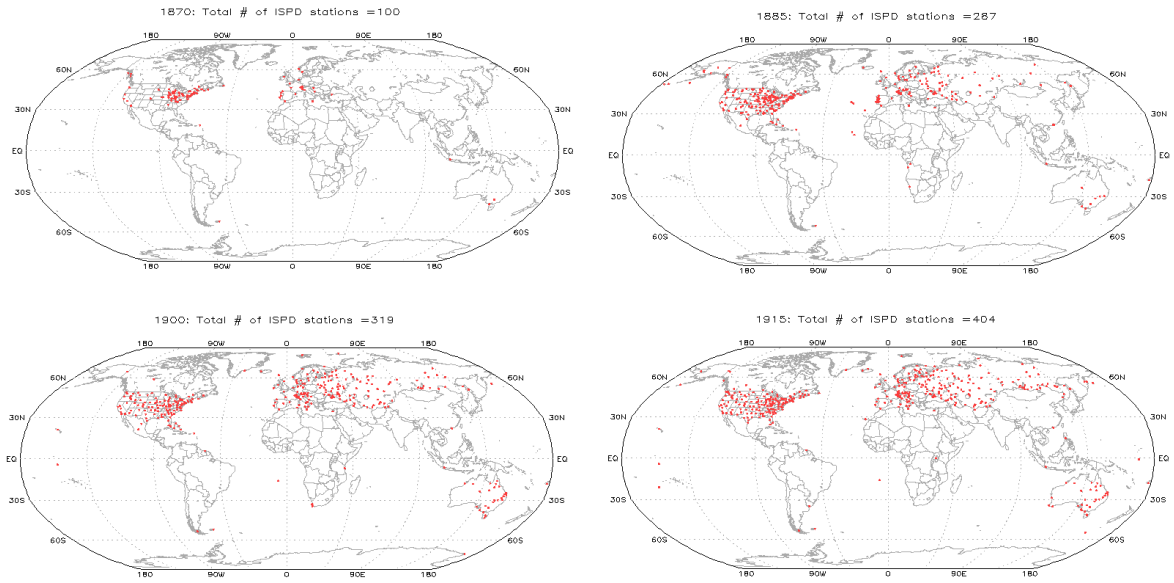

Figure 5.2: Locations of available stations in the ISPD which are assimilated into the 20CR from 4 example years; a) 1870 (100 stations); b) 1885 (287); c) 1900 (319); d) 1915 (404). Plots can be accessed on the ISPD website: https://www.esrl.noaa.gov/psd/data/ISPD/v3.0/

Before such comparisons took place however it was important to check whether the method in Chapter 2 is able to calculate the flow parameters accurately for different grid configurations. In order to assess this, SLP was extracted from each station data grid point from the 20CR. Then the flow parameters were defined from these 4 points at each of the 9 locations shown in Figure 5.1. The westerly and southerly flow components were defined by first interpolating the SLP at the relevant north, east south and west locations. An example of this is shown at the North Sea point is shown in Figure 5.3 with interpolated SLP values represented by the blue points (further information given in appendix D). This interpolation was done so the westerly and southerly flow components can be defined directly from the SLP gradients. The latitudes and longitudes were picked

to try and calculate the atmospheric circulation pattern at the central point between the 4 SLP stations. This is done because the 'conventional' grid patterns discussed in Chapters 2-4 define atmospheric circulation at the point in the middle of the grid configuration.

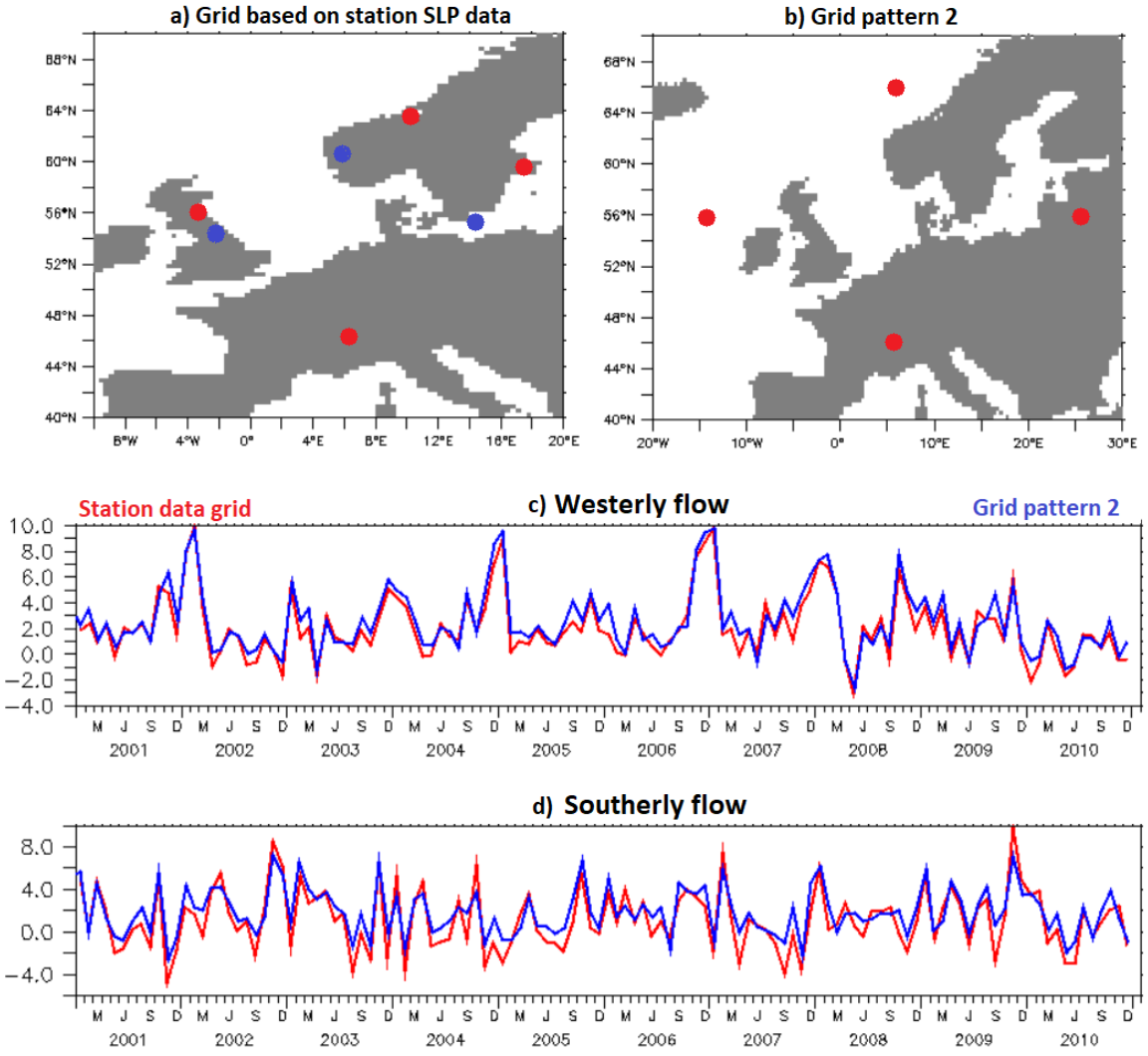

Figure 5.3: A comparison of flow parameters (in ms^{-1}) at the North Sea point; a) Grid pattern based on station SLP data. Stations of SLP data are shown in red. Interpolated points of SLP are shown in blue and these are used to calculate the flow parameters; b) The most similar conventional grid pattern (from Figure 3.7) to panel a which is used as a comparison; c) Westerly flow values from both the grid patterns covering the period 2001-2010. The red line shows westerly flow derived from the grid in panel a) whilst the blue line is derived from the grid in panel b); d) As with panel c but for southerly flow parameters.

The 20CR westerly and southerly flow parameters calculated from the North Sea grid pattern (panel a)) were compared to the atmospheric circulation parameters from

'conventional' grid pattern 2 shown in Figure 5.3 panel b) and also Figure 3.7. This grid pattern was chosen for comparison as it is most alike to the distribution of station SLP points in panel a). If the flow parameters are very strongly correlated and of the right size then it can be assumed the atmospheric circulation patterns are being calculated accurately as it was shown in Chapter 2 that the flow parameters from 'conventional' grids are very strongly correlated to the ones from the J12 method. The time series in Figure 5.3 for the 'conventional' and station SLP grids are very strongly correlated overall ($r > 0.9$) for both southerly and westerly flow. This confirms that flow parameters can be defined using station data grid configurations. There are some minor differences which are more apparent with a southerly flow but this is to be expected given that flow parameters are calculated from SLP values taken from different regions of the North Atlantic basin. Finally, to confirm the method works for other types of grid configurations and other locations, another time series is shown but this time for a grid pattern covering the North Atlantic (Figure 5.4). The results show that the flow parameters from the different grid configurations again are very strongly correlated with each other.

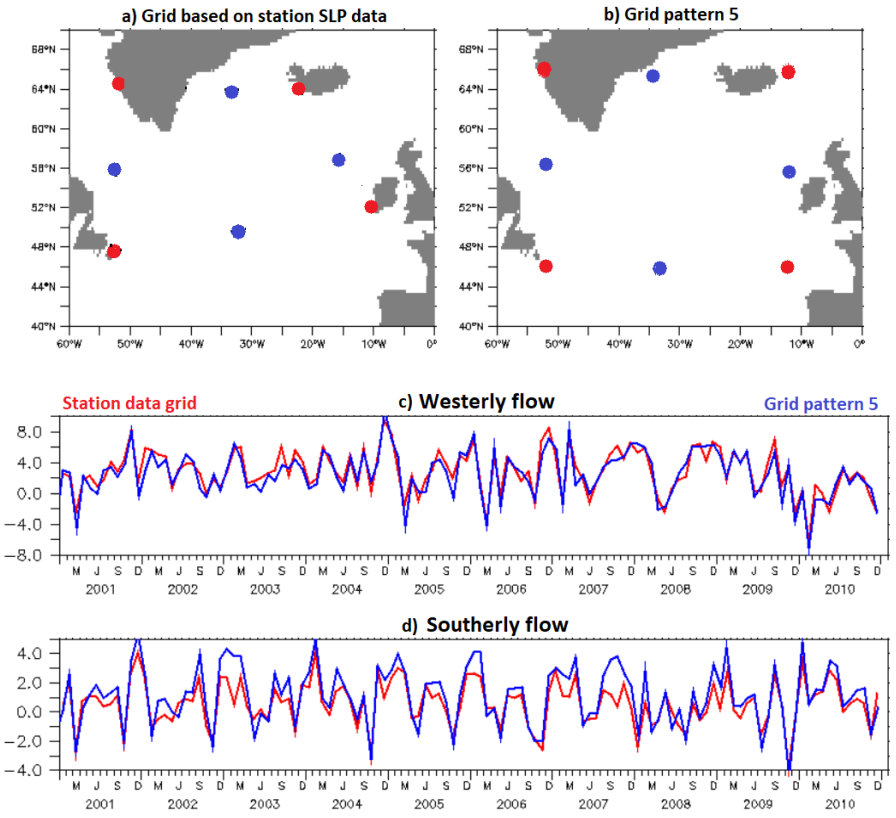

Figure 5.4: As with Figure 5.3 but for a location in the North Atlantic.

A further analysis is provided in Table 5.1 and this shows high correlation coefficients everywhere between 20CR flow parameters defined from Station SLP grid configurations and the conventional configurations from previous chapters. These results provide further confidence that the method developed in this chapter can define atmospheric circulation parameters from station data grid configurations. The southerly flow parameters can sometimes show some weaker correlations, especially in the Bay of Bengal but SLP gradients are particularly slack here. When SLP variability is smaller, differences in the flow parameters due to the grid configurations become more important. This is why correlations tend to be a bit lower in the JJA months when SLP variability is lower.

Overall however the results in this section show that the flow parameters from station grid configurations compare well with the flow parameter calculations from previous chapters. The next sub-section therefore goes through the results of the different CBTA predictions at some of these locations.

Location	Grid pattern	Wflow DJF	Wflow MAM	Wflow JJA	Wflow SON	Sflow DJF	Sflow MAM	Sflow JJA	Sflow SON
North Atl.	5	0.93	0.90	0.84	0.86	0.96	0.94	0.94	0.96
North Sea	2	0.99	0.97	0.89	0.97	0.93	0.91	0.87	0.93
W. of Spain	2	0.99	0.98	0.96	0.98	0.89	0.84	0.8	0.84
Mediterra-nean	4	0.95	0.95	0.90	0.95	0.94	0.86	0.82	0.94
Eastern US	4	0.90	0.85	0.88	0.92	0.94	0.87	0.73	0.86
Bay of Bengal	4	0.97	0.98	0.94	0.99	0.51	0.76	0.61	0.52
W. of New Zealand	4	0.92	0.90	0.95	0.96	0.96	0.96	0.98	0.96
Sea of Japan	4	0.96	0.98	0.98	0.96	0.94	0.96	0.80	0.94
Falklands	4	0.91	0.88	0.96	0.88	0.78	0.83	0.85	0.82

Table 5.1: Correlations between westerly (wflow) and southerly flow (sflow) parameters at different locations and for different seasons. The flow parameters are defined from the grid patterns in Figure 5.1 and then compared to the most similar of the conventional grid configurations shown in Figure 3.7. The conventional grid used for the comparison is listed in column 2.

5.3 CBTAs from different SLP datasets

An issue not discussed in Chapter 4 was the extent to which uncertainties in SLP could affect the model. In the 20CR the uncertainties due to SLP are very low. Out of the 5 uncertainties discussed in Chapter 4, the 20CR SLP uncertainties are smallest, typically contributing to 0-5% to the total uncertainty during the 1971-2010 period used to develop the model. Going further back in time the contribution of SLP to the total uncertainty of a CBTA estimate increases. From 1931-1970 uncertainties in SLP become larger across the whole southern hemisphere. From 1891-1930, SLP uncertainties generally contribute to around 15-30% of the total uncertainty, with exception to the North Atlantic basin (panel c) and Mediterranean where uncertainties are still very small. Even during the 1851-1890 period the contribution of SLP to the total uncertainty of CBTAs in parts of the North Atlantic is below 10% (panel d). The small SLP uncertainties in the North Atlantic indicate there is little variation in SLP between the 26 ensemble members examined so there can be confidence that the CBTA fields from the 20CR won't vary much. Are the SLP uncertainties potentially too low however? This section compares CBTAs from station SLP data (with flow parameters defined as shown in the previous section) and the ERA-20C with the 20CR to answer this question.

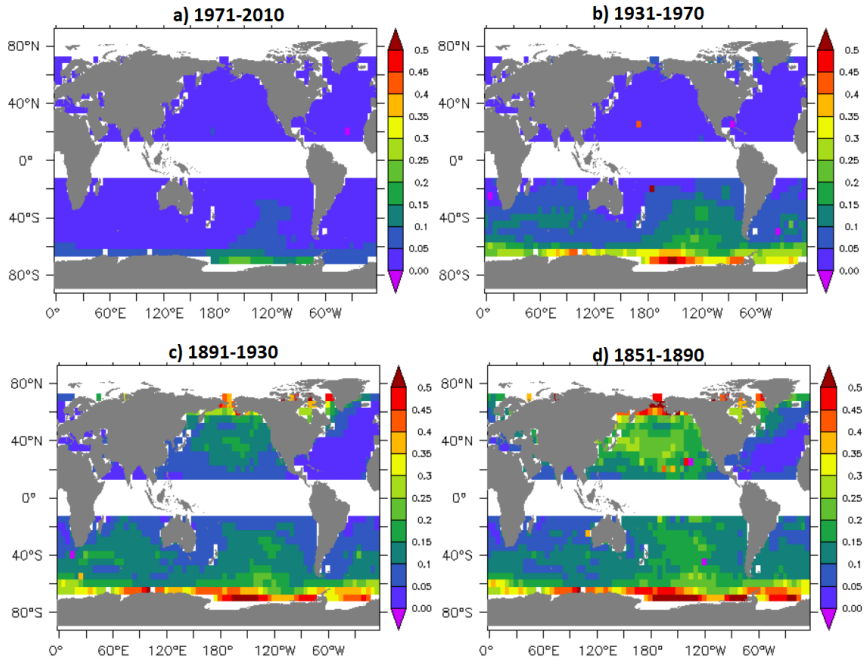

Figure 5.5: The uncertainty in the CBTAs (°C) of chapter 4 due to variations in SLP of 25 ensemble members. The SLP uncertainties are shown for 4 different periods, each covering 40 years.

5.3.1 North Sea time series

In this section time series of CBTAs are analysed at some of the locations shown in Figure 5.1. There are 3 CBTA estimates for each time series, the first from the 20CR flow parameters, second from the ERA-20C and third from the station SLP data. In order to produce the CBTAs for the North Sea using the different SLP data sources, SLP is extracted from the 4 points shown in Figure 5.1a and then the westerly flow, southerly flow and average SLP are calculated. This leaves each month with three different flow directions, flow strengths and average SLP values. For February 2010 for example a CBTA is extracted from 3 different locations on the CBTA field shown in Figure 5.6.

This CBTA field like in previous chapters is based on 20CR SLP and MAT only because the aim of this section is to show how uncertainties in SLP only contribute to variations in the time series of CBTAs. By choosing just the 20CR CBTA field to develop the time series of CBTAs from different SLP data products, the only differences that appear between the 3 different time series are from SLP itself (due to differences in flow indices). It can also be difficult to highlight differences in the CBTA fields between different SLP data products, given there are areas in them which are unconstrained due to a lack of observations (which are sensitive to small changes to the input field).

Time series of CBTAs in the North Sea were analysed again in this section because the atmospheric circulation parameters extend back to cover periods of exceptionally cold winters before 1850. Winters before 1850 in the CET series were generally 1-2^{o}C colder than the 2010s (Parker, Legg and Folland, 1992). Is such cold backed up by the atmospheric circulation parameters or is there a large cold residual that was also present in the early 20th Century across other parts of the world such as the Pacific and Falklands? The North Sea analysis aims to answer that question.

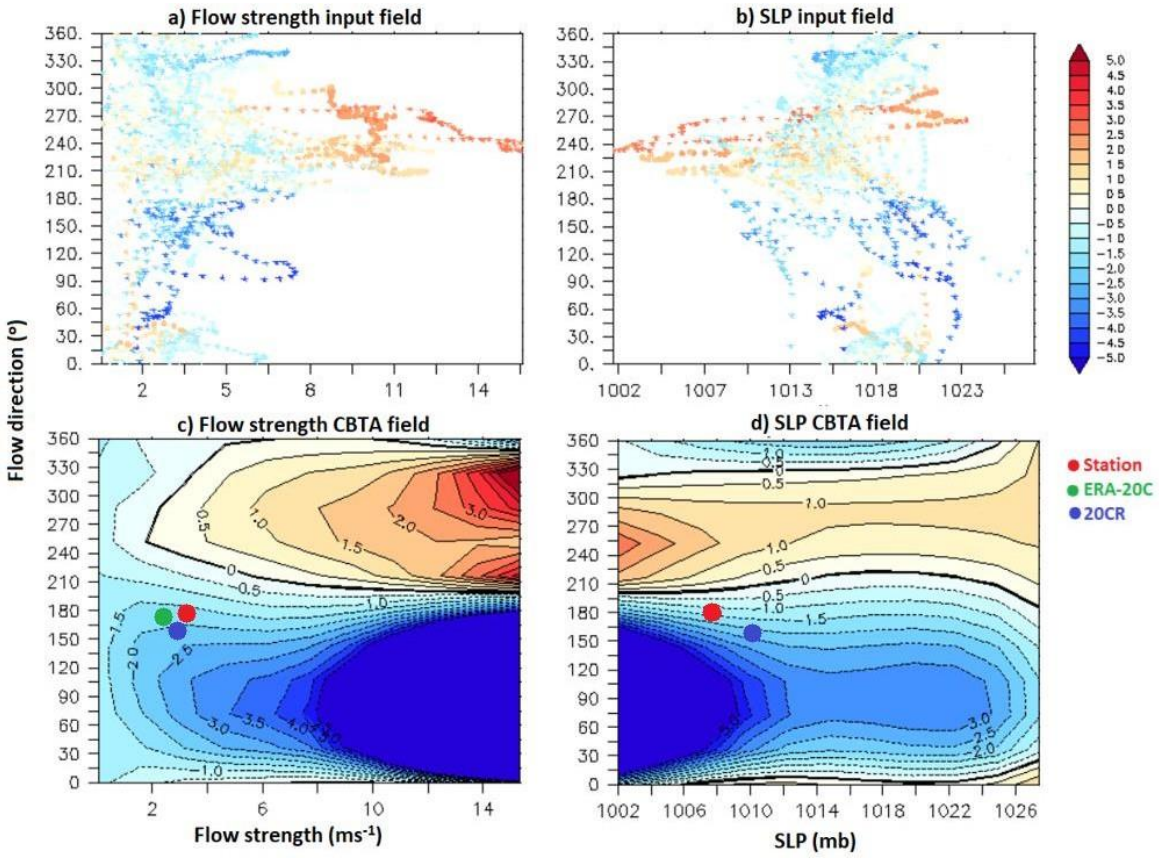

Figure 5.6: February CBTA (°C) fields at the North Sea region showing; a) Flow strength input field, b) SLP input field; c) Flow strength CBTAs; d) SLP CBTAs. CBTAs consist of flow parameters from 1971-2010. The flow parameters for the 3 different SLP datasets are shown for the month of February 2010. The red point represents station data flow parameters, blue from the 20CR and Green from the ERA-20C. In panel b) the red dot closely overlies the green dot.

Time the time series from 1880-2010 are analysed showing results from all 3 SLP datasets. If there is a high level of confidence in the 20CR SLP data then the CBTAs derived from station SLP data, the 20CR and the ERA-20C should be in close agreement. The time series of CBTAs in the North Sea however provide some mixed results (Figure 5.7). During the DJF period all three different time series are in very strong agreement from 1851- 2010 ($r > 0.90$ between station data CBTAs and 20CR CBTAs for example). The same can be said for the MAM period but during the JJA period there are some clear differences between the CBTA time series.

The JJA period of 20CR CBTAs are often much warmer (+1.0°C) then the CBTA time series from station data up until the 1940s, indicating some uncertainty with the SLP data. The

differences during the JJA period are due to an apparent SLP bias in the 20CR over Scandinavia and Eastern Europe where SLP values are too high (~2.5mb). This is in agreement with the analysis by Stryhal and Huth (2017) who suggested the 20CR SLP values were too high from comparisons with the ERA-20C although they looked at data from the 1960s onwards. The result of these biases is that southerly and easterly winds are slightly stronger for the 20CR (shown in the 1930s, Figure 5.8) compared to the station data which is what leads to warmer JJA anomalies. From the 1960s onwards the ERA-20C CBTAs are in closer agreement to the station data but before WWII the ERA-20C CBTAs also appear too warm. In contrast winter CBTA anomalies in the station data are often 0.2°C to 0.3°C higher than the 20CR CBTAs because the flow parameters from station data usually have a stronger westerly flow (again related to the Eastern European SLP biases).

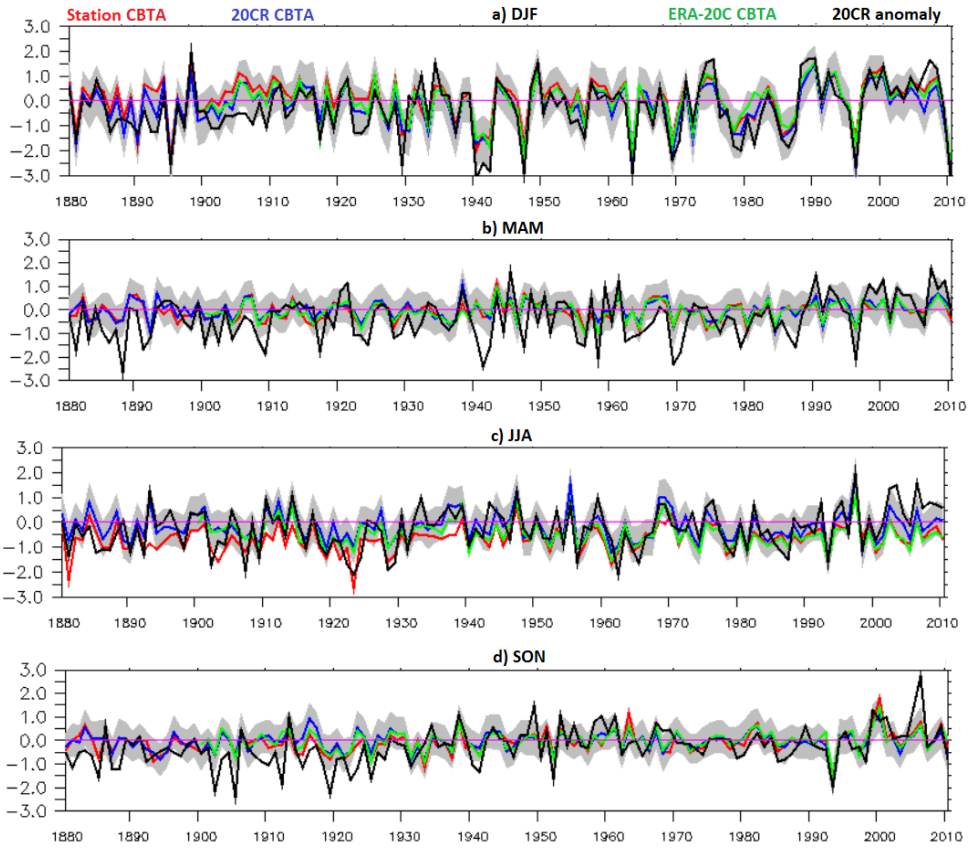

Figure 5.7. Time series of CBTAs (°C) for the North Sea (5E/55N) during four different periods of the year covering the period 1880-2010. The blue time series represents 20CR CBTAs, green represents the ERA-20C and red represents station SLP data. Grey regions mark the 1SD uncertainty bounds of the 20CR time series. The model is built using 1971-2010 20CR flow parameters and MAT as in Chapters 2 and 3.

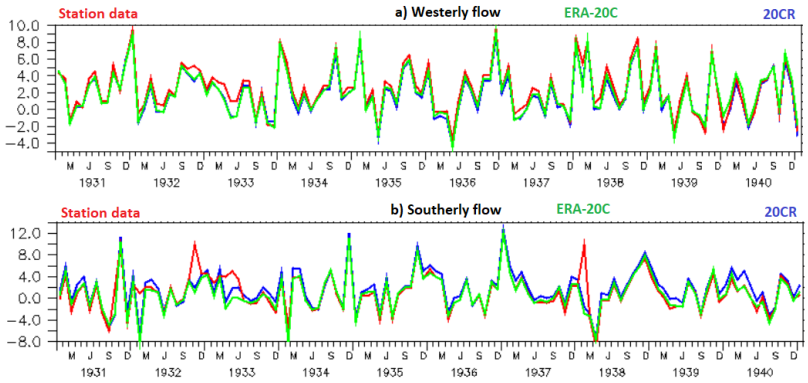

Figure 5.8: Monthly time series of westerly and southerly flow parameters (ms^{-1}) from 2001-2010 over the North Sea region. Flow parameters are calculated from station SLP data (red), 20CR (blue) and the ERA-20C (green).

The differences in SLP between the 20CR, Station SLP and ERA-20C for the North Sea region are shown in Figure 5.9. The areas with the smallest differences in SLP are in Edinburgh (with the exception of the 1930s) and Geneva. Plots are shown for the month of February but the differences in SLP follow a similar theme throughout the year. The SLP values for Edinburgh station SLP data vary closely in accordance with the 20CR with the exception being the late 1910s and during the 1930s. The causes for these differences are not understood but they can be over 10mb on occasion (residuals from panel e). The Geneva SLP series shows little difference with the 20CR throughout whilst Trondheim and Uppsala appear to consistently have a consistent positive SLP bias in the 20CR. These SLP differences do not matter when the variations in SLP are often large, such as the DJF period. However, during the JJA period they are important as Figure 5.7c shows.

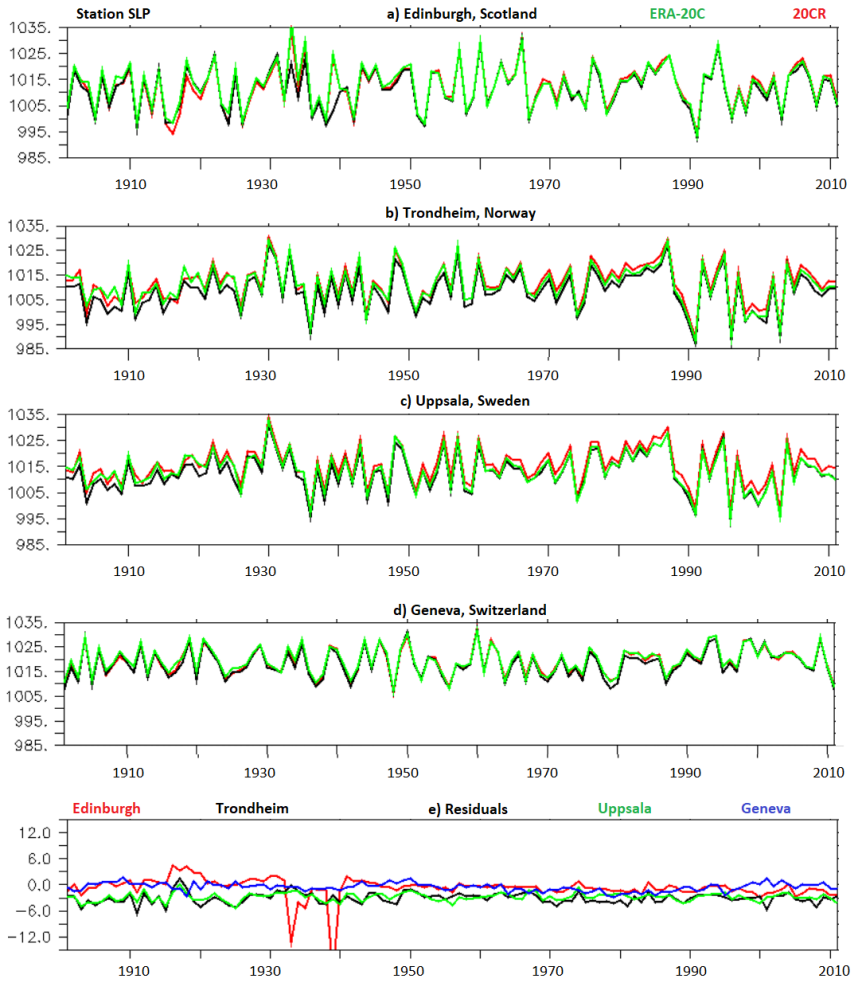

Figure 5.9. Time series of SLP (millibars) for 4 location around the North Sea (6E/56N) region during February. For panels a-d) the red time series represents 20CR CBTAs, green represents the ERA-20C (calculated by using bi-linear interpolation) and black represents station SLP data. Panel e shows the residuals of each of the time series of station SLP – 20CR SLP data.

Aside from uncertainties in the Summer CBTAs, these results are promising because they suggest a high level of confidence should be placed on the CBTA time series at the North Sea based on comparisons from different SLP datasets. With station data in this region going back to 1770 the analysis of CBTAs can be extended back even further. Before the 1850s some interesting features begin to appear when comparing CBTAs with the air temperature over land. Figure 5.10 shows a comparison between DJF station data CBTAs with air temperatures over Copenhagen (the nearest station). The air temperature series over Copenhagen is notably cold up until the mid-19th Century. Such persistence of below average temperatures however is not seen in the CBTA time series. The CBTAs suggest that the winters during this time should not have been cold at all with the CBTAs

fluctuating around the 1971-2010 climatological average. The residuals during the early 19th century are often between -2°C to -4°C and cannot be explained by uncertainties in the model so another factor appears to be causing the cold winters over Copenhagen.

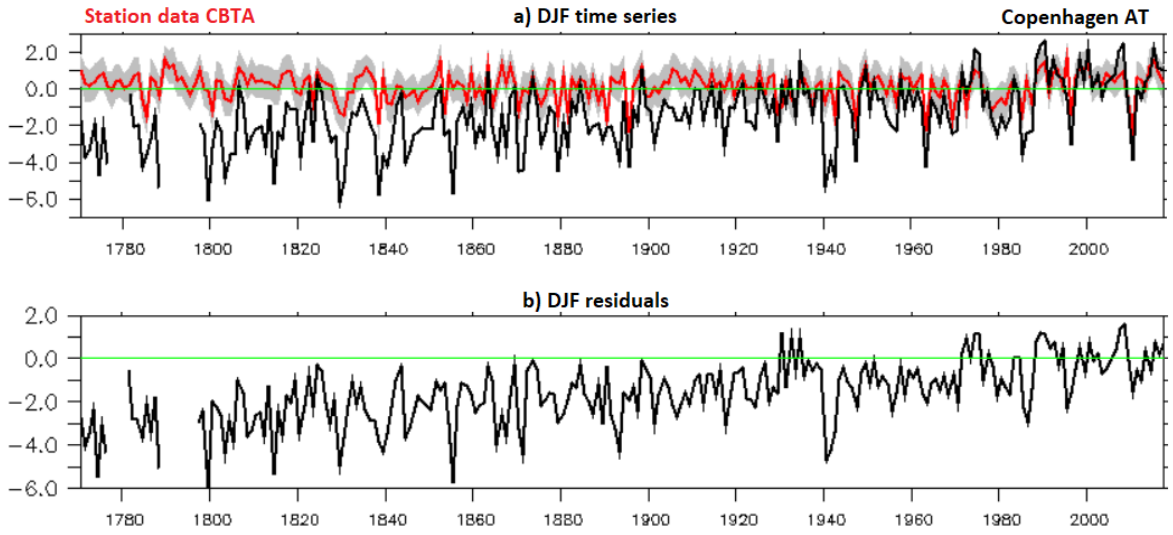

Figure 5.10: a) Extended time series at the North Sea point showing CBTAs (°C) extending back to 1770. Air temperature data for Copenhagen shown in black and is taken from the GHCN version 3; b) Copenhagen AT – Station data CBTA residuals

Some minor differences should be expected between the CBTAs and Copenhagen air temperature however. Land temperature during the DJF period is often influenced by snow cover and when there is snow cover, the albedo from the snow reflects heat back into the atmosphere so nights can be much colder (Foster, Owe and Rango, 1983). Conversely, over the oceans the same effect will not be seen. Despite these differences, the residuals for the time series in Figure 5.10b are still notable and bear some resemblance to those seen in the Pacific and over the Falklands in Chapter 4 which also had periods of notable cold during the early 20th century which couldn't be explained by the model. These results therefore may indicate that a notable warming trend was taking place in the North Sea region before the 1940s (there is a residual warming is 0.15°C per decade up to 1970) as after this period the residuals fluctuate around zero more often, with a weaker warming trend (0.08°C warming per decade, panel b). They perhaps also indicate the unusually cold temperatures in the South Atlantic in the early 20th century may be real as persistent negative residuals are seen elsewhere, though more research is needed.

5.3.2 North Atlantic and west of Spain time series

Results for the North Sea point were encouraging because the different time series of CBTAs were in close agreement despite some SLP differences of varying size. The North Sea region however is an area which has plentiful SLP coverage (J12) so strong agreement should be expected. Can there be confidence with regards to the results further west in the North Atlantic as well? Validation here is important given some key results for this region shown in Chapter 4.

The comparisons between the SLP datasets for this region in Figure 5.11 suggest there can be confidence about the CBTA estimates from the 20CR as time series of SLP are in very close agreement, more so than seen at the North Sea. It could be assumed that all the SLP data assimilated from ICOADS, North America and Europe is sufficient enough to allow for accurate modelling of past SLP in mid-high latitudes of the North Atlantic basin and in NW Europe. Hardly any differences are seen in the time series of Figure 5.11 for all locations from ~1930-2010. The only exception is the station data up until 1930 over Nuuk which is consistently lower than the ERA-20C and the 20CR. Given that both the ERA-20C and the 20CR SLP time series are in close agreement over Greenland, it appears there is a problem with 20CR SLP data and this is backed up by data analysis in the arctic where the gridded SLP data products differed from the station data (Przybylak *et al.*, 2013). Regardless of this discrepancy all the time series of CBTAs are in close agreement so there can be confidence about the results gained from Chapter 4 over this region.

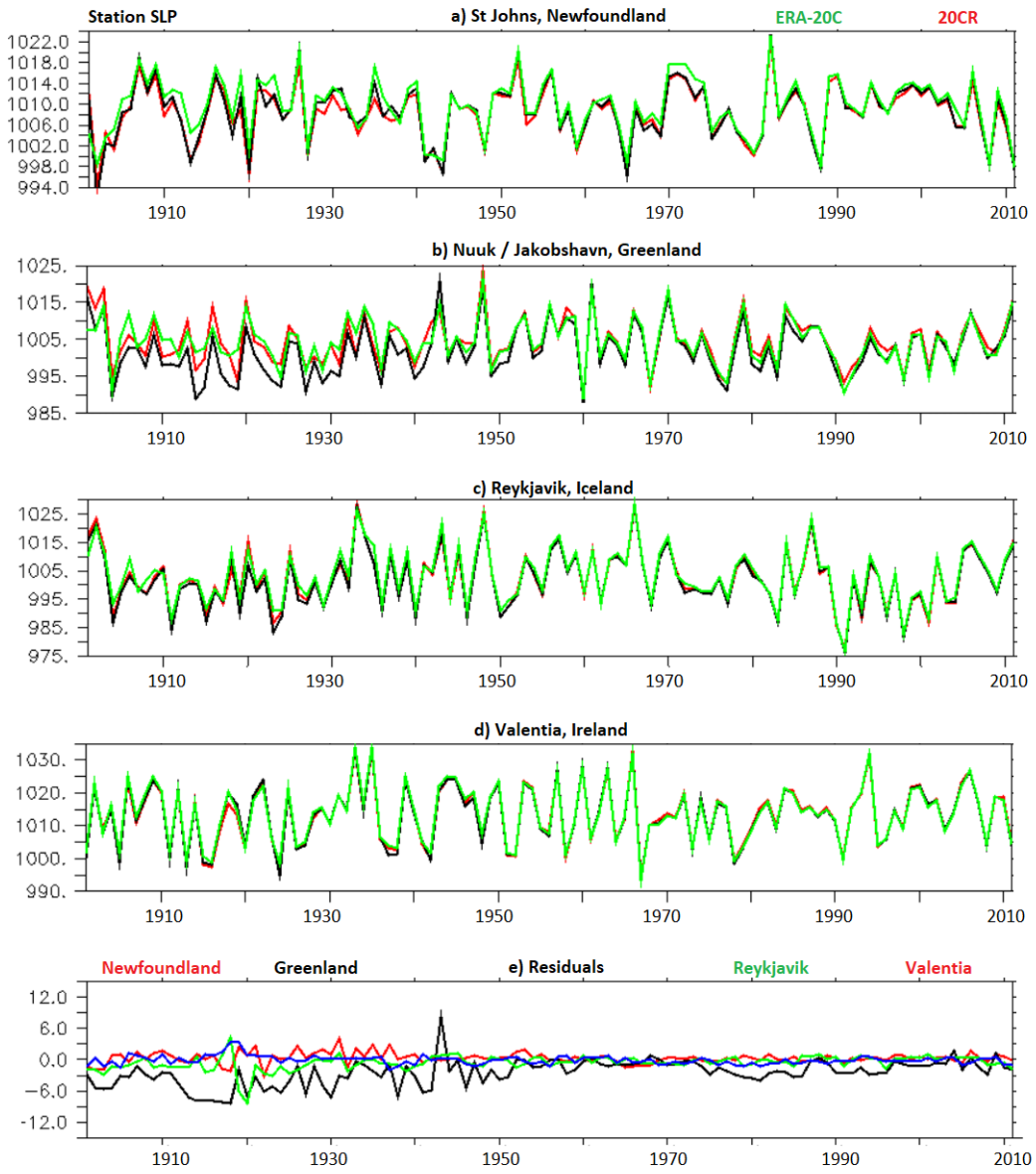

Figure 5.11: As with Figure 5.9 but for stations used in the North Atlantic region (displayed in Figure 5.1a).

Moving further SE in the North Atlantic, a less clear picture begins to emerge with respect to the quality of the 20CR output. Whereas the positive SLP biases Scandinavia appear to be similar throughout, the SLP biases in the Madrid time series do not which has implications for the time series of CBTAs (which is shown in Appendix D). The time series of SLP are shown in Figure 5.12 for the 4 relevant SLP stations covering every month from January 2001 to December 2010. The time series for Ponta Delgada, Valentina and Funchal all appear fine as the residuals appear to be very small with the odd exception.

The time series for Madrid however has a clear annual cycle to the residuals. The Station SLP data is often lower than the ERA-20C and 20CR SLP during the extended summer months (May- October), the reasons for which are not known. The temperature time series of CBTAs as a result during the extended summer months shows some differences between the Station, ERA-20C and 20CR based CBTAs. For other months the time series show little variation between the different CBTAs (Appendix D).

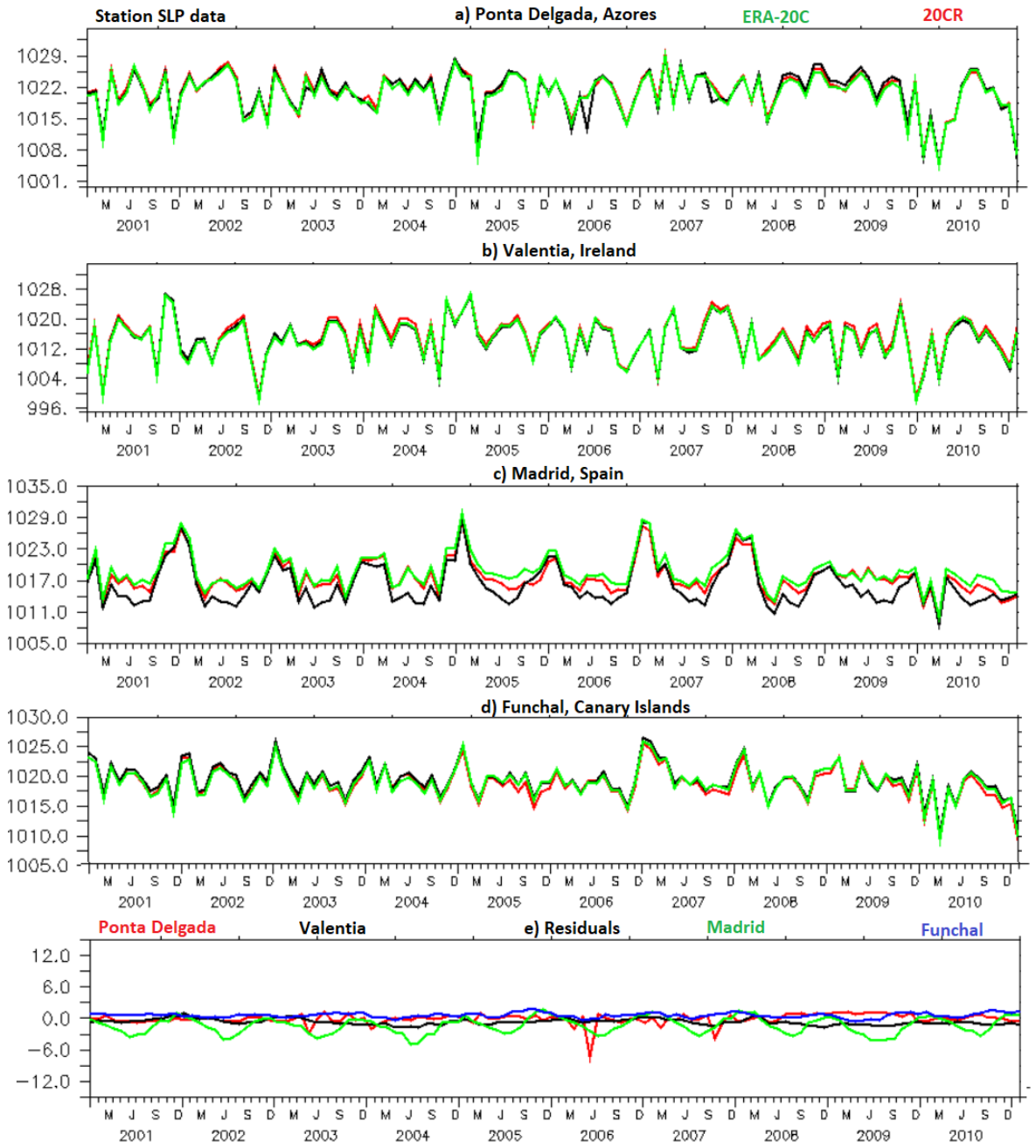

Figure 5.12: Monthly SLP (millibars) values from January 2001-December 2010 for 4 locations (panels a – d) used to calculate atmospheric circulation parameters to the west of Spain. Panel e) shows the Station SLP – 20CR residuals.

5.3.3 Falklands time series and brief discussion of other areas.

The Falklands were identified as an interesting region to study because of variations in the level of SLP data assimilation in the 20CR during earlier years (Jones, Harpham and Lister, 2016) and the unusual cold anomaly that occurred there during the early 20th century (Hegerl *et al.,* 2018). The CBTAs from the 20CR SLP suggested that the cold 20CR MAT during the early 20th Century could not be explained by variability in atmospheric circulation and that some other factors were causing the cold anomalies. CBTAs were therefore also developed from the station, ERA-20C and 20CR SLP values in this region.

The time series of SLP based CBTAs give an uncertain picture of past MAT variability in the Falklands region unfortunately (Figure 5.13). From 1900 to ~1960 for the DJF period good agreement ($r > 0.5$ and all three different time series often stay within uncertainty bounds of the 20CR CBTAs) can be seen between the 3 CBTA datasets but the 1960s to the 1980s see some large contrasts. The most unusual CBTAs are seen with the station data and are most notable during the mid-1960s. The station data CBTAs are especially warm with CBTAs often 1 or 2 degrees above average. Differences in SLP still cause variations in the CBTAs after this point until the present day with the 20CR CBTAs often being the coldest time series.

The large positive anomalies in the station data during the mid-1960s are likely to be the result of biases in station SLP data (Jones, Harpham and Lister, 2015) with the SLP series in Valdividia and Buenos Aires being particular causes for concern. What is surprising is that there are marked differences between the CBTAs for the different time series during the 2000s. During MAM for example, the station data CBTAs are a lot warmer than the 20CR CBTAs. The ERA-20C CBTAs however also agree with the station data rather well indicating some problems with SLP in the 20CR.

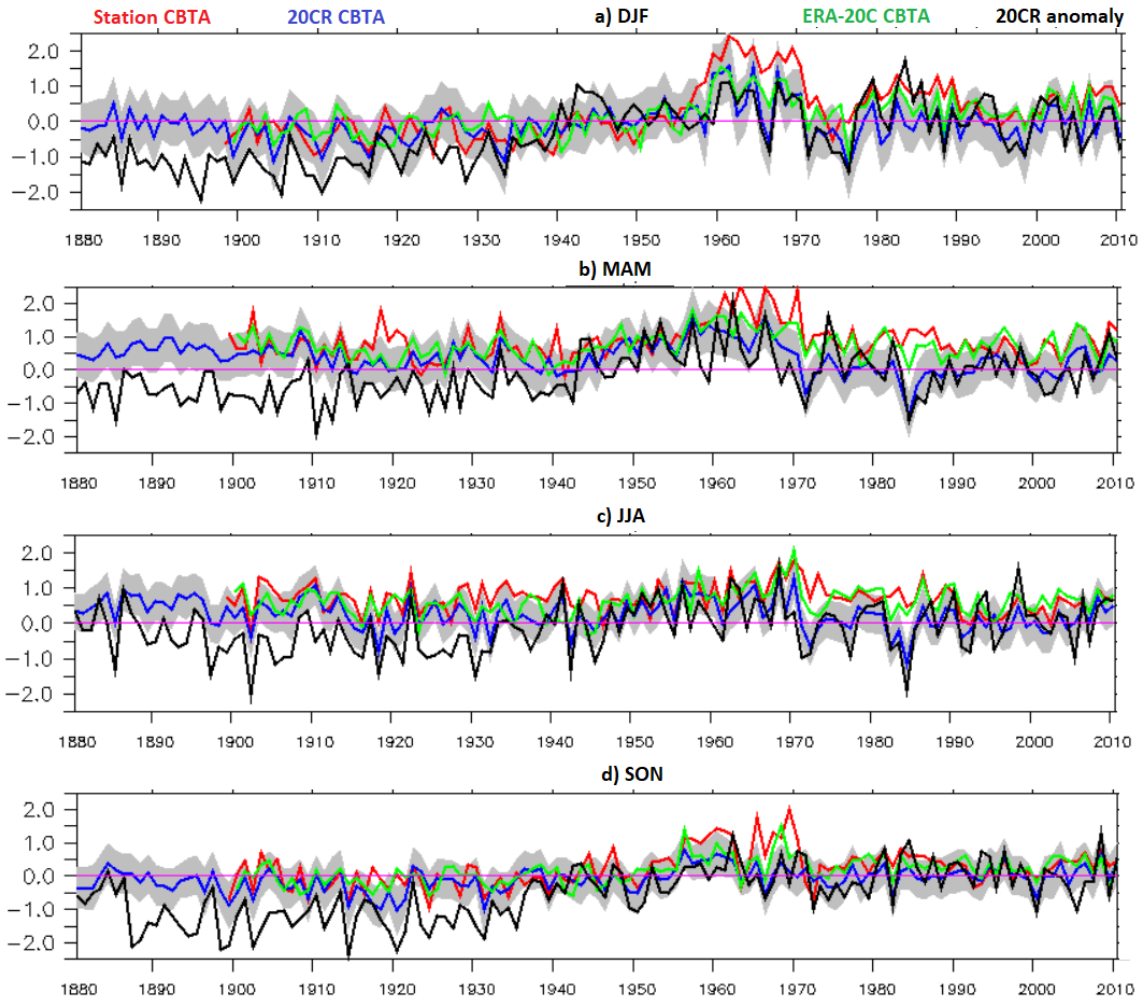

Figure 5.13: As with Figure 5.7 but for a region to the North of the Falklands

When examining the SLP data, the two problematic SLP stations (Buenos Aires and Valdivia) can be clearly seen in Figure 5.14. This shows that there are some issues in what appears to be the 20CR SLP, especially for the DJF period, a time of the year when relationships between temperature and atmospheric circulation are at their strongest according to Chapter 4. The Falklands and Southern Chile time series also appear to have biases, but these are generally smaller according to panel e). The main contributor to the uncertainties in the CBTAs in Figure 5.12 appears to be the annual cycle of SLP data over Buenos Aires. How these uncertainties affect the westerly and southerly flow parameters is also shown by the time series plots in Figure 5.15 from 2001-2010, which demonstrates how uncertain the 20CR SLP data is which goes towards developing the prediction model itself.

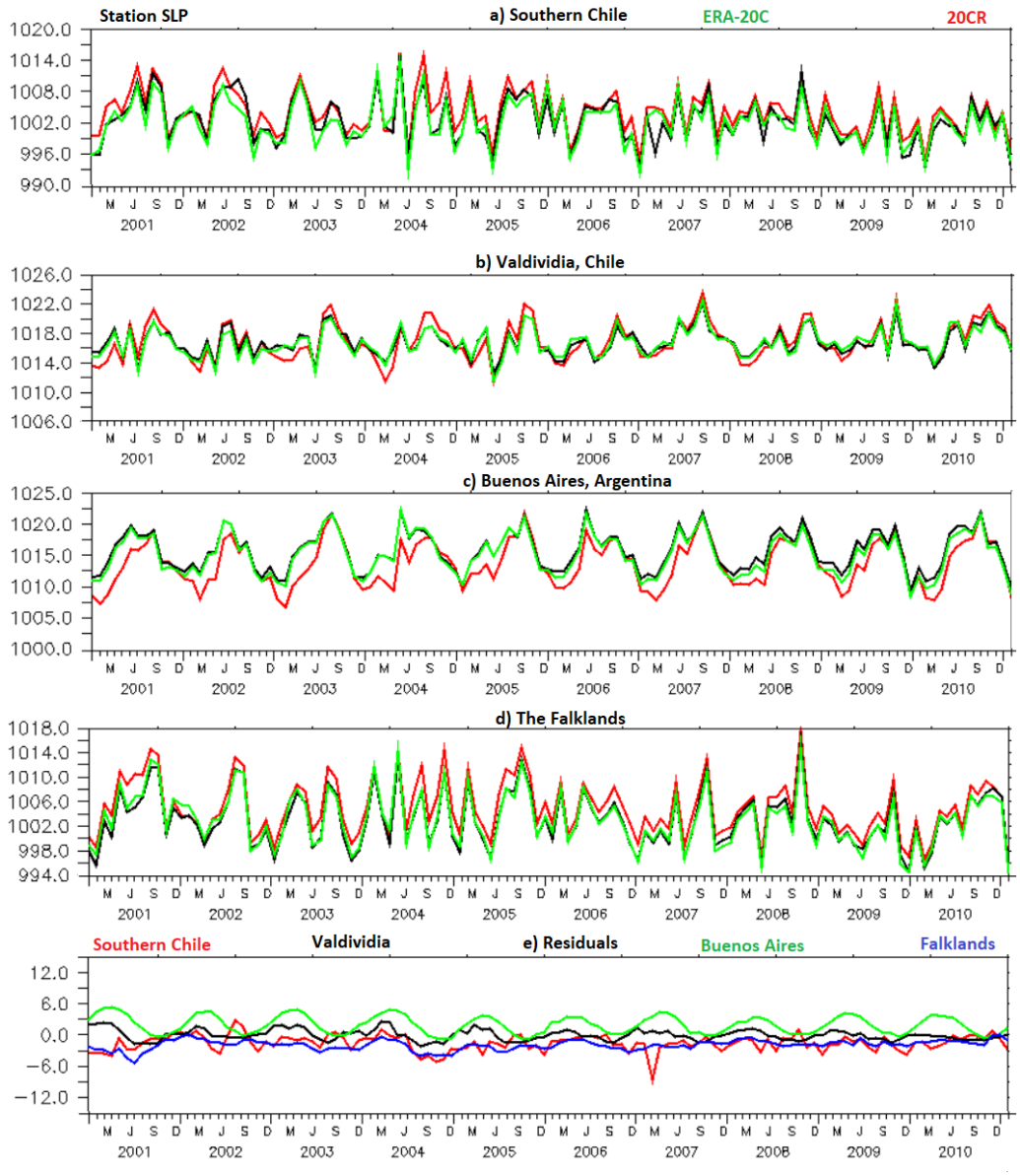

Figure 5.14: As with Figure 5.12 but for the Falklands region (months January 2001 to December 2010).

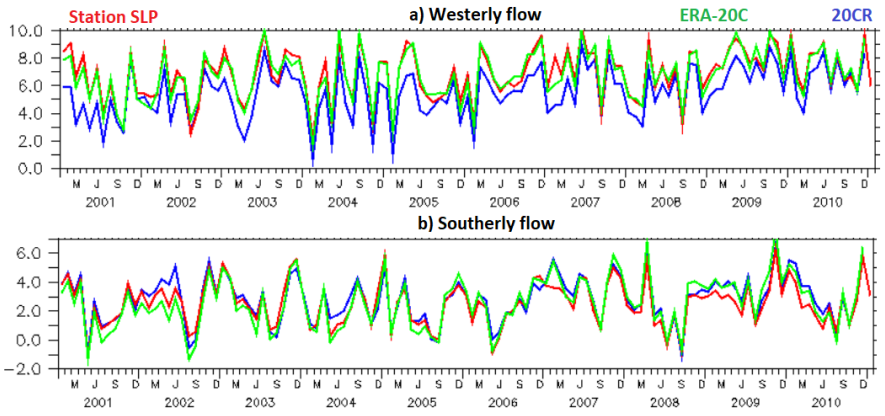

Figure 5.15: As with Figure 5.8 but for the region to the North of the Falklands

The problems with SLP become more complicated further back in time as shown with Figure 5.16. In earlier years SLP data appears very uncertain over the Falkland Islands area itself. Up until 1955 SLP for the station data is often 3-6mb lower than the 20CR SLP (panel e) with the most notable differences being from 1915-1925. The ERA-20C follows the station data closest indicating again more problems with 20CR SLP in this region.

SLP residuals are also large over the Southern Chile region and also appear to show that 20CR SLP is too high for many of the earlier years of the time series (panel a). The time series over Buenos Aires has a more consistent positive residual throughout its duration (panel c) and this indicates 20CR SLP is too low. The time series over Valdividia is a particular cause for concern because the magnitude of the apparent negative bias in the 20CR varies. The negative 20CR SLP bias is particularly large from 1930-1950 and 1995-2005, whilst from 1955-1970 the station SLP time series has similar SLP values to the 20CR SLP. Varying magnitudes of SLP bias mean the correlation between station SLP and 20CR SLP is weaker than at other locations from 1931-2010 ($r < 0.6$).

In summary, the SLP over the Falklands region appears to be particularly uncertain. Over far southern latitudes, 20CR SLP estimates appear to be too high whilst over mid latitudes they appear to be too low. Therefore, the 20CR is underestimating the westerly flow at higher southern latitudes over this region. Such uncertainties are evident during the 1971-2010 period used to build the model and lead to the disagreements in the CBTA time series shown in Figure 5.13.

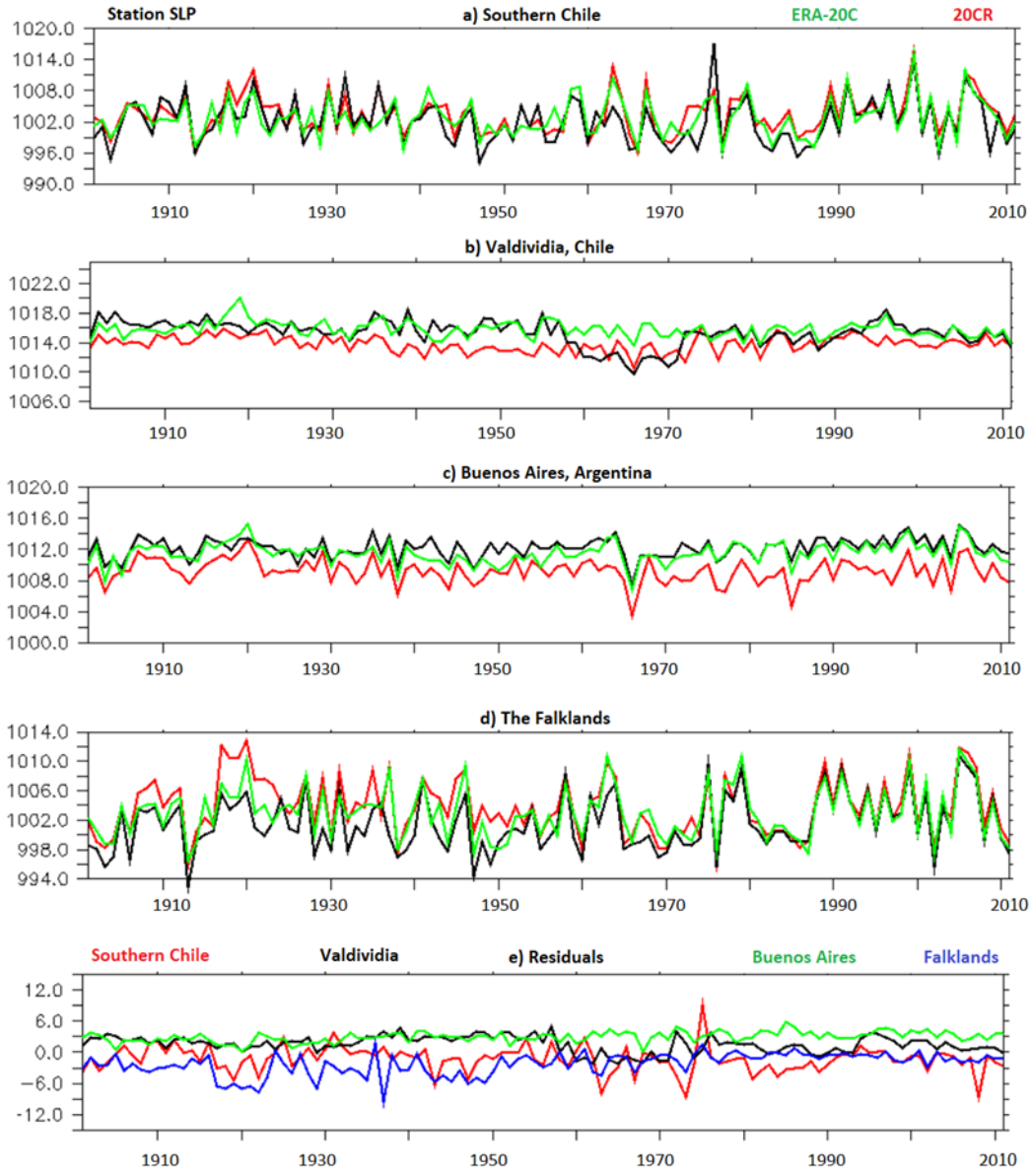

Figure 5.16: As with Figure 5.12 but this plot focuses on Februaries from 1900-2010 over the Falklands region.

Finally, time series of CBTAs were also generated for some other locations shown in Figure 5.1 to assess the quality of the 20CR SLP data over these regions. The results in Figure 5.17 are mixed with the time series in the Sea of Japan another cause for concern. The CBTAs from the 20CR and Station SLP are in strong agreement for the 1971-2010 period used the build the CBTA model. From 1900-1950 however the station data CBTAs often fluctuate around or above zero whilst the 20CR SLP anomalies are generally cold. The ERA-20C SLP appears to disagree with the 20CR and Station data SLP especially during

the 1980s. As for the Falklands region there appears to be disagreement between the CBTAs during the 1971-2010 period used to develop the model which means this caution should be applied when using the 20CR or ERA-20C in this region also. The source of disagreement comes with the strength of the Siberian high in the east of the region. This plays an important role in moderating the depth of the cold advecting out of Siberia (Ding and Krishnamurti, 1987). A stronger Siberian high means more persistent cold air outbreaks over the continent. The CBTAs suggest SLP over the Nagasaki and Verhoyansk regions may be too low.

The other time series appear to be more promising. Panel b) looks at MAT to the North of Bermuda. From ~1935-2010 the CBTAs from the different SLP datasets are in good agreement but before this point the station SLP CBTAs are often much warmer. For the west of New Zealand time series (panel c) the CBTAs agree well throughout from 1895-2010 with a few minor exceptions. Not all areas of the Southern hemisphere are problematic as the Falklands time series would suggest. The analysis in this section however is limited in scope geographically as there are few long-term station SLP datasets over the Pacific with only Tahiti, Honolulu and the west coast of the USA stations available. There is also a lack of stations in the South Atlantic.

The results in this section show some interesting contrasts between the available SLP and MAT datasets. Whereas there is good agreement with most of the different CBTA time series in higher latitudes of the North Atlantic and NW Europe, the picture becomes far more complicated in the Falklands where there are known issues with the 20CR SLP data. Whether the results from the Falklands and Japan are anomalous compared to the rest of the ocean basin is difficult to say at this point but time series over the North Atlantic and to the west of New Zealand look fairly promising at least. Overall the conclusions agree with Jones, Harpham and Lister, (2015) and Ferguson and Villarini, (2014) which suggested there are problems with 20CR SLP during earlier years away from the North Atlantic. It is recommended that future studies look at SLP from a variety of sources when performing time series analysis of CBTAs as a result.

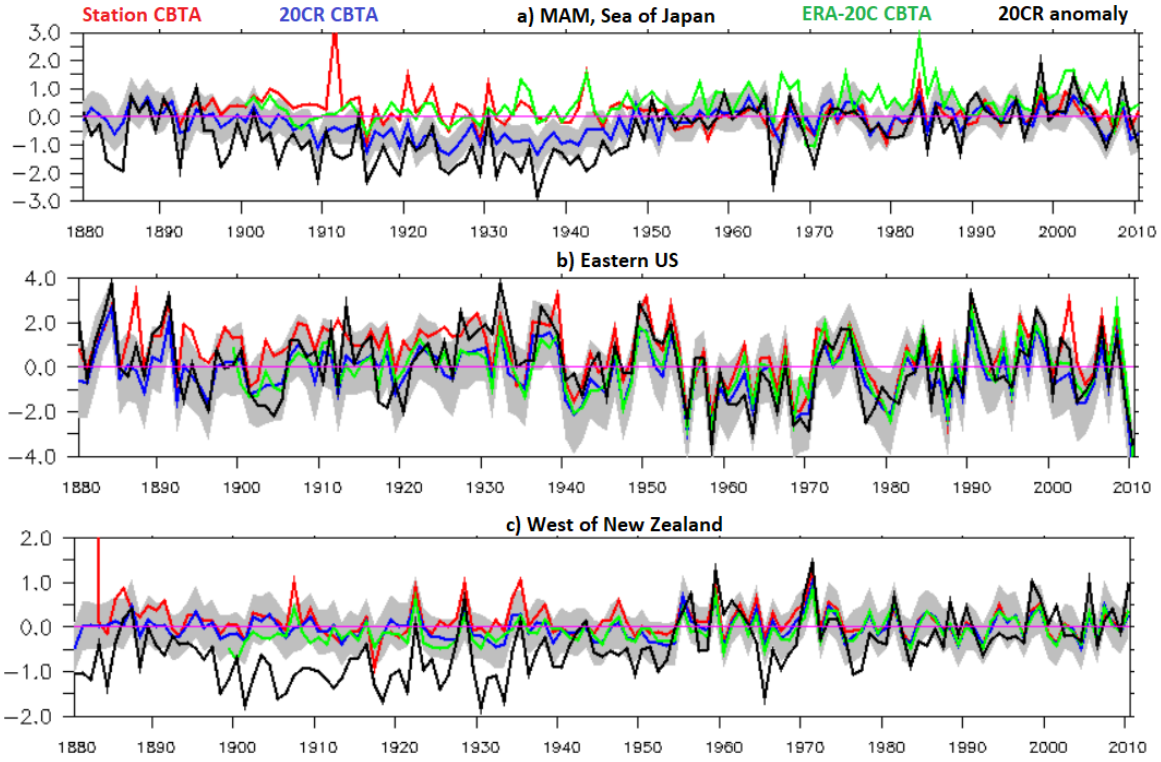

Figure 5.17: As with Figure 5.7 but panel a) looks at CBTA anomalies for the MAM period over the Sea of Japan; b) The DJF period near the Eastern US and c) The DJF period for the west of New Zealand.

5.4 Further temperature analysis using CBTAs

5.4.1 Comparison between 20CR MAT and HadNMAT2

In this section a brief comparison between the CBTAs and HadNMAT2 is performed to see whether any potential discrepancies with 20CR MAT can be identified. Then a comparison between SST datasets is performed with SST estimates based on land air temperature datasets over the North Sea and Newfoundland regions. First, Figure 5.18 shows some time series of 20CR MAT and HadNMAT2 for the month of December over some of the locations shown in Figure 5.1. The month of December was chosen as in many of the locations in the previous section, the strongest relationships between temperature and atmospheric circulation are found during the DJF period. An individual month was chosen due to the missing data in HadNMAT2 which may affect seasonal means.

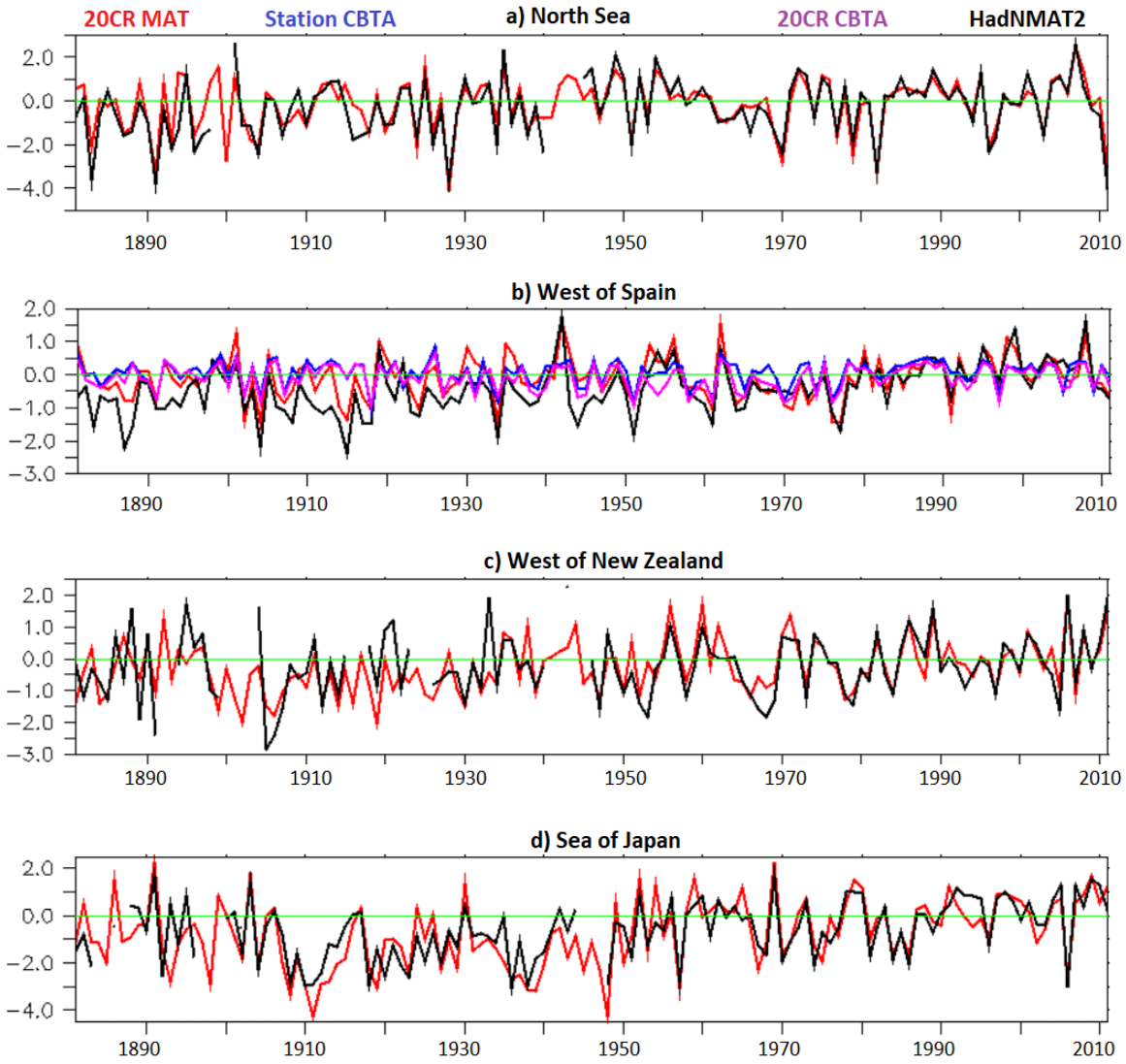

Figure 5.18: Time series of HadNMAT2 and 20CR MAT anomalies (°C) at 4 different locations for the month of December. Panel a) shows a time series for the North Sea; b) for the West of Spain with the CBTAs from the previous section shown for comparison; c) the region to the west of New Zealand; d) Sea of Japan.

For the time series over the North Sea, West of New Zealand and over the Sea of Japan, there is very strong agreement between 20CR MAT and HadNMAT2. Most of these time series only show brief periods of small differences between the two MAT datasets and there isn't a persistent pattern to these differences. The exception to this is the MAT anomalies to the west of Spain (b) which from the 1950s onwards is in close agreement with HadNMAT2. Before 1950 however HadNMAT2 is consistently colder than 20CR MAT,

especially from 1880-1915 where HadNMAT2 can be up to 1^{o}C colder than 20CR MAT. Interestingly during this month, the connections between temperature and atmospheric circulation to the West of Spain are quite strong. There is also good agreement between the station data CBTAs and 20CR CBTAs. Both CBTA time series tend to follow the 20CR MAT much more closely which indicates that HadNMAT2 is too cold over this region during earlier years.

5.4.2 Land air temperature and 20CR SST differences

Another way to analyse the marine climate record is to look at air temperature measured over land and examine its differences with nearby SST. In this section the North Sea and Newfoundland land temperature data are examined as both locations have homogenised daily and monthly air temperature data and provide an additional analysis to the plots in Figure 5.18. The first area analysed in this section is the North Sea time series 20CR SST, taken just to the east of Hull at 54N/2E. Land Air Temperature (LAT) data is taken from the CET series (Parker, Legg and Folland, 1992). The CET (used to represent LAT in this region) minus North Sea 20CR SST is then calculated and a model of CBTAs is developed from this.

The advantages of looking at the LAT / SST differences is that it allows for a model that is not fully dependent on the 20CR temperature data (as LAT is used instead of 20CR MAT). Looking at the SST-LAT differences should also reduce the climate change signal, as both time series are warming (Jones 2016). Provided the CBTAs and observed LAT- SST differences are strongly correlated, then there should be a good estimate of the SST value based on the recorded LAT. The differences between LAT and SST are expressed as monthly anomalies because there is an annual cycle in the difference between LAT and SST. In the North Sea for example, SSTs are at their coldest in early spring compared to January/February for nearby LAT. As a result, LAT is often warmer than SST during the MAM months with the reverse pattern seen during the SON period (Figure 5.19a). The anomalies are with respect to the 1971-2010 climatological average as with previous chapters.

Some variability in the SSTs due to atmospheric circulation is expected as shown in panels b) and c) for the North Sea and Newfoundland regions respectively during the DJF period.

However, the impact of atmospheric circulation is much stronger on LAT than SST especially during the DJF period, as shown in Figure 5.19b and c. As a result, there is a strong connection between atmospheric circulation and LAT – SST differences as this section will show. Results in this section only focus on the DJF period because LAT is more heavily influenced by atmospheric circulation then SST at this time. During other seasons both LAT and SST are influenced by atmospheric circulation to a similar degree so the model doesn't perform as well.

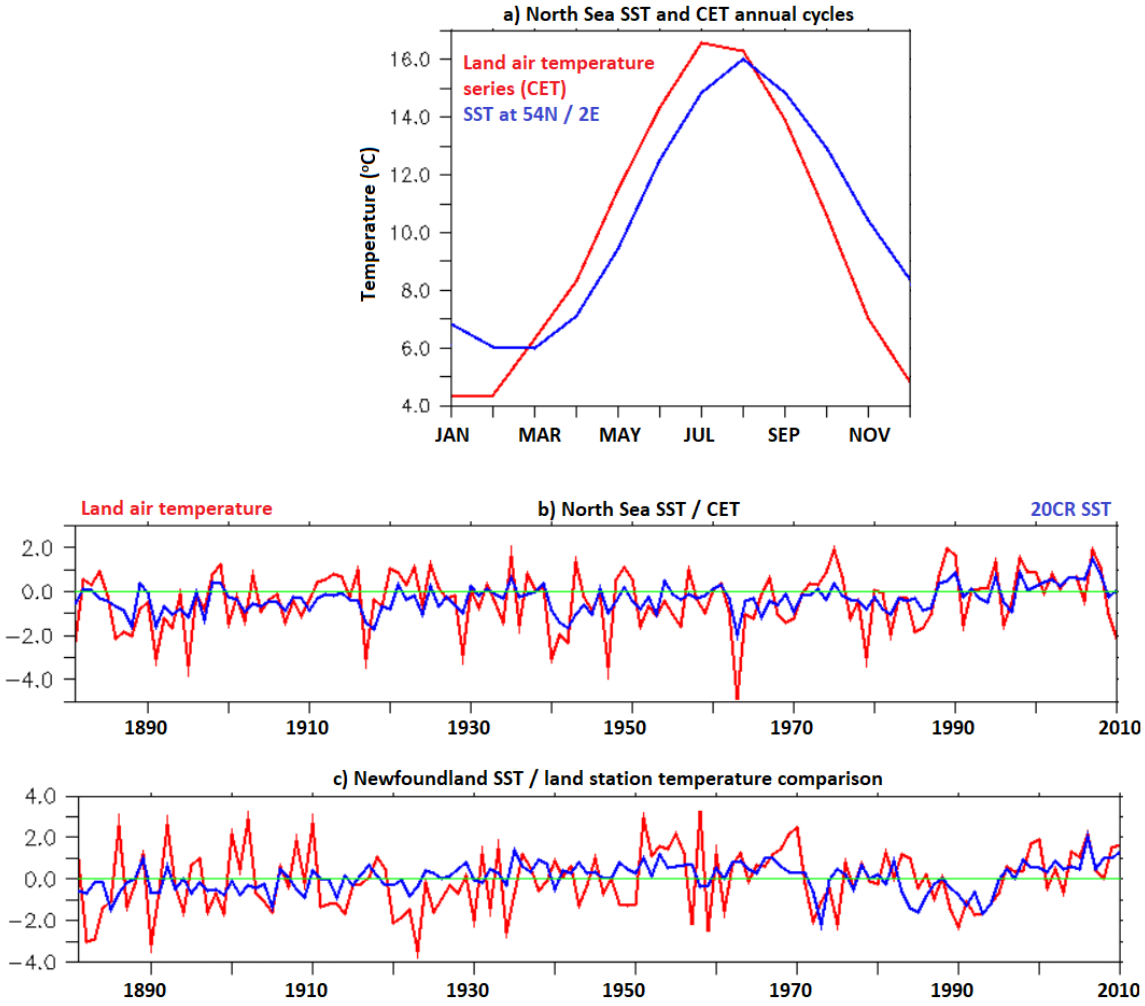

Figure 5.19: a) Annual cycle of monthly CET and SST at a point in the North Sea (2E/54N). based on data from 1971-2010; b) North Sea DJF SST and CET from 1881-2010; c) As with b) but for Newfoundland LAT (taken from St John's station) and SST (48W/50N).

The North Sea CBTA fields and their uncertainties are shown for the month of February in Figure 5.20. As expected, the CBTA fields are have similar patterns to those seen in Figure

2.7 where sampling is good as shown in panels c) and d). Some areas of the CBTA field have little data such as those in panels a) and b) and as a result some of the CBTAs are very large but the total uncertainties will take coverage issues into account as per previous results. Uncertainties for this region are generally between 0.4°C and 0.8°C for both the category and misfit uncertainties as shown in panels e) and f). The total uncertainties in the NW North Atlantic region are generally between 0.7°C and 1°C for the combined CBTAs.

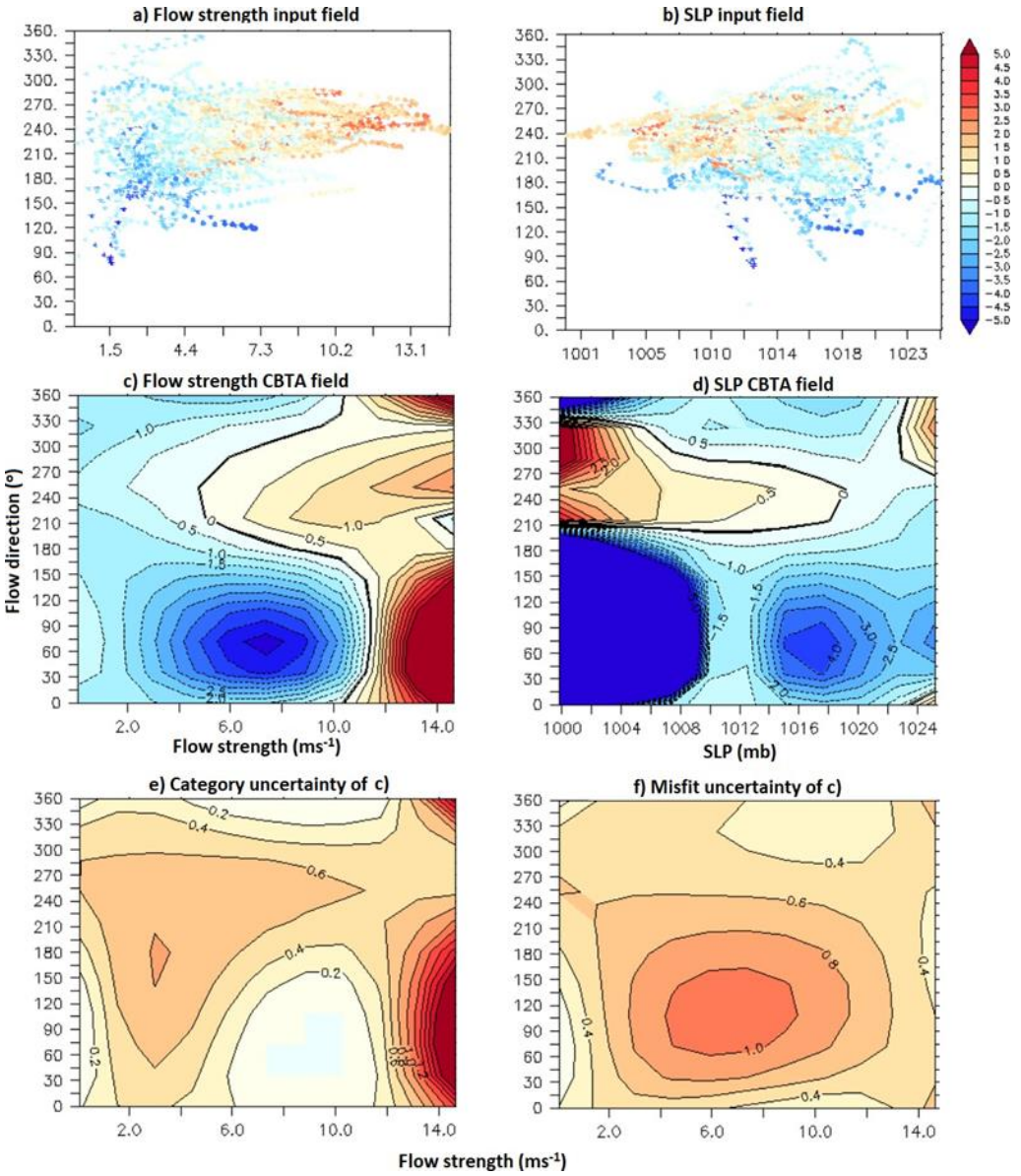

Figure 5.20: February CBTA fields for the North Sea point, based on CET-20CR SST differences. Panels a) and b) show the flow strength and SLP CBTA fields respectively. Panels e) and f) show the input data that contributes towards the flow strength and SLP CBTA fields respectively. Black points represent input data from February and blue points from January and March. Panels e) and f) show the category and misfit uncertainties of the flow strength CBTA field.

The time series of the CBTAs are shown in Figure 5.21 and demonstrate that they are very strongly correlated to the CET-SST difference. The correlation coefficient during the 1971-2010 period is 0.81 and this relationship persists further back in time (r = 0.77 for the whole series). There are a few instances where the CBTA model does not perform as well such as for some of the winters in the mid-late 1990s. During this period the residuals can be as high as +1.0°C (panel b) but the CET-SST estimate is usually within the 1SD uncertainty bounds of the CBTA time series. The residuals from 1930-2010 generally fluctuate between -0.5°C to +0.5°C and they show that the noise in the time series of panel a) has been reduced (as the standard deviation of the residuals is less than the CET-SST anomaly). There is however a period in the mid-1910s to mid-1920s when the CET-SST anomalies are often between 0.5°C to 1.0°C above the CBTA time series (highlighted on panel b)). Either the DJF CET series is too warm during this time or 20CR SSTs are too cold. To calculate an SST anomaly, the expected difference between the actual CET and SST is subtracted from the monthly CET value and is converted into an SST anomaly.

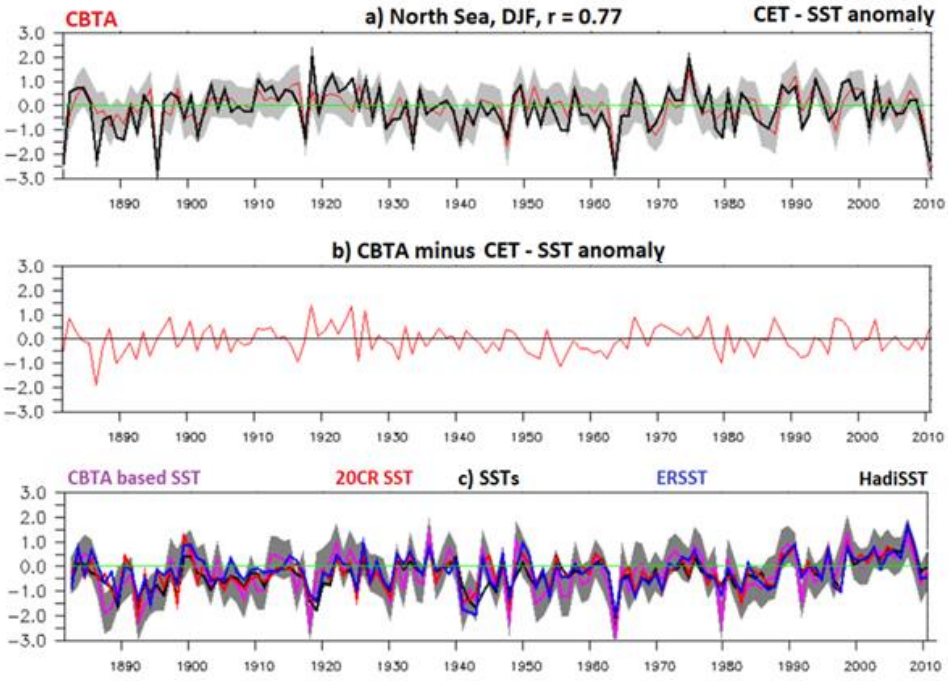

Figure 5.21. CBTA time series at the North Sea but this time the model is developed by taking the difference between the CET and 20CR SST to the east of Hull (2E/54N). Panel a) shows the time series of CBTAs and CET – SST anomaly differences. Grey regions indicate the 1SD uncertainty bounds of the CBTAs. Panel b) shows the residuals of panel a). Panel c) shows a time series of SST estimates at 2E/54N. The CBTA based SSTs are driven by the CET values and are shown in purple, accompanied by uncertainty estimates. The 20CR SSTs are shown in red, ERSSTv5 in blue and HadISST (Rayner et al., 2003) in black.

The estimated SST is then compared to other SST time series with the results shown in Panel c). Aside from some differences in some of the severely cold winters (e.g. 1887/88, 1916/17, 1978/79), the SST predictions driven by the CBTAs and CET perform well. There is good agreement throughout the time series in the North Sea from 1880-2010 but there are hints that SSTs from 1918-1926 may be too cold in this region. Conversely the CBTA SSTs also suggest 1951-1964 SSTs in the North Sea may be too warm. The analysis here suggests that this method can be applied to other coastal land air temperature stations, however the strong correlation shown for the DJF period in panel a) is not apparent for other seasons. The model is therefore limited to only being useful during the DJF months in this area.

With the promising results seen in the North Sea region, it was decided to also analyse the land air temperature-SST differences in Newfoundland. Here the DJF air temperature over St Johns in Newfoundland is examined (SJN – homogenised and available from the Environment Canada website) its difference with SST at 48W/50N is calculated. The time series of data can be seen in Figure 5.22a). Unfortunately, the correlation seen in this time series is not as strong (r = 0.66 from 1880-2010 and r = 0.72 from 1971-2010). It appears that the flow parameters are not as good at predicting severely cold winters in SJN compared to in the North Sea region as the winter of 1974/75 for example shows. The SJN-SST anomaly in this instance is ~-3.0^{o}C yet the CBTA estimate is only -1.0^{o}C.

A string of particularly cold winters is seen in SJN from 1920 to 1950 that are not well predicted by the CBTA model. Residuals are often between -1.0^{o}C and -2.0^{o}C as shown in panel b). The time series here does look suspicious, as the residuals from 1950-2010 generally hover around zero. It could be assumed that SSTs from 1920 to 1950 over this region are too warm and as a result the SJN-SST differences are too big (warm SSTs and cold air temperatures) but more analysis is needed. Overall though this section provides another method for comparing MAT/ SST with CBTA estimates and there are many more coastal stations or marine stations/ that can be explored.

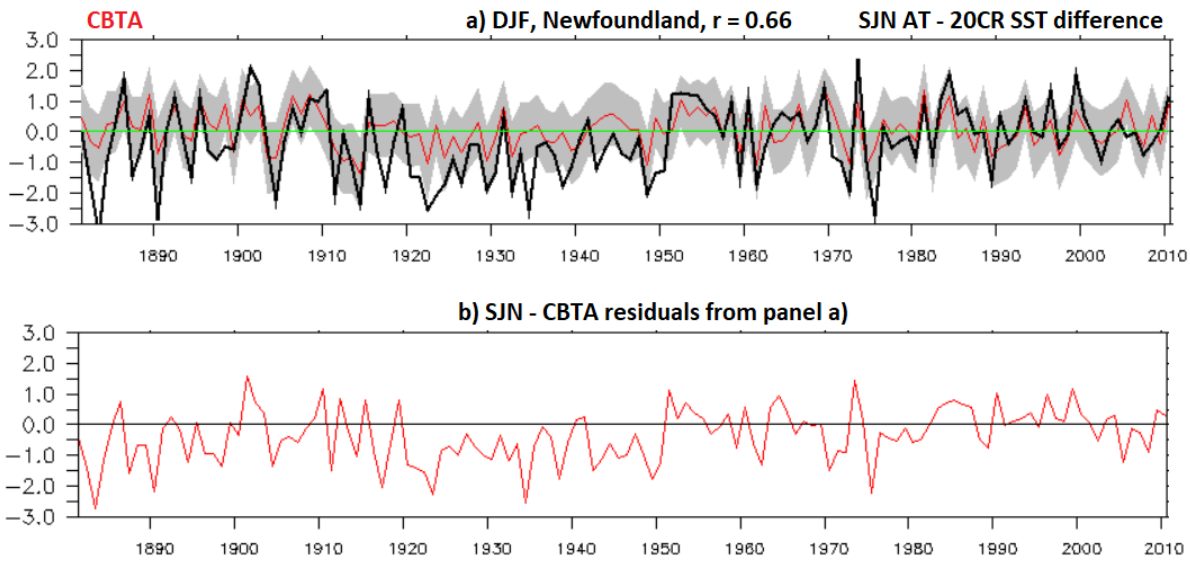

Figure 5.22: As with Figure 5.21 panels a) and b) but for the Newfoundland area.

5.5 Conclusions

The aim of this chapter was to verify the results of Chapter 4, by developing prediction models that weren't entirely dependent on the 20CR. The chapter sought to answer the following questions.

1) Can the method of defining atmospheric circulation be applied to different grid configurations of SLP observations?

This question was addressed in Section 5.2 and the results clearly indicated that the method developed in Chapter 2 was capable of calculating the westerly and southerly flow parameters to a high degree of accuracy using station data grid patterns. To test this the 20CR flow parameters were calculated for each of the nine grid patterns analysed and then compared to the 20CR flow parameters to those based on conventional grid patterns introduced in Chapter 3. Correlation coefficients for the westerly flow calculations were above 0.9 for most of the seasons at each of the locations analysed. Results were less good where the SLP gradients were especially slack as shown by the correlation coefficients for the Bay of Bengal. Overall however, it is concluded that the method of calculating flow parameters can be applied to station data and could come into use for future studies in the research field of synoptic climatology. Flow parameters

were then calculated from the station, 20CR and ERA-20C SLP values, which led to an attempt to answer the second question in the introduction.

2) Can there be confidence with regards to time series of 20CR CBTAs based on comparisons with CBTAs generated from other SLP datasets?

CBTA time series were generated from flow parameters calculated from 20CR, ERA-20C and station data SLP. The results were surprising as the North Sea CBTAs showed some uncertainty in the different CBTAs, more so in the summer months when SLP gradients are usually shallower. The causes of the differences between the 20CR CBTAs and the station data was the presence of an apparent positive SLP bias over Scandinavia in the 20CR, something identified in previous studies (e.g. Stryhal and Huth, 2017). Any SLP uncertainties for the stations used in the Central North Atlantic only have a small impact on the time series of CBTAs but this is in contrast to other ocean basins. There appeared to be a major SLP bias in the station data over Northern Argentina / Chile for example which lead to a highly uncertain time series of CBTAs in Figure 5.13. There also isn't enough station SLP data over the Pacific and South Atlantic to validate the results from Chapter 4 20CR CBTAs. Future studies will have to examine the SLP data in ICOADS to assess the quality of 20CR SLP for the Pacific / South Atlantic. The remainder of this chapter as a result of the SLP CBTA analysis focused on the North Atlantic only. The final section addressed the following question in the introduction for this chapter.

3) Can any further insights into MAT be found where there are strong relationships between temperature and atmospheric circulation as well as good SLP data?

From the analysis in Section 5.3, it was concluded that the areas with the least uncertain SLP observations were in the North Atlantic and the strongest relationships between temperature and atmospheric circulation were seen during the DJF period. This restricted the regions where comparisons between the CBTAs with HadNMAT2 data could be made therefore any judgements about its differences with 20CR MAT.

The regions of analysis were shown in Figure 5.18 and most of these time series showed strong agreement between HadNMAT2 and 20CR MAT anyway with the exception being

the December MAT to the West of Spain. This indicated that HadNMAT2 during earlier years may have been too cold in this region.

Further analysis was possible by looking at LAT-SST differences with Newfoundland and the CET region examined. The analysis from this final section suggested North Sea 20CR SST may be too cold in the mid-1910s to mid-1920s (Figure 5.21). In the Newfoundland region there also appears to be problems with 20CR SSTs from 1920 to 1950 as they appear too warm due to the pattern of the residuals but no conclusive statement can be made about the magnitude of any potential bias. The results from this chapter and others however demonstrate time periods of interest for MAT and SST anomalies that should be researched further.

Chapter 6 Summary of the thesis and future work

6.1 Summary of key achievements

1) The J12 approach to defining atmospheric circulation parameters was generalised and was able to be applied to different grid patterns of SLP data.

The method developed in this thesis was able to define key atmospheric circulation parameters such as flow strength using SLP data from only 4 grid points. This was in contrast to the method by J12 who used 16 points of SLP whilst Lityński weather types popular in eastern Europe were based on 25 points of SLP (Phillipp *et al.,* 2010). Correlation coefficients between westerly and southerly flow parameters from different grid configurations are often greater than 0.9 (Table 5.1).

2) The method of developing CBTAs could be applied globally and these were accompanied by useful uncertainty estimates (showing behaviour that is expected).

Many studies have shown that there are links between marine temperature (SST and MAT) and large-scale atmospheric circulation patterns (e.g. Johnstone and Mantua, 2014; Visbeck *et al.,* 2001) but few have looked at how small-scale atmospheric circulation patterns affect local marine climate. Many previous studies producing time series of CBTAs have also haven't usually been accompanied by uncertainty estimates (e.g. Osborn and Jones 2000; Johnstone and Mantua, 2014; Pena Agulo *et al.,* 2016). This study however has considered them and the advantage of this is that when looking back at time series of CBTAs, it was possible to investigate issues such as whether the local atmospheric circulation patterns were changing over time. Time series analysis suggest that uncertainties in the CBTA model are mainly due to factors other than atmospheric circulation. The uncertainties due to the spline method chosen itself were very small indicated by the parametric uncertainties, indicating no dramatic shifts in the atmospheric circulation patterns.

3) Strong relationships between temperature and atmospheric circulation were found over many ocean basins when based on 20CR SLP and MAT.

Correlation coefficients over 0.7 were found between the CBTAs and 20CR MAT in many places during the 1971-2010 DJF period. Such strong connections were found over the North Sea, NW North Atlantic, the US Pacific, east of Japan and over the Southern Oceans which may be related to the peak amplitude of ENSO events during the boreal winter (Santoso, Mcphaden and Cai, 2017). Relationships were generally weaker outside of these months (with the exception of parts of the Southern Hemisphere) and with data not used to build the model (e.g. from 1931- 1970). CBTAs however were also developed using data from the 1931-1970 period and the interannual variability of this time series was strongly correlated ($r > 0.80$) with the CBTAs developed from 1971-2010 data over most areas. It was therefore concluded the relationships between temperature and atmospheric circulation have generally remained consistent over time.

4) Global temperatures will carry on increasing regardless of what atmospheric circulation does because of the climate change signal (Hartmann *et al.,* 2013). The AMO was also identified as a key influence in the North Atlantic.

This was emphasised by the time series plot in Figure 4.12 which showed globally averaged CBTAs developed by using 1971-2010 data. The CBTAs revert to a value close to zero over large scales which is expected but the global CBTA averages mask some fairly strong variations. This is especially the case during the DJF period over the North Atlantic where a strong AMO signal remains from the DJF period residuals for 20CR MAT, highlighting how a large component of AMO variability is not driven by atmospheric circulation (and also how other signals being exposed when atmospheric circulations' influence is taken away). The MAT variability over small regions can be reduced markedly when taking the estimated influence of atmospheric circulation away. The CBTAs are therefore more insightful when looking at local rather than large scale temperature variability.

5) The CBTAs from different SLP datasets expose some additional uncertainty in 20CR SLP.

CBTAs were developed from station SLP and ERA-20C data and whilst results looked good over the North Atlantic in spite of some SLP biases, results were less clear elsewhere. Good agreement between the CBTAs from different SLP datasets are also seen over New Zealand and the area around Bermuda but CBTAs vary in the Falklands region and Sea of Japan to a large extent, even during the 1971-2010 period used to build the model in this thesis. Therefore, there cannot be confidence about the 20CR output over these regions until such uncertainties in SLP are resolved because they have implications for surface meteorology (e.g. temperature and rainfall).

6.2 Discussion of aims and results

Marine air temperature is an important climate variable, it plays a key role in the development of GST datasets and provides further evidence of a warming trend in global temperatures since the late 19th Century (Hartmann *et al.,* 2013; Kent *et al.,* 2013). As for the SST however, there are biases in the data and uncertainties related to coverage that have been well documented (Bottomley *et al.,* 1990; Kennedy, 2014; Kent *et al.,* 2013). It is important that these biases are understood in order to improve our understanding of the global temperature record.

Differences between MAT and SST provide the basis for SST corrections in the ERSST products (Smith and Reynolds, 2002) and MAT is also a variable considered by the empirical SST corrections developed by Folland and Parker, (1995). Comparisons between the SST datasets and HadNMAT2 suggest that either HadNMAT2 is too cold or SST is too warm during the 1950s and the early 1900s (Figure 1.4). Due to this it was decided to investigate the potential for atmospheric circulation to provide clarification for some of the differences seen in earlier years. Thompson *et al.,* (2008) were able to find a bias in SST after WWII by looking at the roles of ENSO and the COWL index only, so what could be found if the contribution of small-scale atmospheric circulation to MAT was explored? In order to answer this key question, there must be awareness of the uncertainties in SLP, SST and the relationships between temperature and atmospheric circulation. The following aims were therefore put in place for the thesis and this section addresses how closely they could be met in this thesis:

1) Develop a method which can define atmospheric circulation parameters with gridded or station SLP data over any of the world's oceans (so different SLP datasets can be examined, Chapters 2 and 5).
2) Develop suitable uncertainty estimates for the CBTAs (Chapter 3).
3) Use these circulation parameters to estimate the circulation-dependent contribution to MAT variability over all of the world's oceans using the 20CR. (Chapters 2-4).
4) Analyse whether the CBTAs could potentially identify biases in MAT over the course of its record or other influences (Chapters 4 and 5).
5) Compare the 20CR CBTAs to those based upon other SLP and temperature datasets to further assess the quality of the 20CR reanalysis product (Chapter 5).

To achieve the first aim, Chapter 2 looked into simplifying the most used method for defining atmospheric circulation parameters, that developed by Jenkinson and Collison (1977). The grid pattern can again be seen in Figure 6.1 and consists of 16 points where SLP is extracted. The original purpose of this method was to build a climatology of North Sea storms (Jenkinson and Collinson, 1977). It hasn't been changed in subsequent studies (e.g. Jones, Hulme and Briffa, 1993; J12) despite the fact the Jenkinson and Collision method has been widely used in the research field of synoptic climatology. It also isn't known whether the grid pattern devised by Jenkinson and Collinson, (1977) was the best for analysing the response of temperature to atmospheric circulation patterns. Neither have many studies investigated using simpler grid patterns to define atmospheric circulation parameters.

Chapter 2 proposed to simplify the calculations by using 4 points of SLP only with the key advantage that flow parameters based on just station SLP data alone could be calculated. The flow parameters from the grid pattern in Figure 6.1b were very strongly correlated with those calculated from panel a).

In Chapter 5 the approach went further to look at flow parameters from the station data based grid configurations with 2 example patterns shown in panels c) and d) respectively. The flow parameters from these grid configurations were also strongly correlated to those from the J12 method. It was also tested as to whether the flow parameters were

better at predicting MAT variability than a method based on just regressions of SLP. The level of performance was generally similar during the 1971-2010 period (used to develop the model) between the flow parameter and the regression methods but the flow parameter method worked much better for months before this. Overall it is concluded that the first aim of the thesis could be met as an effective method of predicting temperature from atmospheric circulation patterns was developed, which could be applied globally and to station SLP grid configurations as well as the simpler configurations from gridded SLP data.

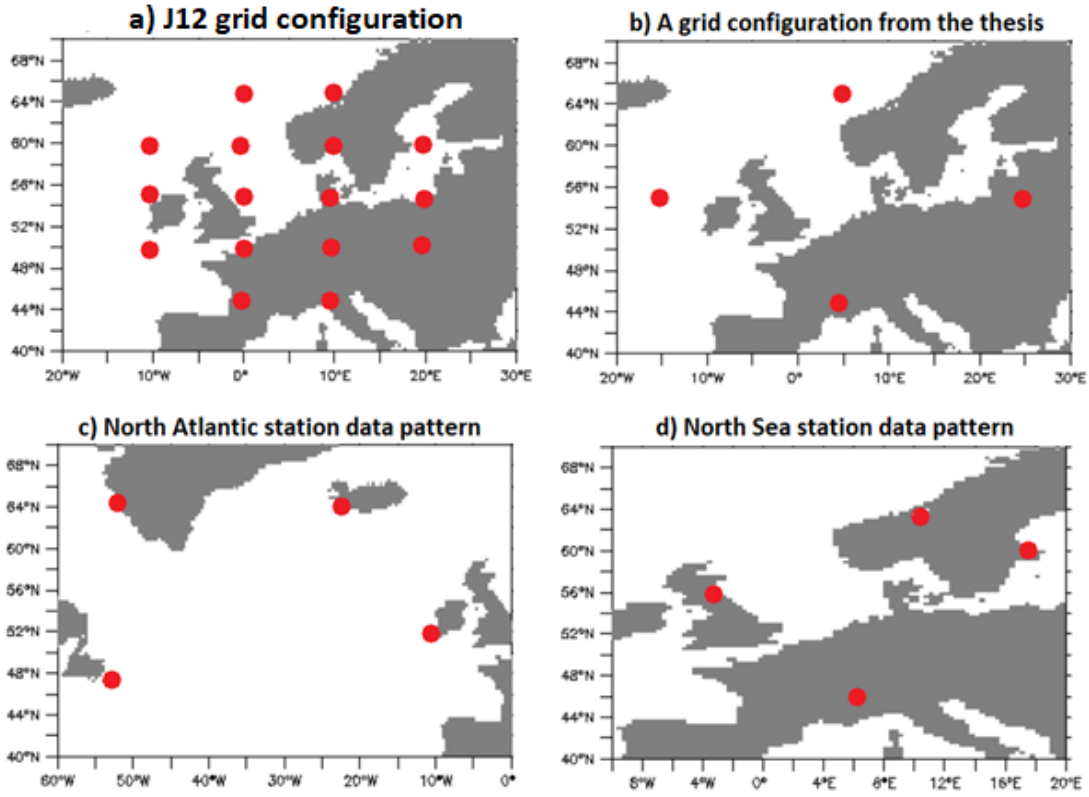

Figure 6.1: Some of the grid configurations shown in this thesis with red points indicating where monthly SLP values are extracted. Panel a) shows the grid configuration used by J12 to define flow parameters. Panel b) shows a grid pattern used in this thesis from Chapter 2. Panels c) and d) show two grid configurations from Chapter 5 based on station SLP data.

The second aim was to develop uncertainty estimates as other time series analysis of CBTAs had no uncertainty estimates (Chen, 2000; Johnstone and Mantua, 2014; Osborn and Jones 2000; Pena-Agulo *et al.,* 2016). This can be problematic if the model is being

used outside a time period used to develop it. This is because some of the months may have atmospheric circulation patterns that are different from those observed during a period used to build the model. As a result, there is a risk that the model output in such instances is uncertain.

The uncertainty model captured the influences on MAT besides atmospheric circulation (category uncertainty), methodological related uncertainties (misfit and parametric uncertainties), uncertainties in the 20CR (SLP uncertainties) and uncertainties in the flow parameters due to the prevailing atmospheric circulation pattern (circulation uncertainties). When these were all combined, accurate uncertainty estimates were developed so it is concluded that aim 2 was met. This was based on the uncertainty analysis and boxplots shown in Chapter 3 and Chapter 4, which showed increasingly large dispersion of residuals with increased uncertainty estimates (shown again in Figure 6.2 for 4 global points selected at random).

The uncertainties helped to understand why the relationships between temperature and atmospheric circulation weaken during earlier years in Chapter 4. The weakening relationship wasn't due to changing atmospheric circulation patterns because the parametric uncertainties didn't increase much when looking at earlier years. This shows that shifts in atmospheric circulation patterns did not have a major impact on uncertainty. Instead the category uncertainties were found to increase when the model was developed from data covering older periods (e.g. 1931 – 1970), indicating the temperature response to atmospheric circulation was more varied in earlier years in the 20CR (Figure 4.28). This is a key reason as to why relationships between temperature and atmospheric circulation are weaker during earlier time periods.

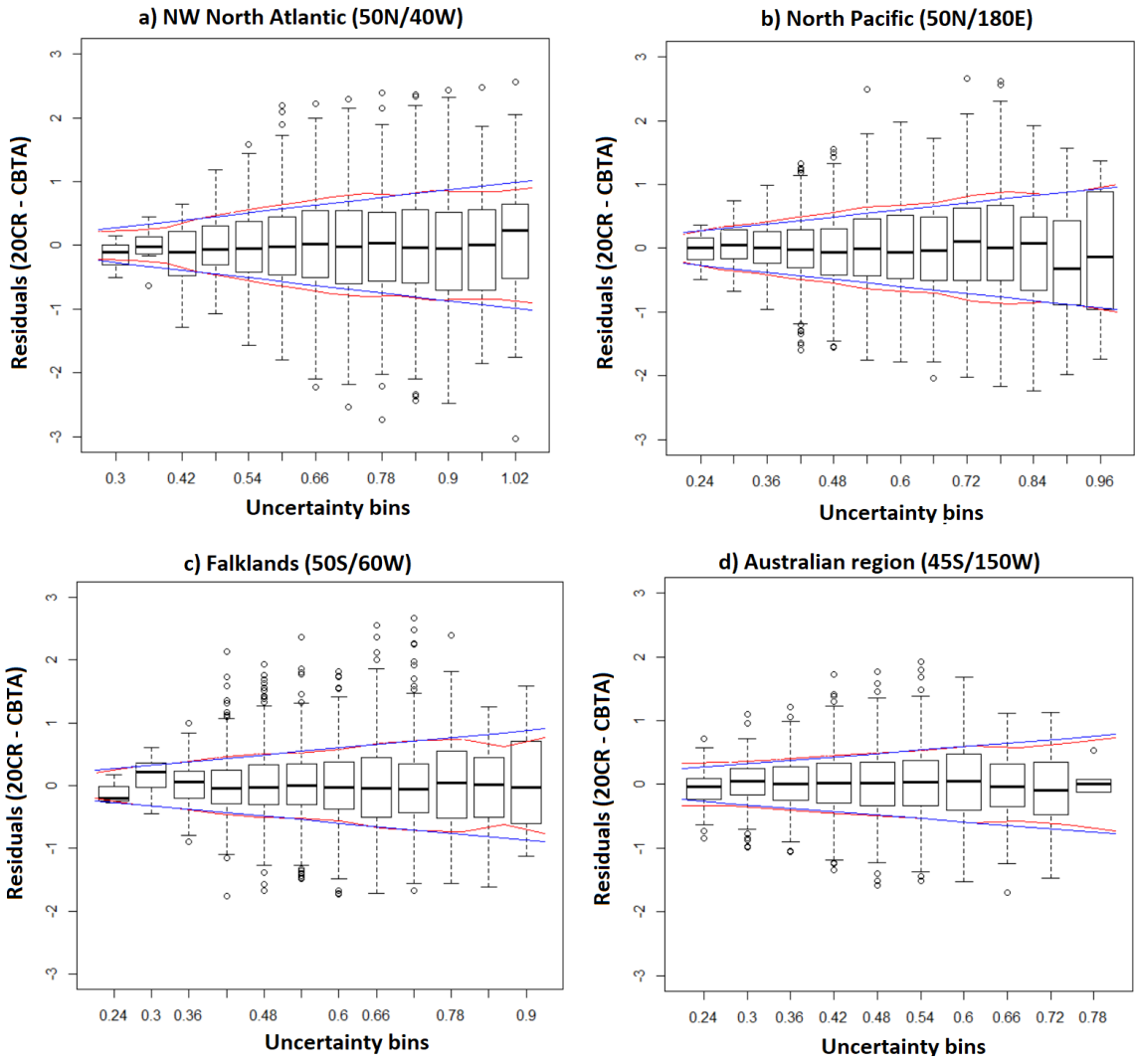

Figure 6.2: Panel a) NW North Atlantic boxplot containing data for all months during the 1971-2010 period, with the total uncertainty on the x axis placed into bins and the distribution of residuals (20CR MAT – CBTA) on the y axis. The boxes represent the upper and lower quartile range of the uncertainty bins whereas the lower and upper extremes of the bins. The line in the middle of the boxes represents the median whilst the circles represent outliers. The red lines represent the standard deviations of the residuals in each bin. Panel b) shows the same as panel a) but for a location in the central North Pacific; c) For the Falklands; d) A region between Australia and New Zealand.

With the uncertainty model formed, Chapter 4 expanded the CBTA method globally to assess the influence of atmospheric circulation on MAT according to the 20CR model output (to address aims 3 and 4). The MAT predictions shown in Chapter 4 were based on a spline method developed in Chapter 2 as this performed better than the alternative stepwise regression method. The global analysis found that model performance was

affected little by changes in grid configurations used to calculate the flow parameters. The results also showed that the spline model could predict 20CR MAT globally with a model developed using data from 1971-2010. Particularly promising results were found during the DJF and MAM periods, especially across higher latitude areas of the North Atlantic and North Pacific. This thesis concludes that aim 3 was also met because the CBTA model could be applied globally and, in many regions, strong relationships were found.

Time series of CBTAs were then analysed over the regions were CBTAs performed best. This was done to reduce the variability of MAT by taking the estimated influence of atmospheric circulation away as with Thompson *et al.,* (2008) and to meet aim 4 of the thesis which sought to identify other influences on MAT besides atmospheric circulation. The results over the North Pacific showed what was to be expected based on previous research into this area (e.g. Osborn and Jones, 2000) in that the strongest relationships occur during the DJF months and there is a trend from negative to positive residuals over time. The Falklands too showed a similar residual pattern to the North Pacific with the exception of the two world wars during the DJF period when 20CR MAT appeared too warm. The NW North Atlantic however did show some more unusual results. Here the relationships between temperature and atmospheric circulation were particularly strong ($r > 0.80$ during the 1971-2010 period) but the residuals were generally positive before the 1971-2010 period. This led this thesis to speculate as to whether 20CR MAT was too warm in earlier years as it goes against the expected trend of atmospheric circulation patterns becoming increasingly warmer as the global climate warms (Hartmann et al., 2013).

Chapter 4 also looked at a model developed by using data from 1931-1970 and it was found the interannual variability of this time series was strongly correlated to the model developed by using 1971-2010 data. The relationships between temperature and atmospheric circulation haven't changed but as the climate warms or cools in any particular region, there becomes an offset when looking at CBTAs over different climate periods. Despite the climate change signal not being captured by the CBTAs, the residual variability of 20CR MAT anomalies was reduced after the CBTA estimates were subtracted. This was most noticeable in the North Atlantic with a key plot from Chapter 4

being shown again below in Figure 6.3. When the CBTAs are removed from 20CR MAT an AMO signal becomes much clearer in the residuals of both the NE and NW Atlantic. It was therefore concluded in Chapter 4 that the CBTAs could also highlight other influences on temperature such as ocean circulation meaning aim 4 was also met. Figure 6.4 also shows another key plot from chapter 4, which highlighted how much of the variance from 20CR MAT was reduced over individual grid cells as a result of taking away the CBTAs.

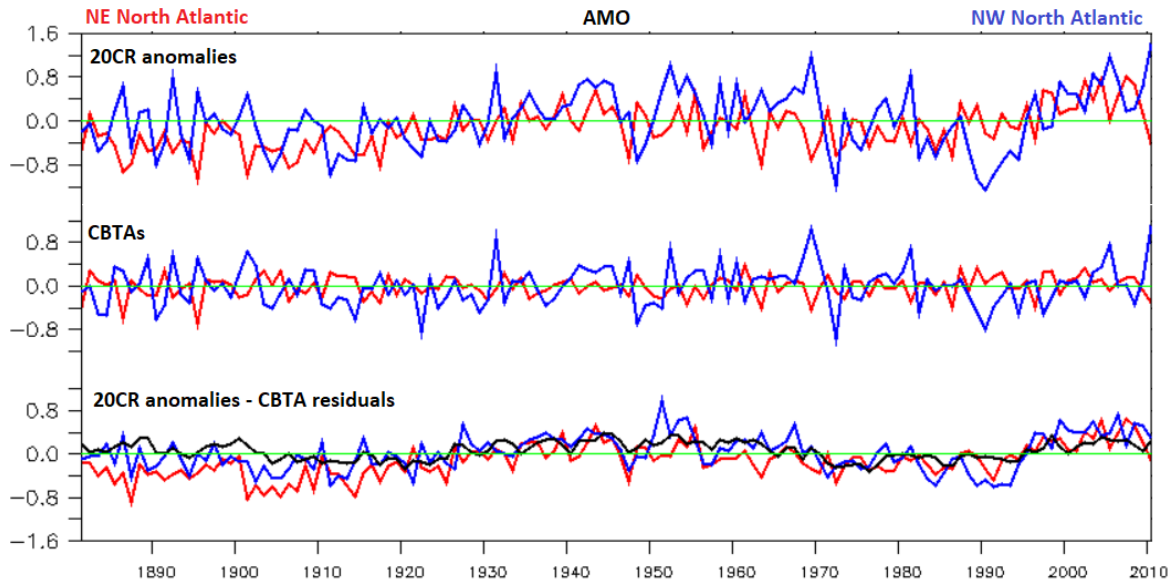

Figure 6.3: Time series of anomalies over the NE Atlantic (red) and the NW Atlantic (blue) from 1880 to 2010. Time series in the top part of the plot show the 20CR anomalies, the middle shows the CBTAs and the bottom part shows the residuals. The AMO time series from Enfield et al (2001) is overlaid for comparison (black).

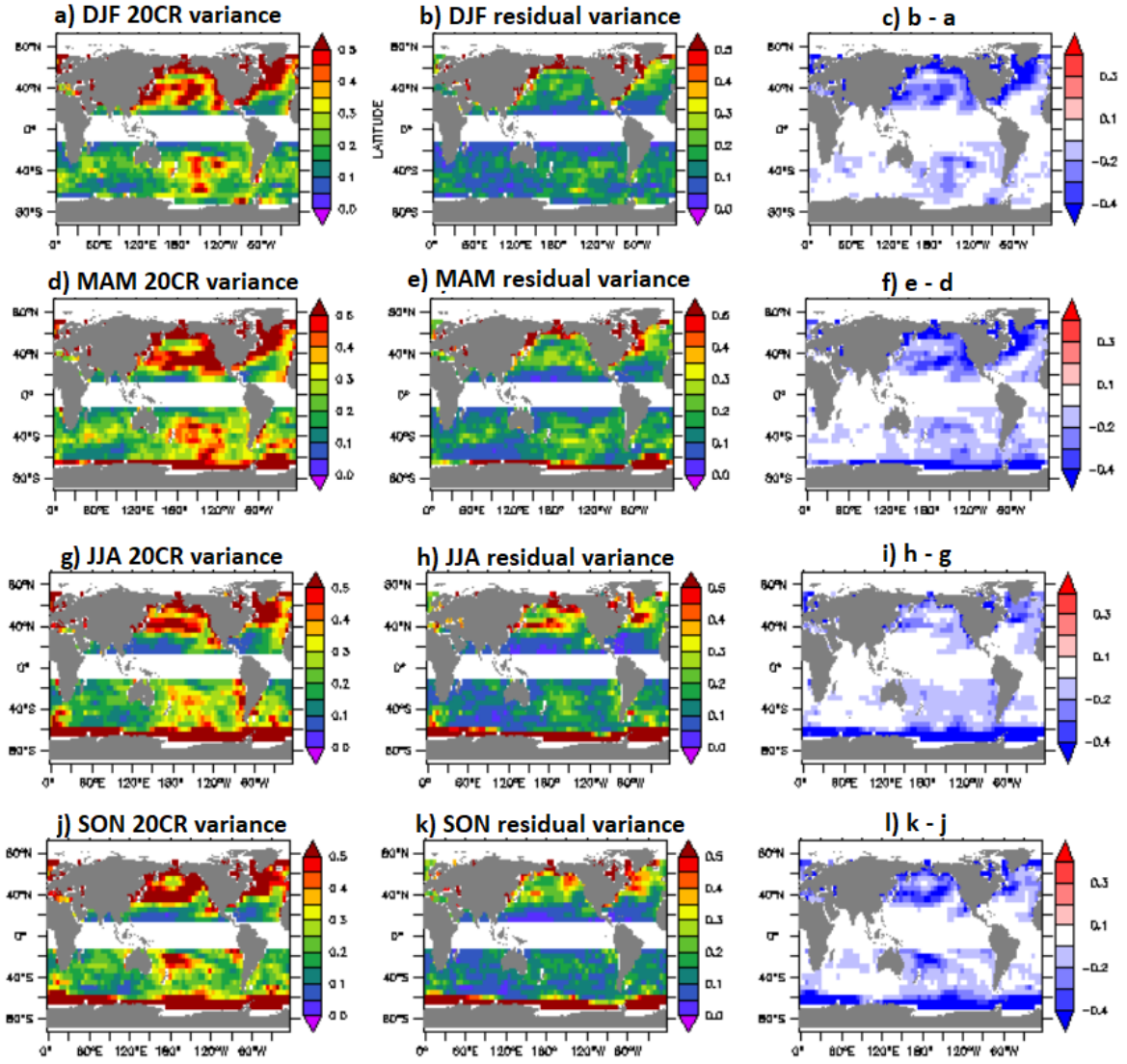

Figure 6.4: Global maps of variances and their differences for the 1971-2010 period. Panel a) shows DJF variances in the 20CR; b) Variance remaining in the 20CR when the CBTA variance has been taken away from panel a); c) the differences between the residual and 20CR MAT variance. Blue areas indicate where 20CR MAT variance has been reduced due to taking the estimated influence of atmospheric circulation away from 20CR MAT; Panels (d-f) as with panels a-c) but for the MAM period; Panels (g-i) JJA; Panels (j-k) SON. Units in $^{o}C^{2}$.

The final aim was to see whether there could be confidence with regards to the 20CR SLP and MAT data by comparing model results based on different datasets. The results from this section highlight the importance of using different SLP datasets when doing time series analyses such as those in this thesis. Figure 6.5 shows an example of where SLP looks particularly uncertain to the North of the Falklands. The level of disagreement during the 1971-2010 period used to build the model is a concern here and led to

questions with regards to the data quality of the 20CR in this region. For the North Atlantic results were far more promising with good agreement from the CBTAs based on different data sources and over most locations HadNMAT2 was in close agreement with 20CR MAT, the exception was December MAT to the West of Spain with the CBTAs and 20CR MAT suggesting HadNMAT2 was too cold.

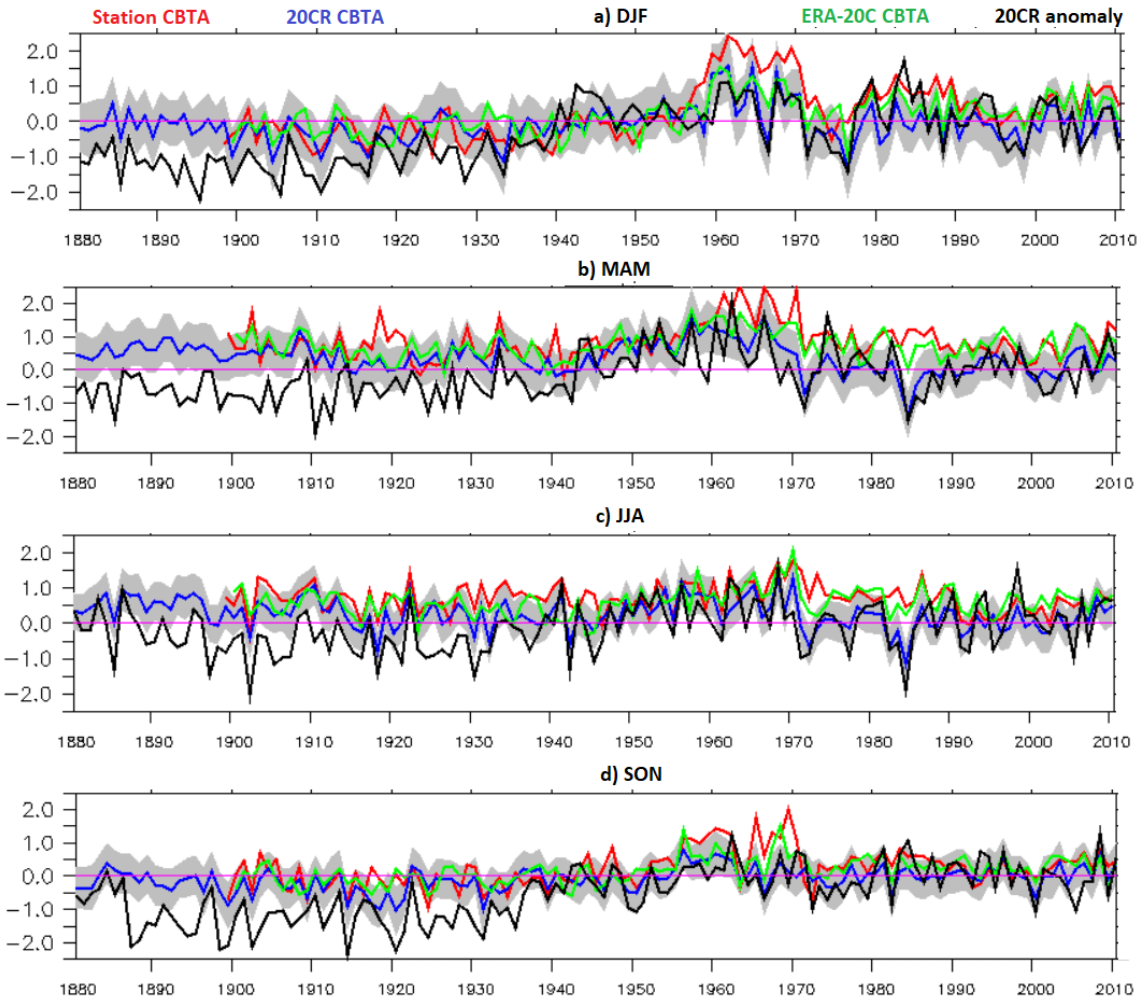

Figure 6.5: Time series of CBTAs for the North Sea (6E/56N) during four different periods of the year covering the period 1880-2010. The blue time series represents 20CR CBTAs, green represents the ERA-20C and red represents station SLP data. Grey regions mark the 1SD uncertainty bounds of the 20CR time series.

6.3 Suggestions for future research

This section gives 3 areas of research that should be pursued to build on this thesis. The first area of concern is:

1) Other SLP datasets and atmospheric circulation parameters need to be examined

The 20CR is used frequently for climate studies however this thesis showed evidence of biases in SLP that are yet to be resolved. Future studies should therefore consider multiple reanalysis / SLP products to interpret time series of CBTAs. Some of the biases such as those over Eastern Europe appear to be a permanent feature of the 20CR SLP in this region, other biases do not appear to be permanent and of a fixed nature (such as over South America) and lead to questions with regards to the quality of the 20CR in certain areas. This thesis only provided a glimpse of the SLP uncertainties across different products.

In addition to the ERA-20C and station data used in Chapter 4, future CBTA analysis could also use the HADSLP2 and ICOADS wind strength datasets. The ICOADS wind data for example contains westerly and southerly flow strengths over 2^{o} latitude / longitude grid points. Coverage from the mid -19th century to the present day is similar to that seen for MAT and SST climate variables (Freeman *et al.,* 2017).

Figure 6.6 shows a plot of ICOADS westerly flow values over the North Atlantic basin for February 2000. Westerly winds are particularly strong over much of the region between 40N-55N whilst between Iceland and Greenland the westerly flow values are strongly negative, indicating persistent easterly winds. Such a pattern is consistent with a deep Icelandic Low. From the differences in westerly flow values it appears the wind data in ICOADS could be used to calculate flow shear or be used as a proxy for the average SLP. The time series of westerly and southerly flows over 50N/40W in panels b) and c) show that the westerly and southerly flow parameters defined from grid pattern 2 (Figure 3.7) are very strongly correlated with those from ICOADS ($r > 0.9$, for the month of February). It would be interesting to see how the results of a MAT prediction model from ICOADS data would compare to those presented in Chapter 4.

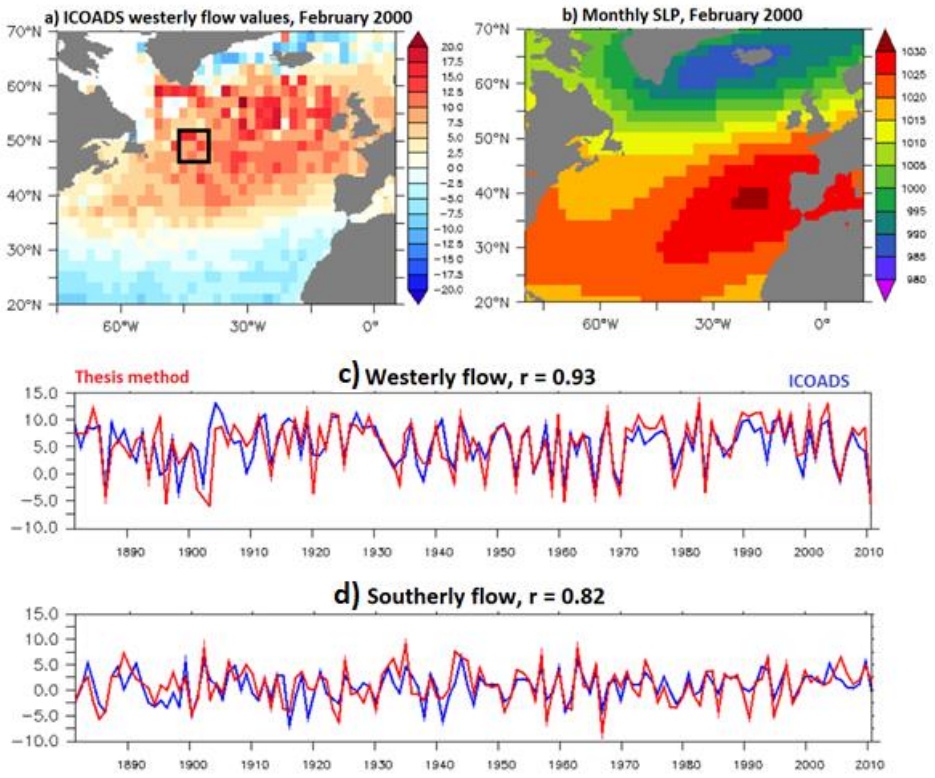

Figure 6.6: Panel a) Westerly flow values (m/s) from ICOADS release 3.0 for the month of February 2000. Red boxes indicate westerly flows in a grid box and blue boxes show easterly flows. Panel b) shows the 20CR SLP values over the North Atlantic basin for the same month; Panels c) and d) show monthly westerly and southerly flow values from ICOADS and the flow parameters defined in this thesis from the grid configuration in Figure 2.2a. Time series are from the black box shown in panel a) and are for the month of February. Correlation coefficients listed are for the 1951-2010 with the wind speeds (m/s) shown in the y axes.

2) Apply the CBTA model over land regions

Given that strong relationships between 20CR air temperature and atmospheric circulation were found over the oceans, future studies should apply the same method over land. The underlying SST may have affected MAT in addition to atmospheric circulation which may have acted as a limitation on the model. SST will be less of an influence on land temperature series even in areas such as England. Figure 6.7 for example shows CBTA time series for Central England which as with previous chapters was built on relationships between 20CR air temperature and atmospheric circulation. Compared to the CBTA model over the North Sea the correlation coefficients are even

higher (Table 6.1), As a further comparison the correlations from 1881-1999 are compared to those done by a similar study (Osborn and Jones, 2000). Again, the correlations are close to the ones seen in their study or slightly higher. The spline method in this thesis could be applied in a similar manner to the Moberg *et al.,* (2003) study to flag potential biases in earlier land station temperature datasets.

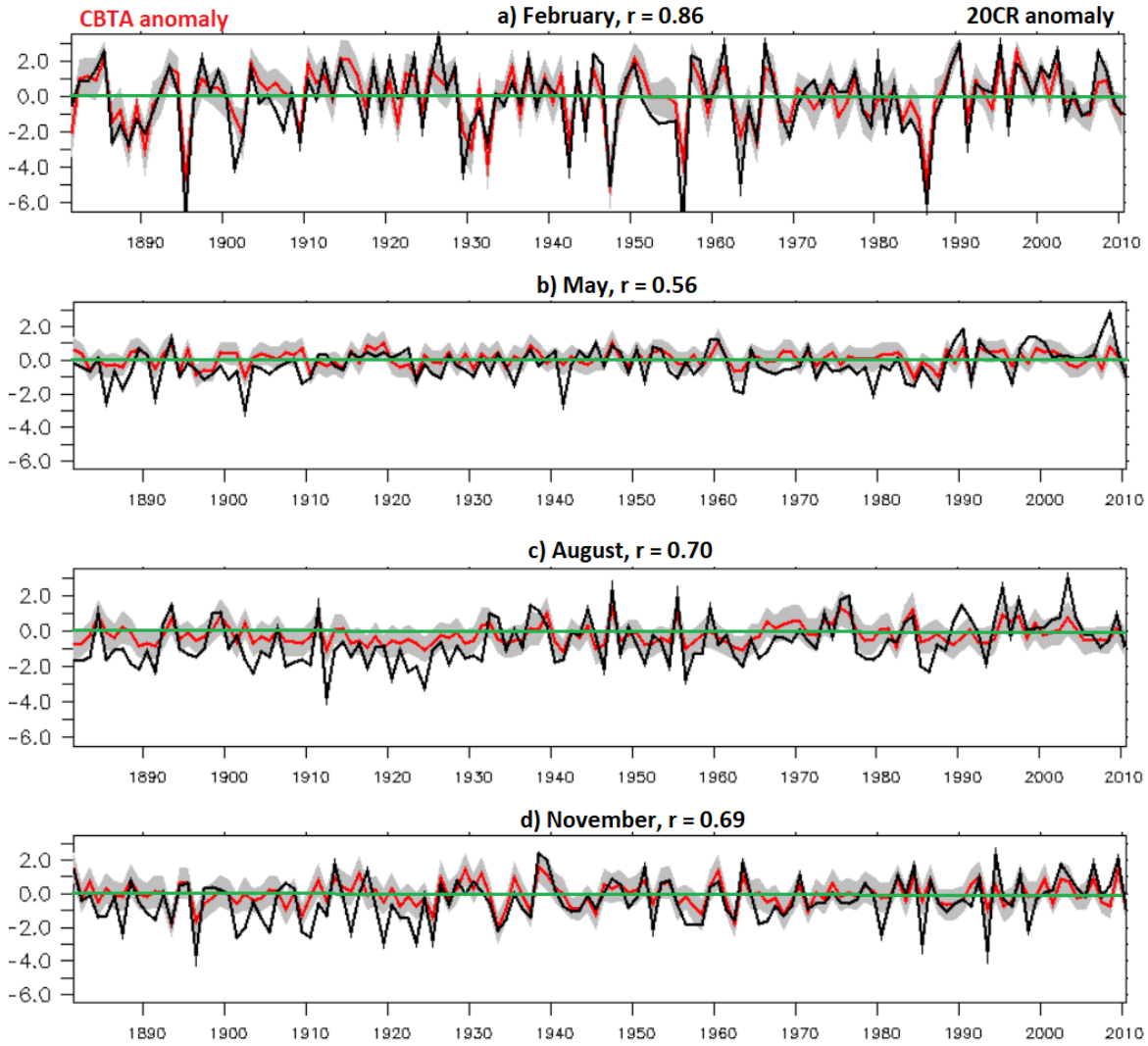

Figure 6.7: Time series of CBTAs and 20CR MAT anomalies for 4 different months of the year over a land point at 50N/0W. Grey regions represent 1SD uncertainty bounds.

Time period	DJF	MAM	JJA	SON
1971-2010	0.89	0.62	0.75	0.78
1931-1970	0.89	0.61	0.44	0.49
1881-1999	0.86 (0.78)	0.57 (0.47)	0.61 (0.65)	0.62 (0.60)

Table 6.1: Seasonal correlation coefficients between 20CR MAT and the CBTAs. For the 1881-1999 period, the correlations from the Osborn and Jones, (2000) study are shown in brackets.

3) Examine daily relationships between temperature and atmospheric circulation

This thesis focused on monthly relationships and whilst this did allow for comparisons between the 20CR and station SLP data, there may be important variations in atmospheric circulation within a month that could be overlooked by focusing on the monthly means. Two different monthly mean SLP patterns are shown in Figure 6.8. These months have similar flow directions, flow strengths and average SLP values, yet the monthly MAT anomalies are different. Only by looking at the daily variations is it clear why differences in the 20CR MAT anomalies occur. Both months had a frequent flow from the west but the SW winds were stronger during December 1993 but occurred on a smaller number of days.

December 1993 had also had a few days of cold northerly winds which resulted in a MAT anomaly close to average (J12). December 1994 however had persistent SW winds over several days bringing particularly mild air from the subtropical North Atlantic at times. The persistence of circulation types within a month can only be identified when looking at daily data, so it's possible the results from this thesis can be improved further by taking daily variations into account.

The results from this thesis for the 20CR suggest it should be fine to look at daily CBTAs over many areas of the North Atlantic and NW Europe when looking at timescales of over a century. The 20CR does not assimilate monthly SLP observations yet in these regions the 20CR flow parameters and station SLP data are in close agreement. In future versions of the 20CR, daily SLP observations will be assimilated from newer versions of the ISPD and ICOADS. ICOADS release 3.0 contains many more observations during the two world wars and the mid-19th century (Freeman *et al.,* 2017) improving the 20CR further. Meanwhile daily SLP observations are being digitised by various projects (Brohan *et al.*, 2009; Allan *et al.*, 2011) and will only serve to further improve the reanalysis products, expanding the number of regions where there could be confidence with regards to daily variations in atmospheric circulation on long timescales (over 50 years).

Finally, using daily data will yield large sample sizes which contain no overlap meaning better uncertainty estimates. The coverage of the CBTA field in areas such as the North Sea will also be improved as atmospheric circulation is more variable at daily timescales.

This thesis used monthly data because many of the marine climate datasets are only available at a monthly timescale. The results here however suggest that in areas such as the North Atlantic, future studies could also focus on daily MAT and SLP 20CR data given the favourable comparisons with HadNMAT2 and station SLP timescales.

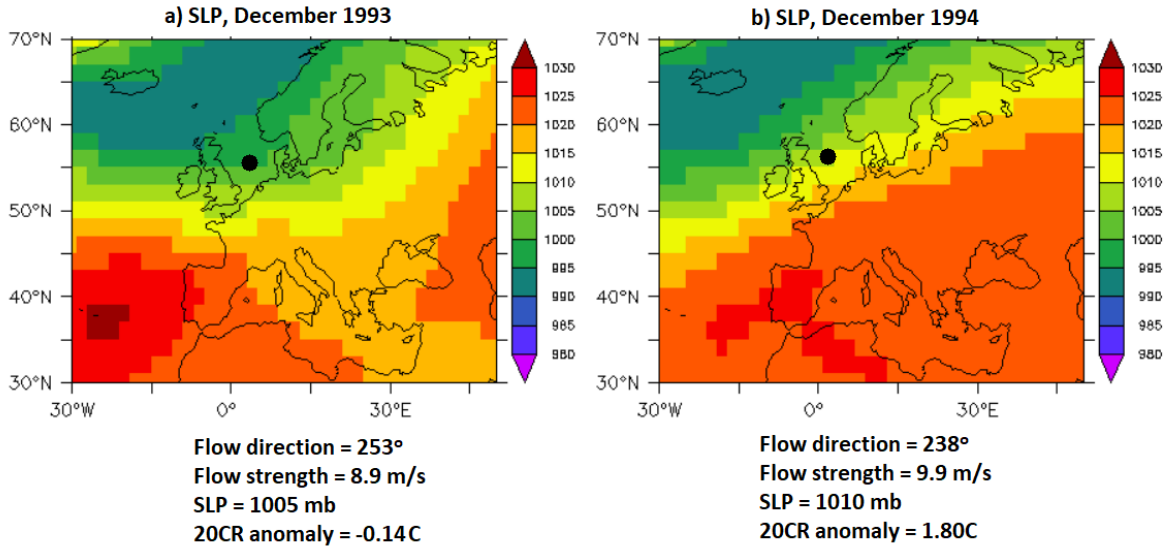

Figure 6.8: Average SLP for 2 months with the flow parameters (defined from the grid pattern in Figure 2.2a) listed underneath.

6.4 Concluding remarks

Historical records of past temperature are important for understanding the earth's climate and these show an unequivocal warming trend since the mid-19th Century (Hartmann *et al.,* 2013). Global temperatures are expected to pass the threshold for dangerous climate change (2^{o}C) by the year 2050 (Karmalkar and Bradley, 2017). In order to understand the potential impacts of this warming, it is important to understand the past variations in climate and the contribution of various influences on it. One way in which this can be done in to disentangle the variations in past temperature that have occurred by excluding different components. This thesis aimed to assess the role that atmospheric circulation has played in past climate variability over the oceans, with a particular focus on MAT.

The results from this thesis suggest that while climate change is the biggest influence on global MAT, atmospheric circulation is a very important influence on a local scale. Subtracting the estimated influence of atmospheric circulation highlighted other influences on climate such as the AMO. The residual variability also raised some questions about the positive anomalies in 20CR over the North Atlantic in the mid-20th century and the negative HadNMAT2 anomalies to the west of Spain before the 1950s. The time series was also accompanied with accurate uncertainty estimates for interpreting time series of temperature data. The method presented in this thesis could become a valuable tool in the research field in synoptic climatology and with further application over land and at daily timescales, more discrepancies in the temperature data may be found.

Appendix A

This section shows appendices from Chapter 2.

A.1 Jones, Harpham and Briffa (2012) Method for calculating flow parameters

This section shows the method used by J12 to calculate atmospheric circulation parameters. The grid configuration can be seen in Figure A1:

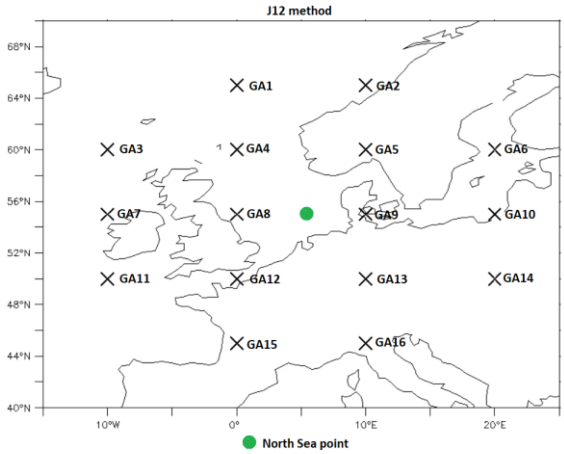

Figure A1: Locations of points where SLP is extracted from the 20CR reanalysis for the method which has been developed by J12.

To estimate flow direction the westerly and southerly flow components must be calculated. The text in bold refers to points in Figure A1:

$$\text{Westerly flow: } W = 0.5(\mathbf{GA12} + \mathbf{GA13}) - 0.5(\mathbf{GA4} + \mathbf{GA5})$$

$$\text{Southerly flow: } S = S_{dist1}\,[0.25(\mathbf{GA5} + (2 \times \mathbf{GA9}) + \mathbf{GA13}) - 0.25(\mathbf{GA4} + (2\ X\ \mathbf{GA8}) + \mathbf{GA12})]$$

$$S_{dist1}\,(1.74) = 1/\cos(lat)$$

$$\text{Flow strength: } F = (S^2 + W^2)^{1/2}$$

The westerly flow component is calculated from the South-North SLP gradient. For the southerly flow component, six points around the North Sea Point are used. Points **GA8** and **GA9** are given a higher weighting because they are closer to the North Sea point in green (Figure A1a). A constant (S_{dist1}) is also used because the distance between lines of

longitude varies with latitude and are closer to each other towards the poles. The S_{dist1} constant is needed to provide an accurate estimate of the southerly geostrophic wind at different latitudes. Flow strength is also calculated which is a quadrature sum of the southerly and westerly flow estimates.

The flow direction is calculated using the calculation $\tan^{-1}$ (*W/S*). For all values of flow direction to fall correctly within 0° and 360° the following adjustments need to be made (as $\tan^{-1}$ (*W/S*) values fall between -90 and 90° when converting from radians to degrees):

- If *W* and *S* > 0.0, add 180°
- If *W* > 0.0 and *S* < 0.0 add 360°
- If *W* < 0.0 and *S* > 0.0 add 180°

The shear parameter calculates the variations in flow strength around the North Sea point from South-North and from East-West. This is then used later as an estimate of the flow curl (flow curvature). The shear parameters are calculated using the following terms:

Westerly shear: $ZW = W_{cori1}$ [0.5(**GA15** + **G16**) – 0.5(**GA8** + **GA9**)] – W_{cori2} [0.5(**GA8** + **GA9**)] – 0.5(**GA1** + **GA2**)]

Southerly shear: $ZS = S_{dist2}$ *

$$\left[\begin{array}{c} 0.25\ (\mathbf{GA6} + (2 \times \mathbf{GA10}) + \mathbf{GA14}) - 0.25(\mathbf{GA5} + (2 \times \mathbf{GA9}) + \mathbf{G1A3}) - \\ 0.25(\mathbf{GA4} + (2 \times \mathbf{GA8}) + \mathbf{GA12}) + 0.25(\mathbf{GA3} + (2 \times \mathbf{GA7}) + \mathbf{GA11}) \end{array}\right]$$

Resultant shear: $Z = ZW + ZS$

W_{cori1} (1.07) = sin(lat)/sin(*lat* – 5°)

W_{cori2} (0.95) = sin(lat)/sin(*lat* + 5°)

S_{dist2} (1.52) = 1/ (2(cos (*lat*) ^{2}))

For westerly shear, the same formula used to estimate the westerly flow component is applied to the North (60°N) and South (50°N) of the North Sea point (55°N). These SLP gradients can identify variations in flow direction and strength around a given region. The

ZW calculation identifies whether there is a cyclonic or anticyclonic flow component using south-north SLP gradients.

Two constants are also used in the westerly shear calculations because the estimated westerly geostrophic wind components are taken at two different latitudes (In Figure A1 these are 50°N and 60°N respectively). The constants are based on the differences in the Coriolis parameter at these latitudes compared to that of the North Sea point at 55°N. The Coriolis parameter varies with latitude, with a minimum of zero at the equator and a maximum at the poles. For westerly shear calculations at 55°N, W_{cori1} is larger because the Coriolis parameter at 50°N is smaller. A smaller weighting is applied at 60°N because the Coriolis parameter is higher.

The southerly flow shear calculates SLP gradients to the east and west of the UK, if the southerly wind is stronger to the east of the UK this indicates cyclonic flow component (positive value for ZS) is present. The sum of these two terms is the Resultant shear (*Z*).

A.2 Thesis method for calculating flow parameters

This appendix subsection shows the SLP gradients which are calculated for the flow parameters in this chapter. In contrast to the J12) method only 4 SLP points are used to define atmospheric circulation parameters in this thesis (Figure A2)

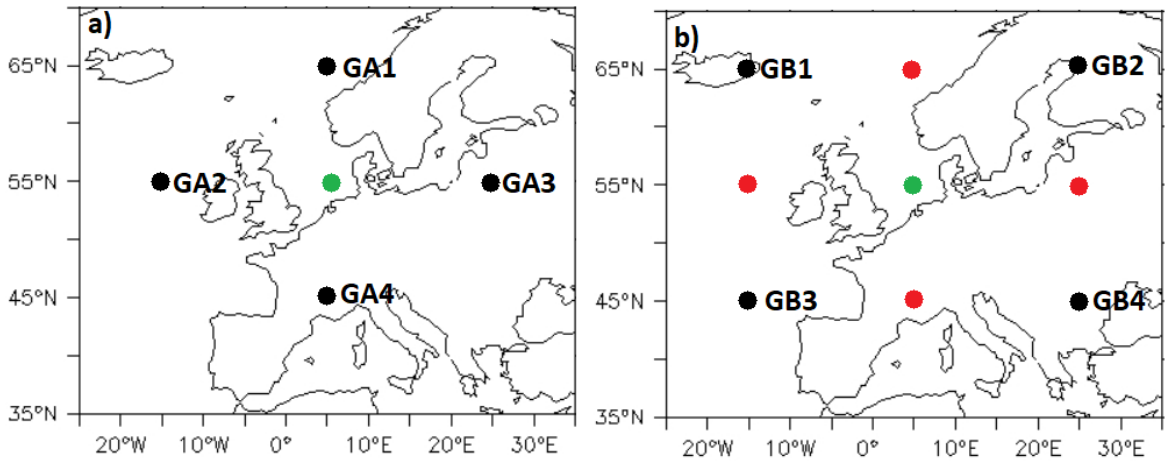

Figure A2: 2 grid configurations used to define atmospheric circulation parameters in this chapter. Panel a) is referred to as the diamond configuration whilst panel b) is the square configuration. SLP is not extracted from the North Sea point shown in green. Red points in panel b) represent interpolated SLP values.

The westerly and southerly SLP gradients are as follows from Figure A1 panel a):

$$Westerly\ flow = GA4 - GA1$$

$$Southerly\ flow = GA3 - GA2$$

For panel b) the calculations are similar but linear interpolation is required to get the SLP at the red points. No scaling is required due to the use of the Haversine formula to calculate distances between points.

A.3 Global correlations between average SLP and flow shear

This part of the appendix shows a Figure with the correlation between the average SLP from the 4 points in the diamond grid configuration and the shear as calculated by J12. This consists of monthly data from 1851-2011 and is shown across each point in the ocean. The correlations are negative because higher SLP is represented by negative shear values (anticyclonic synoptics).

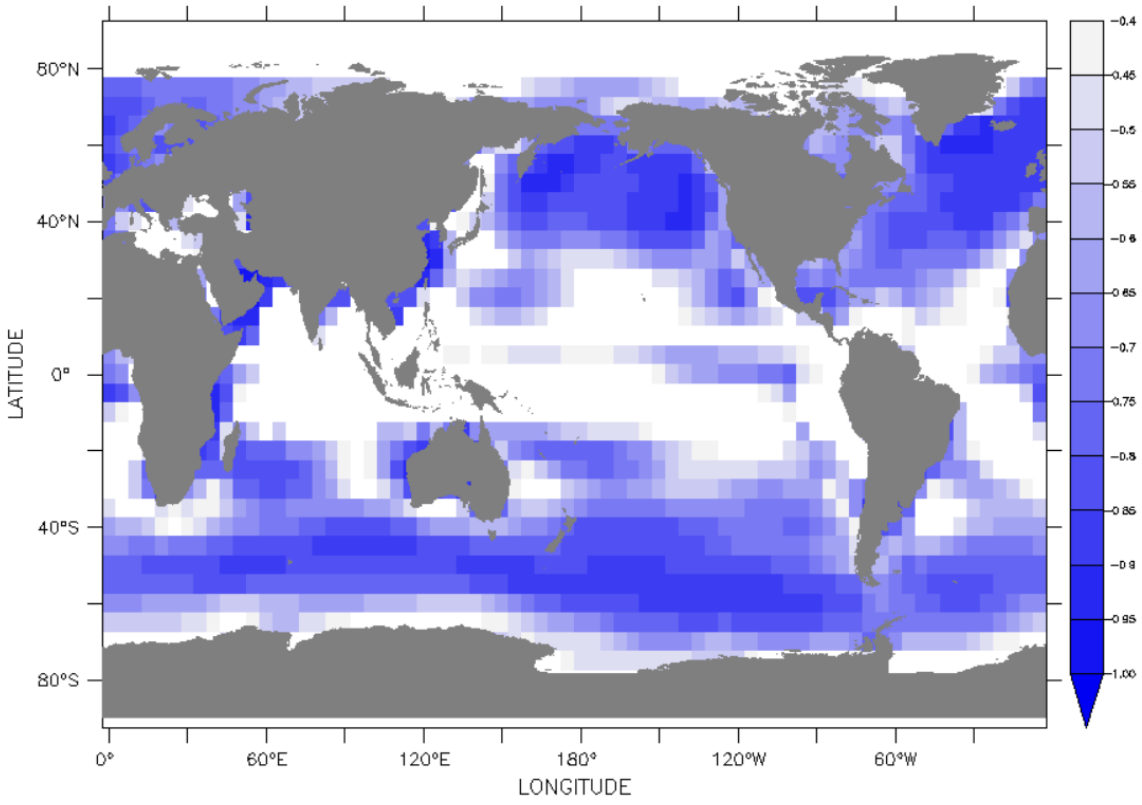

Figure A3: Correlation between SLP and total flow shear from Jones *et al* (2012), using monthly data from 1851-2011.

Appendix B

This appendix shows a plot to accompany Figure 3.5 in Chapter 3. The Uncertainty fields in Figure B1 show that where the category uncertainty estimates are low the parametric uncertainties are high. The parametric uncertainties are high in these regions because there are no observations to constrain the spline approximation.

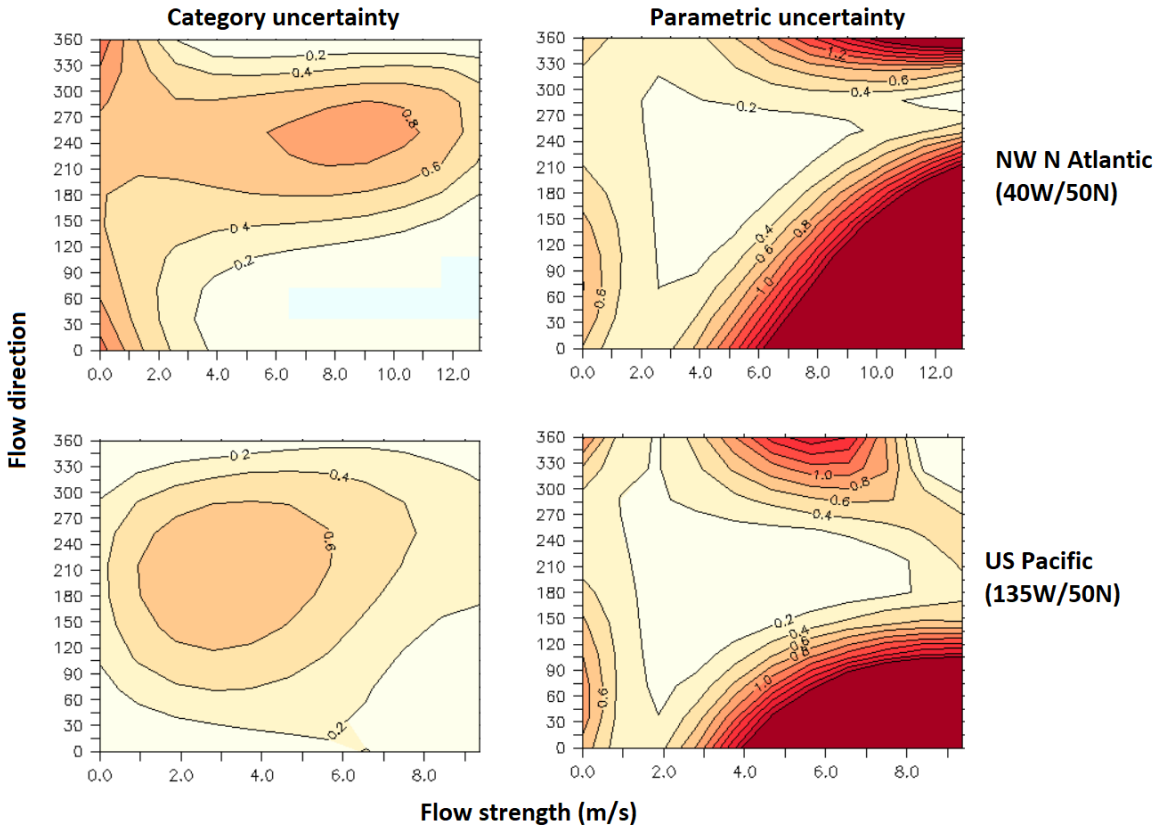

Figure B1: Category and parametric uncertainties for the February flow strength CBTA fields. Two locations at the NW North Atlantic and US Pacific are shown.

Appendix C

This section shows Figures relevant to Chapter 4. The first Figure (C1) shows a comparison of the correlation coefficients for the spline method and the stepwise quadratic regression for the 1971-2010 period (outside the period used to build the model). The Figure C1 shows that the spline method and regression method have similar levels of performance, although for the 1931-1970 period the spline model performs much better.

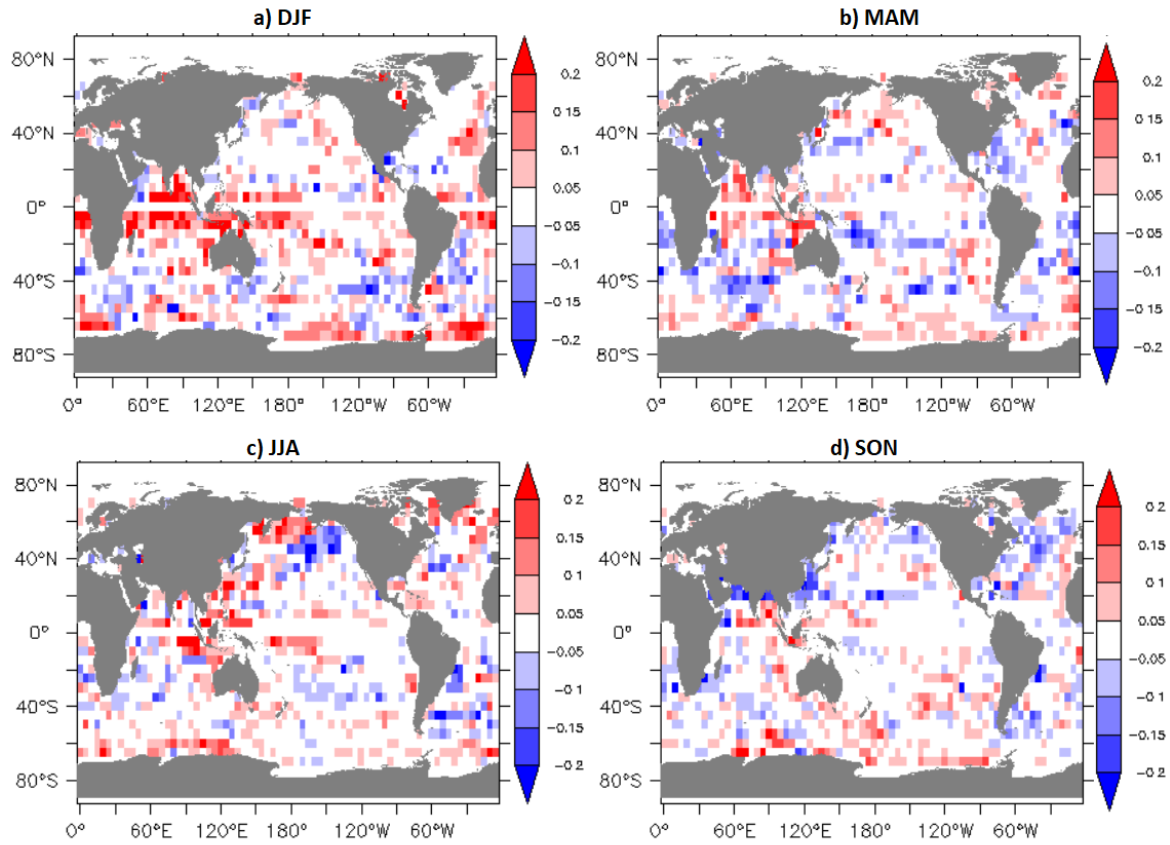

Figure C1: Comparison between the correlation coefficients from the CBTA method and regression method for each season. Red grid cells indicate where the CBTA method performs better whereas blue cells indicate where the regression method is best. White cells show where there is little difference in performance between the two methods. Results are shown for the 1971-2010 period.

The second Figure (C2) shows a comparison of the variances in the 20CR 2 metre air temperature for two different periods (1931-1970 and 1971-2010 in panels a) and b) respectively). The differences between panels a) and b) are shown in panel c). The key results are those for the Southern Ocean which has much less temperature anomaly variability during earlier years and this explains the large drop in uncertainty values occurring alongside a drop in the correlation coefficient when comparing data from 1931-1970 to that from 1971-2010.

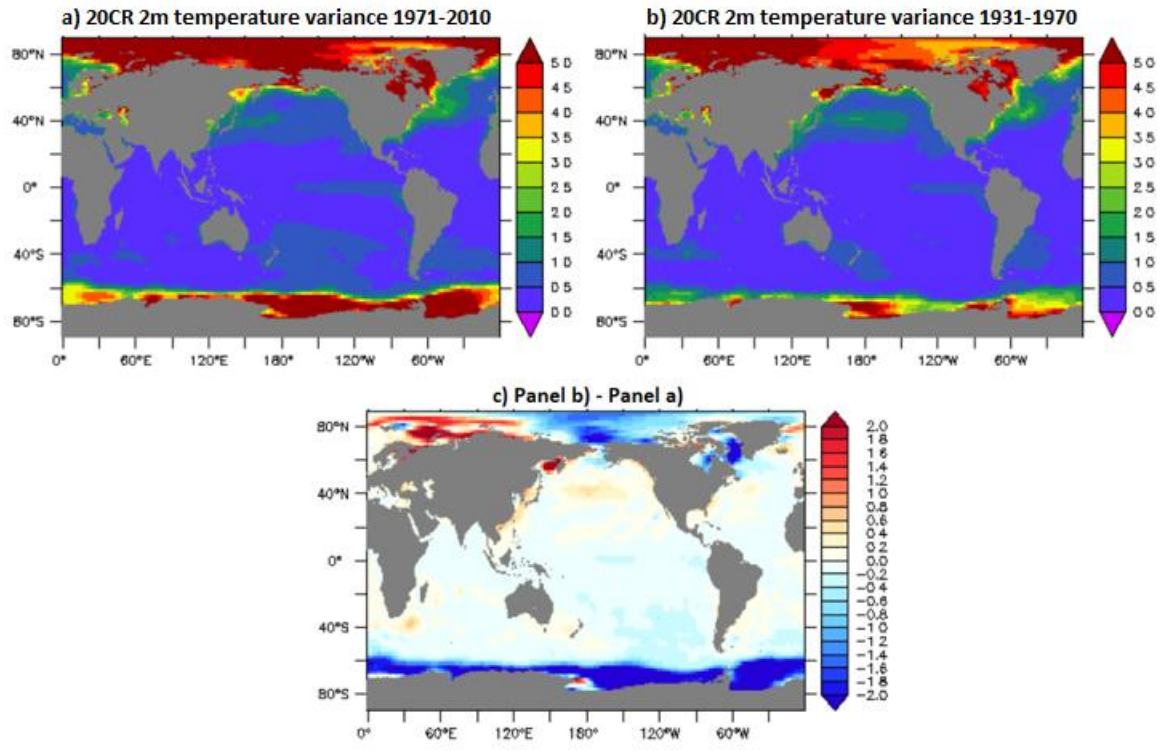

Figure C2: Panel a) Variance of 20CR 2 metre air temperature ($^oC^2$) based on all months from 1971-2010; b) as with panel a) but with results from 1931-1970; c) differences in variances between the two 40-year periods. Blue areas indicate where variance is smaller during the 1931-1970 period compared to 1971-2010 and vice versa.

Appendix D

This section refers to extra analysis from Chapter 5.

D.1 Steps for calculating flow parameters from station data grid patterns

In order to calculate the flow parameters from station data. The following steps are taken:

- The maximum and minimum latitude values are taken and the point in between these latitudes is taken (Figure D1a). SLP values are then interpolated at these points when necessary using the two relevant station SLP points (panels b and c). The SLP gradient between the two interpolated points in blue are then used to calculate the v flow (southerly flow component).
- The same process is applied with the longitude values in order to calculate the u flow component (westerly flow). The other steps taken to calculate the flow

parameters are those described in Chapter 2. Using the haversine formula and Coriolis parameter etc. to calculate flow strengths in ms^{-1}.

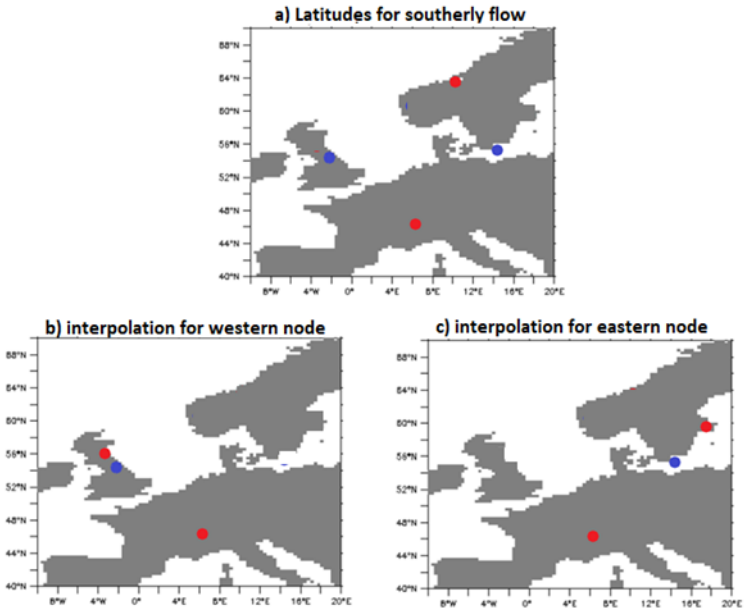

Figure D1: Steps taken to calculate southerly flow from station SLP data. The latitudes taken to calculate southerly flow are determined by the positions of the furthest north and south SLP points (panel a), then SLP is interpolated to calculate values at the blue points in panels b) and c). Southerly flow can be directly calculated from the SLP gradient at both these interpolated points.

D.2 Other results from Chapter 5

Table D1 shows a list of all the stations of SLP used to create the CBTA time series. Some major gaps (10 years or more) are present in some time series. Data from Jakobshavn is used to fill in gaps in the Nuuk series in the mid-20th century. Whilst Vladivostock, Valdividia and Punta Arenas also contain some gaps and are extended by overlapping time series in Ussuriysk, Punta Galera, Islotes Evang respectively.

Station Name	Country	Lat	Lon	Start	End	Data source
St Johns	Canada	47.6N	52.7W	1852	2017	World Surface Climatology (WSC) / Slonosky
Nuuk	Greenland	64.2N	51.7W	1873	2017	WSC
Jakobshavn	Greenland	69.2N	51.1W	1873	2017	WSC
Reykjavik	Iceland	64.2N	21.9W	1821	2017	Jones, Jonsson and Wheeler (1997)
Valentia	Ireland	51.9N	10.4W	1866	2017	Jones et al., (1999)
Edinburgh	UK	55.9N	3.4W	1770	2017	Jones et al., (1999)
Uppsala	Sweden	59.9N	17.6E	1722	2017	Jones et al., (1999)
Trondheim	Norway	63.4N	10.4E	1768	2017	Jones et al., (1999)
Geneva	Switzerland	46.2N	6.1E	1768	2017	Jones et al., (1999)
Madrid	Spain	40.4N	3.7W	1786	2017	Jones et al., (1999)
Funchal	Portugal	32.7N	16.9W	1865	2017	Jones et al., (1999)
Ponta Delgada	Portugal	37.7N	25.7W	1865	2017	Jones et al., (1999)
Malta	Malta	35.9N	14.4E	1852	2017	Jones et al., (1999)
Cairo	Egypt	30N	31.2E	1869	2017	Jones et al., (1999)
Istanbul	Turkey	41N	29E	1856	2017	Jones et al., (1999)
Detroit	USA	42.3N	83.1W	1873	2017	WSC
Charleston	USA	32.8N	79.9W	1873	2017	WSC
Prince Edward Island	Canada	46.5N	63.4W	1874	2017	WSC
Bermuda	USA	32.3N	64.7W	1861	2017	WSC
Madras	India	13.1N	80.3E	1796	2017	Allan *et al.*, 2002
Calcutta	India	22.6N	88.4E	1855	2017	WSC
Agra	India	27.2N	78E	1875	2017	HADSLP2 station data
Port Blair	Indonesia	11.6N	92.7E	1871	2017	HADSLP2 station data
Sydney	Australia	33.4S	151.2E	1859	2018	WSC
Hobart	Australia	42.9S	147.3E	1841	2017	Turney *et al.*, 2016
Auckland	New Zealand	36.9S	174.8E	1863	2017	NIWA
Dunedin	New Zealand	45.9S	170.6E	1864	2017	NIWA
Ussuriysk	Russia	43.8N	131.9E	1890	1950	WSC
Vladivostock	Russia	43.1N	131.9E	1921	2018	WSC
Nagasaki	Japan	32.8N	129.9E	1826	2018	Können *et al.*, 2003
Tokyo	Japan	35.4N	139.5E	1876	2018	JMA
Sapporo	Japan	43.1N	141.2E	1886	2018	JMA
Punta Galera	Chile	40S	73.7W	1899	1957	WSC
Valdividia	Chile	39.6S	73.1W	1941	2018	WSC
Buenos Aires	Argentina	34.6S	58.4W	1856	2018	HADSLP2 station data
Falklands	UK	51.7S	59.5W	1859	2018	Turney *et al., (2016)*
Punta Arenas	Chile	53.2S	70.9W	1941	2018	WSC
Islotes Evang	Chile	52.4S	75.1W	1899	1950	WSC

Table D1: Stations of SLP data used in Chapter 5, data from New Zealand (NIWA), the Japanese Meteorological Agency (JMA), the World Surface Climatology Network (*https://rda.ucar.edu/datasets/ds570.0/*)

D.3 Time series of CBTAs from different SLP datasets

This section shows some more time series of CBTAs from Station data, the ERA-20C and the 20CR. The first time series shows CBTAs over the Central North Atlantic region (location shown Figure 5.1a) and this also shows little disagreement between the three CBTA datasets. The 20CR MAT time series during the DJF period from 1900 to 1920 is colder than the others, whilst the 1930-1950 period appears to be too warm.

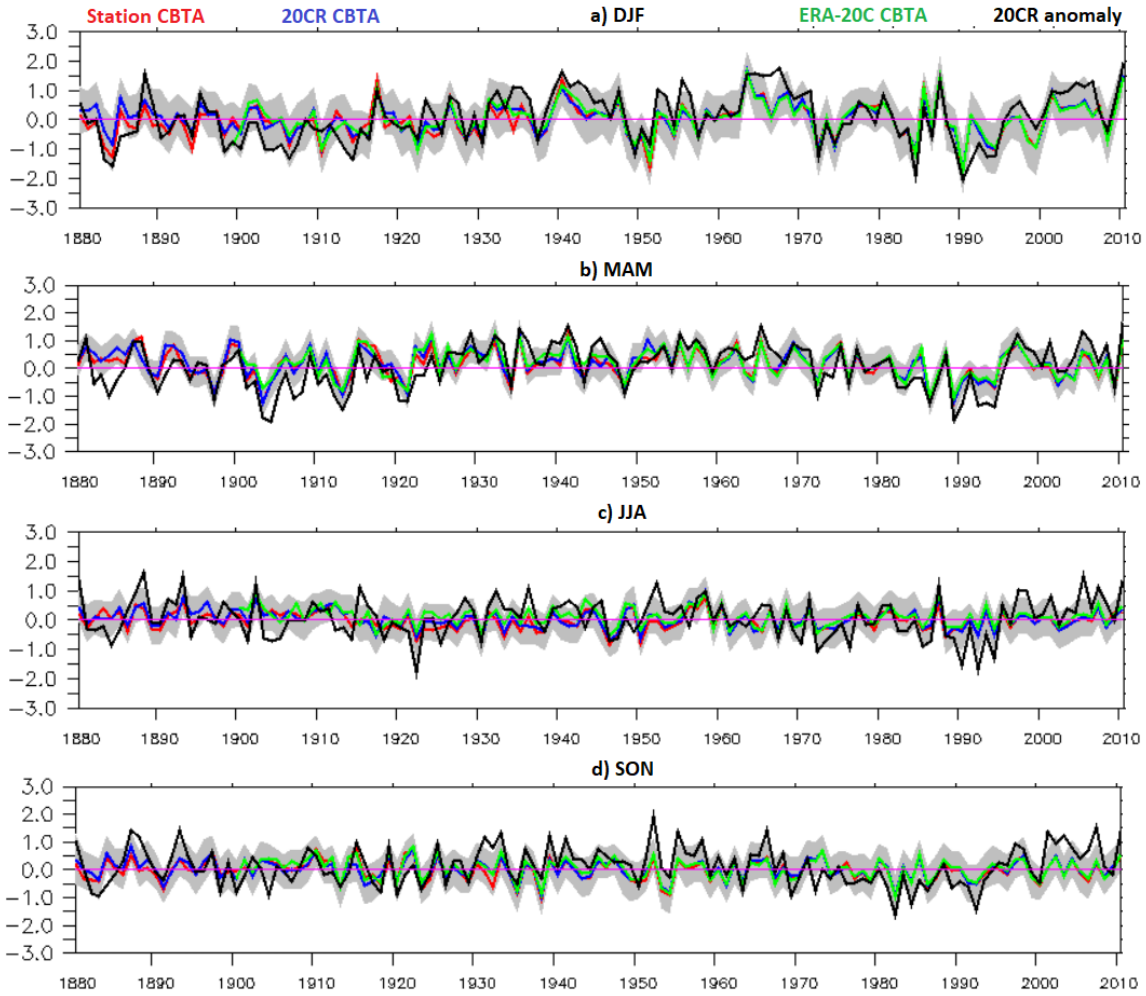

Figure D2: Time series of CBTAs for the North Atlantic region (shown in Figure 5.1a) during four different periods of the year covering the period 1880-2010. The blue time series represents 20CR CBTAs, black shows the 20CR MAT, green represents the ERA-20C and red represents station SLP data. Grey regions mark the 1SD uncertainty bounds of the 20CR time series. The model is developed using 1971-2010 flow parameters as in Chapters 2 and 3.

Figure D3 shows some more time series of CBTAs from the West of Spain between the different SLP data sources.

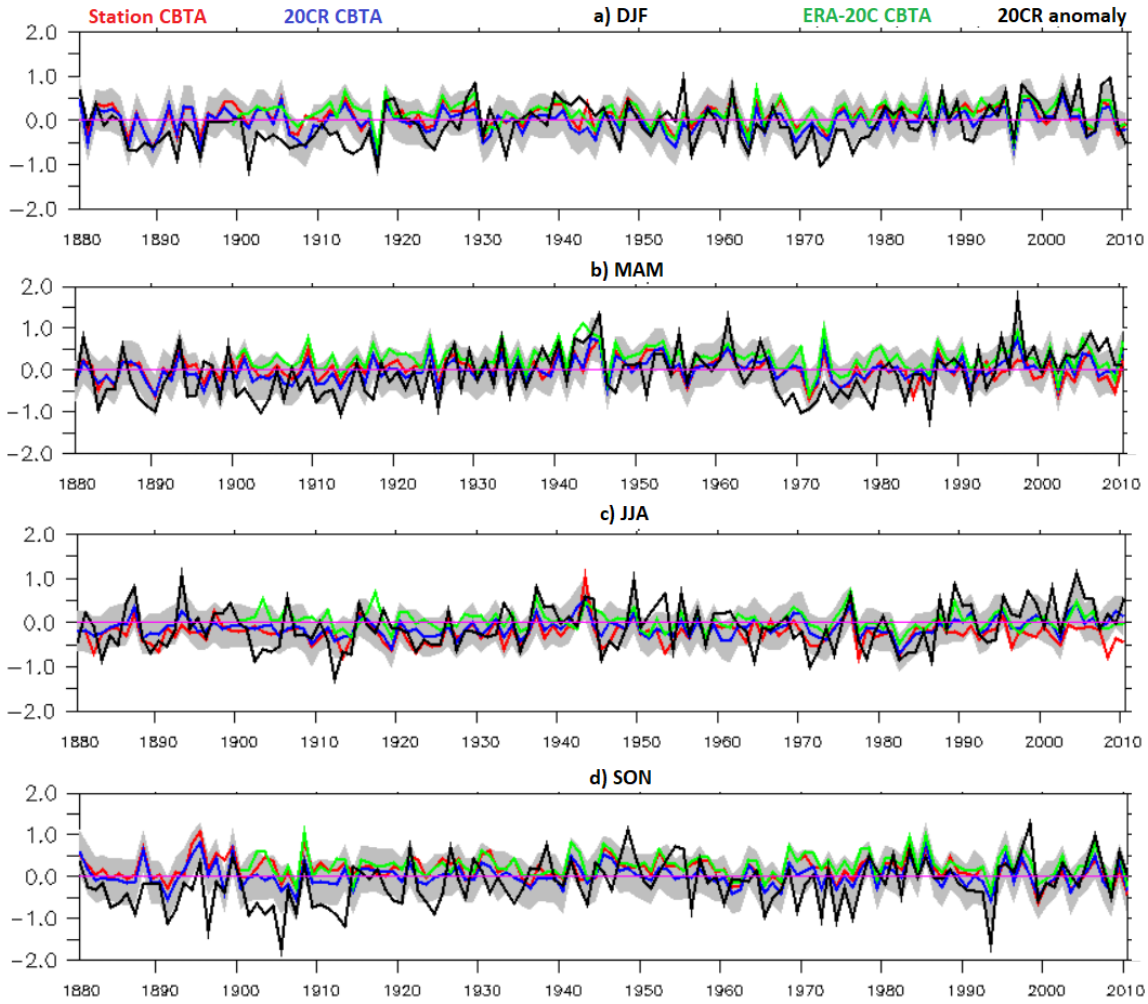

Figure D3: As with Figure D2 but showing results for an area to the West of Spain (16W/42N).

References

Abatzoglou, J. T., Rupp, D. E. and Mote, P. W. (2014) 'Questionable evidence of natural warming of the northwestern United States', *Proceedings of the National Academy of Sciences of the United States of America*, 111(52), pp. E5605–E5606. doi: 10.1073/pnas.1421311112.

Alexander, M. A., Halimeda Kilbourne, K. and Nye, J. A. (2014) 'Climate variability during warm and cold phases of the Atlantic Multidecadal Oscillation (AMO) 1871-2008', *Journal of Marine Systems*, 133(February), pp. 14–26. doi: 10.1016/j.jmarsys.2013.07.017.

Allan, R. and Ansell, T. (2006) 'A new globally complete monthly historical gridded mean sea level pressure dataset (HadSLP2): 1850-2004', *Journal of Climate*, 19(22), pp. 5816–5842. doi: 10.1175/JCLI3937.1.

Allan, R., Brohan, P., Compo, G. P., Stone, R., Luterbacher, J. and Brönnimann, S. (2011) 'The international atmospheric circulation reconstructions over the earth (ACRE) initiative', *Bulletin of the American Meteorological Society*, 92(11), pp. 1421–1425. doi: 10.1175/2011BAMS3218.1.

Allan, R. J., Reason, C. J. C., Carroll, P. and Jones, P. D. (2002) 'A reconstruction of Madras (Chennai) mean sea-level pressure using instrumental records from the late 18th and early 19th centuries', *International Journal of Climatology*, 22(9), pp. 1119–1142. doi: 10.1002/joc.678.

Basnett, T. and Parker, D. (1997) *Development of the Global Mean Sea Level Pressure Data Set GMSLP2*. Bracknell, U.K..: Hadley Centre for Climate Prediction and Research: Meteorological Office.

Beck, C., Jacobeit, J. and Jones, P. D. (2006) 'Frequency and within-type variations of large- scale circulation types and their effects on low-frequency climate variability in central Europe since 1780', *International Journal of Climatology*, 27(4), pp. 473–491. doi: 10.1002/joc.

Berry, D. I. and Kent, E. C. (2011) 'Air-Sea fluxes from ICOADS: The construction of a new

gridded dataset with uncertainty estimates', *International Journal of Climatology*, 31(7), pp. 987–1001. doi: 10.1002/joc.2059.

Böhm, R., Jones, P. D., Hiebl, J., Frank, D., Brunetti, M. and Maugeri, M. (2010) 'The early instrumental warm-bias: A solution for long central European temperature series 1760-2007', *Climatic Change*, 101(1), pp. 41–67. doi: 10.1007/s10584-009-9649-4.

Bojinski, S., Verstraete, M., Peterson, T. C., Richter, C., Simmons, A. and Zemp, M. (2014) 'The concept of essential climate variables in support of climate research, applications, and policy', *Bulletin of the American Meteorological Society*, 95(9), pp. 1431–1443. doi: 10.1175/BAMS-D-13-00047.1.

Bottomley, M., Folland, C. ., Hsiung, J., Newell, R. . and Parker, D. . (1990) *Global Ocean Surface Temperature Atlas (Gosta)*. Bracknell, U.K: Meteorological Office.

Brandsma, T. and van der Meulen, J. . (2007) 'Thermometer screen intercomparison in De Bilt (theNetherlands) – Part II: Description and modeling of meantemperature differences and extremes', *International Journal of Climatology*, 28(3), pp. 389–400. doi: 10.1002/joc.

Brohan, P., Allan, R., Freeman, J. E., Waple, A. M., Wheeler, D., Wilkinson, C. and Woodruff, S. (2009) 'Marine observations of old weather', *Bulletin of the American Meteorological Society*, 90(2), pp. 219–230. doi: 10.1175/2008BAMS2522.1.

Bulgin, C. E., Embury, O. and Merchant, C. J. (2016) 'Sampling uncertainty in gridded sea surface temperature products and Advanced Very High Resolution Radiometer (AVHRR) Global Area Coverage (GAC) data', *Remote Sensing of Environment*. Elsevier Inc., 177, pp. 287–294. doi: 10.1016/j.rse.2016.02.021.

Carella, G., Kent, E. C. and Berry, D. I. (2017) 'A probabilistic approach to ship voyage reconstruction in ICOADS', *International Journal of Climatology*, 37(5), pp. 2233–2247. doi: 10.1002/joc.4492.

Carson, M., Köhl, A., Stammer, D., A. Slangen, A. B., Katsman, C. A., W. van de Wal, R. S., Church, J. and White, N. (2016) 'Coastal sea level changes, observed and projected during the 20th and 21st century', *Climatic Change*, 134(1–2), pp. 269–281. doi: 10.1007/s10584-015-1520-1.

Chen, D. (2000) 'A monthly circulation climatology for Sweden and its application to a winter temperature case study', *International Journal of Climatology*, 20(10), pp. 1067–1076. doi: 10.1002/1097-0088(200008)20:10<1067::AID-JOC528>3.0.CO;2-Q.

Chenoweth, M. (2000) 'A new methodology for homogenization of 19th century marine air temperature data', *Journal of Geophysical Research Atmospheres*, 105(D23), pp. 29145–29154. doi: 10.1029/2000JD900050.

Clarke, A. J. (2014) 'El Niño Physics and El Niño Predictability', *Annual Review of Marine Science*, 6(1), pp. 79–99. doi: 10.1146/annurev-marine-010213-135026.

Compo, G., Whitaker, J., Sardeshmukh, P., Matsui, N., Allan, R., Yin, X., Gleason, B., Vose, R., Rutledge, G., Bessimoulin, P., Bronniman, S., Brunet, M., Crouthamel, R., Grant, A., Groisman, P., Jones, P., Kruk, M., Kruger, A., Marshall, G., Maugeri, M., Mok, H., Nordli, O., Ross, T., Trigo, R., Wang, X., Woodruff, S. and Worley, S. (2011). The Twentieth Century Reanalysis project. 137 (634): Quarterly Journal of the Royal Meteorological Society, pp.1-28.

Compo, G. P. (2014) *Towards an improved 20th Century reanalysis version "2c"(1851-2012).* Available at: https://www2.cisl.ucar.edu/sites/default/files/final_Compo_20CRv2c_Seminar_NCAR_EnKF %281%29.pdf .

Compo, G. P., Whitaker, J. and Sardeshmukh, P. (2006) 'Feasibility of a 100-Year Reanalysis Using Only Surface Pressure Data', *Bulletin of the American Meteorological Society*, 87(2), pp. 175–190.

Conway, D., Wilby, R. L. and Jones, P. D. (1996) 'Precipitation and air flow indices over the British Isles', *Climate Research*, 7(2), pp. 169–183. doi: 10.3354/cr007169.

Cornes, R. C., Jones, P. D., Briffa, K. R. and Osborn, T. J. (2012) 'A daily series of mean sea-level pressure for London, 1692-2007', *International Journal of Climatology*, 32(5), pp. 641–656. doi: 10.1002/joc.2301.

Cortesi, N., Torralba, V., Gonzalez-Reviriego, N. and Pena-Agulo, D. (2018) *Extra-tropical impact of Lamb weather types on mean temperatures*. Available at:

https://www.researchgate.net/publication/312489624_Extratropical_impact_of_Lamb_weather_types_on_mean_temperatures.

Cowtan, K., Rohde, R. and Hausfather, Z. (2018) 'Evaluating biases in sea surface temperature records using coastal weather stations', *Quarterly Journal of the Royal Meteorological Society*, 144(712), pp. 670–681. doi: 10.1002/qj.3235.

Cram, T., Compo, G., Whitaker, J., Sardeshmukh, P., Matsui, N., Allan, R., Yin, X., Gleason, B., Vose, R., Rutledge, R., Bessemoulin, P., Brönnimann, S., Brunet, M., Crouthamel, R., Grant, A., Groisman, P., Jones, P., Kruk, M., Kruger, A., Marshall, G., Maugeri, M., Mok, H., Nordli O., Ross, T., Trigo, R., Wang, X., Woodruff, S. and Worley S. (2015). The International Surface Pressure Databank version 2, *Geoscience Data Journal*, 2(1), 31–46. doi:10.1002/gdj3.25.

Dee, D. P.; Uppala, S. M.; Simmons, A. J.; Berrisford, P.; Poli, P.; Kobayashi, S.; Andrae, U.; Balmaseda, M. A.; Balsamo, G.; Bauer, P.; Bechtold, P.; Beljaars, A. C. M.; van de Berg, L.; Bidlot, J.; Bormann, N.; Delsol, C.; Dragani, R.; Fuentes, M.; Geer, A. J.; Haimberger, L.; Healy, S. B.; Hersbach, H.; Hólm, E. V.; Isaksen, L.; Kållberg, P.; Köhler, M.; Matricardi, M.; McNally, A. P.; Monge-Sanz, B. M.; Morcrette, J.-J.; Park, B.-K.; Peubey, C.; de Rosnay, P.; Tavolato, C.; Thépaut, J.-N.; Vitart, F. (2011). The ERA-Interim reanalysis: configuration and performance of the data assimilation system. *Quarterly Journal of the Royal Meteorological Society*, 137(656), pp.553-597.

El Dessouky, T. and Jenkinson, A. (1975) *An objective daily catalogue of surface pressure, flow and vorticity indices for Egypt and its use in monthly rainfall forecasting*. Bracknell, U.K: Synoptic Climatology Branch Memorandum, No. 46, Meteorological Office.

Dima, M. and Lohmann, G. (2010) 'Evidence for two distinct modes of large-scale ocean circulation changes over the last century', *Journal of Climate*, 23(1), pp. 5–16. doi: 10.1175/2009JCLI2867.1.

Ding, Y. and Krishnamurti, T. (1987) 'Heat Budget of the Siberian High and the Winter Monsoon', *Monthly Weather Review*, 115(10), pp. 2428–2449.

Donlon, C., Robinson, I., Casey, K., Vazquez-Cuervo, J., Armstrong, E., Arino, O., Gentemann, C., May, D., LeBorgne, P., Piollé, J., Barton, I., Beggs, H., Poulter, D.,

Merchant, C., Bingham, A., Heinz, S., Harris, A., Wick, G., Emery, B., Minnett, P., Evans, R., Llewellyn-Jones, D., Mutlow, C., Reynolds, R., Kawamura, H. and Rayner, N. (2007). The Global Ocean Data Assimilation Experiment High-resolution Sea Surface Temperature Pilot Project. *Bulletin of the American Meteorological Society*, 88(8), pp.1197-1214.

Drijfhout, S., Van Oldenborgh, G. J. and Cimatoribus, A. (2012) 'Is a decline of AMOC causing the warming hole above the North Atlantic in observed and modeled warming patterns?', *Journal of Climate*, 25(24), pp. 8373–8379. doi: 10.1175/JCLI-D-12-00490.1.

Enfield, D. B., Mestas-Nuñez, A. M. and Trimble, P. J. (2001) 'The Atlantic multidecadal oscillation and its relation to rainfall and river flows in the continental U.S', *Geophysical Research Letters*, 28(10), pp. 2077–2080. doi: 10.1029/2000GL012745.

Ferguson, C. R. and Villarini, G. (2012) 'Detecting inhomogeneities in the Twentieth Century Reanalysis over the central United States', *Journal of Geophysical Research Atmospheres*, 117(5), pp. 1–11. doi: 10.1029/2011JD016988.

Ferguson, C. R. and Villarini, G. (2014) 'An evaluation of the statistical homogeneity of the Twentieth Century Reanalysis', *Climate Dynamics*, 42(11–12), pp. 2841–2866. doi: 10.1007/s00382-013-1996-1.

Folland, C. K., Knight, J., Linderholm, H. W., Fereday, D., Ineson, S. and Hurrel, J. W. (2009) 'The summer North Atlantic oscillation: Past, present, and future', *Journal of Climate*, 22(5), pp. 1082–1103. doi: 10.1175/2008JCLI2459.1.

Folland, C. K. and Parker, D. E. (1995) *Correction of instrumental biases in historical sea surface temperature data*, *Quarterly Journal of the Royal Meteorological Society*. doi: 10.1002/qj.49712152206.

Foster, J., Owe, M. and Rango, A. (1983) 'Snow cover and temperature relationships in North America and Eurasia.', *Journal of Climate & Applied Meteorology*, pp. 460–469. doi: 10.1175/1520-0450(1983)022<0460:SCATRI>2.0.CO;2.

Fraedrich, K. (1994) 'An ENSO impact on Europe? A review', *Tellus, Series A*, pp. 541–552.

Freeman, E., Woodruff, S. D., Worley, S. J., Lubker, S. J., Kent, E. C., Angel, W. E., Berry, D. I., Brohan, P., Eastman, R., Gates, L., Gloeden, W., Ji, Z., Lawrimore, J., Rayner, N. A.,

Rosenhagen, G. and Smith, S. R. (2017) 'ICOADS Release 3.0: a major update to the historical marine climate record', *International Journal of Climatology*, 37(5), pp. 2211–2232. doi: 10.1002/joc.4775.

Giese, B. S. and Ray, S. (2011) 'El Niño variability in simple ocean data assimilation (SODA), 1871-2008', *Journal of Geophysical Research: Oceans*, 116(2), pp. 1–17. doi: 10.1029/2010JC006695.

Gillett, N. P., Zwiers, F. W., Weaver, A. J. and Stott, P. A. (2003) 'Detection of human influence on sea-level pressure', *Nature*, 422(6929), pp. 292–294. doi: 10.1038/nature01487.

Golinksi, J. (2007) *British weather and the climate of enlightenment*. Chicago and London: University of Chicago Press.

Hansen, J., Ruedy, R., Sato, M. and Lo, K. (2010) 'Global surface temperature change', *Reviews of Geophysics*, 48(4), pp. 1–29. doi: 10.1029/2010RG000345.

Hartmann, D.L., A.M.G. Klein Tank, M. Rusticucci, L.V. Alexander, S. Brönnimann, Y. Charabi, F.J. Dentener, E.J. Dlugokencky, D.R. Easterling, A. Kaplan, B.J. Soden, P.W. Thorne, M. Wild and P.M. Zhai, 2013: *Observations: Atmosphere and Surface. In: Climate Change 2013: The Physical Science Basis. Contribution of Working Group I to the Fifth Assessment Report of the Intergovernmental Panel on Climate Change [Stocker, T.F., D. Qin, G.-K. Plattner, M. Tignor, S.K. Allen, J. Boschung, A. Nauels, Y. Xia, V. Bex and P.M. Midgley (eds.)]*. Cambridge University Press, Cambridge, United Kingdom and New York, NY, USA, pp. 159–254, doi:10.1017/CBO9781107415324.008.

Hegerl, G. C., Brönnimann, S., Schurer, A. and Cowan, T. (2018) 'The early 20th century warming: Anomalies, causes, and consequences', *Wiley Interdisciplinary Reviews: Climate Change*, 9(4), pp. 1–20. doi: 10.1002/wcc.522.

Hirahara, S., Ishii, M. and Fukuda, Y. (2014) 'Centennial-scale sea surface temperature analysis and its uncertainty', *Journal of Climate*, 27(1), pp. 57–75. doi: 10.1175/JCLI-D-12-00837.1.

Holland, G. and Bruyère, C. L. (2014) 'Recent intense hurricane response to global climate

change', *Climate Dynamics*, 42(3–4), pp. 617–627. doi: 10.1007/s00382-013-1713-0.

Huang, B., Banzon, V. F., Freeman, E., Lawrimore, J., Liu, W., Peterson, T. C., Smith, T. M., Thorne, P. W., Woodruff, S. D. and Zhang, H. M. (2015) 'Extended reconstructed sea surface temperature version 4 (ERSST.v4). Part I: Upgrades and intercomparisons', *Journal of Climate*, 28(3), pp. 911–930. doi: 10.1175/JCLI-D-14-00006.1.

Huang, B., Thorne, P. W., Banzon, V. F., Boyer, T., Chepurin, G., Lawrimore, J. H., Menne, M. J., Smith, T. M., Vose, R. S. and Zhang, H. M. (2017) 'Extended reconstructed Sea surface temperature, Version 5 (ERSSTv5): Upgrades, validations, and intercomparisons', *Journal of Climate*, 30(20), pp. 8179–8205. doi: 10.1175/JCLI-D-16-0836.1.

Huntingford, C., Marsh, T., Scaife, A., Kendon, E., Hannaford, J., Kay, A., Lockwood, M., Prudhomme, C., Reynard, N., Parry, S., Lowe, J., Screen, J., Ward, H., Roberts, M., Stott, P., Bell, V., Bailey, M., Jenkins, A., Legg, T., Otto, F., Massey, N., Schaller, N., Slingo, J. and Allen, M. (2014). Potential influences on the United Kingdom's floods of winter 2013/14. *Nature Climate Change*, 4(9), pp.769-777.

Hurrell, J. W. (1995) 'Decadal trends in the North Atlantic oscillation: Regional temperatures and precipitation', *Science*, 269(5224), pp. 676–679. doi: 10.1126/science.269.5224.676.

Inman, J. (1835) *Navigation and Nautical Astronomy: For the Use of British Seamen*. 3rd Editio. London: W. Woodward, C. & J. Rivington.

James, P. M. (2007) 'An objective classification method for Hess and Brezowsky Grosswetterlagen over Europe', *Theoretical and Applied Climatology*, 88(1–2), pp. 17–42. doi: 10.1007/s00704-006-0239-3.

Jenkinson, A. and Collison, F. (1977) *An initial climatology of gales over the North Sea*. Bracknell, U.K: Synoptic Climatology Branch Memorandum No. 62, Meteorological Office.

Johnstone, J. A. and Mantua, N. J. (2014) 'Atmospheric controls on northeast pacific temperature variability and change, 1900-2012', *Proceedings of the National Academy of Sciences of the United States of America*, 111(40), pp. 14360–14365. doi: 10.1073/pnas.1318371111.

Jones, P. (2016) ‘The reliability of global and hemispheric surface temperature records’, *Advances in Atmospheric Sciences*, 33(3), pp. 269–282. doi: 10.1007/s00376-015-5194-4.

Jones, P., Davies, T., Lister, D., Slonosky, V., Jónsson, T., Bärring, L., Jönsson, P., Maheras, P., Kolyva-Machera, F., Barriendos, M., Martin-Vide, J., Rodriguez, R., Alcoforado, M., Wanner, H., Pfister, C., Luterbacher, J., Rickli, R., Schuepbach, E., Kaas, E., Schmith, T., Jacobeit, J. and Beck, C. (1999). Monthly mean pressure reconstructions for Europe for the 1780–1995 period. International Journal of Climatology, 19(4), pp.347-364.

Jones, P. D., Harpham, C. and Briffa, K. R. (2012) ‘Lamb weather types derived from reanalysis products’, *International Journal of Climatology*, 33(5), pp. 1129–1139. doi: 10.1002/joc.3498.

Jones, P. D., Harpham, C. and Lister, D. (2016) ‘Long-term trends in gale days and storminess for the Falkland Islands’, *International Journal of Climatology*, 36(3), pp. 1413–1427. doi: 10.1002/joc.4434.

Jones, P. D., Hulme, M. and Briffa, K. R. (1993) ‘A comparison of Lamb circulation types with an objective classification scheme’, *International Journal of Climatology*, 13(6), pp. 655–663. doi: 10.1002/joc.3370130606.

Jones, P. D., Jonsson, T. and Wheeler, D. (1997) ‘Extension to the North Atlantic oscillation using early instrumental pressure observations from Gibraltar and south-west Iceland.’, *International Journal of Climatology*, 17(13), pp. 1433–1450. doi: 10.1007/1-4020-3266-8_150.

Jones, P. D., Osborn, T. J., Harpham, C. and Briffa, K. R. (2014) ‘The development of Lamb weather types: From subjective analysis of weather charts to objective approaches using reanalyses’, *Weather*, 69(5), pp. 128–132. doi: 10.1002/wea.2255.

Kalnay, E., Kanamitsu, M., Kistler, R., Collins, W., Deaven, D., Gandin, L., Iredell, M., Saha, S., White, G., Wollen, J., Zhu, Y., Chelliah, M., Ebisuzaki, W., Higgins, W., Janowiak, J., Mo, K., Ropelewski, C., Wang, J., Leetmaa, A., Reynolds, R., Jenne, R. and Joseph, D. (1996). The NCEP/NCAR 40 year reanalysis project. *Bulletin of the American Meteorological Society*, 77: 437–471.

Karl, T. R., Arguez, A., Huang, B., Lawrimore, J. H., McMahon, J. R., Menne, M. J., Peterson, T. C., Vose, R. S. and Zhang, H. M. (2015) 'Possible artifacts of data biases in the recent global surface warming hiatus', *Science*, 348(6242), pp. 1469–1472. doi: 10.1126/science.aaa5632.

Karmalkar, A. V. and Bradley, R. S. (2017) 'Consequences of global warming of 1.5 °c and 2 °c for regional temperature and precipitation changes in the contiguous United States', *PLoS ONE*, 12(1), pp. 1–17. doi: 10.1371/journal.pone.0168697.

Kennedy, J. (2014) 'A review of uncertainty in in situ measurements and data sets of sea surface temperature', *Reviews of Geophysics*, 52(1), pp. 1–32. doi: 10.1002/2013RG000434.Received.

Kennedy, J. J., Rayner, N. A., Smith, R. O., Parker, D. E. and Saunby, M. (2011) 'Reassessing biases and other uncertainties in sea surface temperature observations measured in situ since 1850: 1. Measurement and sampling uncertainties', *Journal of Geophysical Research Atmospheres*, 116(14), pp. 1–22. doi: 10.1029/2010JD015218.

Kent, E., Kennedy, J., Smith, T., Hirahara, S., Huang, B., Kaplan, A., Parker, D., Atkinson, C., Berry, D., Carella, G., Fukuda, Y., Ishii, M., Jones, P., Lindgren, F., Merchant, C., Morak-Bozzo, S., Rayner, N., Venema, V., Yasui, S. and Zhang, H. (2017). A Call for New Approaches to Quantifying Biases in Observations of Sea Surface Temperature. *Bulletin of the American Meteorological Society*, 98(8), pp.1601-1616.

Kent, E. C., Rayner, N. A., Berry, D. I., Saunby, M., Moat, B. I., Kennedy, J. J. and Parker, D. E. (2013) 'Global analysis of night marine air temperature and its uncertainty since 1880: The HadNMAT2 data set', *Journal of Geophysical Research Atmospheres*, 118(3), pp. 1281–1298. doi: 10.1002/jgrd.50152.

Kent, E. C., Woodruff, S. D. and Berry, D. I. (2007) 'Metadata from WMO publication No. 47 and an assessment of voluntary observing ship observation heights in ICOADS', *Journal of Atmospheric and Oceanic Technology*, 24(2), pp. 214–234. doi: 10.1175/JTECH1949.1.

Können, G. P., Zaiki, M., Baede, A. P. M., Mikami, T., Jones, P. D. and Tsukahara, T. (2003) 'Pre-1872 extension of the Japanese instrumental meteorological observation series back to 1819', *Journal of Climate*, 16(1), pp. 118–131. doi: 10.1175/1520-

0442(2003)016<0118:PEOTJI>2.0.CO;2.

Kushnir, Y., Robinson, W. A., Bladé, I., Hall, N. M. J., Peng, S. and Sutton, R. (2002) 'Atmospheric Gcm Response To Extratropical Sst Anomalies : Synthesis and evaluation', *Journal of Climate*, 15(16), pp. 2233–2256.

Lamb, H. (1972) *British Isles weather types and a register of the daily sequence of circulation patterns 1861-1971*, *Geophysical Memoir*. London.

Mantua, N. J., Hare, S. R., Zhang, Y., Wallace, J. M. and Francis, R. C. (1997) 'A Pacific Interdecadal Climate Oscillation with Impacts on Salmon Production', *Bulletin of the American Meteorological Society*, 78(6), pp. 1069–1079. doi: 10.1175/1520-0477(1997)078<1069:APICOW>2.0.CO;2.

Maury, M. (1858) *Explanations and sailing directions to accompany the wind and current charts*. Washington: W.A. Harris.

McCabe, G. J., Palecki, M. A. and Betancourt, J. L. (2004) 'Pacific and Atlantic Ocean influences on multidecadal drought frequency in the United States', *Proceedings of the National Academy of Sciences of the United States of America*, 101(12), pp. 4136–4141. doi: 10.1073/pnas.0306738101.

Merchant, C. J., Embury, O., Roberts-Jones, J., Fiedler, E., Bulgin, C. E., Corlett, G. K., Good, S., McLaren, A., Rayner, N., Morak-Bozzo, S. and Donlon, C. (2014) 'Sea surface temperature datasets for climate applications from Phase 1 of the European Space Agency Climate Change Initiative (SST CCI)', *Geoscience Data Journal*, 1(2), pp. 179–191. doi: 10.1002/gdj3.20.

Moberg, A., Alexandersson, H., Bergström, H. and Jones, P. D. (2003) 'Were southern Swedish summer temperatures before 1860 as warm as measured?', *International Journal of Climatology*, 23(12), pp. 1495–1521. doi: 10.1002/joc.945.

Morice, C. P., Kennedy, J. J., Rayner, N. A. and Jones, P. D. (2012) 'Quantifying uncertainties in global and regional temperature change using an ensemble of observational estimates: The HadCRUT4 data set', *Journal of Geophysical Research Atmospheres*, 117(8), pp. 1–22. doi: 10.1029/2011JD017187.

Msadek, R., Delworth, T. L., Rosati, A., Anderson, W., Vecchi, G., Chang, Y. S., Dixon, K., Gudgel, R. G., Stern, W., Wittenberg, A., Yang, X., Zeng, F., Zhang, R. and Zhang, S. (2014) 'Predicting a decadal shift in North Atlantic climate variability using the GFDL forecast system', *Journal of Climate*, 27(17), pp. 6472–6496. doi: 10.1175/JCLI-D-13-00476.1.

Muller, R., Rohde, R., Jacobsen, R., Muller, E. and Wickham, C. (2013) 'A New Estimate of the Average Earth Surface Land Temperature Spanning 1753 to 2011', *Geoinformatics & Geostatistics: An Overview*, 01(01), pp. 1–7. doi: 10.4172/2327-4581.1000101.

Myers, R. (1990) *Classical and Modern Regression with Applications*. 2nd editio. Boston: PWS Kent Publishing.

Newman, M., Compo, G. P. and Alexander, M. A. (2003) 'ENSO-forced variability of the Pacific decadal oscillation', *Journal of Climate*, 16(23), pp. 3853–3857. doi: 10.1175/1520-0442(2003)016<3853:EVOTPD>2.0.CO;2.

Numerical Algorithms Group (2015) *E02 - Curve and Surface Fitting*. Available online: https://www.nag.co.uk/numeric/fl/nagdoc_fl24/html/E02/e02intro.html , Accessed May 2015.

O'Gorman, P. A. (2015) 'Precipitation Extremes Under Climate Change', *Current Climate Change Reports*, 1(2), pp. 49–59. doi: 10.1007/s40641-015-0009-3.

Van Oldenborgh, G. J. and Van Ulden, A. (2003) 'On the relationship between global warming, local warming in the Netherlands and changes in circulation in the 20th century', *International Journal of Climatology*, 23(14), pp. 1711–1724. doi: 10.1002/joc.966.

Osborn, T. J. and Jones, P. D. (2000) 'Air flow influences on local climate: Observed United Kingdom climate variations', *Atmospheric Science Letters*, 1(1), pp. 62–74. doi: 10.1006/asle.2000.0017.

Parker, D. E. (2009) 'Anomalies of Central England temperature classified by air source', *Journal of Climate*, 22(5), pp. 1069–1081. doi: 10.1175/2008JCLI2250.1.

Parker, D. E., Folland, C. K. and Jackson, M. (1995) 'Marine surface temperature: Observed variations and data requirements', *Climatic Change*, 31(2–4), pp. 559–600. doi: 10.1007/BF01095162.

Parker, D. E., Legg, T. P. and Folland, C. K. (1992) 'A new daily central England temperature series, 1772–1991', *International Journal of Climatology*, 12(4), pp. 317–342. doi: 10.1002/joc.3370120402.

Peña-Angulo, D., Trigo, R. M., Cortesi, N. and González-Hidalgo, J. C. (2016) 'The influence of weather types on the monthly average maximum and minimum temperatures in the Iberian Peninsula', *Atmospheric Research*. Elsevier B.V., 178–179, pp. 217–230. doi: 10.1016/j.atmosres.2016.03.022.

Pérez, E. P., Magaña, V., Caetano, E. and Kusunoki, S. (2014) 'Cold surge activity over the Gulf of Mexico in a warmer climate', *Frontiers in Earth Science*, 2(August), pp. 1–10. doi: 10.3389/feart.2014.00019.

Peterson, T. C. and Vose, R. S. (1997) 'An Overview of the Global Historical Climatology Network Temperature Database', *Bulletin of the American Meteorological Society*, 78(12), pp. 2837–2849. doi: 10.1175/1520-0477(1997)078<2837:AOOTGH>2.0.CO;2.

Philipp, A., Bartholy, J., Beck, C., Erpicum, M., Esteban, P., Fettweis, X., Huth, R., James, P., Jourdain, S., Kreienkamp, F., Krennert, T., Lykoudis, S., Michalides, S., Pianko-Kluczynska, K., Post, P., Álvarez, D., Schiemann, R., Spekat, A. and Tymvios, F. (2010). Cost733cat – A database of weather and circulation type classifications. *Physics and Chemistry of the Earth*, Parts A/B/C, 35(9-12), pp.360-373

Poli, P., Hersbach, H., Dee, D. P., Berrisford, P., Simmons, A. J., Vitart, F., Laloyaux, P., Tan, D. G. H., Peubey, C., Thépaut, J. N., Trémolet, Y., Hólm, E. V., Bonavita, M., Isaksen, L. and Fisher, M. (2016) 'ERA-20C: An atmospheric reanalysis of the twentieth century', *Journal of Climate*, 29(11), pp. 4083–4097. doi: 10.1175/JCLI-D-15-0556.1.

Przybylak, R., Wyszyński, P., Vízi, Z. and Jankowska, J. (2013) 'Atmospheric pressure changes in the Arctic from 1801 to 1920', *International Journal of Climatology*, 33(7), pp. 1730–1760. doi: 10.1002/joc.3546.

Kerr, R. (2000) ‘A North Atlantic climate pacemaker for the centuries’, *Science*, 288(5473), pp. 1984–1985.

Rahmstorf, S., Box, J. E., Feulner, G., Mann, M. E., Robinson, A., Rutherford, S. and Schaffernicht, E. J. (2015) ‘Exceptional twentieth-century slowdown in Atlantic Ocean overturning circulation’, *Nature Climate Change*, 5(5), pp. 475–480. doi: 10.1038/nclimate2554.

Rayner, N., Parker, D. E., Horton, E., Folland, C. K., Alexander, L., Rowell, D., Kent, E. C. and Kaplan, A. (2003) ‘Global analyses of sea surface temperature, sea ice, and night marine air temperature since the late nineteenth century’, *Journal of Geophysical Research*, 108(D14). doi: 10.1029/2002JD002670.

Rennell, J. (1832) *An investigation of the currents of the Atlantic Ocean and of those which prevail between the Indian ocean and the Atlantic*. London: J. G. and F. Rivington for Lady Rodd.

Robock, A. (2000) ‘Volcanic eruptions and climate’, *Reviews of Geophysics*, 38(2), pp. 191–219. doi: 10.1007/978-1-4020-4411-3_227.

Robson, J., Hodson, D., Hawkins, E. and Sutton, R. (2014) ‘Atlantic overturning in decline?’, *Nature Geoscience*, 7(1), pp. 2–3. doi: 10.1038/ngeo2050.

Ropelewski, C. and Halpert, M. (1987) ‘Global and Regional Scale Precipitation Patterns Associated with the El Niño/Southern Oscillation’, *Monthly Weather Review*, 115(8), pp. 1606–1626.

Santoso, A., Mcphaden, M. J. and Cai, W. (2017) ‘The Defining Characteristics of ENSO Extremes and the Strong 2015/2016 El Niño’, *Reviews of Geophysics*, 55(4), pp. 1079–1129. doi: 10.1002/2017RG000560.

Schmidt, A., Carslaw, K. S., Mann, G. W., Wilson, M., Breider, T. J., Pickering, S. J. and Thordarson, T. (2010) ‘The impact of the 1783-1784 AD Laki eruption on global aerosol formation processes and cloud condensation nuclei’, *Atmospheric Chemistry and Physics*, 10(13), pp. 6025–6041. doi: 10.5194/acp-10-6025-2010.

Schmith, T., Alexandersson, H., Iden, K. and Tuomenvirta, H. (1997) *North Atlantic-*

European pressure observations 1868-1995 (WASA dataset version 1.0). Copenhagen: Danish Meteorological Institute.

Smith, T. M. and Reynolds, R. W. (2002) 'Bias corrections for historical sea surface temperatures based on marine air temperatures', *Journal of Climate*, 15(3), pp. 73–87.

Smith, T. M. and Reynolds, R. W. (2004) 'Reconstruction of monthly mean oceanic sea level pressure based on COADS and station data (1854-1997)', *Journal of Atmospheric and Oceanic Technology*, 21(8), pp. 1272–1282. doi: 10.1175/1520-0426(2004)021<1272:ROMMOS>2.0.CO;2.

Soden, B. J., Wetherald, R. T., Stenchikov, G. L. and Robock, A. (2002) 'Global cooling after the eruption of Mount Pinatubo: A test of climate feedback by water vapor', *Science*, 296(5568), pp. 727–730. doi: 10.1126/science.296.5568.727.

Spellman, G. (2017) 'An assessment of the Jenkinson and Collison synoptic classification to a continental mid-latitude location', *Theoretical and Applied Climatology*, 128(3–4), pp. 731–744. doi: 10.1007/s00704-015-1711-8.

Steele, M., Ermold, W. and Zhang, J. (2008) 'Arctic Ocean surface warming trends over the past 100 years', *Geophysical Research Letters*, 35(2), pp. 1–6. doi: 10.1029/2007GL031651.

Stroeve, J. C., Kattsov, V., Barrett, A., Serreze, M., Pavlova, T., Holland, M. and Meier, W. N. (2012) 'Trends in Arctic sea ice extent from CMIP5, CMIP3 and observations', *Geophysical Research Letters*, 39(16), pp. 1–7. doi: 10.1029/2012GL052676.

Stroeve, J., Serreze, M., Drobot, S., Gearheard, S., Holland, M., Maslanik, J., Meier, W. and Scambos, T. (2008) 'Arctic sea ice extent plummets in 2007', *Eos*, 89(2), pp. 13–14. doi: 10.1029/2008EO020001.

Stryhal, J. and Huth, R. (2017) 'Classifications of winter Euro-Atlantic circulation patterns: An intercomparison of five atmospheric reanalyses', *Journal of Climate*, 30(19), pp. 7847–7861. doi: 10.1175/JCLI-D-17-0059.1.

Taylor, J. (1997) *An Introduction to Error Analysis: The Study of Uncertainties in Physical Measurements*. 2nd editio. Sausalito, California: University Science Books.

Thompson, D. W. J., Kennedy, J. J., Wallace, J. M. and Jones, P. D. (2008) 'A large discontinuity in the mid-twentieth century in observed global-mean surface temperature', *Nature*, 453(7195), pp. 646–649. doi: 10.1038/nature06982.

Thorne, P. W. and Vose, R. S. (2010) 'Reanalyses Suitable for Characterizing Long-Term Trends', *Monthly Weather Review*, 91(3), pp. 353–362. doi: 10.1175/2009BAMS2858.1.

Trenberth, K. E. and Paolino, D. A. (1980) 'The Northern Hemisphere sea-level pressure data set: trends, errors and discontinuities.', *Monthly Weather Review*, pp. 855–872. doi: 10.1175/1520-0493(1980)108<0855:TNHSLP>2.0.CO;2.

Turney, C. S. M., Jones, R. T., Lister, D., Jones, P., Williams, A. N., Hogg, A., Thomas, Z. A., Compo, G. P., Yin, X., Fogwill, C. J., Palmer, J., Colwell, S., Allan, R. and Visbeck, M. (2016) 'Anomalous mid-twentieth century atmospheric circulation change over the South Atlantic compared to the last 6000 years', *Environmental Research Letters*. IOP Publishing, 11(6). doi: 10.1088/1748-9326/11/6/064009.

Vautard, R. and Yiou, P. (2009) 'Control of recent European surface climate change by atmospheric flow', *Geophysical Research Letters*, 36(22), pp. 6–11. doi: 10.1029/2009GL040480.

Veale, L. and Endfield, G. H. (2016) 'Situating 1816, the "year without summer", in the UK', *Geographical Journal*, 182(4), pp. 318–330. doi: 10.1111/geoj.12191.

Vinther, B. M., Andersen, K. K., Hansen, A. W., Schmith, T. and Jones, P. D. (2003) 'Improving the Gibraltar/Reykjavik NAO index', *Geophysical Research Letters*, 30(23). doi: 10.1029/2003GL018220.

Vinther, B. M., Andersen, K. K., Jones, P. D., Briffa, K. R. and Cappelen, J. (2006) 'Extending Greenland temperature records into the late eighteenth century', *Journal of Geophysical Research Atmospheres*, 111(11). doi: 10.1029/2005JD006810.

Visbeck, M., Hurrell, J., Polvani, L. and Cullen, H. (2001) 'The North Atlantic Oscillation: Past, present, and future', *Proceedings of the National Academy of Sciences of the United States of America*, (November), pp. 12876–12877. doi: 10.1073/pnas.231391598.

Wallace, J. M. and Hobbs, P. V. (2006) *Atmospheric science: An introductory survey*. 2nd

editio. Washington: Elsevier.

Wallace, J. M., Zhang, Y. and Renwick, J. A. (1995) 'Dynamic contribution to hemispheric mean temperature trends', *Science*, 270(5237), pp. 780–783. doi: 10.1126/science.270.5237.780.

Wallbrink, H., Koek, F. and Brandsma, T. (2009) *The US Maury collection Metadata 1796 - 1861*, *KNMI*. Available at: http://bibliotheek.knmi.nl/knmipubDIV/HISKLIM/HISKLIM_11.pdf.

Webster, P. J. and Yang, S. (1992) *Monsoon and Enso: Selectively Interactive Systems*, *Quarterly Journal of the Royal Meteorological Society*. doi: 10.1002/qj.49711850705.

Wilby, R. L. and Quinn, N. W. (2013) 'Reconstructing multi-decadal variations in fluvial flood risk using atmospheric circulation patterns', *Journal of Hydrology*. Elsevier B.V., 487, pp. 109–121. doi: 10.1016/j.jhydrol.2013.02.038.

WMO (1983) *Guide to meteorological instruments and methods of observation*. 5th editio. Geneva, Switzerland.

Wolter, K. and Timlin, M. S. (2011) 'El Niño/Southern Oscillation behaviour since 1871 as diagnosed in an extended multivariate ENSO index (MEI.ext)', *International Journal of Climatology*, 31(7), pp. 1074–1087. doi: 10.1002/joc.2336.

Woodruff, S. D., Worley, S. J., Lubker, S. J., Ji, Z., Eric Freeman, J., Berry, D. I., Brohan, P., Kent, E. C., Reynolds, R. W., Smith, S. R. and Wilkinson, C. (2011) 'ICOADS Release 2.5: Extensions and enhancements to the surface marine meteorological archive', *International Journal of Climatology*, 31(7), pp. 951–967. doi: 10.1002/joc.2103.

Xu, Z. X., Takeuchi, K. and Ishidaira, H. (2004) 'Correlation between El Niño-Southern Oscillation (ENSO) and precipitation in South-east Asia and the Pacific region', *Hydrological Processes*, 18(1), pp. 107–123. doi: 10.1002/hyp.1315.

Yulaeva, E. and Wallace, J. M. (1994) 'The signature of ENSO in global temperature and precipitation fields derived from the microwave sounding unit', *Journal of Climate*, pp. 1719–1736. doi: 10.1175/1520-0442(1994)007<1719:TSOEIG>2.0.CO;2.

Zhang, X., Vincent, L. A., Hogg, W. D. and Niitsoo, A. (2000) 'Temperature and precipitation trends in Canada during the 20th century', *Atmosphere - Ocean*, 38(3), pp. 395–429. doi: 10.1080/07055900.2000.9649654.